

Synthesizing Self-Healing and Recyclable Silicones
Using the Diels-Alder Reaction as a Cross-Linker:
Investigation of Various Dienes and Dienophile Systems

Paria Azadi Namin, BSc, MSc

The thesis submitted to the Department of Chemistry in partial fulfillment of
the requirements for the degree of

Master of Science

December, 2019
Brock University
St. Catharines, Ontario

© 2019 Paria Azadi

Equipped with his five senses, man explores the universe
around him and calls the adventure Science. - Edwin
Powell Hubble

One, remember to look up at the stars and not down at your
feet. Two, never give up work. Work gives you meaning
and purpose and life is empty without it. Three, if you are
lucky enough to find love, remember it is there and don't
throw it away. — Stephen Hawking

To my family

Abstract

This thesis focuses on the synthesis of recyclable and self-healing polysiloxane elastomer networks. These features were achieved through the use of thermally reversible Diels-Alder (DA) and retro-Diels-Alder (rDA) reactions. In this work, for the model system, two different dienes (**3** and **8**) and six dienophile were explored, of which five of the dienophiles are commercially available and one of them was synthesized in the lab (**13**) to produce a series of model DA adduct. Model systems consisting of diene-functionalized trisiloxanes and bismaleimides as dienophiles were utilized to develop a fundamental understanding of how the electronic differences in the coupling systems would influence the efficiency of the overall reaction. Then for the elastomers, three different methylhydrosiloxane-dimethylsiloxane copolymer, trimethylsiloxane terminated (PDMS) with different molecular weights and Si-H group mole percentages [**32 a** = 3-4% Si-H and 13000 g/mol; **32 b** = 7-9% Si-H and 5500-6500 g/mol; **32 c** = 25-30% Si-H and 2000-2600 g/mol] were used and functionalized with two different dienes (**3** and **8**) to produce six polymeric diene systems (**33 a**, **33 b**, **33 c**, **34 a**, **34 b** and **34 c**). After analyzing the model systems, the optimal temperature for adduct formation was determined to be between 60 °C – 70 °C, while the rDA reactions occur were found to occur between 90 °C and 110 °C, depending on the system. The tensile strengths of the elastomer systems correlated well with the cross-link densities of individual elastomers (elastomers were elongated between 0.3 cm and 2.54 cm). Furthermore, the hardness of the elastomers also correlated with the cross-link density of the elastomer (Shore 00 values ranged from 32 to 8). However, all of the elastomers displayed a decrease in their Shore 00 values after being damaged and healed. Of particular note in this study are elastomers **35 b** and **35 c**. Not only were these the only examples of

translucent and colourless materials, the elastomers fully cured at room temperature in only 5 h. After mechanical damage the elastomers were heated to 80 °C to induce mobility in the polymer chains, complete healing of the mechanical damage was observed to occur in approximately 3 min and upon cooling to room temperature it cured and got solid again.

Acknowledgement

I would like to express my special thanks of gratitude to my supervisor Dr. Paul Zelisko who gave me this wonderful opportunity working in his research lab. His patience and supportive advises were always appreciable. Without his support and guidance this research would not have been possible.

I would like to extend thanks to my committee members, Prof. Travis Dudding for his generous guidance and Prof. Melanie Pilkington for her support. The constructive comments of my external examiner Dr. Melissa Grunlan helped me through my thesis. I would like to thank Marcia Reid (McMaster University), Liqun Qiu and Razvan Simionescu, for their precious help in collecting and providing technical services for SEM imaging, mass spectrometry and nuclear magnetic resonance respectively.

I would like to thank to all of the past and present members of the Zelisko group. Specially, Dr. Mark Frampton, Kelly Duggan, Zachary Raczewolski, Julio Trevino Silva, Andrea Blais, Phoebe Booth and Laura Voigt for their presence and support in this precious journey. My special thanks go to Sepehr Sepehri and Rozhin Rowshanpour for being there for me when I needed.

At the end, I need to thank my mother, father and sister for their support from the long distance.

Table of Contents

1	Chapter 1: Introduction	1
1.1	Silicon Chemistry	1
1.1.1	Silicon Atom	1
1.2	Fundamentals of Polymer Chemistry	3
1.2.1.1	Thermoplastic and Thermoset Polymers	6
1.2.2	Cross-Linking Chemistry	7
1.2.2.1	Polymer Strength	8
1.2.2.3	Ultimate Elongation of a Polymer	9
1.2.2.4	Young's Modulus	9
1.3	Silicone Chemistry	11
1.3.1	The Hydrosilylation Reaction	14
1.4	Esterification Reactions	16
1.4.1	Enzyme-Mediated Esterification Reactions	18
1.5	Self-Healing Materials	20
1.5.1	Physical Principles of Self-Healing	22
1.5.2	Chemical Principles of Self-Healing	24
1.5.2.1	Covalent Bond Network Formation	25
1.5.2.1.1	Irreversible Networks	25
1.5.2.1.2	Reversible Networks	26
1.5.2.2	Supramolecular Network Formation	27

1.6	The Diels-Alder Reaction.....	28
1.6.1	Diels-Alder Reaction and Mechanism	30
1.6.2	Classification of Diels-Alder Reactions.....	32
1.6.3	Dienes in Diels-Alder Reactions.....	36
1.6.4	Dienophiles in Diels-Alder Reactions	37
1.6.5	Stereochemistry of the Diels-Alder Reaction	38
1.6.6	The Diels-Alder Reaction and Polymer Chemistry	39
1.7	Silicones and the Diels-Alder Reaction	42
1.8	Polymers and the Environment	46
1.9	Hypothesis and Thesis Objectives.....	47
2	Chapter 2: Results and Discussion.....	48
2.1	The Model Systems	48
2.2	Synthesis of Diels-Alder Cross-Linked Siloxane Elastomers.....	68
2.3	Solid-State NMR.....	73
2.4	Imaging the Elastomers	75
2.5	Tensile Strength Measurements	79
2.6	Differential Scanning Calorimetry (DSC) Analysis of Cross-Linked Elastomers	
	83	
2.7	Hardness Measurements.....	84
2.8	Conclusions & Future Outlook	86

1. Chapter 3: Experimental	88
3 Chapter 3: Experimental	88
3.1 Instrumentation.....	88
3.2 Materials.....	89
3.3 Synthesis of the Model Compounds	90
3.3.1 Synthesis of the Diene	90
3.3.1.1 Synthesis of furan-2-ylmethyl undec-10-enoate (3).....	90
3.3.1.2 Synthesis of furanyl-2-methyl-11-(1,1,1,3,5,5,5-heptamethyltrisiloxan-3-yl)undecanoate (5)	91
3.3.1.3 Synthesis of 2-(undec-10-en-1-yl)furan (8).....	92
3.3.1.4 Synthesis of 3-(11-(furan-2-yl)undecyl)-1,1,1,3,5,5,5-heptamethyltrisiloxane (9)	93
3.3.1.5 Synthesis of N-hydroxymethylmaleimide (11)	93
3.3.1.6 Synthesis of tetramethybis[(N-maleimidomethyl)oxy]disiloxane (13).....	94
3.3.1.7 Model Diels-Alder Reactions	95
3.4 Synthesis of the Elastomers	95
3.4.1 Synthesis of furan-2-ylmethylundecanoatesiloxane-dimethylsiloxane copolymers (33 a, 33 b, 33 c).....	95
3.4.2 Synthesis of furan-2-ylmethylundecanoatesiloxane-dimethylsiloxane copolymers (34 a, 34 b, 34 c).....	97
3.4.3 DA Synthesis in the Mould (Elastomers)	98

3.4.3.1.1 Appendix	99
3.4.3.1.2 Vita	150
References.....	151

List of Figures

Figure 1-1. Comparison of carbon and silicon bond formation.....	2
Figure 1-2 Different kinds of polymer structures. a) linear, b) branched, c) star-shaped, d) comb-shaped, e) ladder, f) semi-ladder and g) network ¹⁰ (Adopted from the reference with permission)	3
Figure 1-3 a) Step-growth and b) chain-growth polymerization over time in various temperatures (T) ¹¹ (Adopted from the reference with permission).....	4
Figure 1-4 Step-growth polymerization: a) unreacted monomer, b) 50% reacted, c) 75% reacted, d) 100% reacted (Adopted from the reference with permission)	5
Figure 1-5 Chain-growth polymerization: a) unreacted monomer, b) 50% reacted, c) 75% reacted, d) 100% reacted (Adopted from the reference with permission)	5
Figure 1-6 Some thermosetting polymers: (1) phenolic's high modulus & excellent heat and creep resistance under pressure; (2) urea-formaldehyde resins such as laminates ¹⁸ ...	7
Figure 1-7 Thermoplastic polymers in industry.....	7
Figure 1-8 Dependence of the poly strength to molecular weight.....	8
Figure 1-9 Elongation to break of the polymer.....	9
Figure 1-10 Ratio of stress to the strain (Young's modulus).....	10
Figure 1-11 Possible physical states of polymers	10
Figure 1-12. Applications of silicone polymers.....	13
Figure 1-13 Structure of Karstedt's catalyst ⁴⁷ (Adopted from the reference with permission).....	15

Figure 1-14 Chalk-Harrod and modified Chalk-Harrod mechanism for the hydrosilylation of alkenes ^{50, 51} (Adopted from the reference with permission).....	16
Scheme 1-4 Mechanism for a Fischer esterification ⁵⁵ (Adopted from the reference with permission).....	17
Figure 1-15 Three dimensional structure of Candida antarctica enzyme ⁵⁷ (Adopted from the reference with permission).....	18
Figure 1-16 The active site amino acids of CalB. ⁶³ (Adopted from the reference with permission).....	20
Figure 1-17 Autonomic healing of a polymeric material ⁶⁸ (Adopted from the reference with permission)	22
Figure 1-18. The Wool and O'Connor model for the physical self-healing of polymers ⁶⁵ (Adopted from the reference with permission)	23
Figure 1-19 Different chemical self-healing processes: 1) covalent bond formation, 2) chain entanglement, and 3) supramolecular network formation ⁷⁷ (Adopted from the reference with permission)	25
Figure 1-20 Examples of reversible and irreversible covalent bond network formation in self-healing polymers ⁶⁵ (Adopted from the reference with permission).....	26
Figure 1-21 Reversible interactions to produce supramolecular polymer networks ⁶⁵ (Adopted from the reference with permission).....	27
Figure 1-22 Hydrogen bonds between UPy units leading to polymeric networks ⁷⁸ (Adopted from the reference with permission)	28
Figure 1-23. Frontier molecular orbitals of the reactants in a Diels-Alder Reaction ⁹⁰	30

Figure 1-24. Disrotatory mechanism to obtain two new σ bonds in a Diels-Alder reaction 91	31
Figure 1-25. Suprafacial and antarafacial interactions of p orbitals to form new a σ bond in the Diels-Alder reaction ⁸⁹ (Adopted from the reference with permission)	32
Figure 1-26 Molecular orbital and bonding interactions between butadiene and ethylene in the DA cycloaddition reaction ⁵⁵ (Adopted from the reference with permission)	35
Figure 1-27. Frontier molecular orbital interactions for different categories of DA reactions.	35
Figure 1-28. (a) Poly(butylmethacrylates) and (b) Polysiloxanes modified with furan and maleimide moieties synthesized by Kickelbick et. al. ¹¹⁷ (Adopted from the reference with permission).....	44
Figure 2-1 Different bismaleimides	48
Figure 2-2 ¹ H NMR spectrum of model Diels-Alder adduct 23	52
Figure 2-3 COSY NMR spectrum illustrating the correlation between the endo protons and the bridgehead proton. Note that the exo proton is not correlated with the bridgehead proton	53
Figure 2-4. ¹ H NMR spectra of the reaction between 5 and 13 at different temperatures (40 °C, 50 °C, 60 °C, 70 °C, 80 °C, 85 °C) illustrating maleimide consumption (●) and the formation of the new endocyclic double bond (■), the bridgehead proton (◆), and the exo (▲) and endo (*) adduct products	59

Figure 2-5 VT ¹H NMR spectra of the reaction #1 (40 °C,50 °C, 60 °C, 70 °C, 80 °C) illustrating maleimide consumption (●) and the formation of the new endocyclic double bond (■), the bridgehead proton (◆),and the exo (▲) and endo (*) adduct products 60

Figure 2-6 VT ¹H NMR spectra of the reaction #2 (40 °C,50 °C, 60 °C, 70 °C, 80 °C) illustrating maleimide consumption (●) and the formation of the new endocyclic double bond (■), the bridgehead proton (◆),and the endo (*) adduct products 60

Figure 2-7 VT ¹H NMR spectra of the reaction #3 (40 °C,50 °C, 60 °C, 70 °C, 80 °C) illustrating maleimide consumption (●) and the formation of the new endocyclic double bond (■), the bridgehead proton (◆),and the endo (*) adduct products 61

Figure 2-8 VT ¹H NMR spectra of the reaction #5 (40 °C,50 °C, 60 °C, 70 °C, 80 °C) illustrating maleimide consumption (●) and the formation of the new endocyclic double bond (■), the bridgehead proton (◆),and the exo (▲) and endo (*) adduct products 61

Figure 2-9 VT ¹H NMR spectra of the reaction #6 (40 °C,50 °C, 60 °C, 70 °C, 80 °C) illustrating maleimide consumption (●) and the formation of the new endocyclic double bond (■), the bridgehead proton (◆),and the exo (▲) and endo (*) adduct products 62

Figure 2-10 VT ¹H NMR spectra of the reaction #7 (40 °C,50 °C, 60 °C, 70 °C, 80 °C) illustrating maleimide consumption (●) and the formation of the new endocyclic double bond (■), the bridgehead proton (◆),and the endo (*) adduct products 62

Figure 2-11 VT ¹H NMR spectra of the reaction #8 (40 °C,50 °C, 60 °C, 70 °C, 80 °C) illustrating maleimide consumption (●) and the formation of the new endocyclic double bond (■), the bridgehead proton (◆),and the endo (*) adduct products 63

Figure 2-12 VT ^1H NMR spectra of the reaction #9 (40 °C, 50 °C, 60 °C, 70 °C, 80 °C) illustrating maleimide consumption (●) and the formation of the new endocyclic double bond (■), the bridgehead proton (◆), and the endo (*) adduct products	63
Figure 2-13 VT ^1H NMR spectra of the reaction #10 (40 °C, 50 °C, 60 °C, 70 °C, 80 °C) illustrating maleimide consumption (●) and the formation of the new endocyclic double bond (■), the bridgehead proton (◆), and the exo (▲) and endo (*) adduct products	64
Figure 2-14 VT ^1H NMR spectra of the reaction #11 (40 °C, 50 °C, 60 °C, 70 °C, 80 °C) illustrating maleimide consumption (●) and the formation of the new endocyclic double bond (■), the bridgehead proton (◆), and the endo (*) adduct products	64
Figure 2-15 VT ^1H NMR spectra of the reaction #12 (40 °C, 50 °C, 60 °C, 70 °C, 80 °C) illustrating maleimide consumption (●) and the formation of the new endocyclic double bond (■), the bridgehead proton (◆), and the exo (▲) and endo (*) adduct products	65
Figure 2-16. Computationally-derived electronic charges on (a) N,N'-(1,3-phenylene)bismaleimide and (b) N,N'-(1,4-phenylene)bismaleimide atoms.	66
Figure 2-17. (a) DSC thermograph and (b) TGA analysis for the model DA/rDA reaction between 5 and 13	68
Figure 2-18 Solid-state ^1H NMR of compound 35 b . The peaks at 3.02, 3.40 and 3.68 ppm confirm existence of exo and endo adduct protons.....	74
Figure 2-19 Solid-state ^1H NMR of compound 41 c . The peaks at 3.24 and 3.37 ppm confirm existence of exo and endo adduct protons.....	75
Figure 2-21 Photographs and SEM images for the elastomer made from 35 b : (a), (b), (c) photographs of virgin, bisected, and healed elastomer respectively; (d), (e) SEM images of	

a virgin and healed elastomer at 200 x magnification; (f), (g) the same virgin and healed elastomer imaged at 2.5k x magnification; (h) the healed elastomer imaged at 500 x magnification. The cuts/scars are highlighted in (b), (c), (e), (g), and (h).....	78
Figure 2-22 Images demonstrating the capacity of the elastomers made from 35 b to be remoulded into different shapes and hence recycled.	79
Figure 2-23 Comparing the tensile strength of the 35 b, 36 b, 38 b, 39 b and 40 b	80
Figure 2-24 Comparing the tensile strength of the 41 b, 42 b and 46 b	80
Figure 2-25 Comparing the tensile strenght of the 35 c, 36 c, 38 c and 40 c	81
Figure 2-26 Comparing the tensile strength of elastomer 35 b before and after healing .	82
Figure 2-27 Comparing the tensile strength of elastomer 35 c and after healing	82
Figure 2-28 DSC thermograms for elastomer 35 b	83
Appendix Figure 1 ¹ H NMR of compound 3	99
Appendix Figure 2 ¹³ C NMR of compound 3	100
Appendix Figure 3 ¹ H NMR of compound 8	101
Appendix Figure 4 ¹³ C NMR of compound 8	102
Appendix Figure 5 ¹ H NMR of compound 5	103
Appendix Figure 6 ¹³ C NMR of compound 5	104
Appendix Figure 7 ²⁹ Si NMR of compound 5	105
Appendix Figure 8. ¹ H NMR of compound 9	106
Appendix Figure 9. ¹³ C NMR of compound 9	107

Appendix Figure 10. ^{29}Si NMR of compound 9	108
Appendix Figure 11. ^1H NMR of compound 13	109
Appendix Figure 12. ^{13}C NMR of compound 13	110
Appendix Figure 13. ^{29}Si NMR of compound 13	111
Appendix Figure 14. ^1H NMR of compound 11	112
Appendix Figure 15. ^{13}C NMR of compound 11	113
Appendix Figure 16. DA adduct ^1H NMR of reaction number 1	114
Appendix Figure 17. DA adduct ^1H NMR of reaction number 2	115
Appendix Figure 18. DA adduct ^1H NMR of reaction number 3	116
Appendix Figure 19. DA adduct ^1H NMR of reaction number 4	117
Appendix Figure 20. DA adduct ^1H NMR of reaction number 5	118
Appendix Figure 21. DA adduct ^1H NMR of reaction number 6	119
Appendix Figure 22. DA adduct ^1H NMR of reaction number 7	120
Appendix Figure 23. DA adduct ^1H NMR of reaction number 8	121
Appendix Figure 24. DA adduct ^1H NMR of reaction number 9	122
Appendix Figure 25. DA adduct ^1H NMR of reaction number 10	123
Appendix Figure 26. DA adduct ^1H NMR of reaction number 11	124
Appendix Figure 27. DA adduct ^1H NMR of reaction number 12	125
Appendix Figure 28. DSC analysis of model reaction number 1	126
Appendix Figure 29. DSC analysis of model reaction number 2	126

Appendix Figure 30. DSC analysis of model reaction number 3	127
Appendix Figure 31. DSC analysis of model reaction number 4	127
Appendix Figure 32. DSC analysis of model reaction number 5	128
Appendix Figure 33. DSC analysis of model reaction number 6	128
Appendix Figure 34. DSC analysis of model reaction number 7	129
Appendix Figure 35. DSC analysis of model reaction number 8	129
Appendix Figure 36. DSC analysis of model reaction number 9	130
Appendix Figure 37. DSC analysis of model reaction number 10	130
Appendix Figure 38. DSC analysis of model reaction number 11	131
Appendix Figure 39. DSC analysis of model reaction number 12	131
Appendix Figure 40 ¹ H NMR of compound 33 a	132
Appendix Figure 41 ¹³ C NMR of compound 33 a	133
Appendix Figure 42 ²⁹ Si NMR of compound 33 a	134
Appendix Figure 43 ¹ H NMR of compound 33 b	135
Appendix Figure 44 ¹³ C NMR of compound 33 b	136
Appendix Figure 45 ²⁹ Si NMR of compound 33 b	137
Appendix Figure 46 ¹ H NMR of compound 33 c	138
Appendix Figure 47 ¹³ C NMR of compound 33 c	139
Appendix Figure 48 ²⁹ Si NMR of compound 33 c	140
Appendix Figure 49 ¹ H NMR of compound 34 a	141

Appendix Figure 50 ^{13}C NMR of compound 34 a	142
Appendix Figure 51 ^{29}Si NMR of compound 34 a	143
Appendix Figure 52 ^1H NMR of compound 34 b	144
Appendix Figure 53 ^{13}C NMR of compound 34 b	145
Appendix Figure 54 ^{29}Si NMR of compound 34 b	146
Appendix Figure 55 ^1H NMR of compound 34 c	147
Appendix Figure 56 ^{13}C NMR of compound 34 c	148
Appendix Figure 57 ^{29}Si NMR of compound 34 c	149

List of Schemes

Scheme 1-1 nucleophilic attack on carbon and silicon atoms (Adopted from reference with permission)	2
Scheme 1-2 Hydrosilylation reaction using peroxide as catalyst	14
Scheme 1-3 A hydrosilylation reaction and the possible side reactions that can occur when using Karstedt's catalyst ⁴⁸ (Adopted from the reference with permission).....	15
Scheme 1-5 Esterification using N435 as a catalyst ⁶² (Adopted from the reference with permission).....	19
Scheme 1-6. Examples of different cycloaddition reactions and their mechanisms ⁸²	29
Scheme 1-7. The first reported DA reaction by Diels and Alder in 1928 ⁸⁴	29
Scheme 1-8. Regioselectivity in normal and inverse demand DA reactions ⁹⁹	34
Scheme 1-9. The s-cis and s-trans conformation of conjugated dienes.....	36
Scheme 1-10. Locked s-trans conformations.....	37
Scheme 1-11. The endo and exo orientations possible in a Diels-Alder reaction ¹⁰⁶	38
Scheme 1-12. Polymeric dienes using bismaleimides as a cross-linking agent ¹¹⁴	40
Scheme 1-13 Synthesis of (1) bis(dienophile), (2) bis(diene) and (3) long flexible chain by Lehn group ¹¹⁵ (Adapted from the reference with permission).....	41
Scheme 1-14 The rubber product synthesised by Picchioni et. al. using a thermoreversible DA reaction ¹¹⁶ (Adapted from the reference with permission).....	42
Scheme 1-15. Polymeric dienophiles using a bisfuran as a cross-linking agent ¹¹⁴	43

Scheme 1-16 Healable elastomers PDMS elastomers synthesized by Xia et al. ¹¹³ (Adapted from the reference with permission)	45
Scheme 1-17 Temperature-controlled self-healing elastomers synthesized from siloxane chain grafted with maleimide moiety and POSS ¹¹⁸	46
Scheme 2-3 Synthesis of dienophile 13 ¹²³	50
Scheme 2-4 The model Diels-Alder reaction between compounds 5 and 13	51
Scheme 2-5.....	Error! Bookmark not defined.
Scheme 2-5. Synthesis of ester-furan-modified elastomers using trimethylsilyl-terminated poly(dimethylsiloxane-co-methylhydrosiloxane) with different molecular weights and Si-H concentrations	69
Scheme 2-6 Synthesis of alkyl-furan-modified elastomers using trimethylsilyl-terminated poly(dimethylsiloxane-co-methylhydrosiloxane with different molecular weights and Si-H concentrations	69
Scheme 2-7 DA reactions in the mould with diene 33 a , 33 b , 33 c and dienophile 13-18	71
Scheme 2-8 DA reactions in the mould with diene 34 a , 34 b , 34 c and dienophile 13-18	72
Scheme 2-9 A graphical of Diels-Alder reactions between furan-modified silicones and bismaleimides leading to elastomer formation.	73

List of Tables

Table 1-1 Bond strength comparison between silicon and other atoms	2
Table 1-2. Different types of dienes ¹⁰²	36
Table 1-3. Examples of common dienophiles ⁵⁶	38
Table 2-1. Model Diels-Alder reactions of furanyl-2-methyl-11-(1,1,1,3,5,5,5-heptamethyltrisiloxan-3-yl)undecanoate with 6 different dienophiles.	54
Table 2-2. Model Diels-Alder reactions of 3-(11-(furan-2-yl)undecyl)-1,1,1,3,5,5,5-heptamethyltrisiloxane with six different dienophiles	55
Table 2-3. Optimized reaction condition for the all of the model systems. The red numbers denote the reaction conditions that resulted in the highest overall yield.	56
Table 2-4 Hardness measurements of synthesized elastomers before and after healing ..	84
Table 2-5 Summary of Diels-Alder cross-linked silicone elastomers. ^a	86
Table 3-1 Moles and masses used for synthesizing compounds 33 a , 33 b and 33 c and their yields	96
Table 3-2 Moles and masses used for synthesizing compounds 34 a , 34 b and 34 c and their yields	98

Abbreviations

N435	Novozyme-435
DA	Diels-Alder
DSC	Differential Scanning Calorimeter
FMO	Frontier Molecular Orbital
HOMO	Highest Occupied Molecular Orbital
IR	Infrared Spectroscopy
LUMO	Lowest Unoccupied Molecular Orbital
MO	Molecular Orbitals
MS	Mass Spectrometry
NMR	Nuclear Magnetic Resonance
PDMS	Polydimethylsiloxane
POSS	Polyhedral Oligomeric Silsesquioxane
rDA	retro Diels-Alder
ROMP	Ring-Opening Metathesis Polymerization
SEM	Scanning Electron Microscopy
TGA	Thermogravimetric Analysis
THF	Tetrahydrofuran
Upy	2-ureido-4[1H]-pyrimidinone

Chapter 1: Introduction

1.1 Silicon Chemistry

1.1.1 Silicon Atom

Silicon (Si) is found in Group 14 ($3s^2 3p^2$) of the Periodic Table and is classified as a metalloid and semiconductor. Silicon is the second most abundant element in the Earth's crust (28%) after oxygen and is commonly found as silicon dioxide (SiO_2). Given that silicon is located in the same group as carbon it is often anticipated that silicon will display a similar chemical behaviour to carbon. However, the two elements have two distinct chemical differences that lead to different relevant reactivities under the same conditions (Figure *I-1*)^{1,2}. Firstly, the silicon atom's van der Waals radius is 50% larger than that of carbon, which results in longer bond lengths between silicon and other elements compared to similar bonds for carbon (Table *I-1*). Consequently, the rotational barrier for silicon is lower than for carbon, which ultimately results in less stable π bonds to silicon. Secondly, the weaker electronegativity of silicon when compared to carbon, has a significant effect on bond polarity that results in some unique bond strengths and enables reactions that are not possible with carbon-based chemistry (Table *I-1*). For instance, the Si-F bond is one of the strongest single bonds between atoms in the Periodic Table whereas the C-F bond is a relatively weak bond. In addition, the Si-H bond is quite weak while the C-H bond is extraordinarily strong.³ Except when it is bonded to electropositive elements such as alkali metals, silicon is typically the electropositive atom in the bonds that it forms. As a result, nucleophilic attack occurs at $\text{Si}^{\delta+}$ in a Si-H molecule whereas with a C-H bond the nucleophilic attack takes place at $\text{H}^{\delta+}$ (Scheme *I-1*).⁴

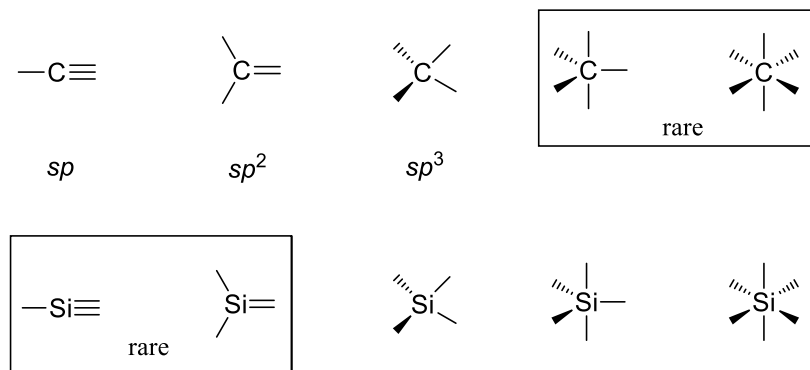
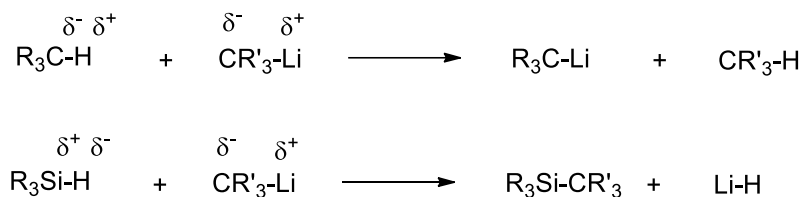


Figure 1-1. Comparison of carbon and silicon bond formation



Scheme 1-1 nucleophilic attack on carbon and silicon atoms (Adopted from reference with permission)

Although both atoms (Si and C) are found in Group 14, silicon does not always react in a similar manner when compared to carbon (Scheme 1-1). For instance, silicon has only recently been shown to be capable of forming stable double and triple bonds⁵⁻⁹. On the other hand, silicon's capacity to form hypervalent species, makes silicon special in terms of nucleophilic substitution reactions with lower activation energies.

Table 1-1 Bond strength comparison between silicon and other atoms

Atom	Electronegativity	σ -Bond Strength (Kcal/mol) (KJ/mol)		Average Bond Lengths (Å)	
Si	1.7	C-C	83	347.27	C-C 1.54
H	2.1	C-Si	76	317.98	C-Si 1.87
C	2.5	Si-Si	53	221.75	
Cl	3	C-H	83	347.27	C-O 1.43
N	3	Si-H	76	317.98	Si-O 1.66
O	3.5	C-O	86	359.82	
F	4	Si-O	108	451.87	
		C-N	83	347.27	
		Si-N	76	317.98	
		C-F	116	485.34	
		Si-F	135	564.84	

1.2 Fundamentals of Polymer Chemistry

Polymer is being defined as a large molecule chain (macromolecules) consisting of smaller units (monomers) that are connected to each other through a covalent bond. These units can be connected in various methods and produce different kinds of polymer structures such as linear, branched, star-shaped, comb-shaped, ladder, semi-ladder and network structures (Figure 1-2).¹⁰

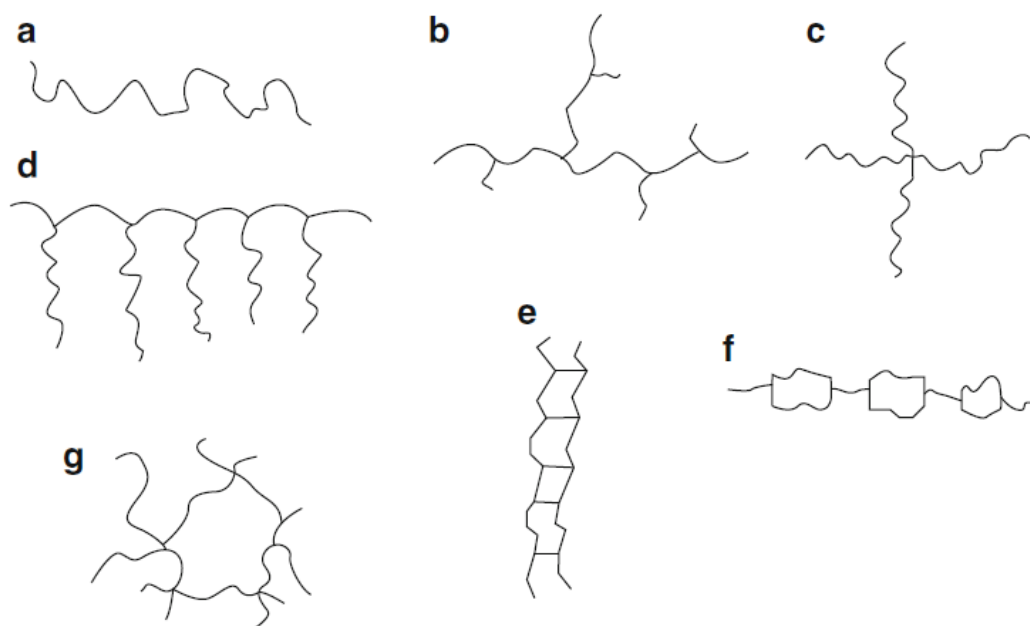


Figure 1-2 Different kinds of polymer structures. a) linear, b) branched, c) star-shaped, d) comb-shaped, e) ladder, f) semi-ladder and g) network¹⁰ (Adopted from the reference with permission)

The molecular weight of each polymer depends on the number of repeating units which is called the degree of polymerization (DP) and is showing with a number or letter. For instance, the molecular weight of polystyrene with DP of 100 would be 100×104 . If there is only one kind of monomer repeating along the polymer chain, the polymer will be called “homopolymer” while having more than one kind of monomer make a copolymer. If there

is orderliness for these repeating units they are called alternating copolymers, otherwise they will be called random copolymers.¹¹

Carothers (1929)¹² was the first one who represented a classification for polymers according to their repeating units (addition or condensation polymers). This classification depends on the similarity of atoms in repeating units compared to starting monomer. Thus, addition polymer is the one in which the same atoms in monomer is repeating along the polymer chain, while condensation polymers contain less atoms due to the side reactions occurring during the polymerization. Yet, this classification failed to include all kinds of polymers. As a result, Flory¹³ introduced the polymerization mechanism to be used to categorize polymers which can be either step-growth or chain growth polymerization. Step-growth polymerization takes place modestly. Said otherwise, the monomers unite step by step to produce polymer chain slowly over time. However, in the chain-growth polymerization, chain propagation occurs rapidly from the active sides of the monomers and the process may take only few seconds. In other words, the molecular weight increases consecutively by the linkage of the monomers (Figure 1-3).

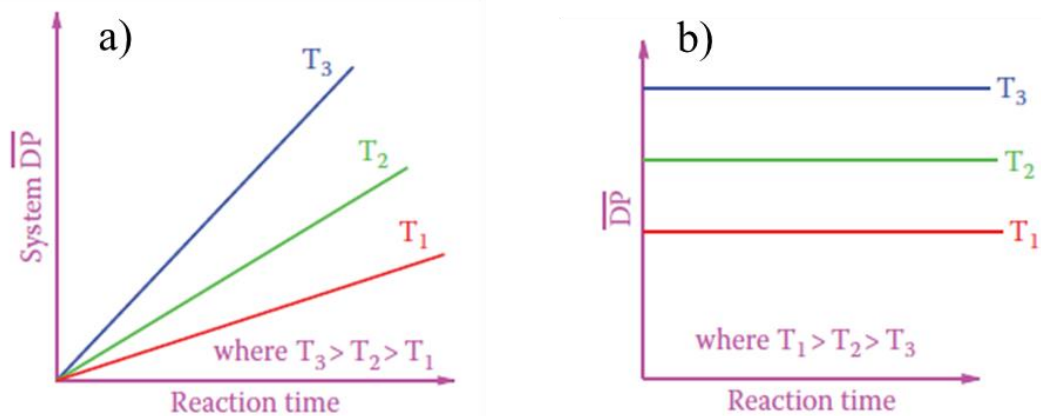


Figure 1-3 a) Step-growth and b) chain-growth polymerization over time in various temperatures (T)¹¹(Adopted from the reference with permission)

The schematic of step-growth and chain-growth polymerization have been illustrated in Figure 1-4 and Figure 1-5 respectively.¹⁴

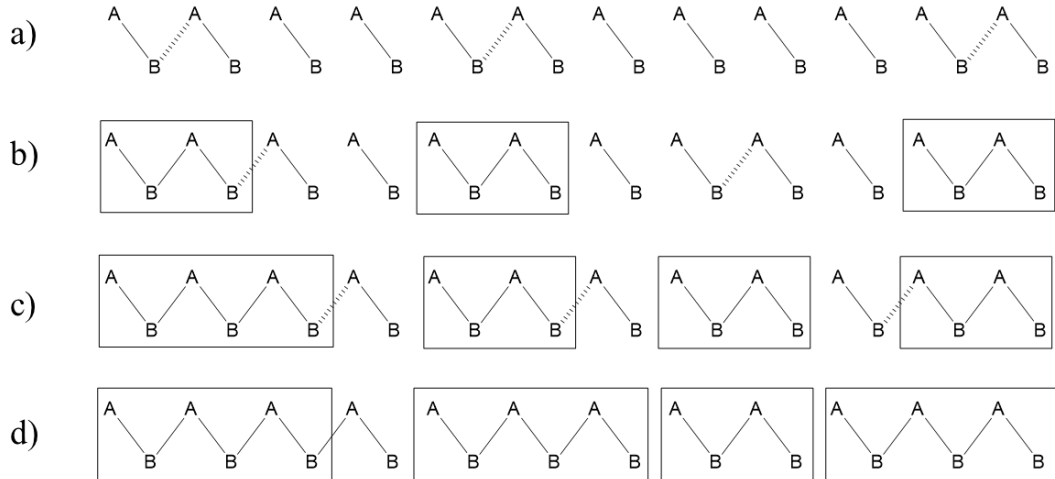


Figure 1-4 Step-growth polymerization: a) unreacted monomer, b) 50% reacted, c) 75% reacted, d) 100% reacted (Adopted from the reference with permission)

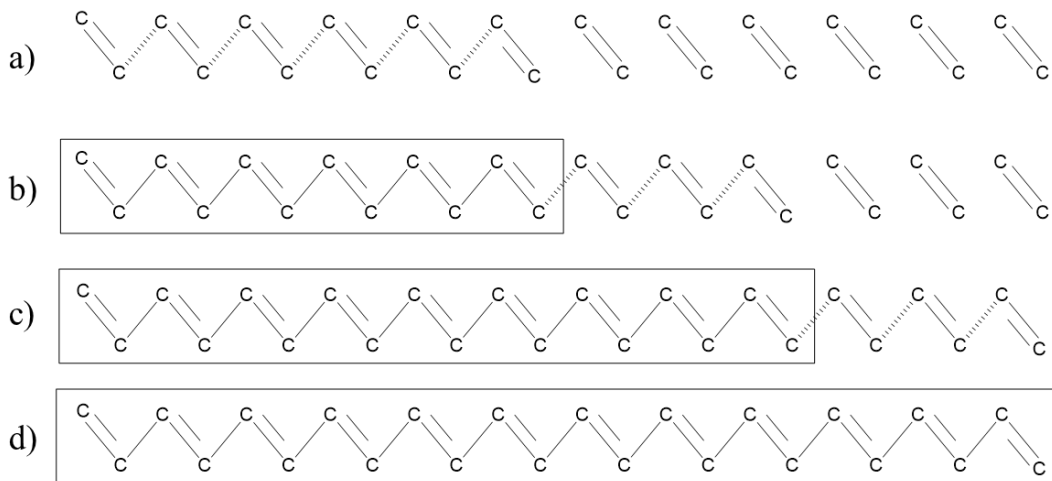


Figure 1-5 Chain-growth polymerization: a) unreacted monomer, b) 50% reacted, c) 75% reacted, d) 100% reacted (Adopted from the reference with permission)

In addition to these classifications, polymers can be categorized based on their response to temperature. As it was mentioned before, one type of polymers is network

structure that can be formed when linear or branched polymers adding together. The process of producing these networks through covalent bonds is called cross-linking. Cross-linked polymers, experience a fast acceleration in molecular weight that cannot flow or melt easily. These kinds of polymers are classified as thermosets and the ones that are not cross-linked (linear or branched) and can flow or melt are in the group of thermoplastic polymers.

1.2.1.1 Thermoplastic and Thermoset Polymers

Thermoplastics and thermoset polymers are the two main general class of polymers. Distinguishing these two classes of polymers is possible by examining the effect that temperature has on the elastic modulus of the polymers. Polymers that can be repeatedly softened and hardened by variations in temperature are classed as thermoplastics and typically the individual polymer strands can move independently of each other. On the other hand, thermoset polymers possess individual chains that are covalently bonded to each other (highly cross-linked). As a result, once these types of polymers are formed into solids they cannot return to a liquid state.¹⁵ Thermoset polymers are typically tougher and more brittle than thermoplastics and cannot flow as a viscous liquid and do not display a T_m . Elastomers are examples of thermoset polymers that are lightly cross-linked and typically have a T_g value lower than room temperature; the polymer chains can be reversibly stretched without being degraded and/or deformed.^{16,17} Phenolic and urea formaldehyde resins, unsaturated polyesters, and epoxy resins are some examples of thermosetting polymers. And some examples of thermoplastics are polyethylene, polypropylene, polystyrene, and poly(vinyl chloride) (Figure 1-6 and Figure 1-7).¹⁵

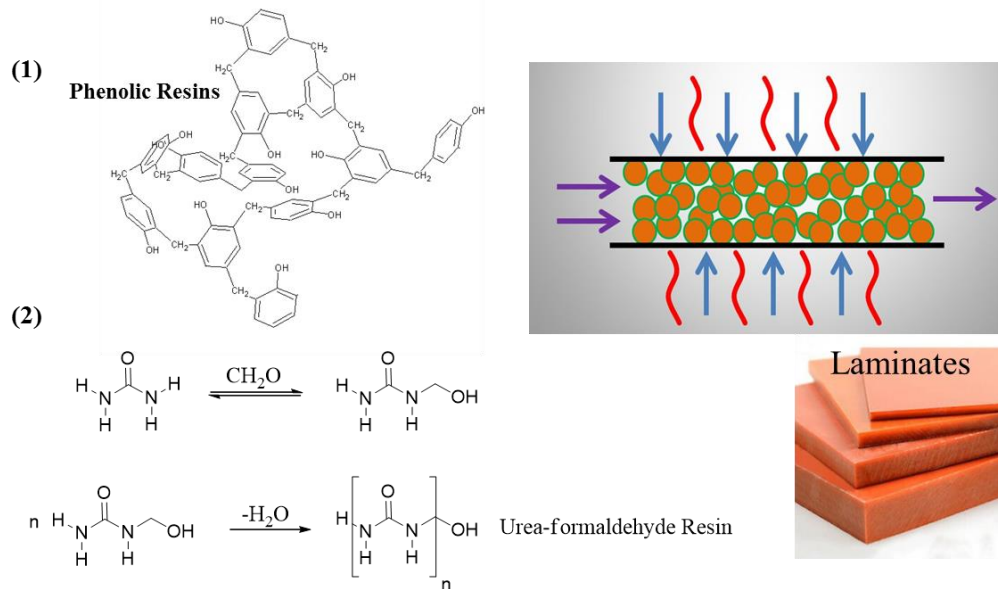


Figure 1-6 Some thermosetting polymers: (1) phenolic's high modulus & excellent heat and creep resistance under pressure; (2) urea-formaldehyde resins such as laminates¹⁸

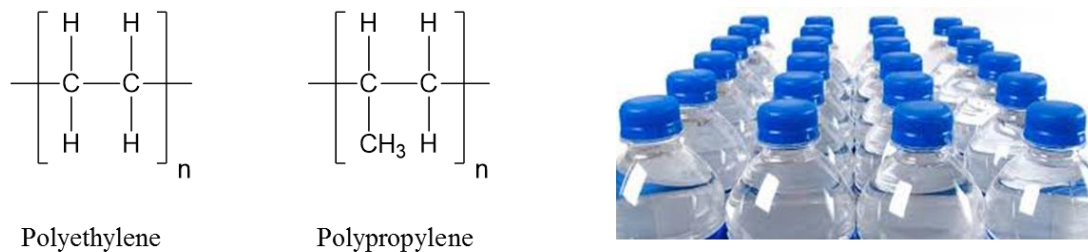


Figure 1-7 Thermoplastic polymers in industry

1.2.2 Cross-Linking Chemistry

Cross-linking is typically an irreversible process in polymer chemistry that is used to improve the mechanical properties of polymers such as strength, elongation, tensile modulus (Young's modulus), toughness, and viscoelasticity. However, highly cross-linked materials are more fragile and are prone to cracking.¹⁹ In order to make the cross-linked polymers more efficient and reusable, reversible cross-linking have been introduced as kind of a self-healing process.^{20,21} Typically, the reversible cross-links require an external

stimulus such as heat or chemical activation to occur.^{22,23} The Diels-Alder/retro Diels-Alder (Section 1.6) is one example of a reversible cross-link employed in polymer chemistry.

1.2.2.1 Polymer Strength

The strength of a polymer is represented by the stress required to break a polymer sample. The applied stress can take on a number of different forms such as tensile (stretching of the polymer), compressional (compressing the polymer), flexural (bending of the polymer), torsional (twisting of the polymer), and impact stressors (hammering on the polymer).²⁴ As a result, highly cross-linked polymers are stronger due to the greater networking and restricted motions of the polymer chains. However, tougher polymers are more brittle and are more prone to cracking. The features effecting the poly strength are molecular weight (Figure 1-8), cross-linking and crystallinity. Thus, the polymers strength can be ordered as linear < branched < cross-linked < network.

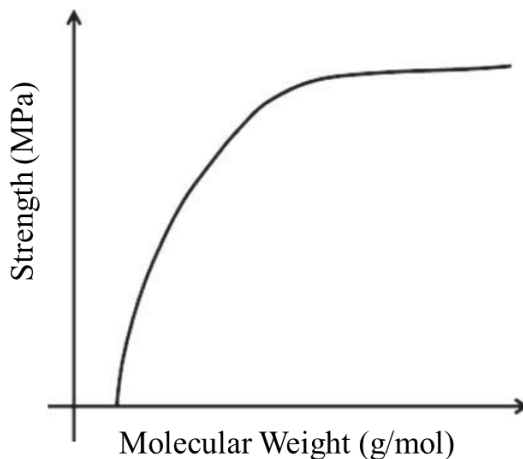


Figure 1-8 Dependence of the poly strength to molecular weight

1.2.2.3 Ultimate Elongation of a Polymer

The percentage of elongation of a polymer is the ratio between the polymer's increased length and initial length after breakage at a controlled temperature (Figure 1-9). In other words, elongation can be calculated by the relative increase in length. $\epsilon = (\Delta L/L) \times 100$. Thermoplastics have the highest elongation percentage (>100%) compared to other materials.^{25,26}

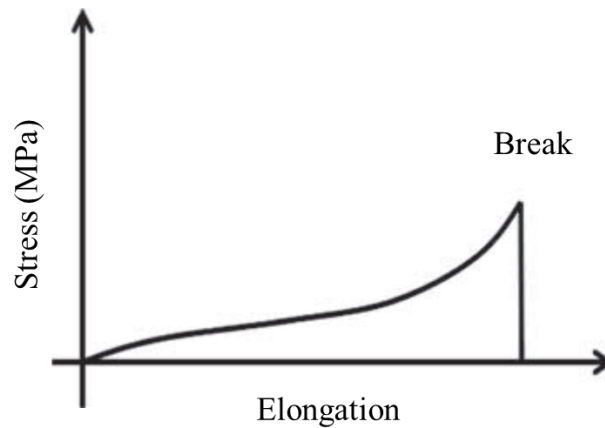


Figure 1-9 Elongation to break of the polymer

1.2.2.4 Young's Modulus

The elastic modulus, or Young's modulus, is a measure of the stiffness of solid materials that can be measured by the ratio of stress to the strain in a linearly elastic region of the material (Figure 1-10). For polymers, the mechanical properties are dependent on temperature since the polymers would be in different physical phases at different temperatures. At lower temperatures polymers are typically more brittle and tougher due to lower internal energies (glassy). The glass transition state (T_g) can be defined as a temperature where a polymer in a crystalline phase converts to a flexible and pliable polymer that can be shaped (amorphous phase). Furthermore, the melting temperature (T_m)

of a polymer is the temperature at which polymer chains can flow freely such as in a viscous liquid (Figure 1-11).²⁷

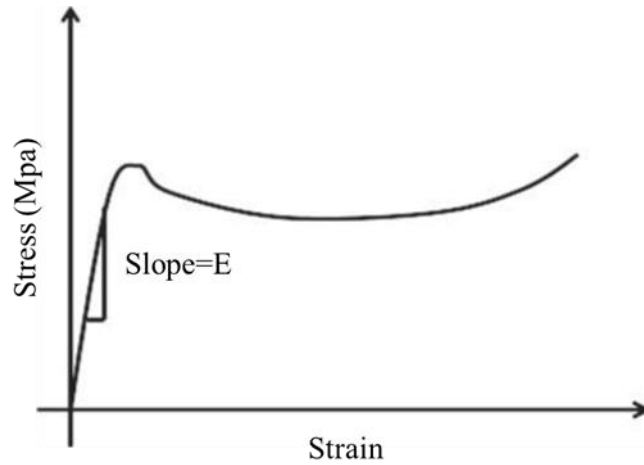


Figure 1-10 Ratio of stress to the strain (Young's modulus)

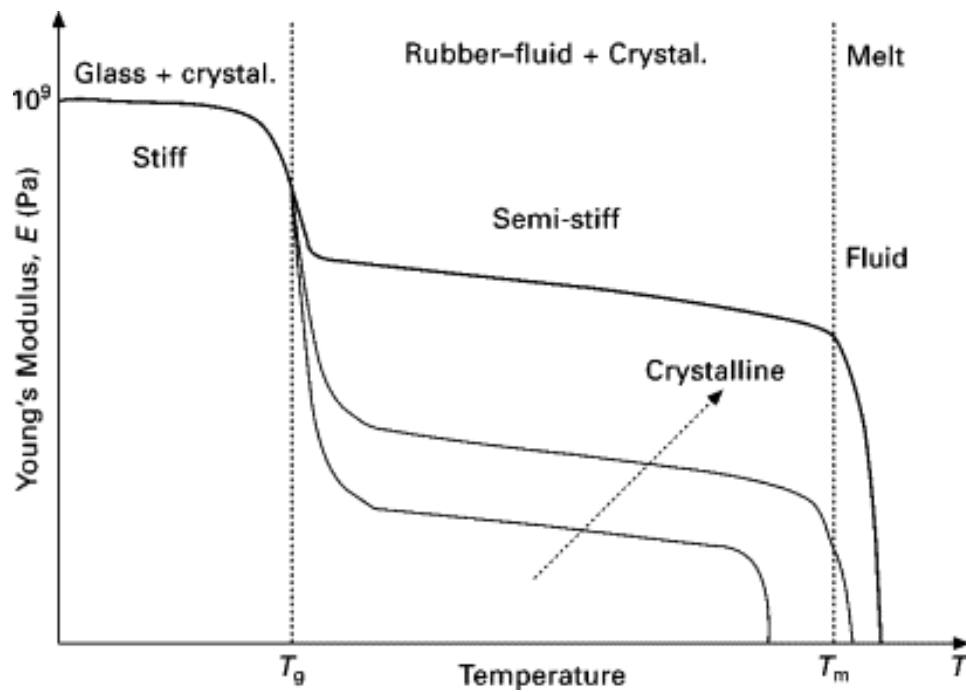


Figure 1-11 Possible physical states of polymers

1.3 Silicone Chemistry

Silicones, or polysiloxanes $(RR'SiO)_n$, are polymers that consist of an inorganic backbone chain of Si-O bonds and organic side groups typically consisting of methyl groups. Silicone polymers have found a variety of applications in fields such as the pharmaceutical industry, the electronics industry, and the automotive industry (Figure 1-12).²⁸⁻²⁹ Silicones can be formulated into different forms such as solids, liquids, semi-viscous pastes, greases, oils, and rubbers. In these various forms silicones exhibit thermal stability, electrical resistance, hydrophobicity, low thermal conductivity (insulator), low chemical reactivity, and low toxicity. These properties have led to silicones

being utilized for the production of insulator coatings, anti-foaming agents, water repellent coatings, mold-release agents, and as a component of agricultural products.

Siloxanes are thermally stable and typically exhibit consistent behaviour over a wide range of temperatures (-100 °C to 350 °C).²⁹ The thermal stability of silicones can be examined via the polymers' degradation rate, maximum degradation temperature, residue yield, and the temperature at which degradation commences.^{30,31} The relative permittivity of silicone compounds is very low and is independent of molecular weight of the polymer and temperature.^{32,33} For instance, the relative permittivity of oligomers (lower molecular weight compounds, < 100 repeat units) and higher molecular weight compounds is almost the same (~2.75). As a comparison, water and acetone have relative permittivity values of 20.7 and 78.5 respectively. Even if the silicone undergoes thermal decomposition, the polymer will decompose to silica, which is in and of itself still an excellent insulator. This has led to silicone polymers being used in industrial coatings and insulators.³⁴

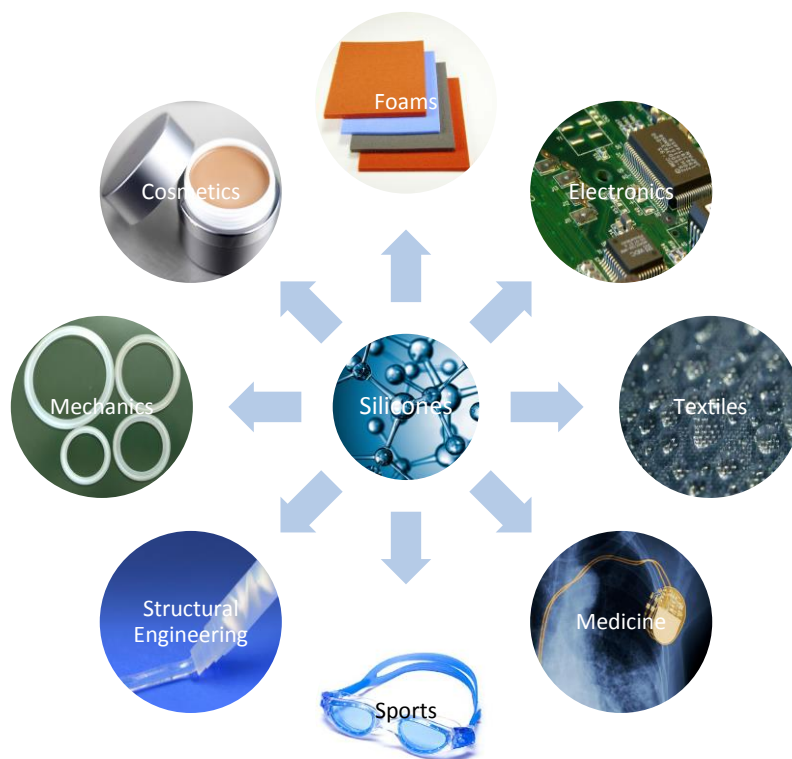


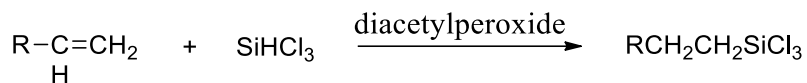
Figure 1-12. Applications of silicone polymers

One of the other advantages of silicone polymers is their surface hydrophobicity, which is mostly the result of hydrophobic methyl side groups and the flexibility of the polymer backbone that reduces wettability of the coated surface.³⁵ The chain flexibility is the result of the relatively large angle of the Si-O-Si bonds (145°) and the low bending force constant of the chain. Moreover, the longer Si-O bond (1.64 \AA) versus C-C bond (1.53 \AA) decreases steric hindrance and intramolecular blocking. As a result, silicone polymers can be used for the prevention of adhesion in automobile tire moulds.

Functionalizing silicone polymers can be used to manipulate their physical and structural properties, such as their capacity to form cross-links.

1.3.1 The Hydrosilylation Reaction

There are so many methods to produce cross-linked polymers such as using free radicals, radiation, and click chemistry.³⁶⁻³⁸ One of the most common methods used to functionalize silicone polymers to obtain a new C-Si bond from carbon-carbon multiple bond is the hydrosilylation reaction. For this reaction an Si-H group on the polymer chain adds to an unsaturated bond.^{39,40} The hydrosilylation reaction is usually catalyzed by transition-metal (precious or non-precious) complexes that can include, but are not limited to, platinum, rhodium, iridium, iron, nickel, aluminum, boron, alkaline-earth metals, copper, and titanium. Of these catalysts platinum and rhodium tend to be the most reactive producing higher yields even when utilized at room temperature.⁴¹ The first hydrosilylation reaction was performed by Sommer *et al.* in 1947 using peroxide as a catalyst (Scheme 1-2).⁴²



Scheme 1-2 Hydrosilylation reaction using peroxide as catalyst

Two metal-based catalysts, Speier's catalyst (late 1950s)⁴³ and Karstedt's catalyst (early 1970s)⁴⁴, typically are the most commonly used of the hydrosilylation catalysts. Speier's catalyst is a homogeneous transition metal catalyst obtained from the organic solution of hexachloroplatinic acid $\text{H}_2\text{PtCl}_6 \cdot 6\text{H}_2\text{O}$ in isopropyl alcohol (1-10%).⁴¹ Karstedt's catalyst (Figure 1-13) $\text{Pt}_2[(\text{CH}_2 = \text{CHSiMe}_2)_2]_3$, given its relatively high solubility in polysiloxane compounds and high selectivity and reactivity, has become known as the catalyst of choice for hydrosilylation reactions involving Polydimethylsiloxane (PDMS) compounds.^{45,46}

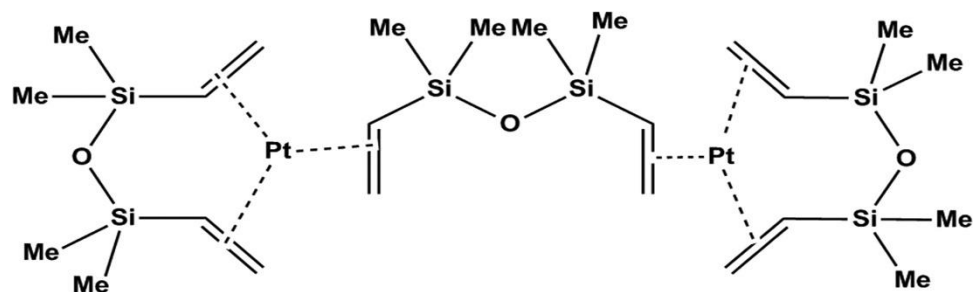
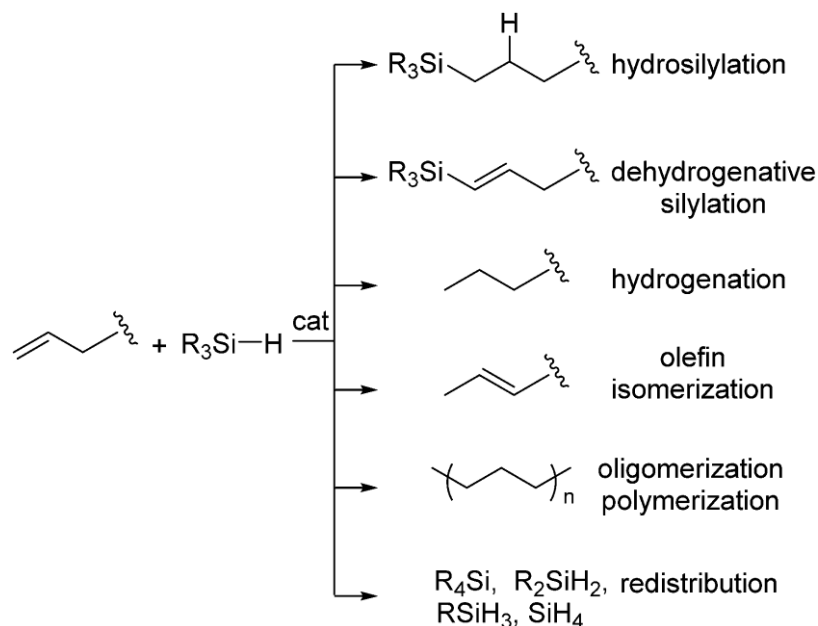


Figure 1-13 Structure of Karstedt's catalyst ⁴⁷ (Adopted from the reference with permission)

However, the use of Karstedt's catalyst in hydrosilylation reactions is not without its shortcomings; a number side reactions are possible (Scheme 1-3). Some of the possible side reactions include dehydrogenative silylation, hydrogenation of olefins, isomerization of olefins, olefin oligomerization, and redistribution of hydrosilanes.^{48,49} However, given the platinum stability of these particular platinum compounds towards heat, moisture, and oxygen, Karstedt's catalyst is still the primary for both academic and industrial scale reactions.⁴¹



Scheme 1-3 A hydrosilylation reaction and the possible side reactions that can occur when using Karstedt's catalyst ⁴⁸ (Adopted from the reference with permission)

The hydrosilylation catalytic cycle using Karstedt's catalyst is illustrated in Figure 1-14.⁵⁰ This mechanism consists of four steps. In the first step the silane compound is coordinated with the platinum complex. Then, the olefin coordinates with the metal complex followed by the production of the new Pt-C single bond in the Chalk-Harrod mechanism, while in the modified mechanism a new silicon-carbon bond is produced. In the last step for the both mechanisms hydrosilylation is been completed and the catalyst is been regenerated.^{51,52}

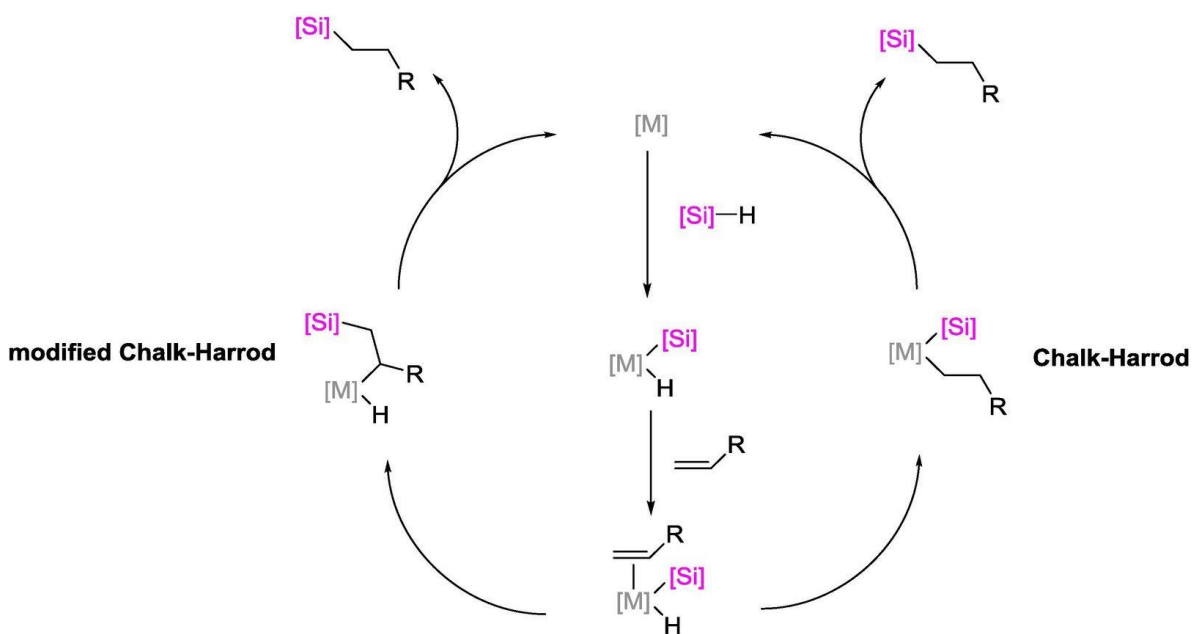
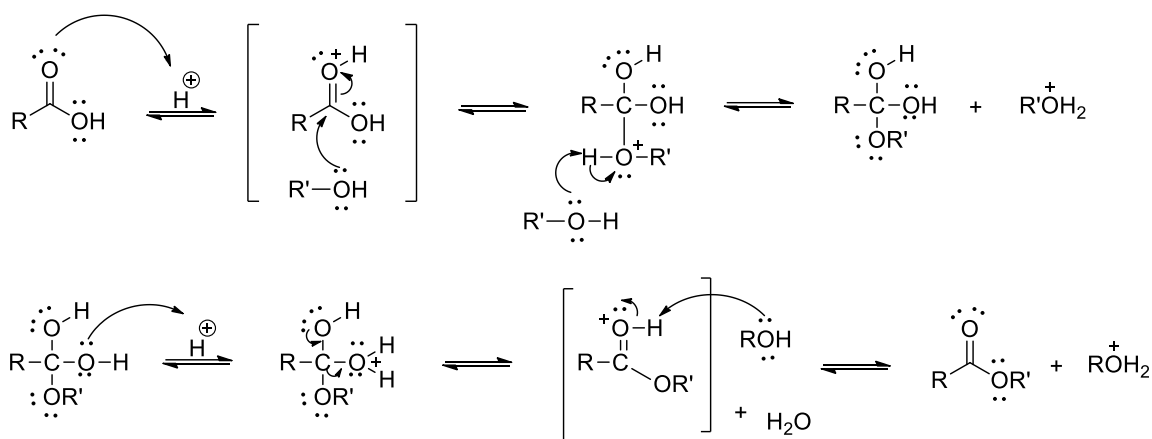


Figure 1-14 Chalk-Harrod and modified Chalk-Harrod mechanism for the hydrosilylation of alkenes ^{50, 51}
(Adopted from the reference with permission)

1.4 Esterification Reactions

In general terms esterification is the conversion of a carboxylic acid and/or one of its derivatives to an ester via a reaction with an alcohol. The reaction between alcohols and carboxylic acids in the presence of an acid catalyst (Fischer esterification)^{53,54} or base can lead to ester production (Scheme 1-4)⁵⁵, although reactions under basic conditions are not

optimal. Carboxylic acids are weak acids ($pK_a \sim 5$) while alcohols are even weaker still ($pK_a \sim 16$). Comparing the acidity of these two functional groups carboxylic acids are 1×10^{11} times stronger acids than alcohols. As a result, a base would deprotonate the carboxyl acid, which would lead to the formation of a carboxylate conjugate base that would decrease the electrophilic nature of the carbonyl carbon as a result of resonance stabilization of the negative charge on oxygen.⁵⁵



Scheme 1-4 Mechanism for a Fischer esterification⁵⁵ (Adopted from the reference with permission)

Acid-catalyzed esterification reactions are an equilibrium process. As a result, obtaining high yield requires shifting the reaction equilibrium toward the products. To achieve this either excess amounts of starting materials should be used, or the products should be removed from the reaction flask in order to force the reaction to compensate and generate more of the product. One strategy for employing Le Chatelier's Principle in these reactions is through the use of dehydrating agents such as molecular sieves in the reaction flask, or by actively removing the product water using a Dean-Stark apparatus, which ensures the continuous removal of water from the reaction flask.⁵⁶

1.4.1 Enzyme-Mediated Esterification Reactions

Recently, the use of enzymes as catalysts for various kinds of organic reactions such as hydrolysis, C-C bond formation, and redox reactions has gained popularity. Enzymatic catalysts are being used in both industry and academia as a replacement for catalytic metals and organocatalysis. Generally, the three dimensional structure of enzymes makes them a perfect catalyst due to their high chemoselectivity and stereoselectivity (regio-, diastereo- and enantioselectivity). The ribbon structure of a most common catalytic enzyme, lipase B from the yeast *Candida antarctica* is shown in Figure 1-15.^{57,58}

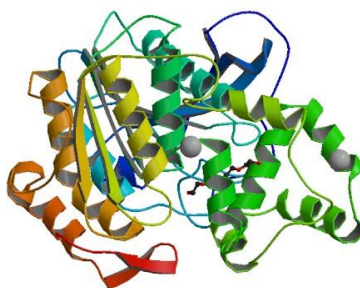
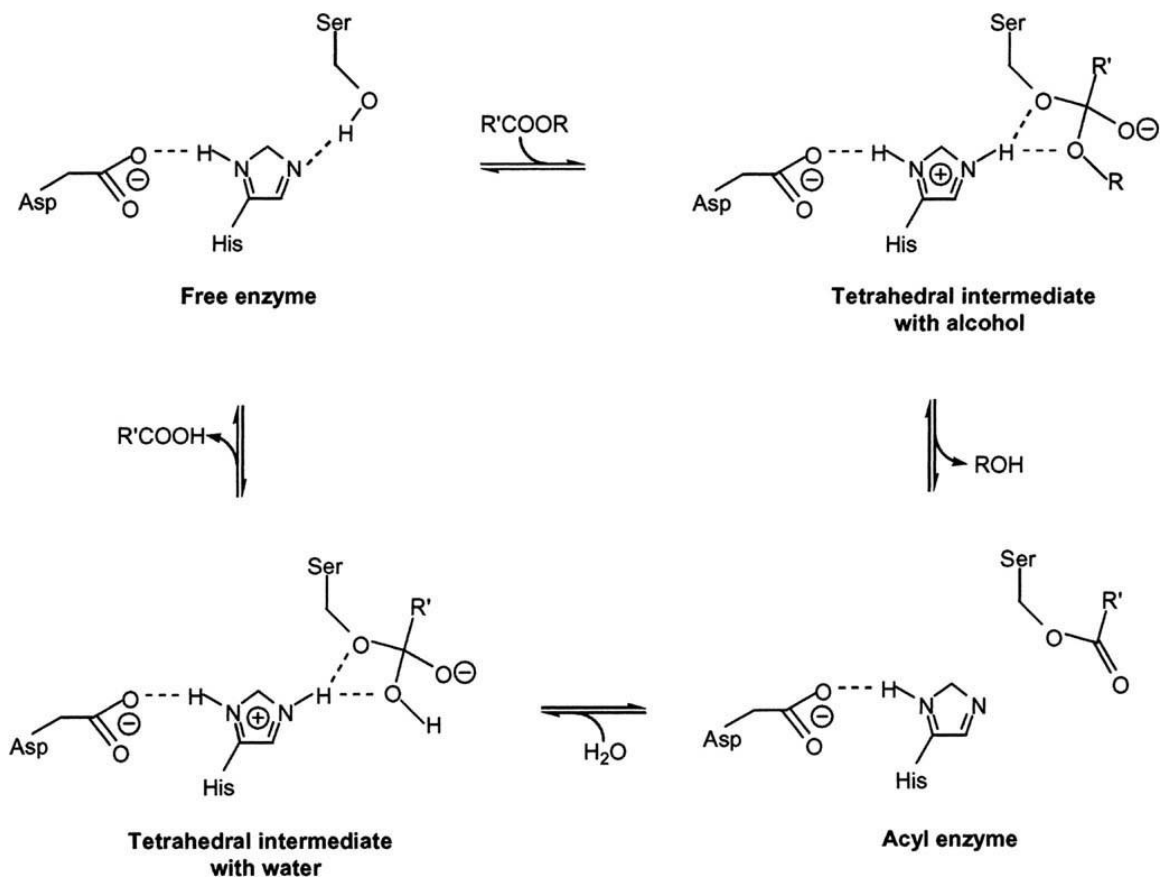


Figure 1-15 Three dimensional structure of *Candida antarctica* enzyme⁵⁷ (**Adopted from the reference with permission**)

Novozyme-435 (N435) is a commercially available immobilized lipase B from *C. antarctica* (CalB) that has been used as a catalyst for esterification reactions. Kazlauskas' rule explains that (*R*)-enantiomers of bulky substituents are more favourable for this enzyme compared to (*S*)-enantiomers. Furthermore, as the difference in the size increases, so does the selectivity between the two enantiomers.⁵⁹⁻⁶¹ Consequently, esterification, transesterification, and polymerization reactions using N435 as a catalyst (Scheme 1-5) are more stereo- and enantio-selective than traditional acid-catalyzed reactions.



Scheme 1-5 Esterification using N435 as a catalyst ⁶²(Adopted from the reference with permission)

The lipase's active site consists of histidine, serine, and aspartate amino acids as basic, nucleophilic, and basic units respectively (Figure 1-16). The enzymes' high stereoselectivity for secondary alcohols is the result of the active site binding pocket consisting of Thr42, Ser47, and Trp104.⁶³ One of the benefits of N435 is that it can be recovered, recycled, and be used repeatedly.⁶⁴ As can be seen in Scheme 1-5, the reaction between the enzyme and a carboxylic acid leads to a tetrahedral intermediate transition state that is stabilized by three hydrogen bond donors. The removal of water produces an acyl enzyme intermediate that can be attacked by an alcohol to produce the ester-like intermediate. Finally, the ester product is ejected and the catalyst is regenerated.

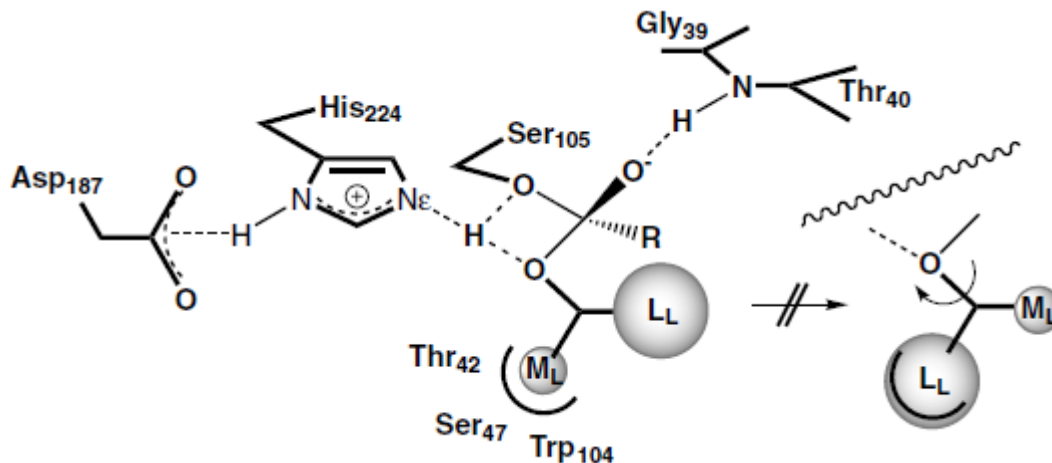


Figure 1-16 The active site amino acids of CalB.⁶³ (Adopted from the reference with permission)

1.5 Self-Healing Materials

Methods such as gluing, fusing and mending are often used to repair damaged surfaces caused by degradation and material failure.⁶⁵ Given the global reliance on polymer-based materials highly durable materials with extended life times are in high demand as the result of a desire to lower repair and maintenance costs. The concept of self-healing polymeric materials comes from the natural healing of cuts and wounds in human beings and other species.²²

Two general types of healing mechanisms exist: healing resulting from a chemical reaction or from sort of physical interaction. Self-healing materials ideally have the capacity to repair or heal themselves (automatically and autonomously) without any external stimulus. However, most synthetic materials are not capable of performing spontaneous repairs. Currently there is two types of self-healing processes: (1) autonomic, which occurs without any external stimulus; and (2) nonautonomic, which requires some

form of external activation.^{66,67} The self-healing of materials (e.g., polymers, coatings, concrete, *etc.*) can be categorized into two distinct processes as follows⁶⁸:

1. Healing through the release of a healing agent or agents
2. Healing via reversible cross-links

For the first strategy an active healing agent is incorporated into the polymeric product during its production. These active agents are typically liquids that are contained in microcapsules, channels, or fibers. After mechanical damage to the polymeric material the reactive liquids pour from their encapsulating structure into the crack and start the self-repairing process typically employing catalysts or hardeners to congeal and fix the crack. In other words, the fracture of the liquid-containing capsules is the driving force for the release of the active agents and commencement of the healing process (Figure 1-17). Unfortunately, this method of healing, which is categorized as autonomic self-healing because no external energy is involved in the healing process and crack closure, can typically only be utilized once per region of material; once the healing compounds are consumed no further healing is possible.^{69,70}

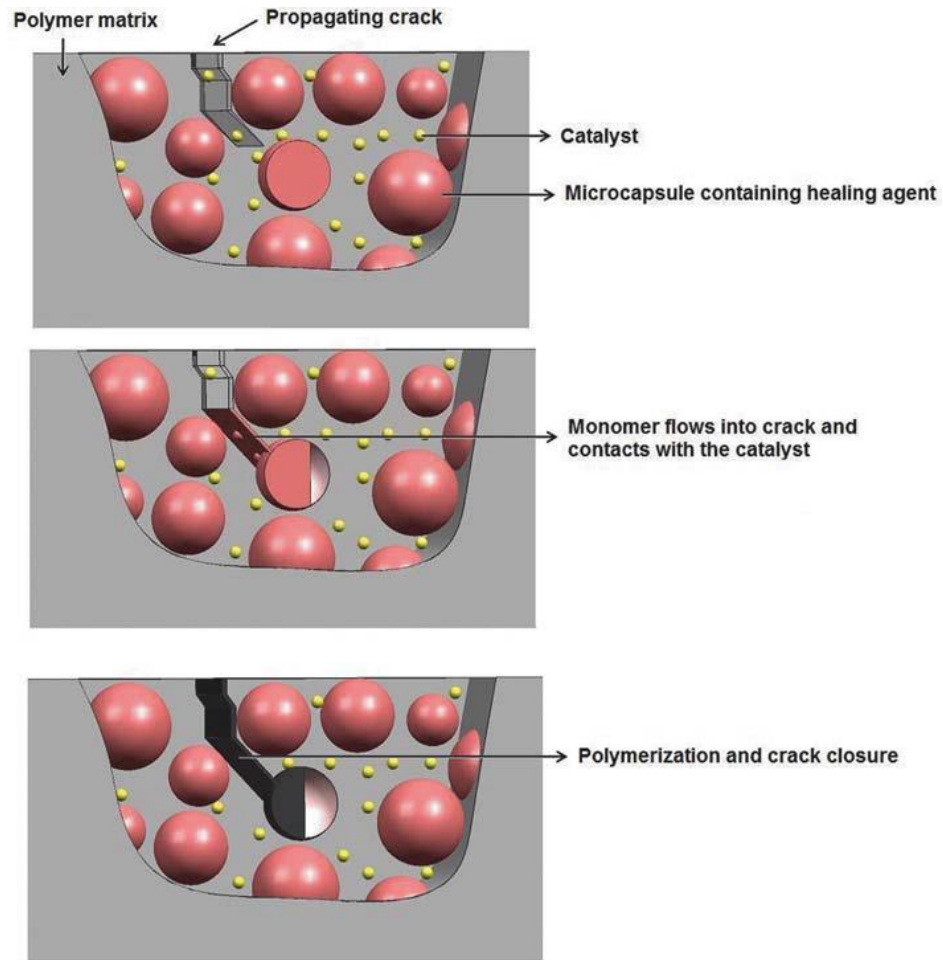


Figure 1-17 Autonomic healing of a polymeric material ⁶⁸(Adopted from the reference with permission)

1.5.1 Physical Principles of Self-Healing

Generally, self-healing is a process by which a material suffers some form of damage but which is subsequently repaired via the reconnection of broken polymer chains either through a chemical or physical interactions.^{71,72} The physical interactions usually occur from the interdiffusion and intermolecular interactions, which are highly dependent on the chemical nature of the polymer and the length of the polymer backbone. However, there are conflicting reports in the literature when it comes to this phenomenon; some reports claim that shorter polymeric chain lengths provide the higher chance of interdiffusion,

while others claim that longer chains produce a stronger entanglement of the polymer chains.⁷³⁻⁷⁴ An excellent summary for these phenomena is the Wool and O'Connor theory⁷⁵ that consist of a five-step process (Figure 1-18) that occurs at, or above, the glass transition temperature of the polymer. At its T_g a polymers is softened and flexible, facilitating the physical self-healing process.

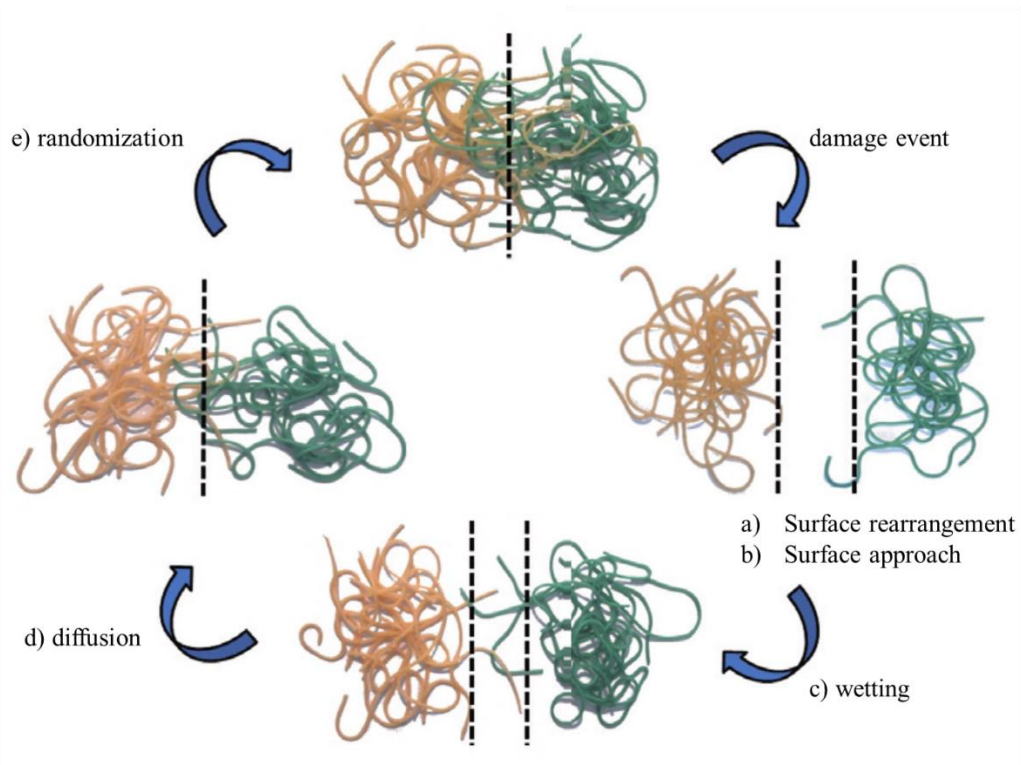


Figure 1-18. The Wool and O'Connor model for the physical self-healing of polymers⁶⁵ (**Adopted from the reference with permission**)

With this theory, since it is a physical process, efficient movement of the different polymeric compartments is the principal consideration in designing a proficient self-healing system. After damage occurred on the polymer's surface (Figure 1-18), surface rearrangement, surface approach, wetting, diffusion, and randomization are the events that must occur in order lead to a cured surface with roughly the same mechanical and physical properties (sometimes the quality lowers over time) as the virgin material. The first two

steps (surface rearrangement and surface approach) are both crucial steps that initiate self-healing process. In order to prevent contact failure of the two collapsed sides, a wetting step must occur in the polymer to provide sufficient mobility on the both sides of the injured area. The wetting process can be gained by either increasing the temperature (i.e., heating the polymer) or by adding solvent to the system.^{18,76} As long as the wetting step is done appropriately, diffusion should occur easily given the increased chain mobility of the polymer ultimately leading to increased contact between two parts of the damaged polymer. Lastly, a randomization step completes the self-healing process and fills the damaged area.

1.5.2 Chemical Principles of Self-Healing

Chemical self-healing is divided into two categories: one is established through covalent bonds that can be both reversible and irreversible processes, and the other is achieved through supramolecular network formation, which is a reversible process (Figure 1-19).⁷⁷

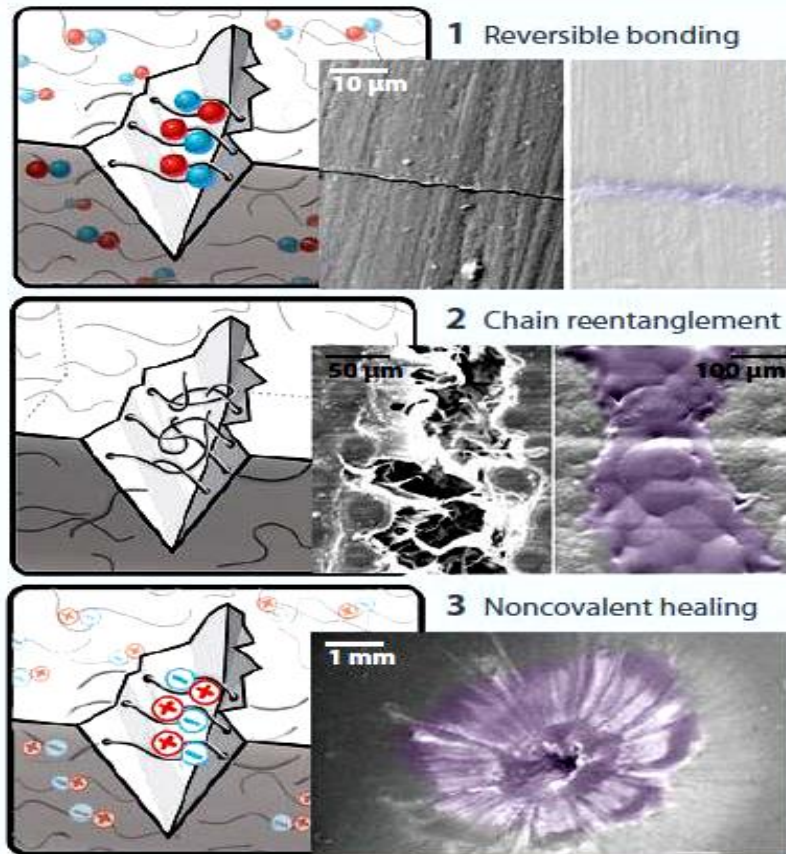


Figure 1-19 Different chemical self-healing processes: 1) covalent bond formation, 2) chain entanglement, and 3) supramolecular network formation ⁷⁷ (Adopted from the reference with permission)

1.5.2.1 Covalent Bond Network Formation

1.5.2.1.1 Irreversible Networks

In the irreversible healing process, one of the common methods involved in healing is encapsulation of active agents within the polymer matrix or the activation of catalysts *in situ* that leads to crack filling and ultimately healing. With this method once damage takes place, the encapsulated active agent releases and reacts with the catalyst at the damage site to produce new covalent bonds. Since this is a one-time process after one damage event occurs all of the active agents will be consumed. This network curing method is referred to as *irreversible covalent bond formation*. The examples of these

kinds of reactions include, but are not limited to ring-opening metathesis polymerization (ROMP), nucleophile addition to epoxides, and click reactions (Figure 1-20).

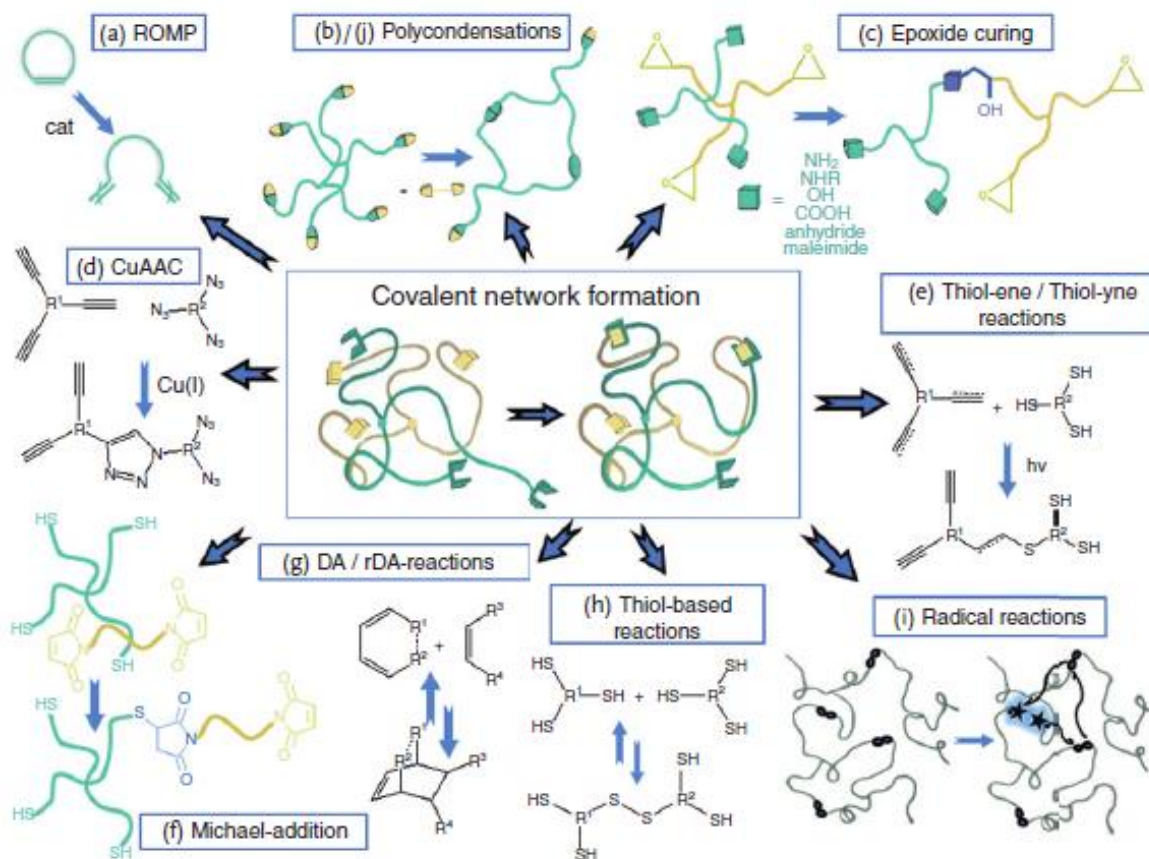


Figure 1-20 Examples of reversible and irreversible covalent bond network formation in self-healing polymers ⁶⁵ (Adopted from the reference with permission)

1.5.2.1.2 Reversible Networks

Various kinds of reactions produce new covalent bonds that can be applied to the field of self-healing polymer chemistry including: thiol/disulfide linkages, radical-based methods, polycondensation reactions, and Diels-Alder/retro-Diels-Alder (DA/retro-DA) cycloaddition reactions (Figure 1-20). The most widely used reversible covalent bond

system in self-healing studies has been the Diels-Alder reaction, which has the capacity to producing new C-C bond in high yields and with controlled stereochemistry (Section 1.6).⁶⁵

1.5.2.2 Supramolecular Network Formation

Supramolecular polymers are group of monomers connecting to each other through reversible and directional secondary interactions such as hydrogen bonding, ionomers, metal bonding, and π - π stacking interactions (Figure 1-21).⁷⁸

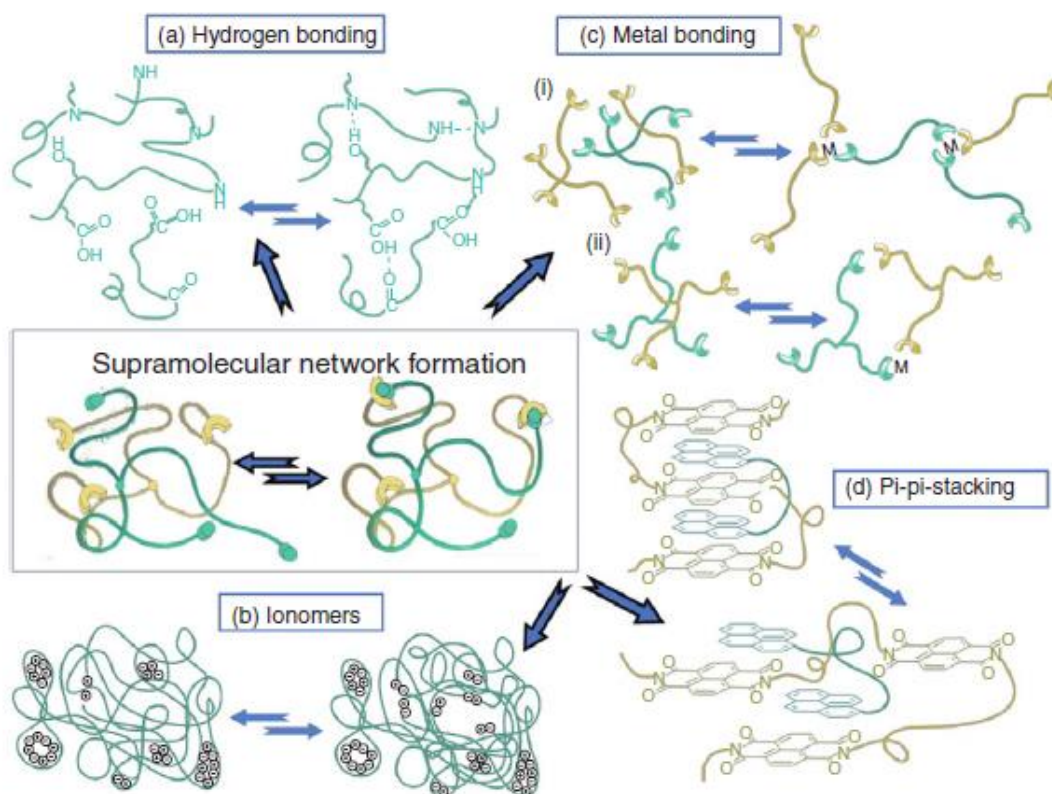


Figure 1-21 Reversible interactions to produce supramolecular polymer networks ⁶⁵(Adopted from the reference with permission)

The first supramolecular network based on hydrogen bonds was developed in 1997 by Meijer *et al.*⁷⁹ using 2-ureido-4[1H]-pyrimidinone (UPy) units capable of forming four

hydrogen bonds. The stability of these bonds and their associated lifetime is something to be considered in order to develop strong polymeric networks. In the specific case involving UPy, the hydrogen bonds are so strong that even after exposing the system to water, despite the competition between water molecules and monomer units to form hydrogen bonds, the connections between the polymer chains remained intact (Figure 1-22).

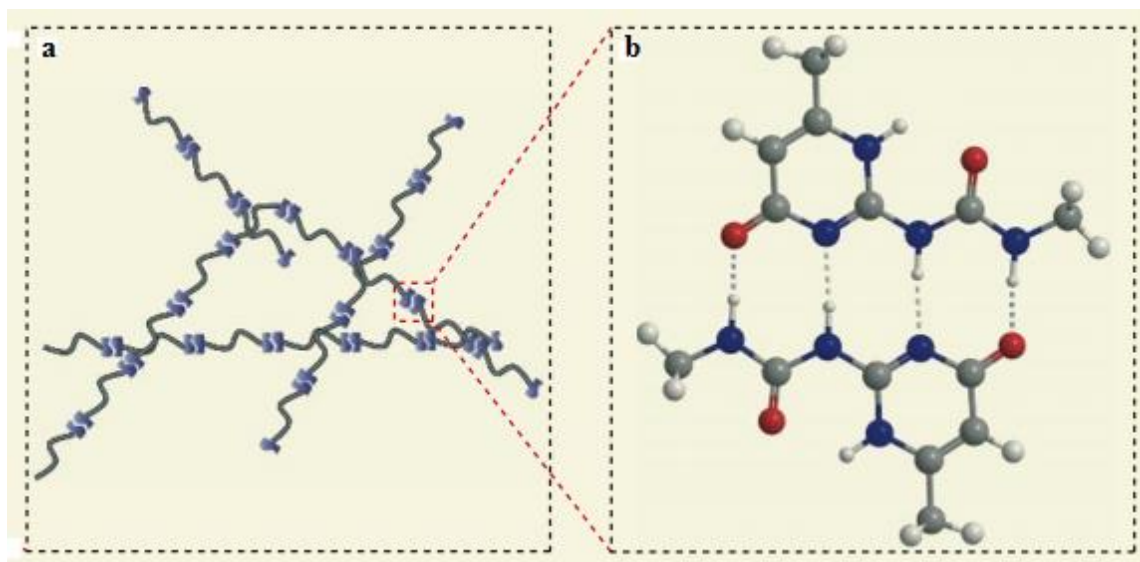
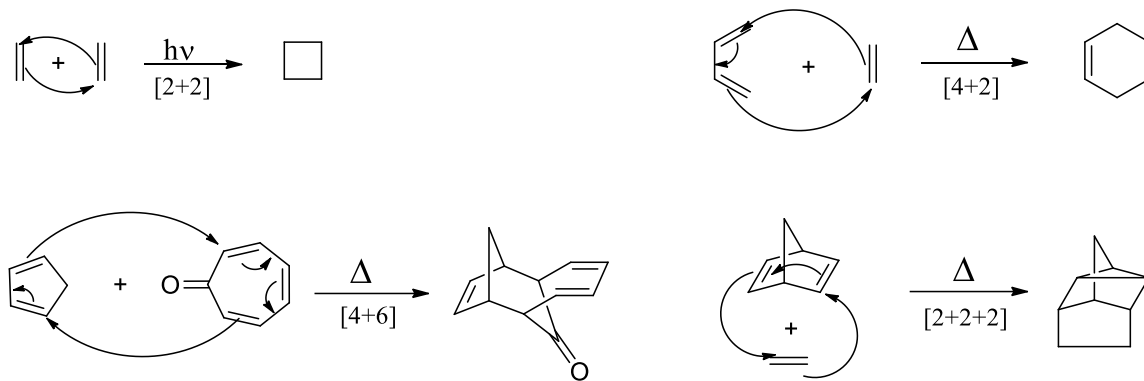


Figure 1-22 Hydrogen bonds between UPy units leading to polymeric networks ⁷⁸ (Adopted from the reference with permission)

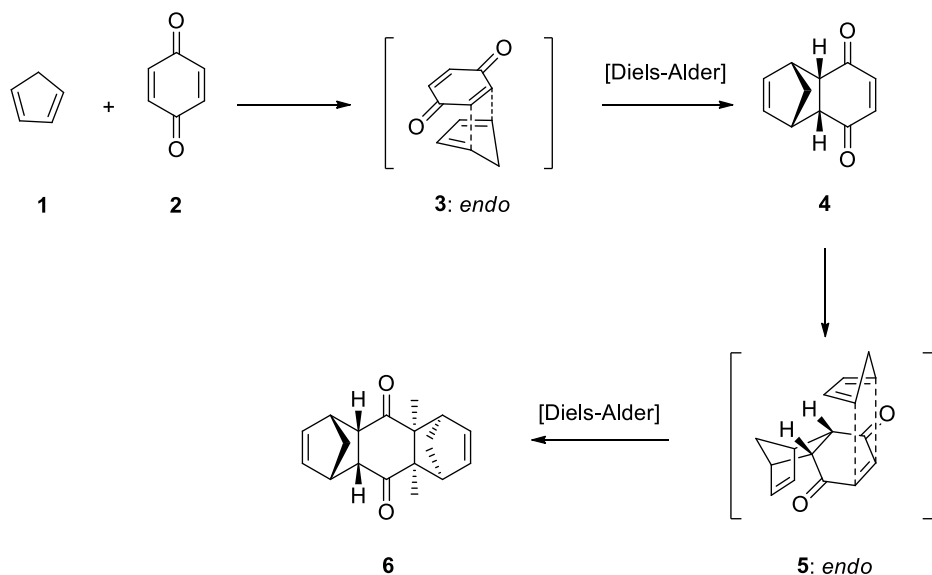
1.6 The Diels-Alder Reaction

Cycloaddition reactions are one group of chemical transformations that can be used for the self-healing and recycling of polymers. Cycloaddition reactions involve the formation of a new cyclic compound from two or more unsaturated starting materials and formation of a new C-C bond. These reactions usually take place under thermal or photochemical conditions with high stereoselectivity (Scheme 1-6).^{80,81}



Scheme 1-6. Examples of different cycloaddition reactions and their mechanisms ⁸²

The focus of this section is the reversible [4+2] cycloaddition known as the Diels-Alder (DA) reaction⁸³ that occurs between a 4-electron nucleophilic conjugated diene and a 2-electron electrophilic dienophile. The history of the DA reaction goes back to 1928 when Otto Diels and his student Kurt Alder reported the reaction of cyclopentadiene and quinone, ultimately leading to the development of a class of reactions that earned them the Noble Prize in Chemistry in 1950 (Scheme 1-7).⁸⁴



Scheme 1-7. The first reported DA reaction by Diels and Alder in 1928 ⁸⁴

1.6.1 Diels-Alder Reaction and Mechanism

The Diels-Alder reaction typically takes place between a diene and an alkene or alkyne (referred to as the dienophile) that not only produces two new σ bonds from a π bond, but that can also result in the creation of up to four new stereo-centers. Cycloaddition reactions can be described using frontier molecular orbital (FMO) theory, which was first introduced by Kenichi Fukui in 1952⁸⁵ and then extended by the Woodward-Hoffman rules in 1965.⁸⁶⁻⁸⁸ According to FMO theory, if the molecular orbitals (MO) symmetry of the reactant is the same as the MOs of product in the ground state, the reaction is feasible thermally, but if reactant MO is the same as the MO of the first excited state of the product, then the reaction is photochemically allowed. And if the MO symmetry of the reactant and product are different, the cycloaddition reaction will not occur in a concerted manner. As a result, the highest occupied molecular orbital (HOMO) of one component and the lowest unoccupied molecular orbital (LUMO) of the other component, should be examined to consider the symmetry and feasibility of the cycloaddition reaction (Figure 1-23).^{82,89}

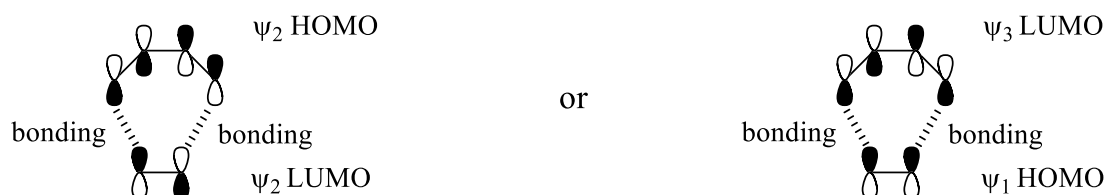


Figure 1-23. Frontier molecular orbitals of the reactants in a Diels-Alder Reaction⁹⁰

The $[\pi_4 + \pi_2]$ cycloaddition occurs via a disrotatory mechanism in order to produce two new σ bonds from two π bonds in a concerted fashion (Figure 1-24).^{91,92}

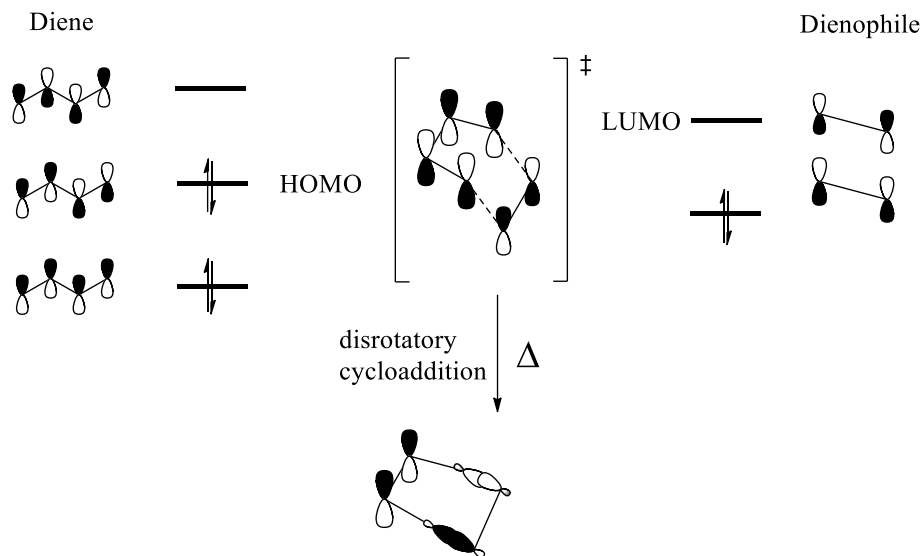


Figure 1-24. Disrotatory mechanism to obtain two new σ bonds in a Diels-Alder reaction ⁹¹

Conrotatory (both sets of orbitals rotate clockwise or both rotate counter clockwise) and disrotatory (one set of orbitals rotates clockwise and the other rotates counter clockwise) processes consist of rotation of frontier molecular orbitals in order to achieve optimal overlap of orbital lobes.⁹⁰

The formation of new σ bond occurs only if the p orbitals of the terminal carbons of the two reactants can overlap with each other properly. This can take place through two mechanisms: (1) suprafacial or (2) antarafacial attack.⁹³ With a suprafacial interaction the same faces of the p orbitals of the π system overlap and in an antarafacial, attack occurs from opposite side (180° twist) of the p orbitals of the π system (Figure 1-25).⁸⁹

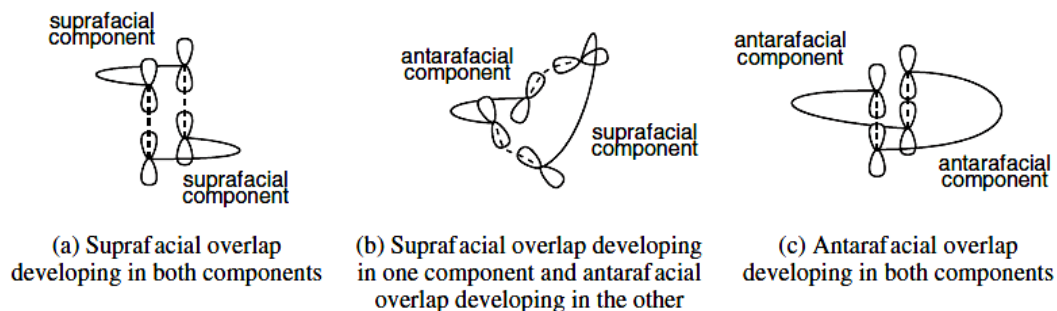


Figure 1-25. Suprafacial and antarafacial interactions of p orbitals to form new σ bond in the Diels-Alder reaction ⁸⁹ (Adopted from the reference with permission)

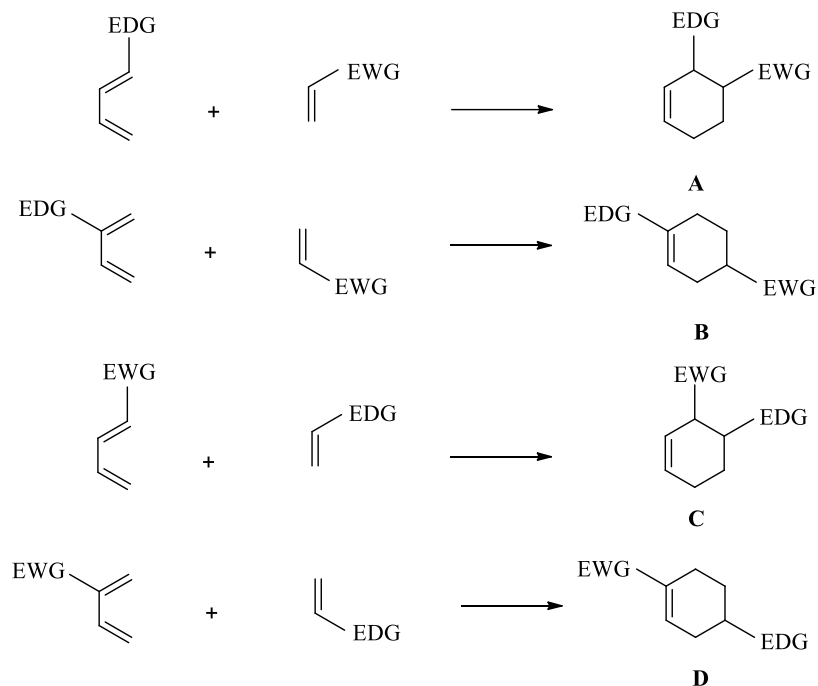
Cycloaddition reactions yielding four to six membered rings should go through suprafacial-suprafacial transition state due to the ring strain.⁵⁶

1.6.2 Classification of Diels-Alder Reactions

The Diels-Alder reaction can be categorized in two different ways: (i) according to the reactants - they can be classified into two groups either as (a) homo-Diels-Alder reaction in which the reactants consist of only hydrocarbon moieties, and (b) hetero-Diels-Alder reactions in which the reactants, either diene or dienophile, possess one or more heteroatoms to produce heterocycles;⁹⁴ (ii) considering the presence of electron withdrawing and electron donating groups on the reactants and their influence on the reaction rate in agreement with Woodward-Hoffman rules. This second category can be divided into three distinct classes:⁹⁵

1. The normal demand Diels-Alder reaction
2. The inverse demand Diels-Alder reaction
3. The neutral Diels-Alder reaction

The reaction rate for the Diels-Alder reaction is related to the energy gap between the HOMO and LUMO orbitals of the diene and dienophile. The lower the gap, the more efficient the orbital overlap and the higher reaction rate. In the normal demand DA reaction, electron donating groups on the diene will increase the energy of the HOMO orbitals and electron withdrawing groups on the dienophile will decrease the energy of LUMO orbitals of dienophile, ultimately resulting in a lower energy gap ($\text{HOMO}_{\text{diene}}\text{-LUMO}_{\text{dienophile}}$) and acceleration of the reaction rate. On the other hand, a similar observation is made for the inverse demand DA reaction ($\text{LUMO}_{\text{diene}}\text{-HOMO}_{\text{dienophile}}$) that also leads to reduction of the energy gap and higher reaction rates. For the neutral DA reaction, the difference between the energy gap of $\text{HOMO}_{\text{diene}}\text{-LUMO}_{\text{dienophile}}$ and $\text{LUMO}_{\text{diene}}\text{-HOMO}_{\text{dienophile}}$ is not considerable. Therefore, both electron withdrawing and electron demanding groups can be presented on the diene and dienophile.⁹⁶⁻⁹⁸ The normal demand DA reaction (A and B adducts) and the inverse demand DA reaction (C and D adducts) have been illustrated in Scheme 1-8.⁹⁹



Scheme 1-8. Regioselectivity in normal and inverse demand DA reactions ⁹⁹

For all of the different DA reactions, the symmetry of the molecular orbitals of the reactant and product should be the same. This phenomenon is known as the conservation of orbital symmetry and leads to a more stable transition state resulting in a concerted cycloaddition reaction (i.e., in accordance with the Woodward-Hoffmann rule).^{91,100} Molecular orbitals and the bonding interactions of the simplest DA reaction between butadiene and ethylene are shown in Figure 1-26, followed by an illustration of the frontier orbital interactions for different electronic demands in Figure 1-27.

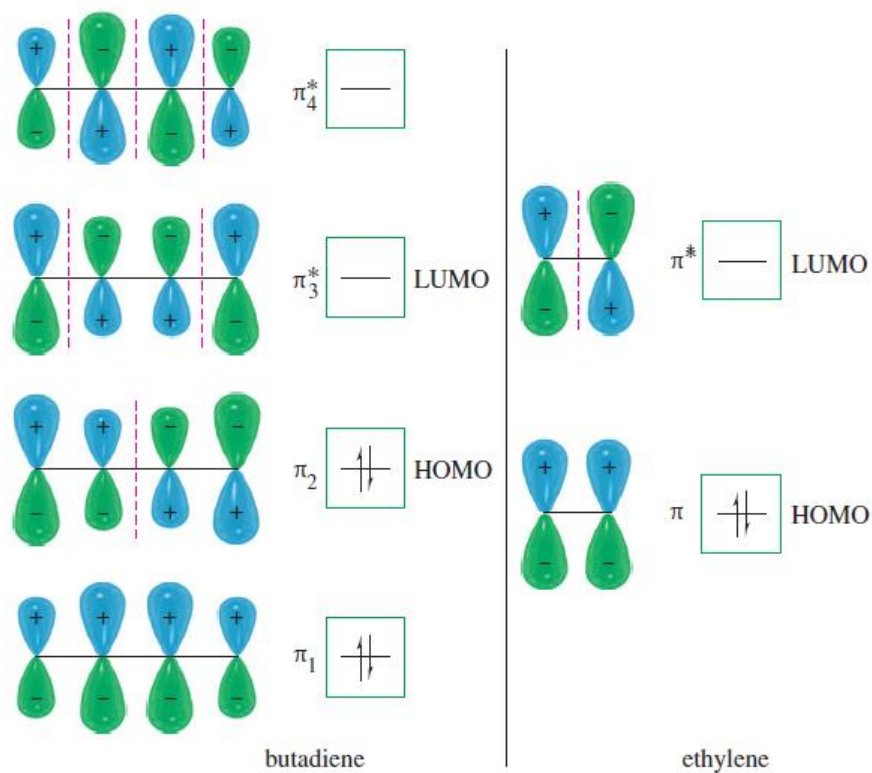


Figure 1-26 Molecular orbital and bonding interactions between butadiene and ethylene in the DA cycloaddition reaction ⁵⁵ (Adopted from the reference with permission)

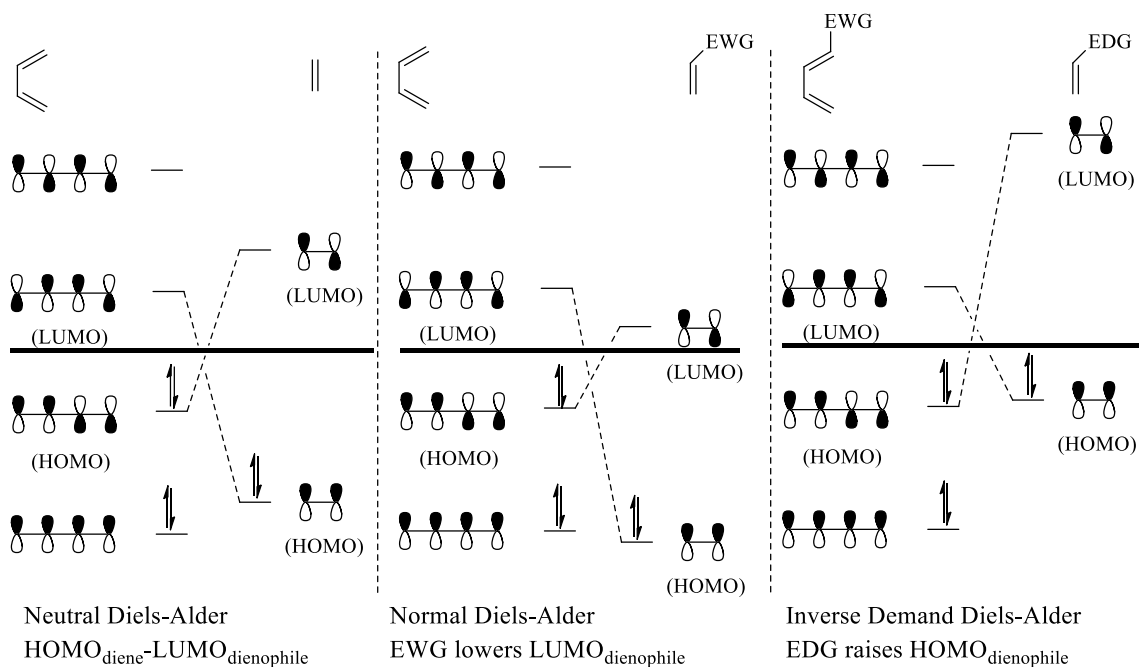
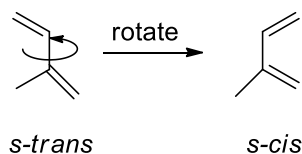


Figure 1-27. Frontier molecular orbital interactions for different categories of DA reactions

Dienes in Diels-Alder Reactions

Dienes in the Diels-Alder reaction can be both cyclic and acyclic with various kinds of substitutions. Conjugated dienes can exist in two conformations: *s-cis* or *s-trans*. As a result of the steric hindrance imparted by the hydrogen atoms on terminal carbons the *s-cis* conformation is less stable. Thus, it is capable of participation in the DA reaction. However, a rotation about the C-C single bond can activate *s-trans* conformer for this reaction (Scheme 1-9).^{56,101}



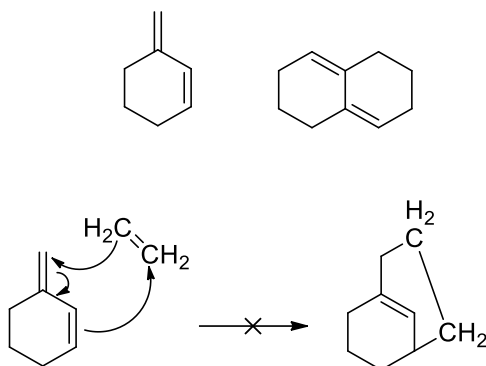
Scheme 1-9. The *s-cis* and *s-trans* conformation of conjugated dienes.

The electronic properties of substituents on the diene and dienophile influence the rate of the DA reaction (Table 1-2). Generally, cyclic dienes are more reactive than open-chain ones.¹⁰²

Table 1-2. Different types of dienes¹⁰²

Open-Chain	Outer Ring	Inner-Outer	Across Ring	Inner Ring

For the locked *s-trans* conformers that cannot undergo a C-C rotation, such as those involving cyclic system, participating as diene in a DA reaction is not possible (Scheme 1-10).⁵⁵



Scheme 1-10. Locked *s-trans* conformations

1.6.3 Dienophiles in Diels-Alder Reactions

Dienophiles are compounds containing double or triple bonds. Since dienes behave like nucleophiles (electron-rich compounds) and dienophiles as electrophiles (electron-deficient compounds) in DA reactions, electron-withdrawing groups on dienophiles can make them better electrophiles by removing electron density from C-C double/triple bond, which leads to more reactive compounds (Table 1-3).^{56,103}

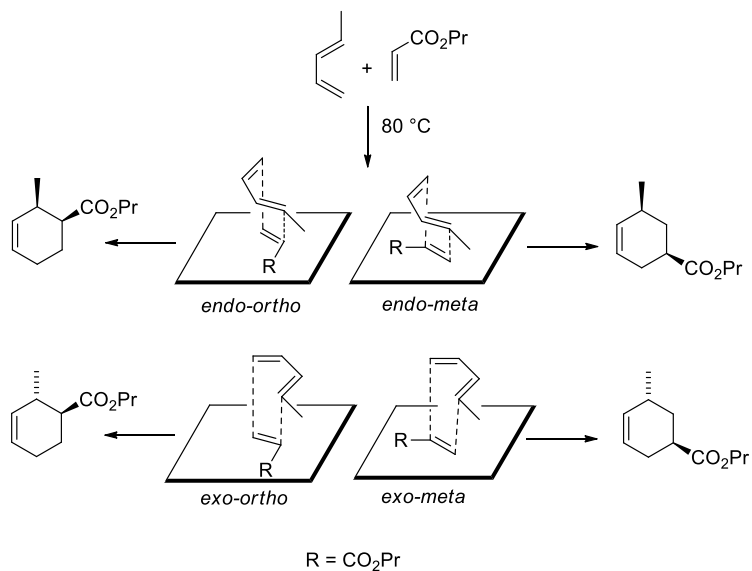
In the DA reaction the stereochemistry of the dienophile is preserved. In other words, a *cis* cyclic adduct will be obtained from a *cis* dienophile and a *trans* dienophile produces a *trans* cyclic adduct.

Table 1-3. Examples of common dienophiles⁵⁶

Acyclic			Cyclic		
$(\text{NC})_2=\text{(CN)}_2$	$\text{MeO}_2\text{CHC}=\text{CHCO}_2\text{Me}$				
	$\text{HC}\equiv\text{CO}_2\text{Me}$				
$\text{CMe}_2=\text{S}$	$\text{Ph}-\text{N}=\text{O}$	$\text{NAr}=\text{NCN}$			
$\text{O}=\text{O}$	$\text{S}=\text{S}$				

1.6.4 Stereochemistry of the Diels-Alder Reaction

The Diels-Alder cycloaddition reaction is capable of producing up to four chiral centers. These chiral centers can be predicted by the suprafacial *endo* and *exo* interactions of the reaction components. For the *endo* transition state, the reactants interact with each other from the most sterically congested position (Alder rule) to produce adducts (Scheme 1-11).^{104,105}



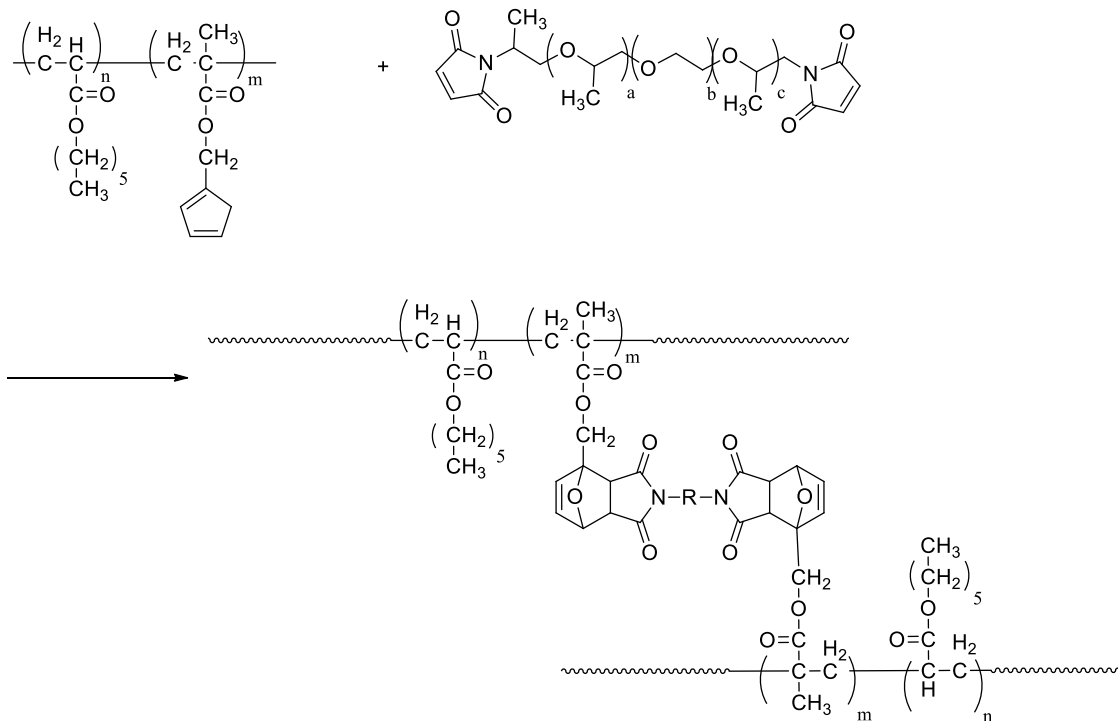
Scheme 1-11. The endo and exo orientations possible in a Diels-Alder reaction¹⁰⁶

The *endo* adduct is the major product as the transition state involves an interaction between the diene and dienophile in such a way that the unsaturated substituent on the dienophile overlaps with the π system of the diene.¹⁰⁷⁻¹⁰⁸

1.6.5 The Diels-Alder Reaction and Polymer Chemistry

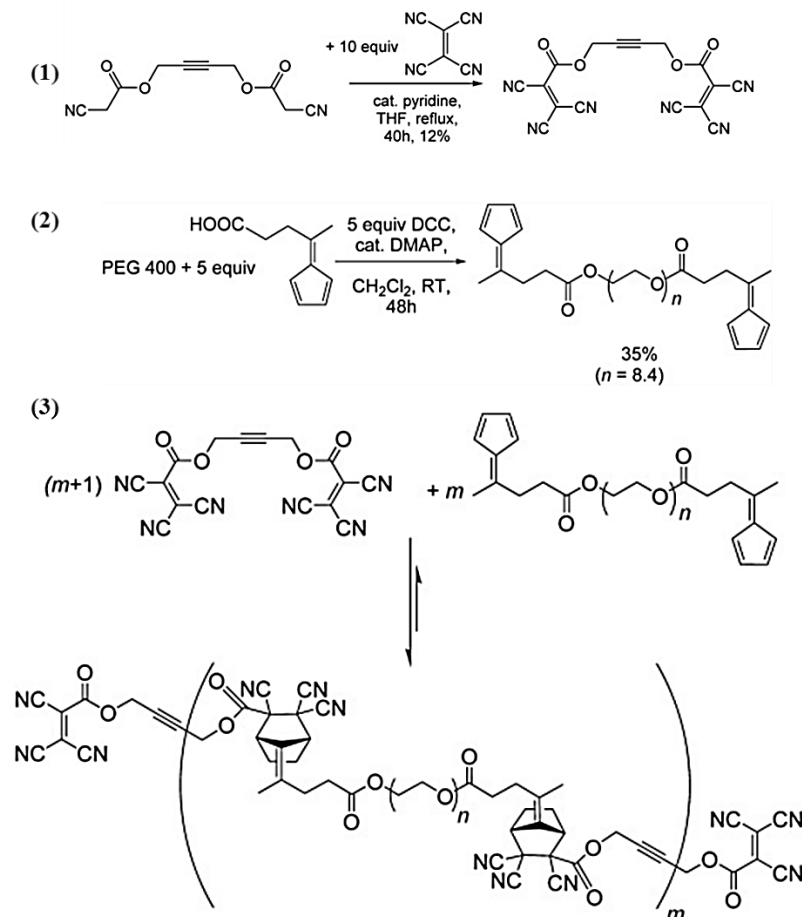
In the past few years, the use of DA reaction in the field of polymer chemistry for self-healing and cross-linking purposes has been increased due to the reaction's thermal and mechanical reversibility and high yields. This thermal reversibility can be used to produce reactive sites *in situ*.¹⁰⁹ Various numbers of these mendable polymeric materials using diene-dienophile systems especially furan-maleimide moieties have been used that are capable of retro DA reaction.¹¹⁰

Among different DA reactants (dienes & dienophiles) furan and maleimide units have garnered attention in polymer chemistry with organic backbone as result of their capacity to reaction at relatively low temperatures (25-70 °C), and the retro DA reaction temperature for these reactants is around 90-110 °C. Thus, the accessible thermally reversible nature of these particular units makes their DA adducts attractive for use in smart, responsive materials under mild condition.^{111,112} Moreover, flexibility of the polymer chains is one of the features that has always been sought for in elastomers to improve the self-healing process. In 2002, Gandini *et. al.*¹¹³ produced low-T_g elastomers using polymeric dienes cross-linked with bismaleimides (Scheme 1-12).



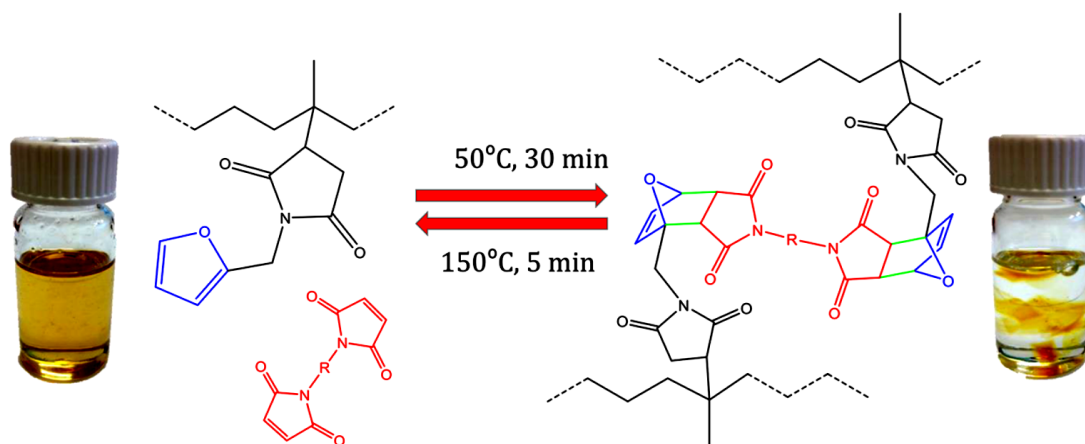
Scheme 1-12. Polymeric dienes using bismaleimides as a cross-linking agent ¹¹⁴

Lehn group in 2009,¹¹⁵ produced dynamers with organic backbone using reversible DA reaction that can be done at room temperature. These synthesized long and highly flexible chains from bis(diene) and bis(dienophile) are capable of self-healing in few minutes at room temperature and produce thin film elastomers that have T_g lower than room temperature that will prevent crystallization of the polymer (Scheme 1-13).



Scheme 1-13 Synthesis of (1) bis(dienophile), (2) bis(diene) and (3) long flexible chain by Lehn group ¹¹⁵
(Adapted from the reference with permission)

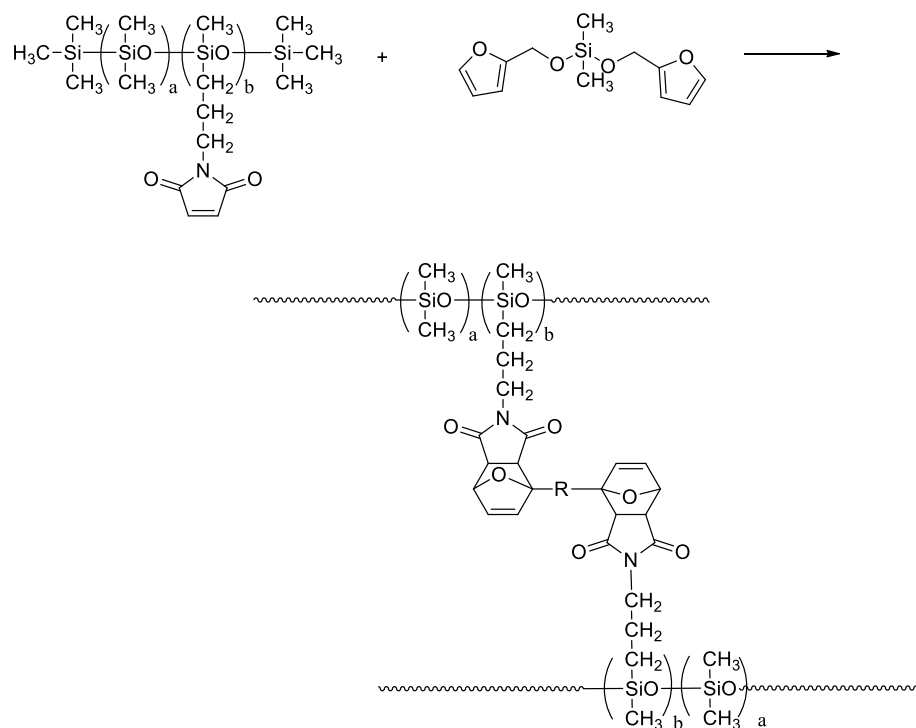
Research reported by Picchioni *et. al.* in 2015 involved the production of a reversible rubber system. In this report commercially available ethylene-propylene rubber was modified with maleic anhydride and then reacted with furfurylamine to form a polymer possessing furan moieties that was subsequently cross-linked with a bismaleimide (dienophile moiety) to produce reversible rubbers (Scheme 1-14).¹¹⁶ In this research, DA reaction occurs at 50 °C -70 °C, whereas rDA is occurring at more than 150 °C.



Scheme 1-14 The rubber product synthesised by Picchioni *et. al.* using a thermoreversible DA reaction ¹¹⁶
(Adapted from the reference with permission)

1.7 Silicones and the Diels-Alder Reaction

One of the earliest examples the DA reaction being applied to silicone chemistry by Gandini *et. al.* in 2002¹¹⁴ involved the use of polymeric dienophiles (synthesized from siloxane copolymers containing pendant propylamine chains) cross-linked to bisfurans (Scheme 1-15) to produce reversible rubbers, especially for tire manufactures to reduce the number of damaged tires.¹¹⁴ It has been indicated in this study that copolymers with lower maleimide units are completely soluble and failed to produce a healable network due to the lack of intermolecular coupling. However, using copolymers with richer reactive moieties were good enough to produce anticipated gel (network).



Scheme 1-15. Polymeric dienophiles using a bisfuran as a cross-linking agent ¹¹⁴

Recently, Kickelbick *et al.*¹¹⁷ in 2015 studied different polysiloxane chains of various molecular weights that were modified with furan and maleimide moieties to increase the flexibility of the resultant elastomers and were able to improve the self-healing properties of these elastomer (Figure 1-28).¹¹⁷ The strength of this study is comparing the flexibility of the synthesized networks (using furan and maleimide) from cross-linking of the nanoparticles with (a) poly(butylmethacrylates) and (b) polysiloxanes. The study shows that rigid thermoplasts (a) undergo less cross-linking reactions compared to modified polysiloxanes (b) that are thermally reversible cross-linked. Thus, polysiloxanes extend the mobility and flexibility of the polymer backbone.

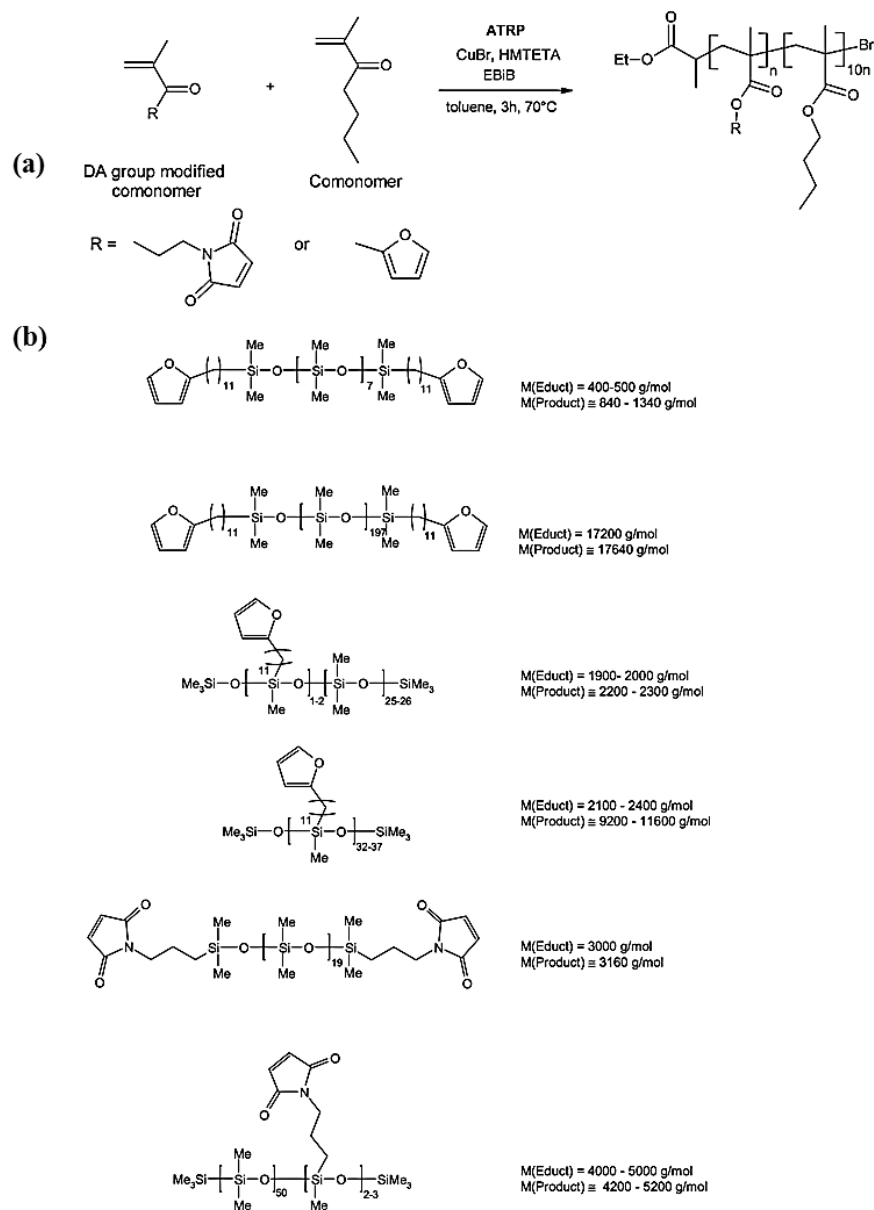
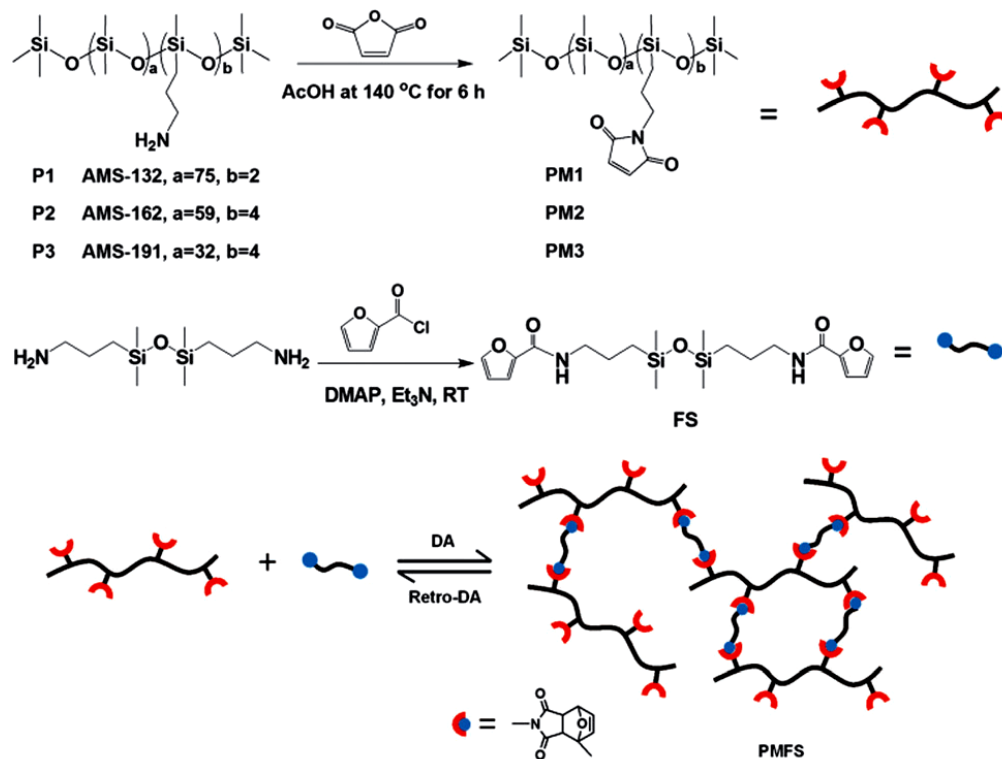


Figure 1-28. (a) Poly(butylmethacrylates) and (b) Polysiloxanes modified with furan and maleimide moieties synthesized by Kikelbick *et al.*¹¹⁷ (Adapted from the reference with permission)

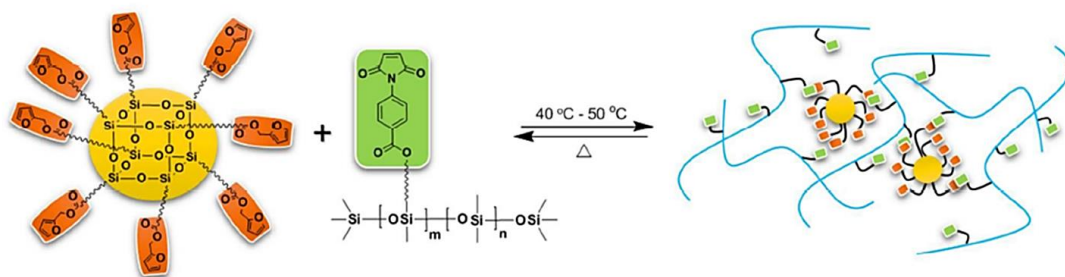
In 2016, Xia *et al.*¹¹³ reported research on polydimethylsiloxane chains including maleimide fragments cross-linked by bisfuran compounds to form healable PDMS elastomers that have potential applications in the biomedical field as artificial skin and tissue engineering scaffolds (Scheme 1-16). In this specific DA reaction the N-H groups

on the furan chain provided hydrogen bonding with the C=O group on the maleimide, which led to better reconnection (healability) after damage occurred.



Scheme 1-16 Healable elastomers PDMS elastomers synthesized by Xia et al.¹¹³ (Adapted from the reference with permission)

Most recently in Zelisko's lab (2017),¹¹⁸ temperature-controlled self-healing elastomers have been synthesized using siloxane chain grafted with maleimide moiety and polyhedral oligomeric silsesquioxane (POSS) modified with furan active groups. The thermally reversible DA reaction between these two diene and dienophile polymeric systems led to cross-linking networks capable of recyclability.



Scheme 1-17 Temperature-controlled self-healing elastomers synthesized from siloxane chain grafted with maleimide moiety and POSS ¹¹⁸

To conclude, according to previous studies that some of them were mentioned in this section, changing the diene and dienophile structures attached to the different PDMS with variable average molecular weight can lead to production of elastomers with different mechanical properties. Moreover, using various diene and dienophile systems can be effective on cross-linking density and self-healing temperature to afford higher quality elastomers.

1.8 Polymers and the Environment

In the beginning of 19th century, production of rubber and then plastic materials expanded rapidly. The waste disposal of these kinds of modern polymeric materials with the ancient methods were impossible since the plastics are non-biodegradable.¹¹⁹ The marine conservation society in 2008 found that over 50% of the litter is plastic, consisting of 7393 plastic bags, 7025 pieces of plastic trays and cups and 16243 plastic drinks bottles which is 77% more than plastic waste in 1994. Burning the plastics in the open air leads to spreading the poisonous chemicals and harmful greenhouse gases such as CO₂ and methane that causes global warming and effects on livings health as well. As a result, discovering the recycling and recovery methods have become an interesting and necessary topic to be achieved. The use of plastics in the twentieth century rose dramatically especially in the

packaging (30% of all synthetic polymers) due to the plastics light weight, transparency, flexibility and low cost.¹²⁰ In regards with the applications of plastics and their properties, environmentalists' priority is to recycle and reuse these materials after their service life which is both economically and environmentally advantageous because it takes two-third less energy to use recycled plastics at the first step of material production other than using the virgin plastics.¹²¹ Because of the high usage and applications of polymers in different aspects of modern human lifestyle, it cannot be expected to decrease or eliminate the usage of these materials. Yet, it is required to recycle these building blocks to prevent the misuse of these polymeric compounds.

1.9 Hypothesis and Thesis Objectives

Pollution by polymers is a growing concern, especially because of the disposable nature of many polymers; this issue could be addressed by developing methodologies for prolonging lifetimes of polymers, especially for ones as ubiquitous as silicones. Although there have been reports of self-healing silicone systems based on the Diels-Alder reaction, the systems are rather limited, especially as it pertains to low temperature (>50°C) self-healing phenomena. Given the existing data involving self-healing polymers and the Diels-Alder reaction,^{112,113,116,117} it is hypothesized that it is possible to synthesize a silicone elastomeric system that has the capacity to self-heal at room temperature, and ultimately to be recycled. The combination of various siloxane-based maleimide and furan systems in the synthesis of silicone elastomers will be explored to confirm or refute this hypothesis.

Chapter 2: Results and Discussion

In this section the cross-linking, self-healing, and recyclability of silicone elastomers will be examined and discussed. The characterization and analysis of model compounds was then extended to polymeric systems in the form of elastomers.

2.1 The Model Systems

In order to synthesize a library of model compounds, two different dienes and six different dienophiles were used to investigate Diels-Alder (DA) and retro Diels-Alder (rDA) reactions involving these compounds. The studies involving the model compounds were designed to establish the optimal temperatures for DA/rDA reactions to afford the highest adduct yield, so that these conditions could then be extended to polymeric siloxane systems. The procedures contained in this section are thoroughly outlined in Chapter 1.

Both of the diene systems were synthesized through a two-step reaction that is illustrated in Scheme 2-1¹²² and Scheme 2-2.¹¹⁷ All of the bisdienophiles (Figure 2-1) used in these studies (**14**, **15**, **16**, **17**, **18**), were commercially available except for **13**, which was obtained from a two-step reaction (Scheme 2-3).¹²³

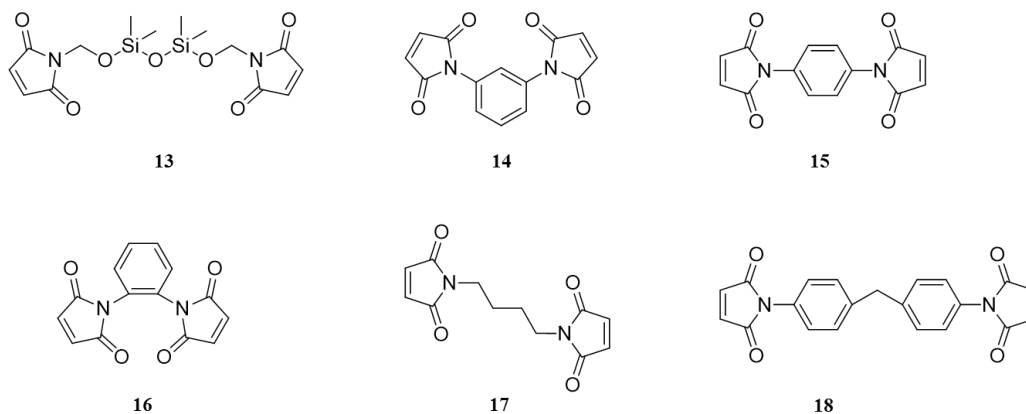
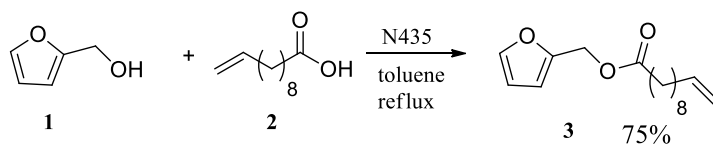
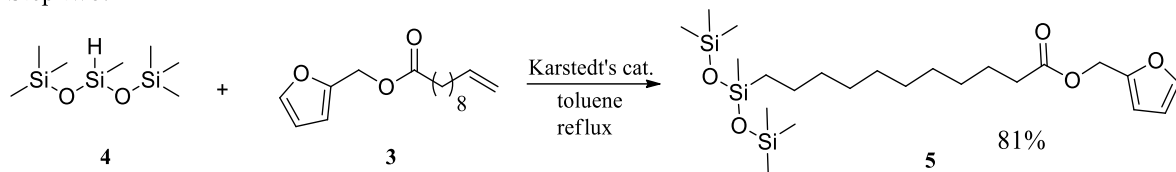


Figure 2-1 Different bismaleimides

Step one:



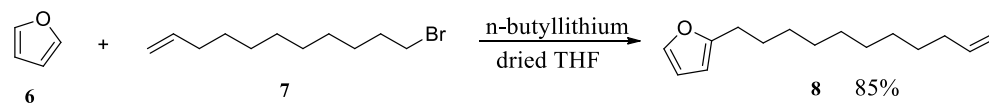
Step two:



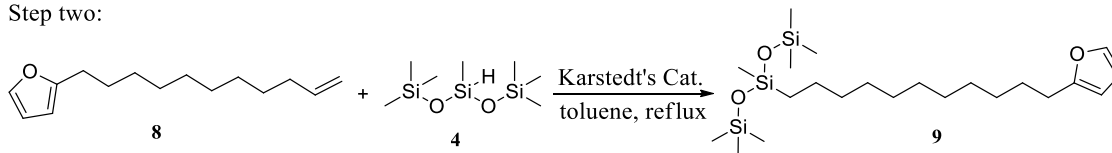
Scheme 2-1 The chemoenzymatic synthesis of model furan-modified trisiloxane (diene) 5

Synthesizing one of the model diene systems (5) as was mentioned before, was done in a two-step reaction. In the first step, chemoenzymatic esterification was done to produce compound 3 with 75% yield followed by a hydrosilylation reaction in the presence of Karstedt's catalyst to obtain compound 5 in 81% yield.

Step one:

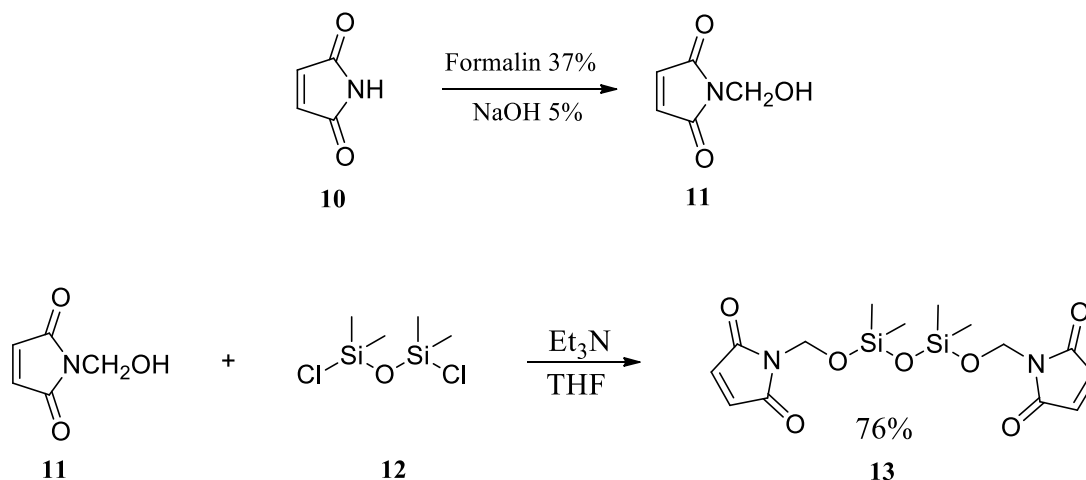


Step two:



Scheme 2-2 Synthesis of the model furan-modified trisiloxane (diene) 9.

Compound 6 was treated with n-butyllithium to yield a furanyl-2-lithium. The furanyl-2-lithium subsequently performed a nucleophilic substitution on 7 to afford 8 in an 85% yield.

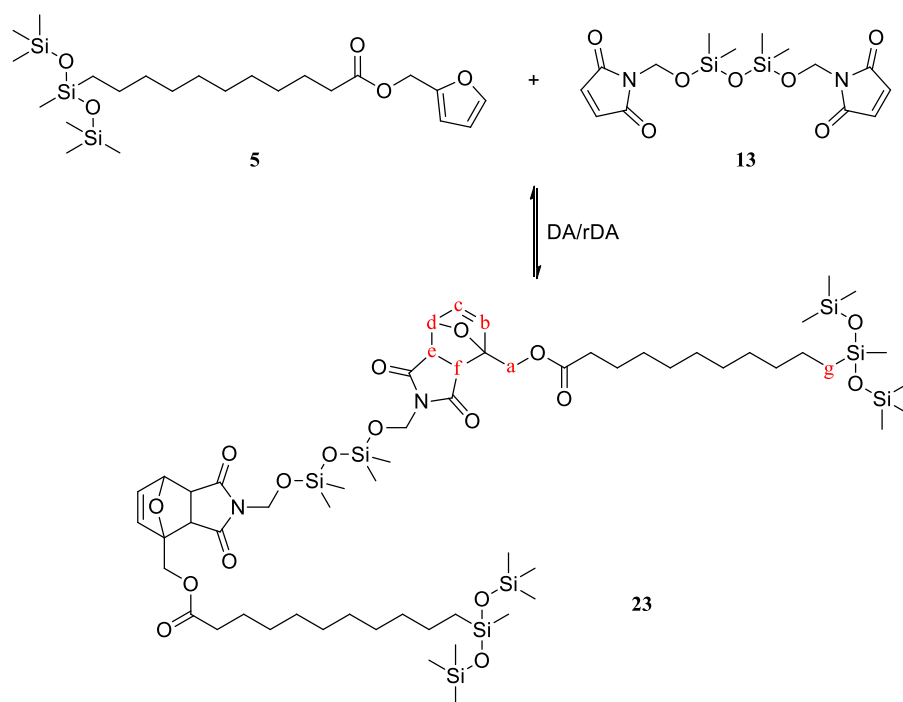


Scheme 2-3 Synthesis of dienophile **13**¹²³

Overall 12 different model DA reactions were investigated in this study. For every Diels-Alder reaction, equimolar amounts of the diene and dienophile were reacted in the absence of solvent at temperatures ranging from 40 °C to 80 °C to optimize maleimide conversion (Table 2-1, Table 2-2, Table 2-3) Since the chemical transformation in all of these reactions is the same, the discussion will focus on the reaction between **5** and **13** (Scheme 2-4), but can easily be extrapolated to the other Diels-Alder reactions involving the model compounds.

The disappearance of bismaleimide alkene resonance at 5.2 ppm in the ¹H NMR (Figure 2-2) confirmed the consumption of the maleimide ring. Moreover, the two doublets corresponding to the alkene protons of the newly synthesized cyclohexene ring (Scheme 2-4, Figure 2-2) were observed at 6.41 and 6.44 ppm indicating the successful formation of the Diels-Alder adduct. The bridgehead proton of the adduct was assigned to the resonance at 5.35 ppm. The most shielded protons (0.41-0.46 ppm) were used as reference protons to calculate the *exo* and *endo* adducts ratios (Figure 2-2). Furthermore, a

gCOSY NMR spectrum (Figure 2-3) was acquired to confirm that the resonances at 3.02-3.04 and 3.40-3.71 ppm corresponded to the *exo* and *endo* adducts, respectively. Owing to $\sim 90^\circ$ dihedral angle between proton d and the *exo* proton e (Scheme 2-4), the correlation between these two protons are not observable in the gCOSY NMR spectrum. As a result, the protons were assigned as follows: 3.02 (e-*exo*), 3.04 (f-*exo*), 3.41 (e-*endo*), 3.69 (f-*endo*) (Figure 2-2).



Scheme 2-4 The model Diels-Alder reaction between compounds **5** and **13**

All of the model adducts that were synthesized, and the corresponding starting materials are summarized in Table 2-2. Reactions number 1-6 occurred between model ester furan **5** and six unique bismaleimide compounds while reactions 7-12 involved an aliphatic furan and the same bismaleimides compounds used for reactions 1-6. So, from now on bismaleimides will be named as number 13 to 18 for the ease of labeling.

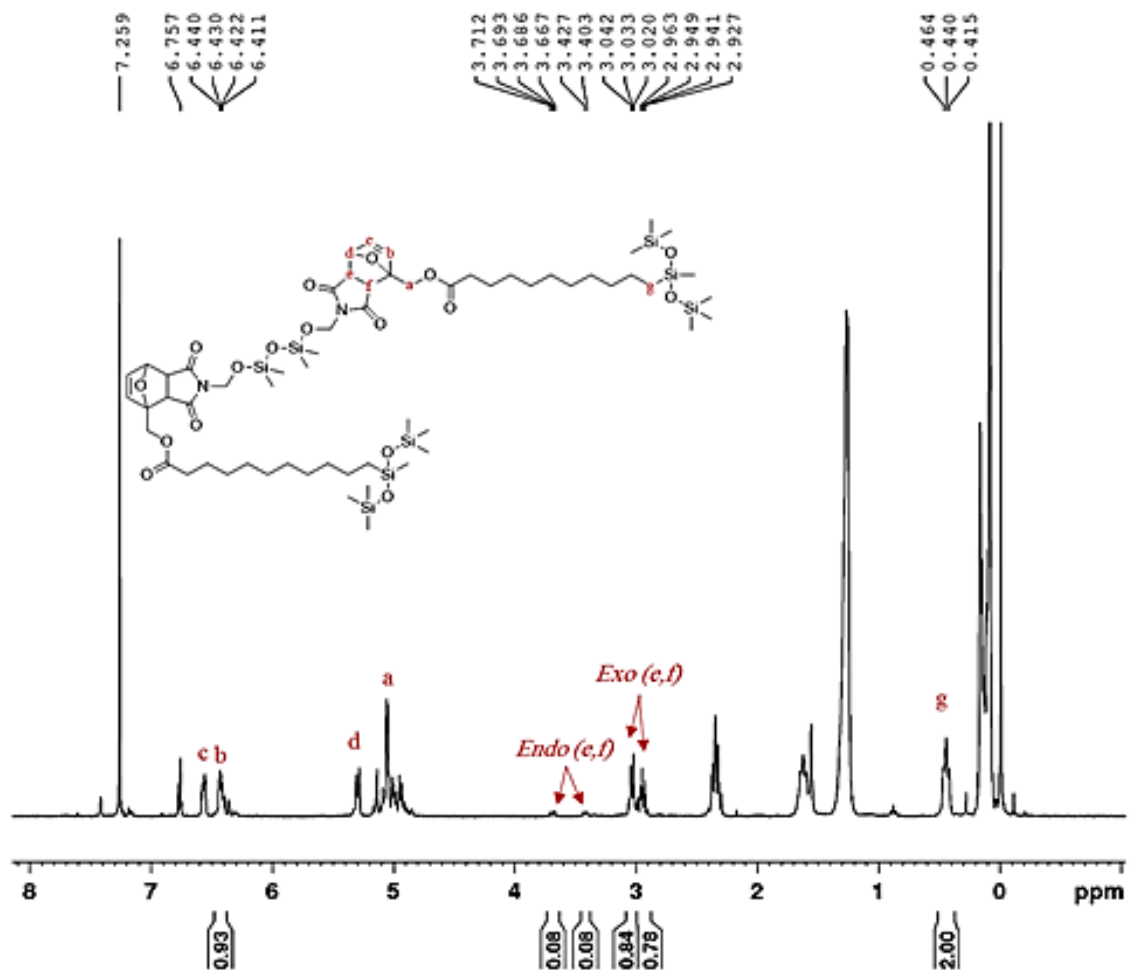


Figure 2-2 ¹H NMR spectrum of model Diels-Alder adduct **23**

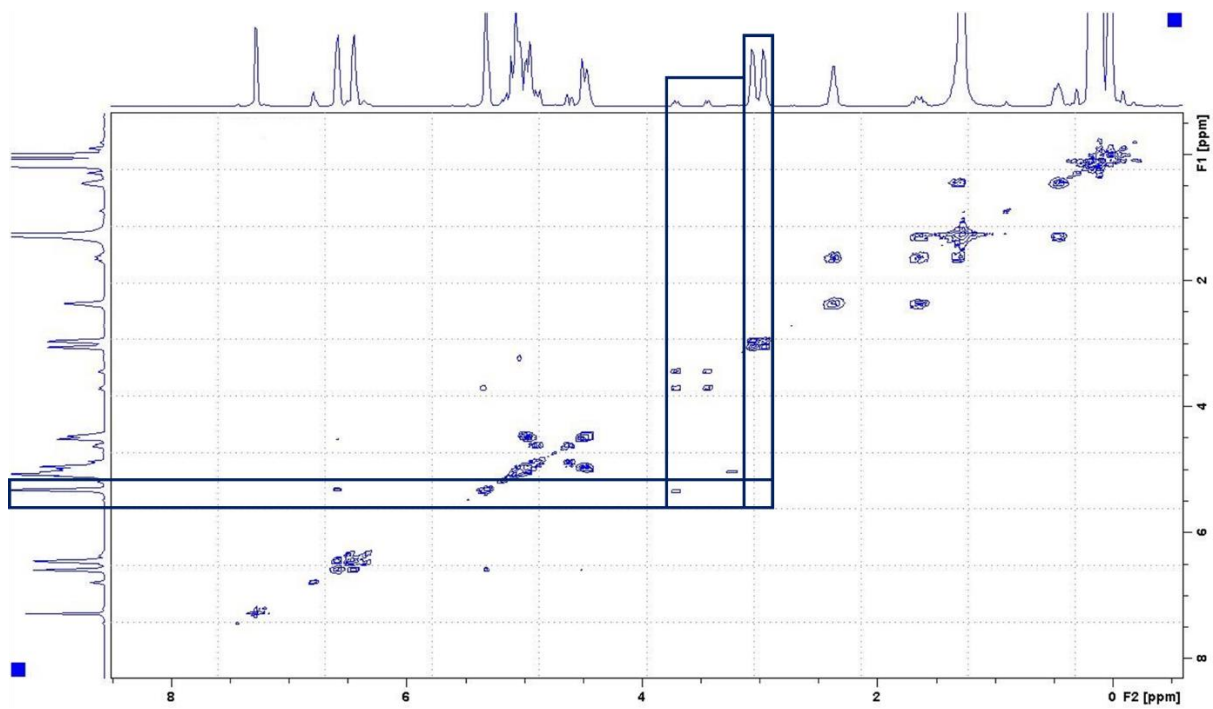


Figure 2-3 COSY NMR spectrum illustrating the correlation between the endo protons and the bridgehead proton. Note that the exo proton is not correlated with the bridgehead proton

Table 2-1. Model Diels-Alder reactions of furanyl-2-methyl-11-(1,1,1,3,5,5,5-heptamethyltrisiloxan-3-yl)undecanoate with 6 different dienophiles

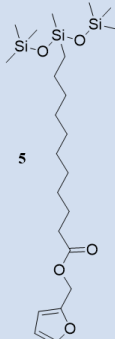
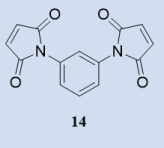
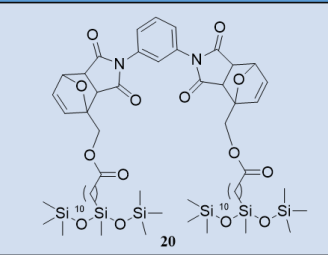
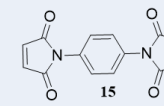
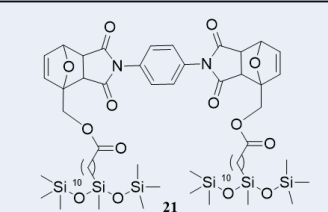
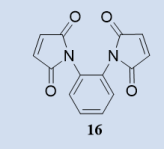
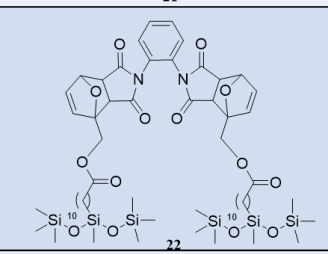
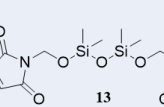
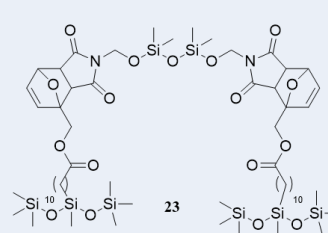
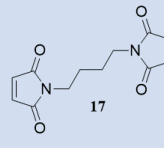
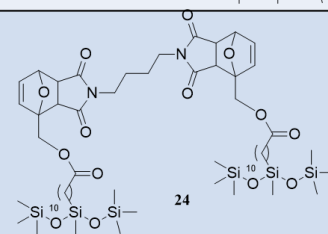
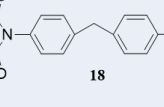
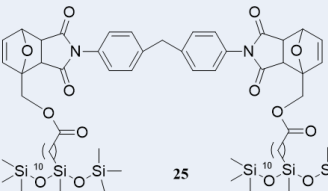

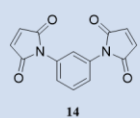
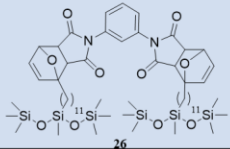
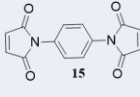
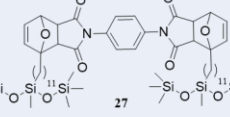
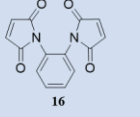
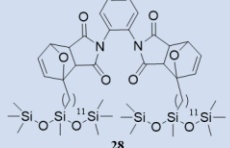
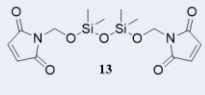
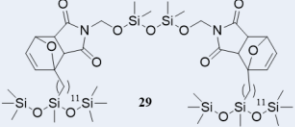
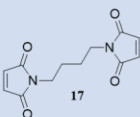
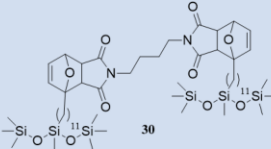
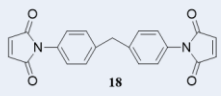
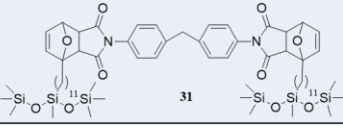
Reaction Number	Diene	Dienophile	DA Adduct
1		 <p>14</p>	 <p>20</p>
2		 <p>15</p>	 <p>21</p>
3		 <p>16</p>	 <p>22</p>
4		 <p>13</p>	 <p>23</p>
5		 <p>17</p>	 <p>24</p>
6		 <p>18</p>	 <p>25</p>

Table 2-2. Model Diels-Alder reactions of 3-(11-(furan-2-yl)undecyl)-1,1,1,3,5,5,5-heptomethyltrisiloxane with six different dienophiles

Reaction Number	Diene	Dienophile	DA Adduct
7		 14	 26
8		 15	 27
9		 16	 28
10		 13	 29
11		 17	 30
12		 18	 31

In order to optimize the conversion of the bismaleimide compounds to the corresponding Diels-Alder adduct, a range of temperatures from 40 °C to 80 °C was applied to all of the model systems and the maleimide consumption, amount of *exo* adduct formation, and overall yield of the reactions was determined using ¹H NMR (Table 2-3). Based on these data it was determined that, for the model compounds, the optimal temperature for the reactions was between 65 °C and 75 °C over a period of 24 h.

Table 2-3. Optimized reaction condition for the all of the model systems. The red numbers denote the reaction conditions that resulted in the highest overall yield

Reaction Number*	Reaction Temperature	Total Yield (%)	<i>exo</i> (%)	<i>endo</i> (%)
1	40 °C	0	0	0
	50 °C	4	3	1
	60 °C	10	5	5
	70 °C	88	79	9
	80 °C	81	74	7
2	40 °C	0	0	0
	50 °C	0	0	0
	60 °C	10	7	3
	70 °C	22	19	3
	80 °C	37	37	0
3	40 °C	10	6	4
	50 °C	10	6	4
	60 °C	67	58	9
	70 °C	62	56	6
	80 °C	52	40	12
4	40 °C	83	35	48
	50 °C	85	28	57
	60 °C	90	78	11
	70 °C	93	84	9
	80 °C	76	68	8
5	40 °C	0	0	0
	50 °C	0	0	0
	60 °C	86	48	38
	70 °C	89	54	35
	80 °C	10	10	0
6	40 °C	11	3	6
	50 °C	8	1	6
	60 °C	51	37	14
	70 °C	65	55	10
	80 °C	63	55	8
7	40 °C	13	9	4
	50 °C	6	4	2
	60 °C	38	38	0
	70 °C	30	27	3

	80 °C	8	5	3
8	40 °C	0	0	0
	50 °C	0	0	0
	60 °C	7	6	1
	70 °C	22	19	3
	80 °C	16	16	0
9	40 °C	8	4	4
	50 °C	8	3	5
	60 °C	20	14	6
	70 °C	34	27	7
	80 °C	13	9	4
10	40 °C	88	66	22
	50 °C	84	53	31
	60 °C	79	73	6
	70 °C	63	56	7
	80 °C	63	54	9
11	40 °C	7	4	3
	50 °C	6	6	0
	60 °C	27	20	7
	70 °C	40	33	7
	80 °C	28	26	2
12	40 °C	0	0	0
	50 °C	0	0	0
	60 °C	10	9	1
	70 °C	19	15	4
	80 °C	19	16	3

* Reaction numbers correspond to those listed in Table 2-1 and Table 2-2

Of all the model reactions, two presented some rather unique results. Comparing the yields of the reactions 4 and 10 with the others, it becomes apparent that these two systems resulted in relatively high conversion of the maleimide compound at 40 °C while the other reactions required higher temperatures (>50 °C) to achieve similar levels of maleimide conversion. These results encouraged me to attempt the DA reaction using the novel tetramethyldisiloxane-bismaleimide **13** at room temperature and over a shorter timeframe. Quite unexpectedly the reaction produced 80% conversion of the maleimide in 5 h at room temperature; to the best of our knowledge this represents the first reported instance of a siloxane-based Diels-Alder reaction taking place at room temperature. Under these conditions the *endo* isomer was the major product but the concentration of the *exo* isomer could be increased by increasing the reaction temperature and the reaction time. Given that the purpose of the Diels-Alder reaction in this thesis is to form covalent bonds between silicone polymers, the formation of a Diels-Alder adduct between polymer chains was of paramount concern, and not whether the adduct was the result of a predominantly *endo* or *exo* cycloaddition. These results were obtained only for the newly synthesized bismaleimide **13**; none of the commercially available bismaleimide compounds underwent the Diels-Alder reaction at room temperature.

To better understand the nature of the DA/rDA process, the reaction between 5 and 13 was monitored using variable temperature (VT) ¹H NMR experiments (Figure 2-4). Examination of the NMR spectra revealed that the resonance at 5.2 ppm (●) corresponding to the maleimide alkene protons disappeared as the temperature increased, signifying that the DA reaction was taking place, and then reappeared once the temperature reached 85 °C indicating that the rDA reaction was now the dominant reaction. The formation of the new

endocyclic double bond formation (■) and endo/exo protons (*/▲) and their subsequent disappearance over the experimental temperature range can be clearly observed. The retro DA reaction for both reactions 4 and 10 begins at 70 °C and 60 °C degrees, respectively, and continues to completion at 85 °C (Figure 2-4, Table 2-3). These data suggest that 85 °C which would be the ideal temperature at which all of the Diels-Alder linkages in the elastomers could be reversed and the material could be recycled. The variable ¹H NMR data for each model experiment have been shown in Figure 2-5 to Figure 2-15.

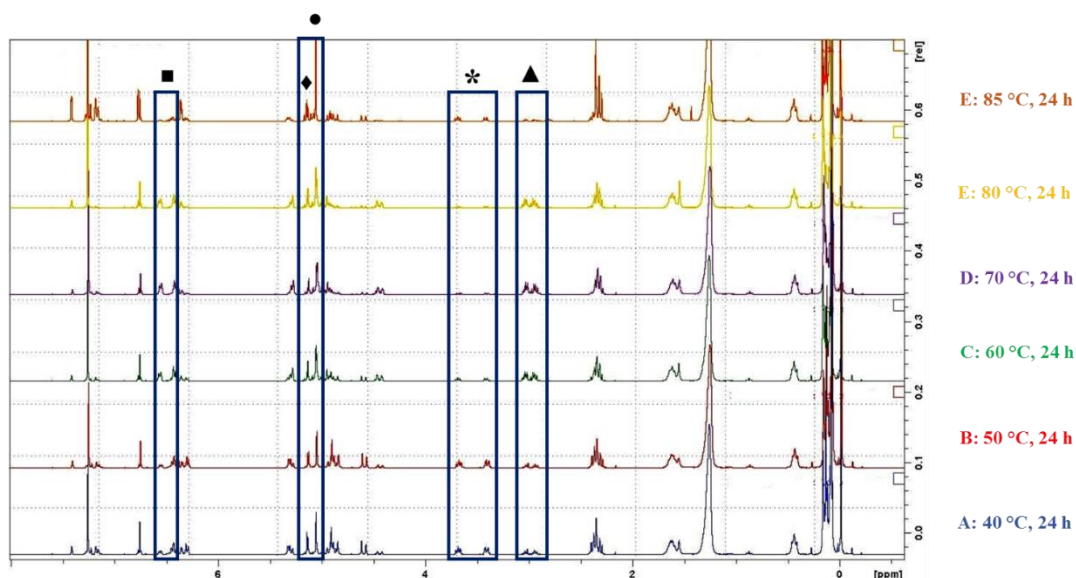


Figure 2-4. ¹H NMR spectra of the reaction between **5** and **13** at different temperatures (40 °C, 50 °C, 60 °C, 70 °C, 80 °C, 85 °C) illustrating maleimide consumption (●) and the formation of the new endocyclic double bond (■), the bridgehead proton (◆), and the exo (▲) and endo (*) adduct products

The VT NMR of the reaction number 6 (Figure 2-6), the progress of the reaction (maleimide consumption and bridgehead proton appearance) is really slow owing to the lower yield of adduct compared to the others. Moreover, no *endo* adduct is observed in this reaction. The same thing can be observed for reaction number 3 in Figure 2-7.

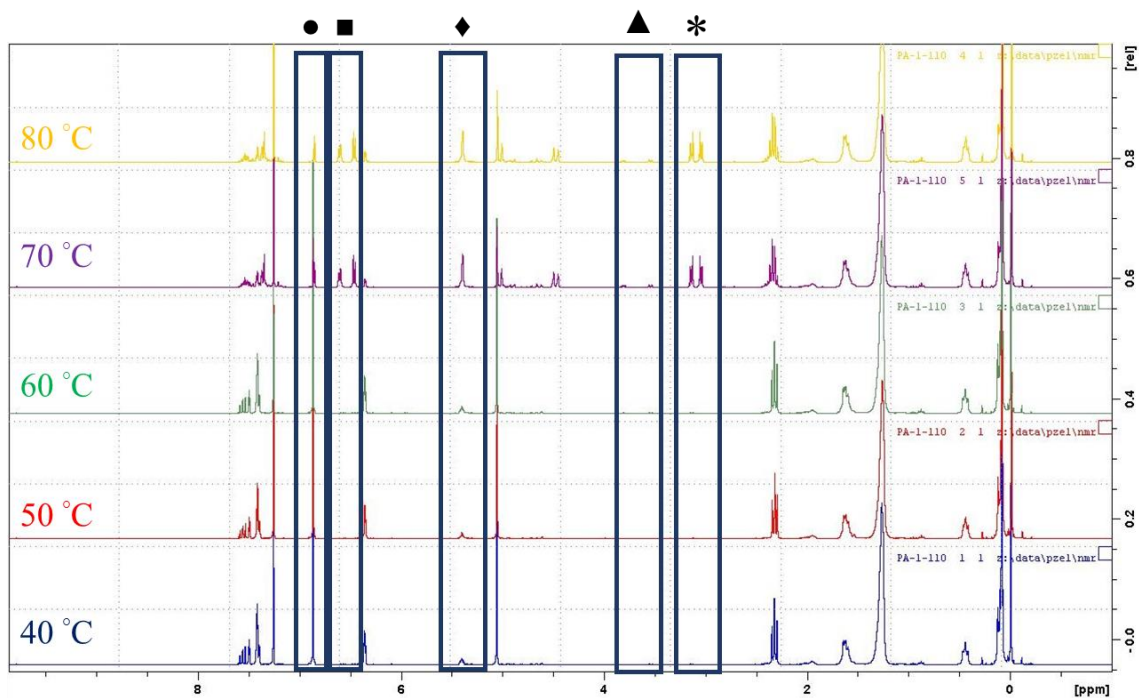


Figure 2-5 VT ^1H NMR spectra of the reaction #1 (40 °C, 50 °C, 60 °C, 70 °C, 80 °C) illustrating maleimide consumption (●) and the formation of the new endocyclic double bond (■), the bridgehead proton (◆), and the exo (▲) and endo (*) adduct products

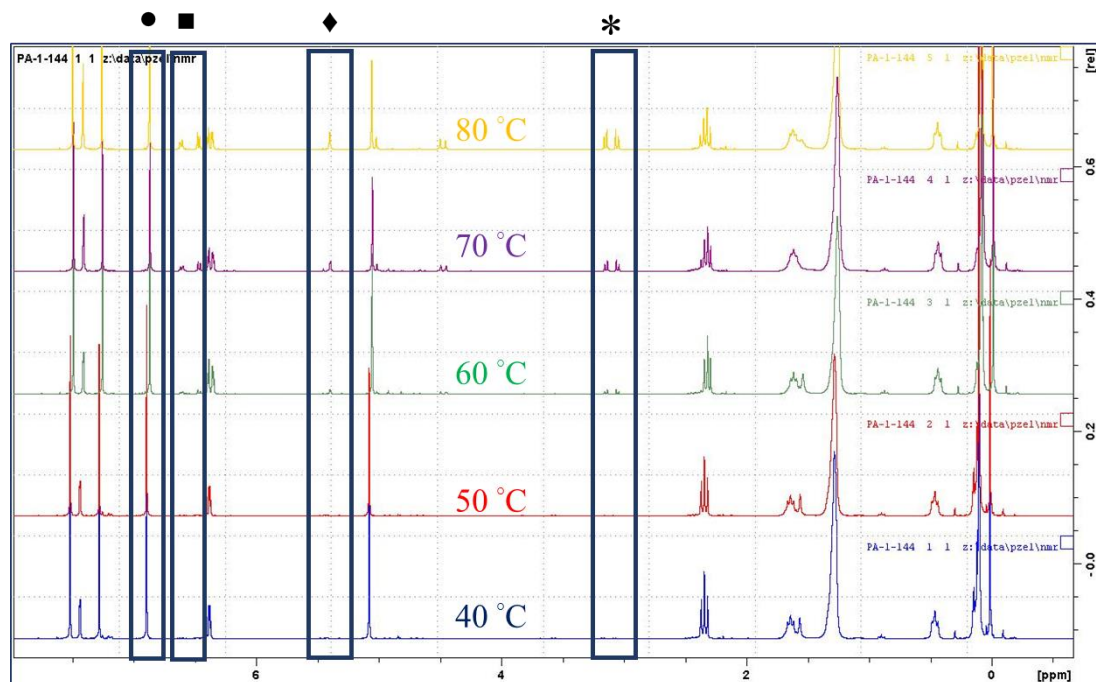


Figure 2-6 VT ^1H NMR spectra of the reaction #2 (40 °C, 50 °C, 60 °C, 70 °C, 80 °C) illustrating maleimide consumption (●) and the formation of the new endocyclic double bond (■), the bridgehead proton (◆), and the endo (*) adduct products

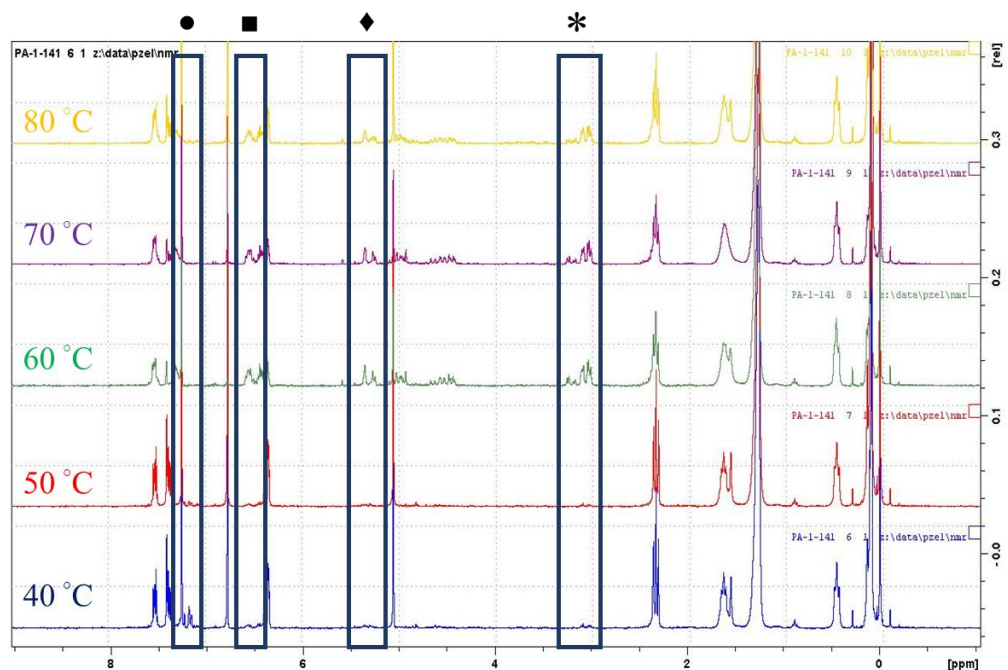


Figure 2-7 VT ^1H NMR spectra of the reaction #3 (40 °C, 50 °C, 60 °C, 70 °C, 80 °C) illustrating maleimide consumption (●) and the formation of the new endocyclic double bond (■), the bridgehead proton (◆), and the endo (*) adduct products

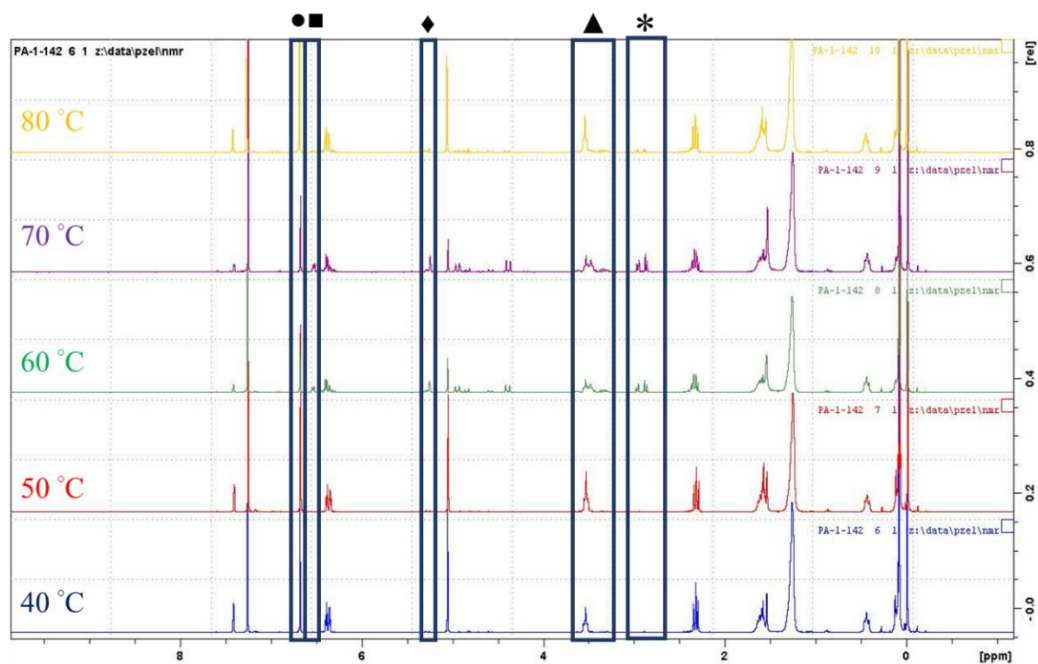


Figure 2-8 VT ^1H NMR spectra of the reaction #5 (40 °C, 50 °C, 60 °C, 70 °C, 80 °C) illustrating maleimide consumption (●) and the formation of the new endocyclic double bond (■), the bridgehead proton (◆), and the exo (▲) and endo (*) adduct products

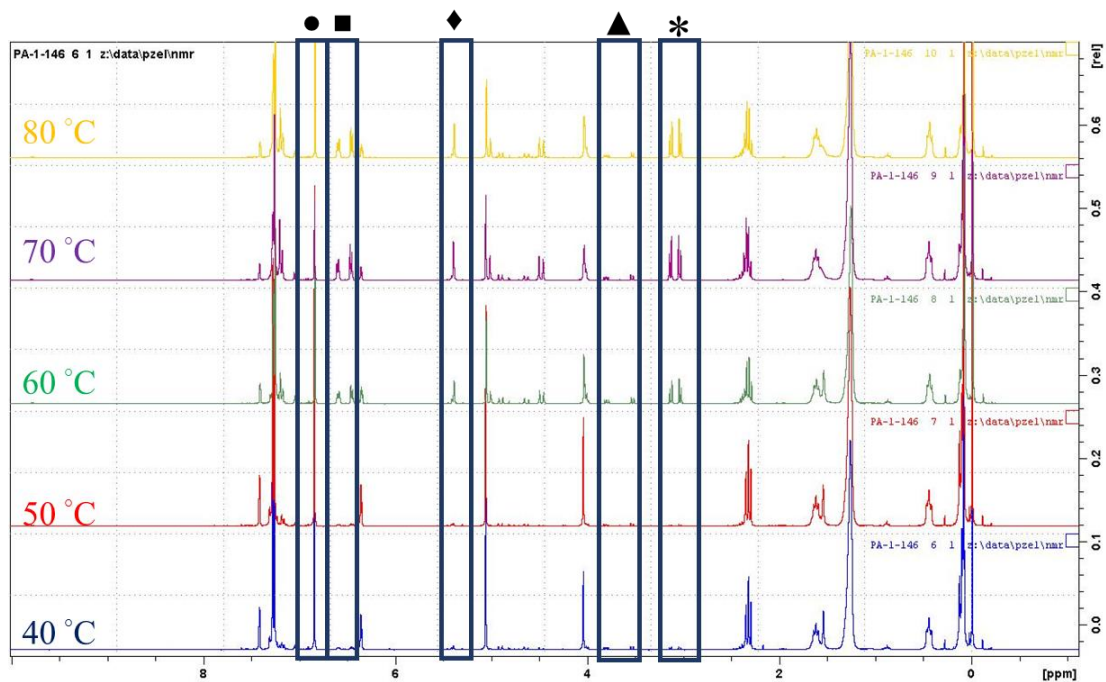


Figure 2-9 VT ^1H NMR spectra of the reaction #6 (40 °C, 50 °C, 60 °C, 70 °C, 80 °C) illustrating maleimide consumption (●) and the formation of the new endocyclic double bond (■), the bridgehead proton (◆), and the exo (▲) and endo (*) adduct products

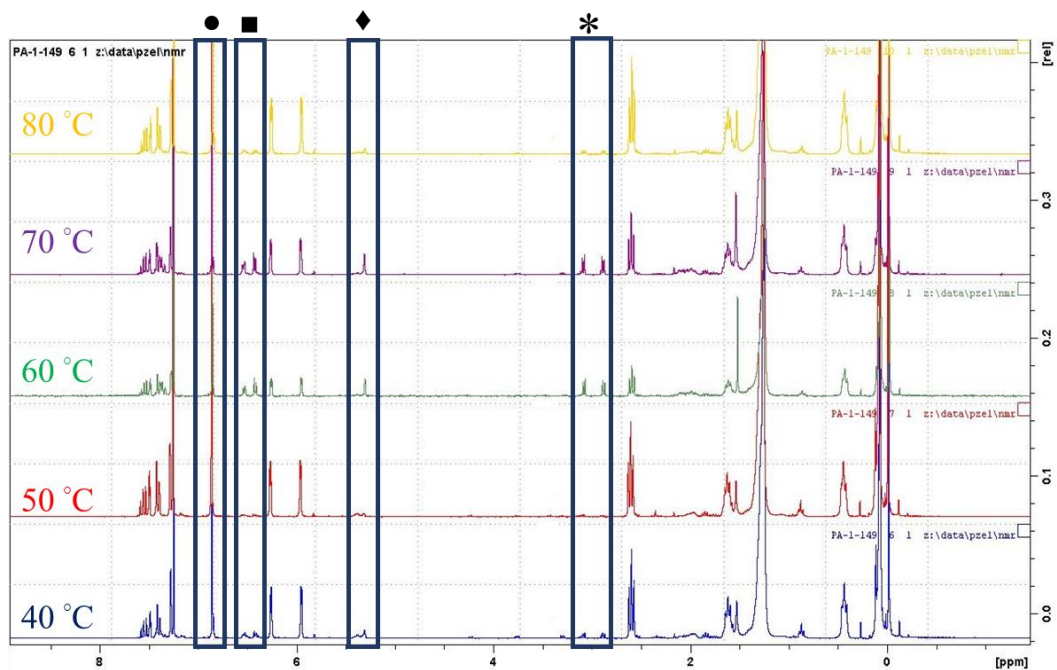


Figure 2-10 VT ^1H NMR spectra of the reaction #7 (40 °C, 50 °C, 60 °C, 70 °C, 80 °C) illustrating maleimide consumption (●) and the formation of the new endocyclic double bond (■), the bridgehead proton (◆), and the endo (*) adduct products

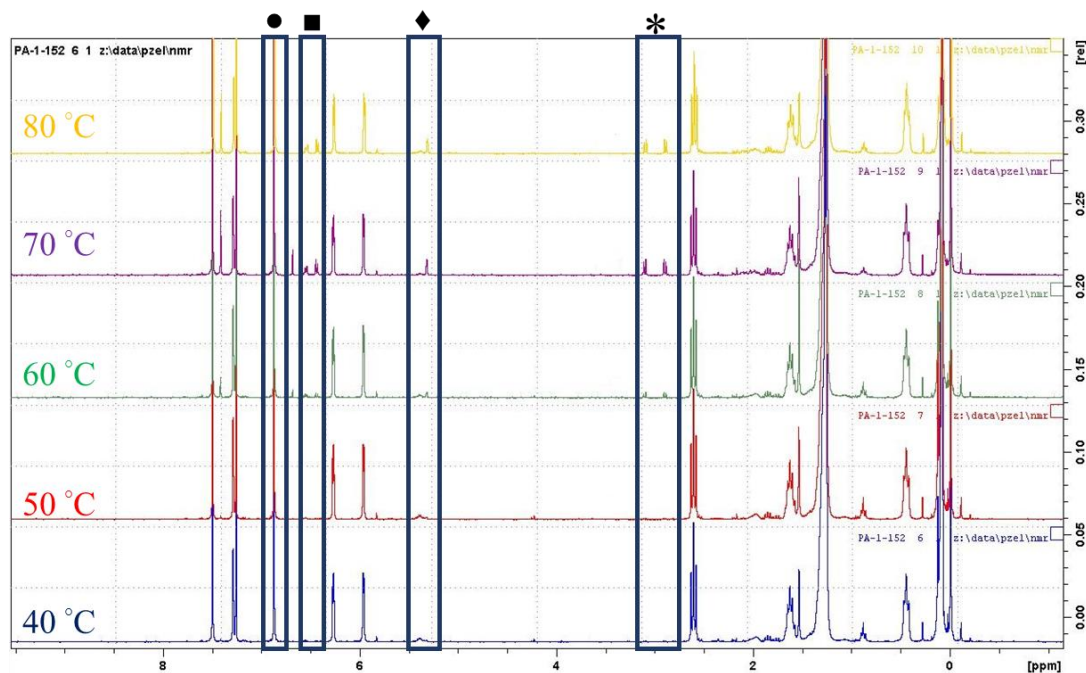


Figure 2-11 VT ^1H NMR spectra of the reaction #8 (40 °C, 50 °C, 60 °C, 70 °C, 80 °C) illustrating maleimide consumption (●) and the formation of the new endocyclic double bond (■), the bridgehead proton (◆), and the endo (*) adduct products

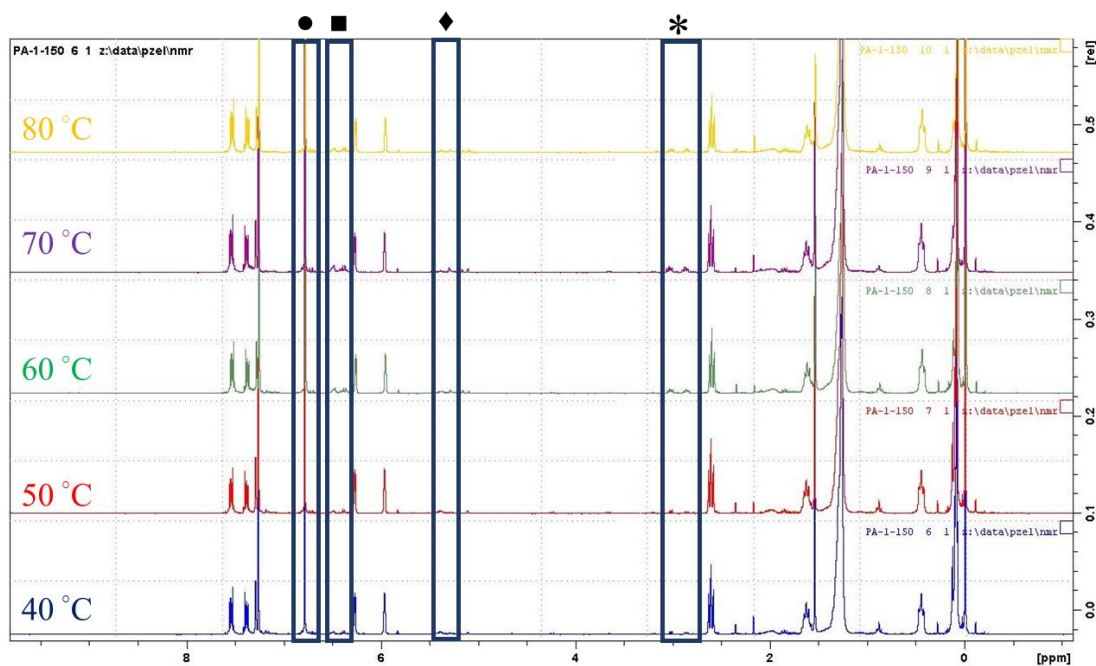


Figure 2-12 VT ^1H NMR spectra of the reaction #9 (40 °C, 50 °C, 60 °C, 70 °C, 80 °C) illustrating maleimide consumption (●) and the formation of the new endocyclic double bond (■), the bridgehead proton (◆), and the endo (*) adduct products

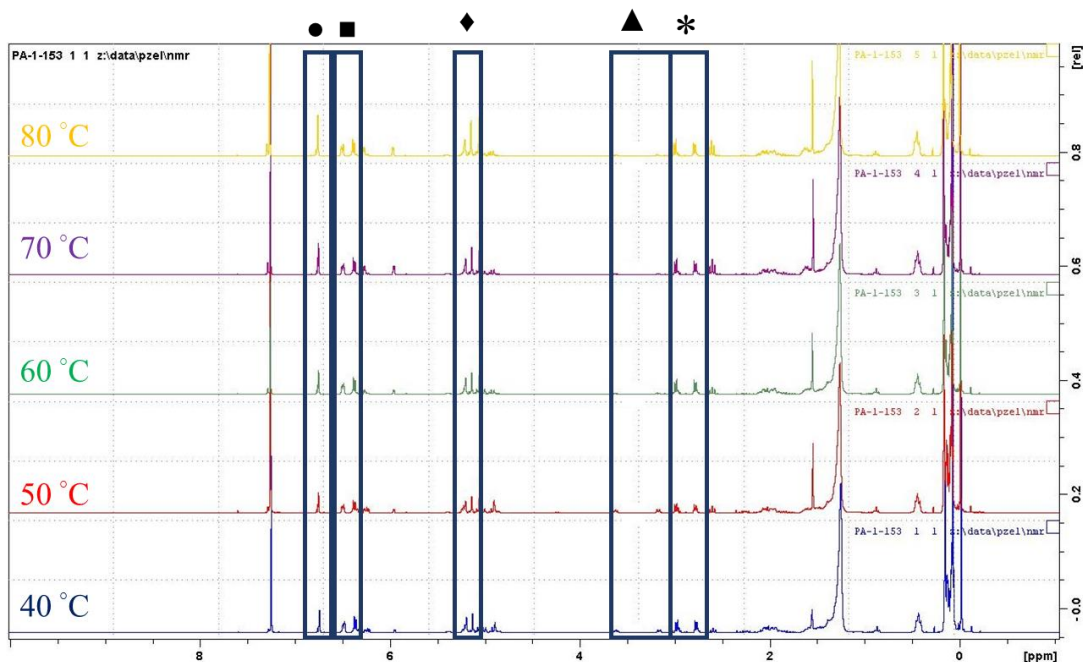


Figure 2-13 VT ^1H NMR spectra of the reaction #10 (40 °C, 50 °C, 60 °C, 70 °C, 80 °C) illustrating maleimide consumption (●) and the formation of the new endocyclic double bond (■), the bridgehead proton (◆), and the exo (▲) and endo (*) adduct products

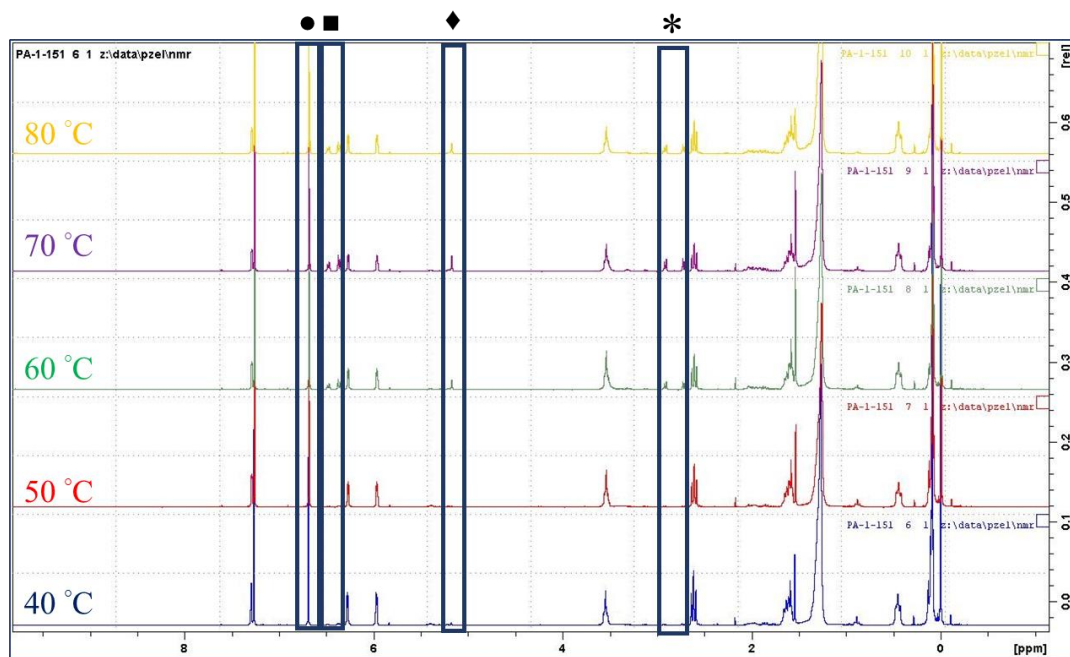


Figure 2-14 VT ^1H NMR spectra of the reaction #11 (40 °C, 50 °C, 60 °C, 70 °C, 80 °C) illustrating maleimide consumption (●) and the formation of the new endocyclic double bond (■), the bridgehead proton (◆), and the endo (*) adduct products

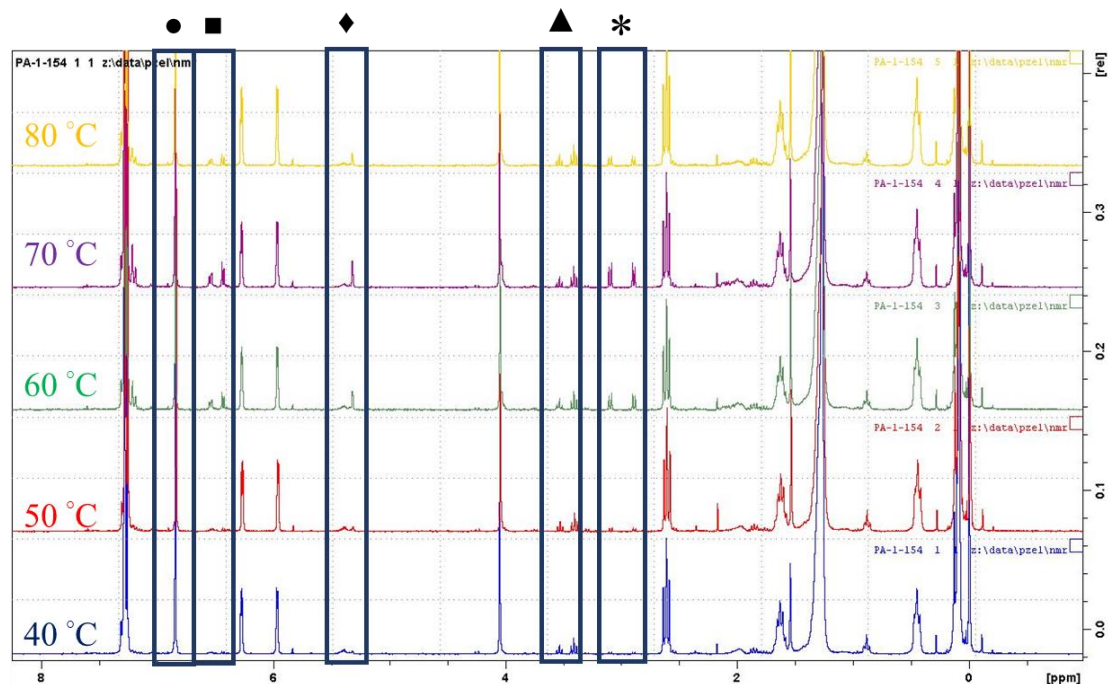


Figure 2-15 VT ^1H NMR spectra of the reaction #12 (40 °C, 50 °C, 60 °C, 70 °C, 80 °C) illustrating maleimide consumption (●) and the formation of the new endocyclic double bond (■), the bridgehead proton (◆), and the exo (▲) and endo (*) adduct products

Among three *ortho* **14**, *para* **15**, and *meta* **16** phenylenebismaleimides, the reactivity of the *meta* compound **16** in the model DA reactions was the highest. The relatively low reactivity of *ortho* compound **14** was attributed to the steric hindrance of the two maleimide rings, which inhibit addition of a furan ring attached to a bulky siloxane chain. It was anticipated that the *para* compound **15** would be more reactive in the model DA reactions than the *meta* analogue **16** owing to the planarity of **15** and the maximal distance between the two maleimide rings. The arrangement of the maleimide rings in **15** diminishes steric hindrance and should, in theory increase the yield of the cycloaddition reaction. However, this was not the case. As the steric considerations appeared to favour successful adduct formation, some basic calculations were performed by Dr. Travis Dudding (Brock University,

Department of Chemistry) to try and elucidate an electronic explanation for the lack of reactivity associated with **15** (Figure 2-16).

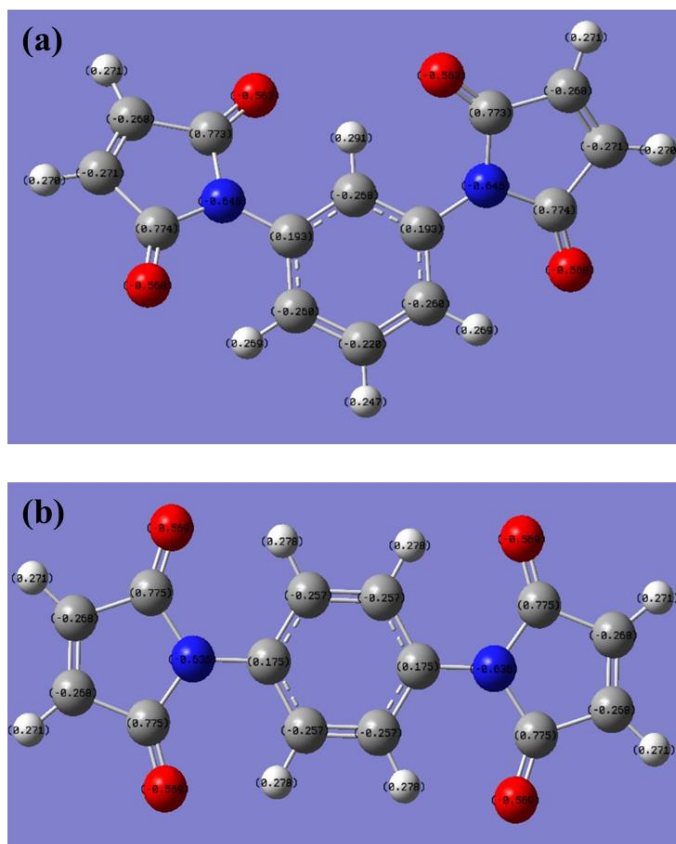
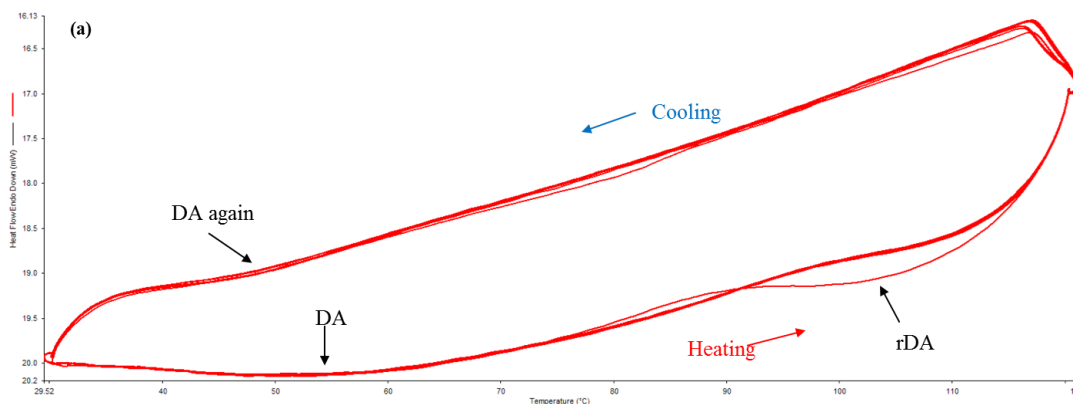


Figure 2-16. Computationally-derived electronic charges on (a) *N,N'*-(1,3-phenylene)bismaleimide and (b) *N,N'*-(1,4-phenylene)bismaleimide atoms.

As can be seen in Figure 2-16, the *meta* **16** and *para* **15** compounds are virtually identical from an electronic standpoint, suggesting that electronic charge distribution is not the key factor responsible for the difference in reactivities between these two species.

DSC (Differential Scanning Calorimetry) and TGA (Thermogravimetric Analysis) analyses were performed for each model reaction to study the DA/rDA equilibrium and the reversibility of the system. The samples prepared from 1:1 mixture, by mass, of the diene:dienophile of interest mixed in a flask and stirred in the absence of solvent at 80 °C

for 24 h to yield the DA adduct in approximately 85% (not for all of the model systems). Then, three cycles of heating and cooling were applied to each sample from 30 °C to 120 °C with a ± 4 °C heating/cooling rate. The DSC and TGA thermographs for the reaction between **5** and **13** (Figure 2-17) is discussed here as a representative sample of all the model reactions. The thermal experiments subjected the sample to 7 heating/cooling cycles seven times at a ± 4 °C heating/cooling rate with the hold time of 20, 30 and 40 min in order to examine the system's stability, repeatability, and reversibility. The DSC trace for the reaction between **5** and **13** (Figure 2-17a) shows that for the the model system the DA and retro DA reactions occur at around 55 °C and 105 °C, respectively; the DA reaction occurs again in the cooling cycle at roughly 50 °C. The stability of the heating and cooling process over the course of 7 cycles confirmed the recyclability and repeatability of DA/rDA reaction. The remaining 11 thermographs for the other model reactions can be found in the Appendix; these systems displayed similar thermal behaviours to the model reaction between **5** and **13**.



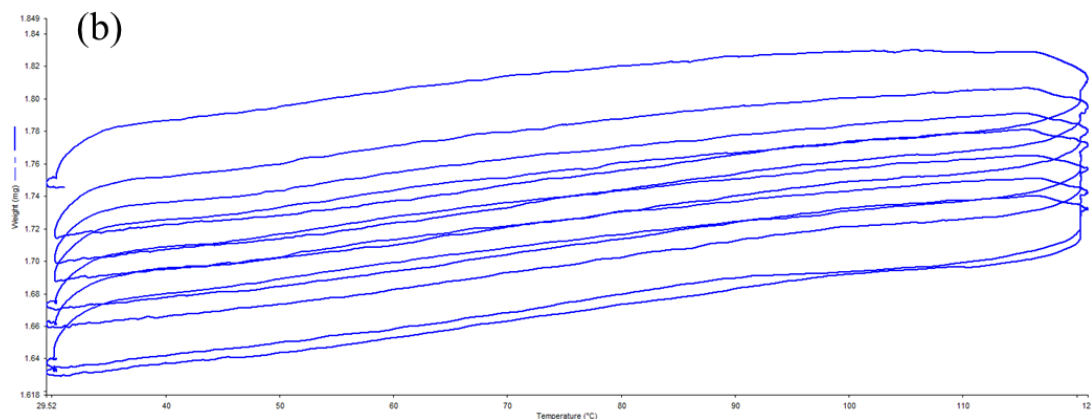


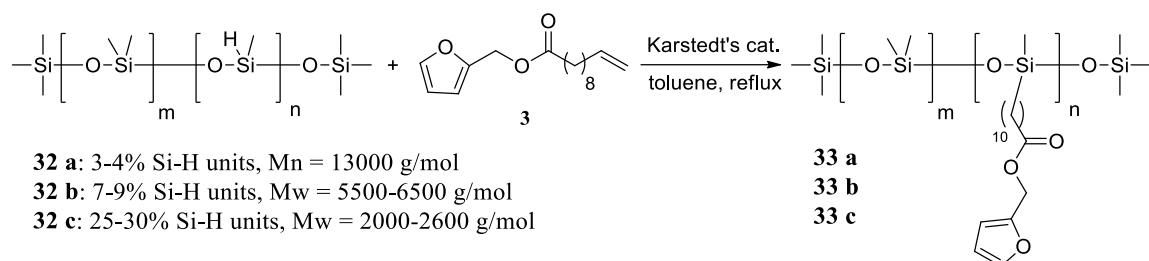
Figure 2-17. (a) DSC thermograph and (b) TGA analysis for the model DA/rDA reaction between **5** and **13**

Moreover, the TGA trace (Figure 2-17b) indicated that the compounds do not demonstrate appreciable degradation as evidenced by weight loss after being subjected to 7 heating and cooling cycles. This is evidenced by the minimal weight loss (from 1.75 mg to 1.63 mg observed for the reaction mixture indicating that the reaction mixtures are capable of undergoing multiple DA/rDA reactions.

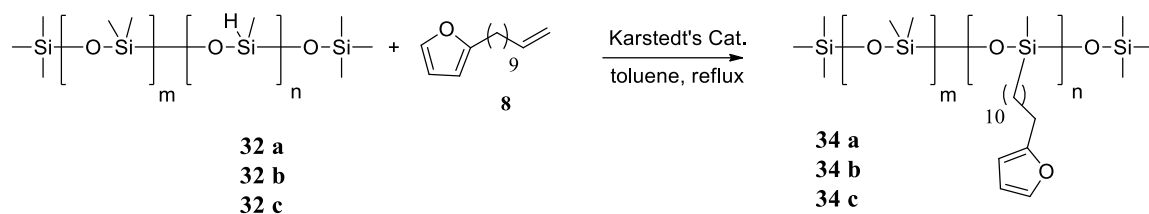
2.2 Synthesis of Diels-Alder Cross-Linked Siloxane Elastomers

In an effort to better understand the target elastomeric systems, 12 different model DA adducts were synthesized over varying timeframes and temperatures. This data was then extended to the synthesis of elastomeric silicone materials cross-linked using the Diels-Alder reaction. Using three different siloxane polymers (**32 a**, **32 b** and **32 c**) with varying concentrations of the furan diene, with two different furan moieties (**3** and **8**) generated six different diene systems (Scheme 2-5 and

Scheme 2-6) that could be reacted with six different dienophiles to yield 36 different elastomers. All of the elastomers were synthesized with a 1:1 mole ratio of diene:dienophile (Scheme 2-7, Scheme 2-8).



Scheme 2-5. Synthesis of ester-furan-modified elastomers using trimethylsilyl-terminated poly(dimethylsiloxane-co-methylhydrosiloxane) with different molecular weights and Si-H concentrations

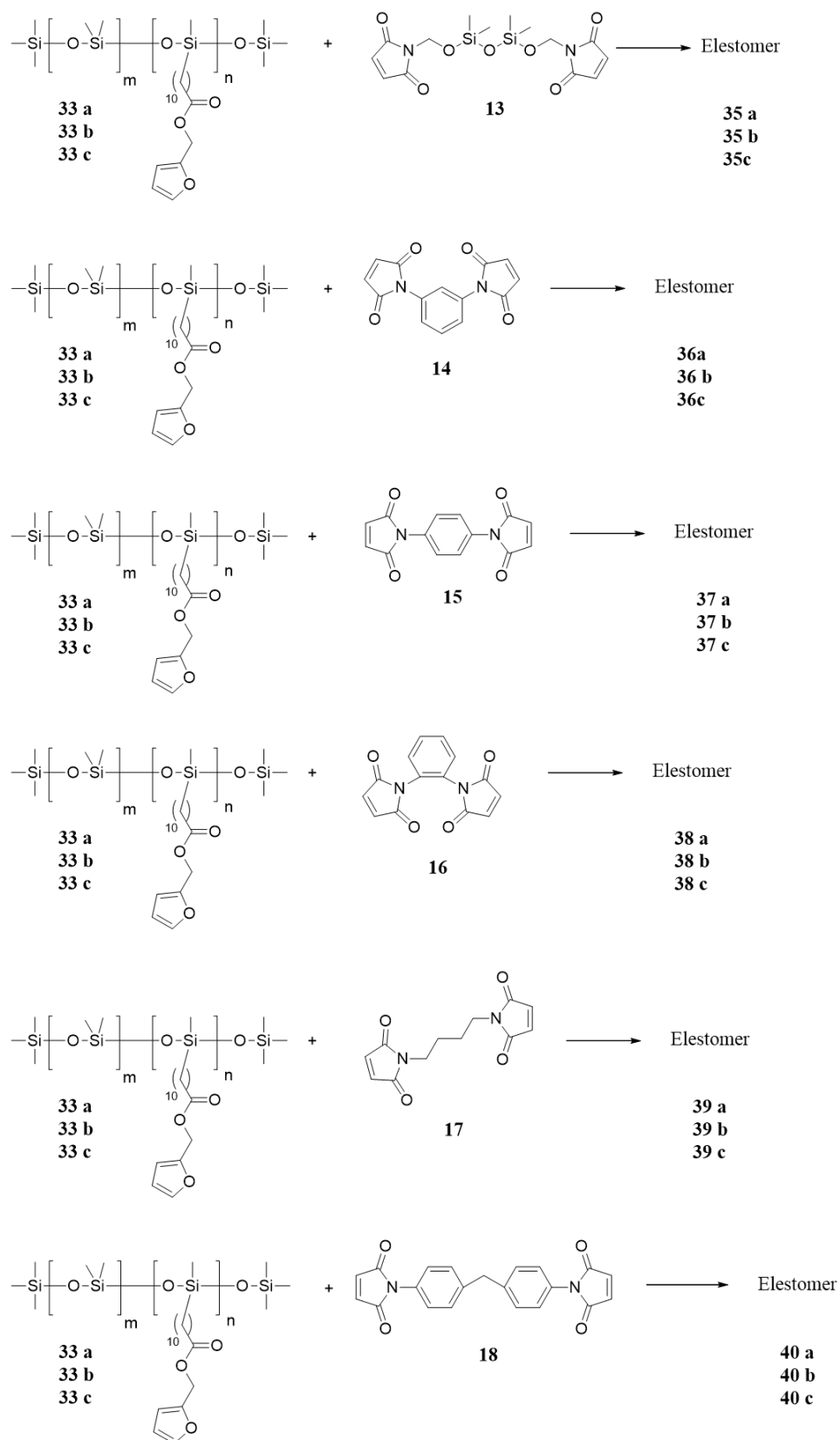


Scheme 2-6 Synthesis of alkyl-furan-modified elastomers using trimethylsilyl-terminated poly(dimethylsiloxane-co-methylhydrosiloxane) with different molecular weights and Si-H concentrations

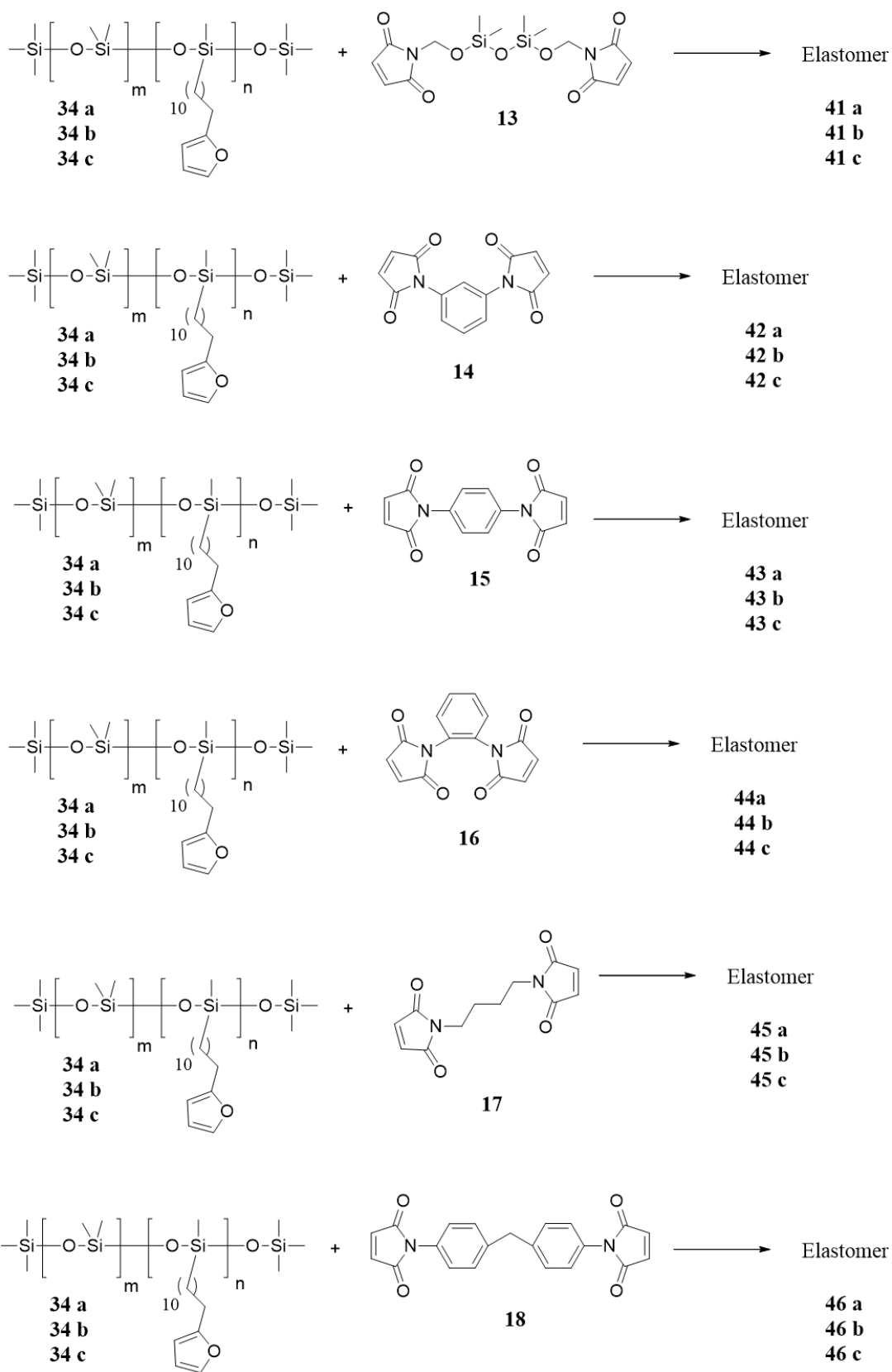
Synthesizing cross-linked siloxane elastomers using the Diels-Alder reaction required that the number of diene units along the polymer backbone be calculated. In this study, three different concentrations of Si-H moieties along the PDMS backbone were examined. The first one possessed 3-4 mol% of methylhydrosiloxane units over a PDMS polymer with an average molecular weight (M_n) of 13,000 g/mol. From the ^1H NMR spectrum of the product it was determined that **33 a** and **34 a** possessed approximately 1 furan moiety for every 32 dimethylsiloxane units, which means half of this number represents the amount of bismaleimides **13-18** required for the reaction since the cross-linker possesses two dienophile units. The second system (**33 b** and **34 b**), was 7-9 mol% methylhydrosiloxane units a molecular weight of 5,500-6,500 g/mol, leaving approximately 1 furan unit for every 13 dimethyl siloxane units in the polymer backbone. For (**33 c** and **34 c**), which was 25-30 mol% methylhydrosiloxane with a molecular weight

range of 2,000-2,600 g/mol, the polymer contained 1 furan unit for every 3 dimethyl siloxane groups. The solvent-free Diels-Alder reaction (Scheme 2-7, Scheme 2-8, Scheme 2-9) was performed in a polytetrafluoroethylene (PTFE, Teflon™) mould (37.6 mm L x 13.8 mm W x 3 mm D) with three cavities. Once the components of the reaction were placed in the mould the entire system was placed in an oven and the elastomers were permitted to cure. Among all of these 36 elastomers, 15 of them worked perfectly and produced solid elastomers with different colours ranging from clear and colourless, light yellow to brownish. Furthermore, each of the elastomers indicate various mechanical properties (elongation and hardness) that will be discuss later. Moreover, 5 of the elastomers didn't cure completely (liquid on the top) mostly because of the low cross-link density. 12 of all didn't cure at all and it was expectable according to the model systems. Eventually, 4 of the DA reactions in the mould were not attempted in spite of the data from the model reactions because the cost of the bismaleimide was prohibitive.

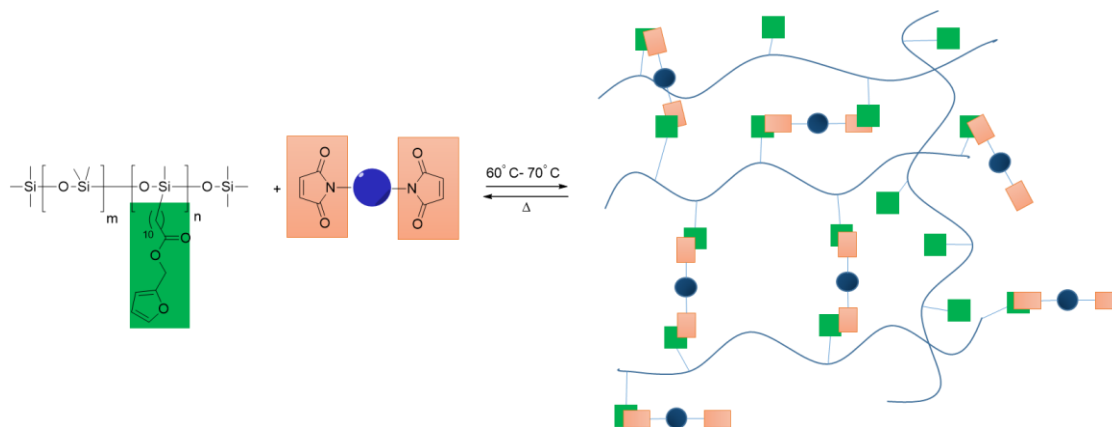
In the following sections, the reasons of why some of the elastomers worked perfectly, some of them cured incomplete and some of them did not cure at all, will be discussed in more details.



Scheme 2-7 DA reactions in the mould with diene **33 a**, **33 b**, **33 c** and dienophile **13-18**



Scheme 2-8 DA reactions in the mould with diene **34 a**, **34 b**, **34 c** and dienophile **13-18**



Scheme 2-9 A graphical of Diels-Alder reactions between furan-modified silicones and bismaleimides leading to elastomer formation.

All of the elastomers utilizing the commercially available dienophiles (**14-18**) were synthesized at temperatures ranging from 60 °C to 70 °C in an oven over the course of 24 to 48 h. These results were consistent with earlier work in the Zelisko lab involving elastomer formation utilizing diene- and dienophile-modified siloxane polymers.¹¹⁸ However, silicone elastomers utilizing bismaleimide **13** as the dienophile were fully formed at room temperature in only 5 h. Since the temperature for the both model and polymeric DA reaction for this specific bismaleimide **13** were lower compared to the other systems (models and elastomers), the retro DA also occurred at 80 °C (Figure 2-4), compared to the other systems that typically displayed the onset of the rDA reaction at approximately 100 °C. To the best of my knowledge this is the first, and only, reported case of a self-healing silicone elastomer based on the Diels-Alder reaction where healing occurs at room temperature.

2.3 Solid-State NMR

Solid-state ¹H NMR analysis of the cross-linked PDMS elastomer confirmed the appearance of adduct peak on the spectra at around 3 ppm as it was observed previously

on the model adduct ^1H NMR. Solid-state NMR were taken from two of the elastomers (**35 b** and **41 c**) and have been shown in Figure 2-18 and Figure 2-19 respectively. So, the results extended to the other synthesized elastomers.

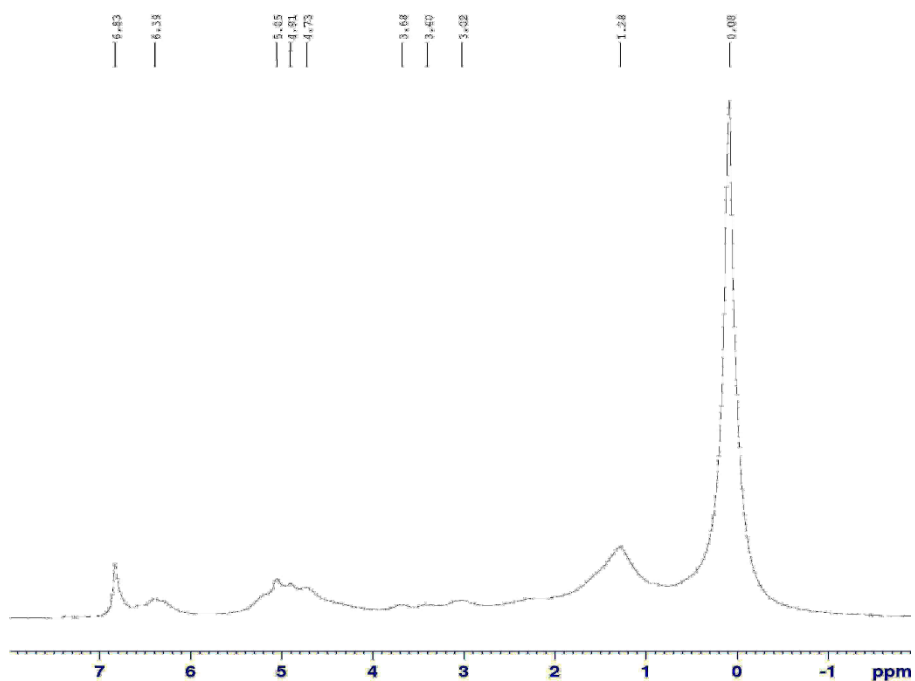


Figure 2-18 Solid-state ^1H NMR of compound **35 b**. The peaks at 3.02, 3.40 and 3.68 ppm confirm existence of exo and endo adduct protons

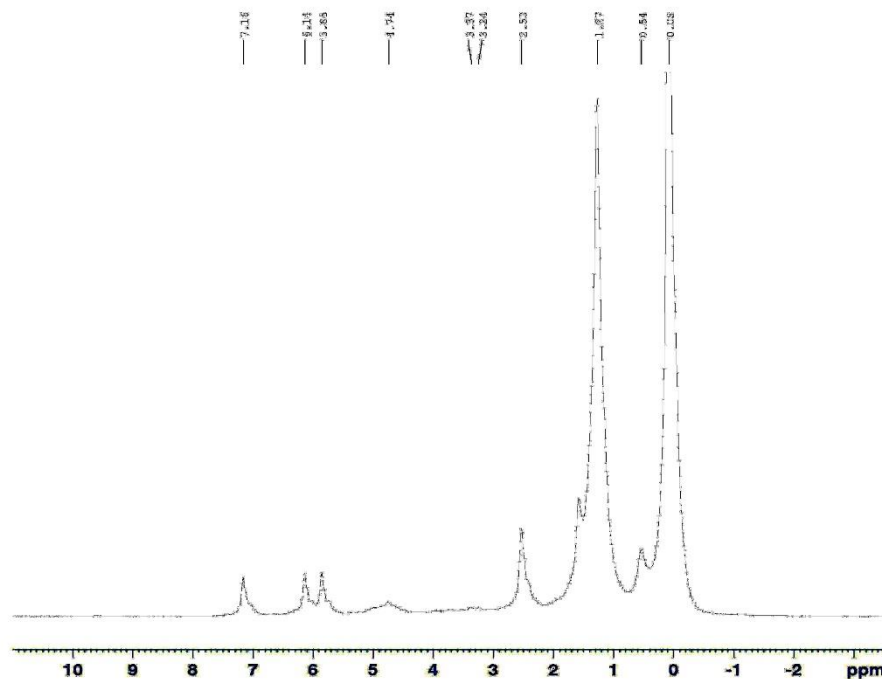


Figure 2-19 Solid-state ^1H NMR of compound **41 c**. The peaks at 3.24 and 3.37 ppm confirm existence of exo and endo adduct protons

2.4 Imaging the Elastomers

In addition to using solid state ^1H NMR to confirm the self-healing and reversible nature of the DA reactions in the silicone elastomers, optical and scanning electron microscopy (SEM) were used to observe the surface of virgin and healed elastomer surfaces for an elastomer (**36 b**) made by reacting **33 b** and bismaleimide **14** (Figure 2-20), chosen at random from all synthesized elastomers involving the commercially available bismaleimides. One can observe a faint scratch on the surface of the elastomers after self-healing. Even though a scar is visible on the surface of the elastomer, the silicone material was completely healed (i.e., one solid elastomer rather than two individual pieces). The elastomer was imaged at

various magnifications to truly understand the implications of the healing process on the surface of the elastomeric material.

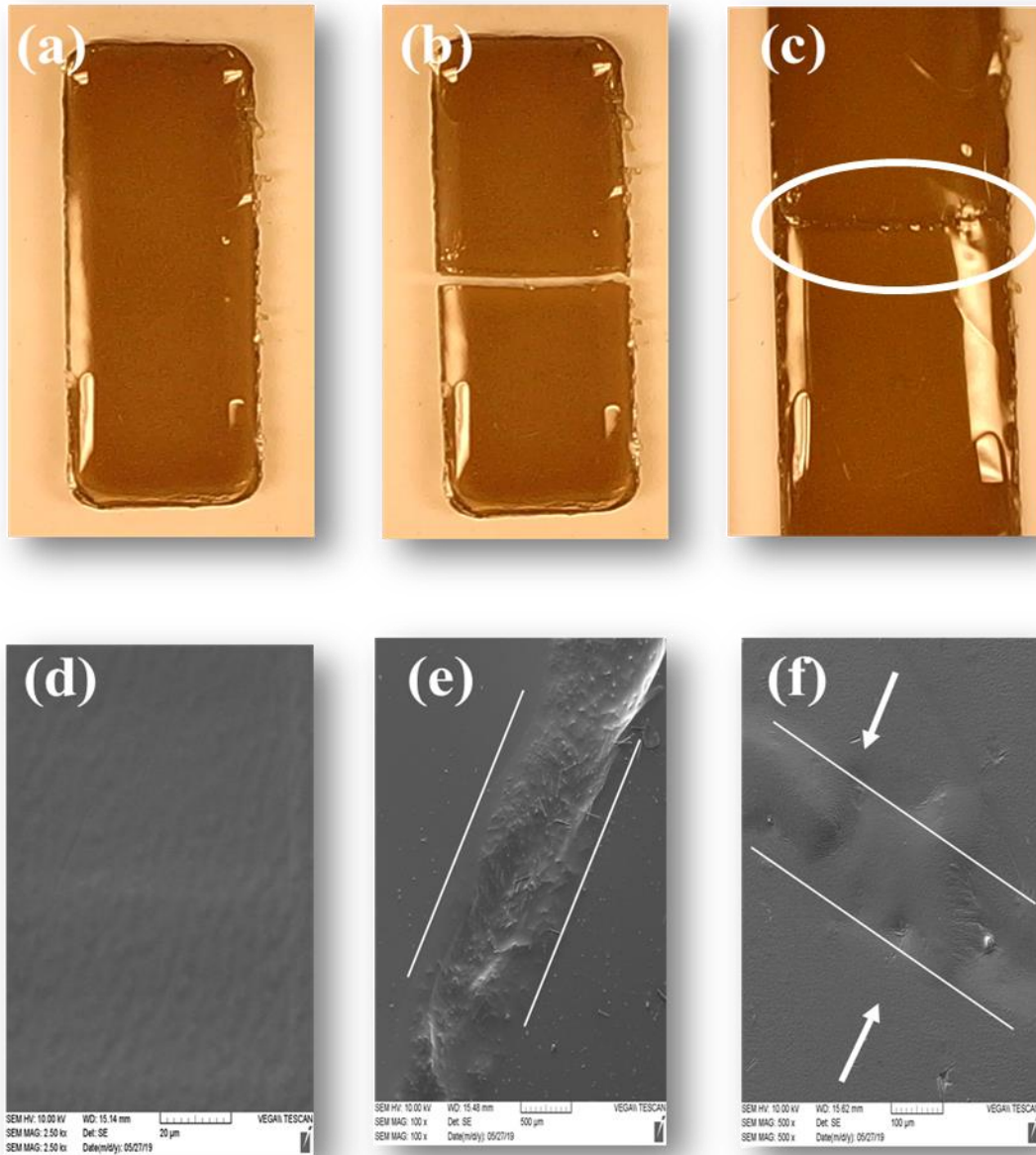


Figure 2-20. Optical microscopy images of (top) and scanning electron microscopy (SEM) images (bottom) of 36 b virgin elastomer (a) & (d), bisected elastomer (b), and the “scar” of a healed elastomer (c), (e), & (f) obtained by heating the sample to 120 °C and then permitting it to cool and heal

The elastomers made using the commercially available dienophiles (**14-18**) were all yellow to light brown in colour. However, elastomers formulated using **13** as the dienophile were all clear and colourless (Figure 2-21 (a), (b), and (c)). SEM imaging of the elastomer **35 b** revealed an extremely well healed elastomer – the scar was nearly imperceptible. These data suggest that silicone elastomers employing **13** as the cross-linker are more efficient not only in terms of their initial synthesis, but also with respect to their self-healing, which was observed to occur in 2-3 min after heating the sample to 80 °C to increase chain mobility within the elastomer.

In addition to developing a self-healing silicone elastomer in an effort to extend the useful lifetimes of such materials, it was also of interest to look at the capacity of these elastomers to be recycled; specifically it was of interest to examine the efficiency with which the elastomers could be remoulded into different forms and subsequently reused, a feat that is not trivial with traditional silicone elastomers. To explore the capacity of the elastomers to be recycled, specifically through remoulding, a sample of the elastomer made from **35 b** was heated to 80 °C in a small vial. The solid sample underwent the retro-Diels-Alder reaction and became fluid. After cooling and being left at the room temperature for a few hours the sample underwent the Diels-Alder reaction to form a solid elastomer once again, this time in the cylindrical shape of the vial (Figure 2-22).

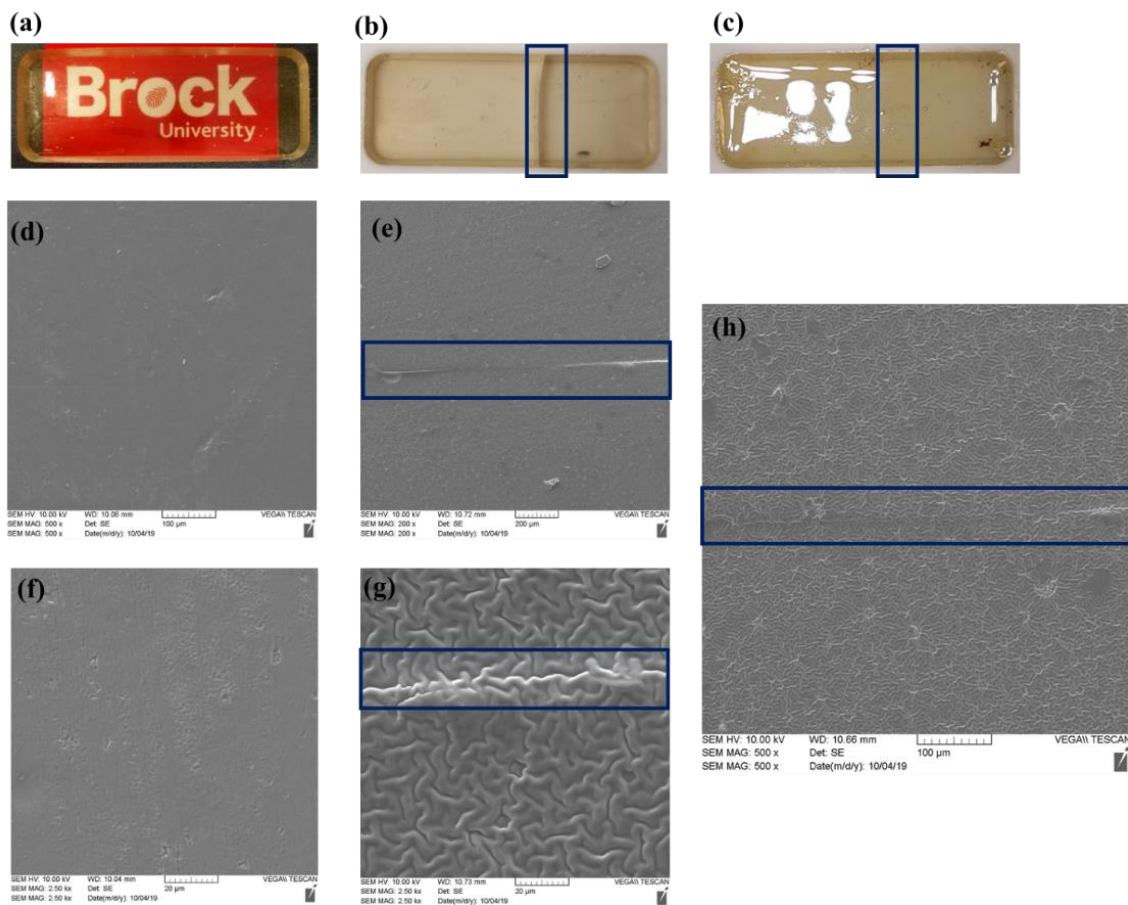


Figure 2-21 Photographs and SEM images for the elastomer made from **35 b**: (a), (b), (c) photographs of virgin, bisected, and healed elastomer respectively; (d), (e) SEM images of a virgin and healed elastomer at 200 x magnification; (f), (g) the same virgin and healed elastomer imaged at 2.5k x magnification; (h) the healed elastomer imaged at 500 x magnification. The cuts/scars are highlighted in (b), (c), (e), (g), and (h).

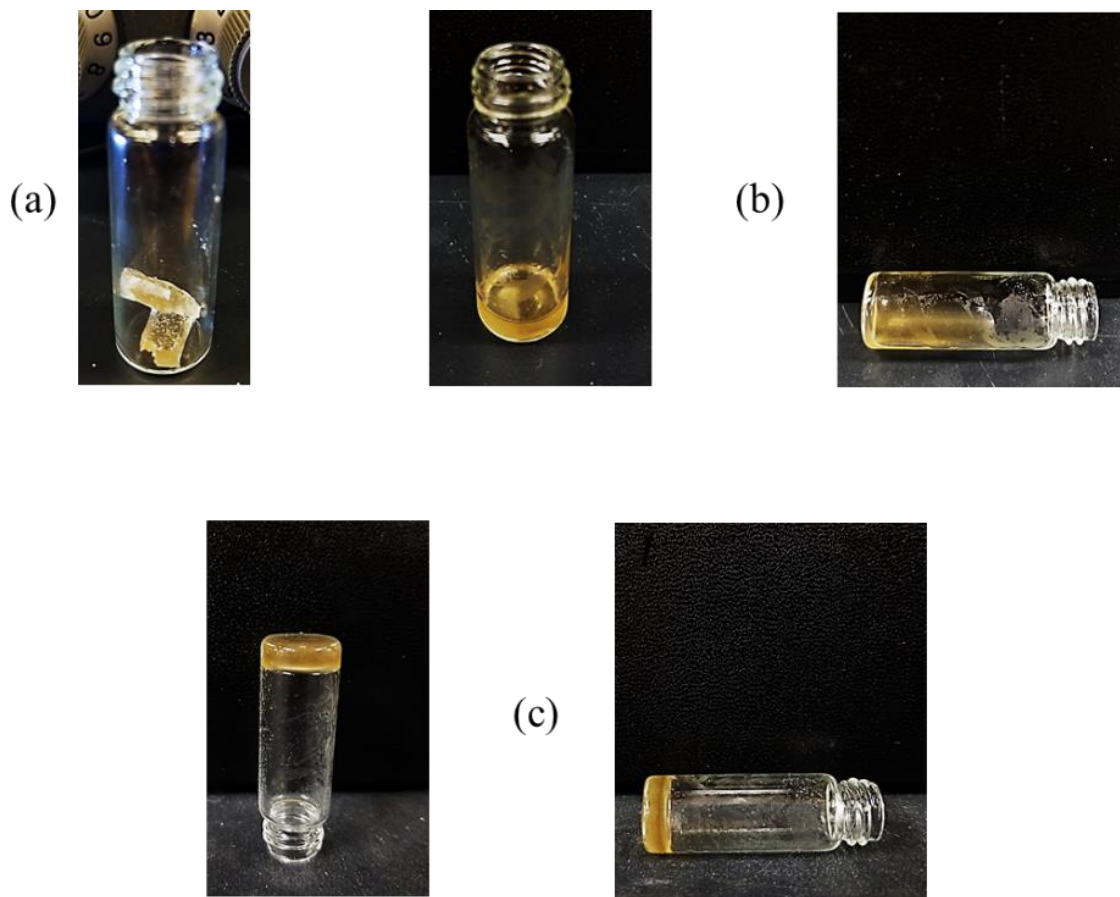


Figure 2-22 Images demonstrating the capacity of the elastomers made from **35 b** to be remoulded into different shapes and hence recycled.

2.5 Tensile Strength Measurements

The tensile strength of the polysiloxane elastomers was examined for virgin elastomers and for elastomers that had been healed (Figure 2-23). **36 a** required the application of a greater force (12 N) than the other elastomers in this series, but it broke after only being elongated by roughly 1.27 cm. Elastomer **35 b** was elongated by 3.3 cm but suffered catastrophic failure after the application of only 1 N of force.

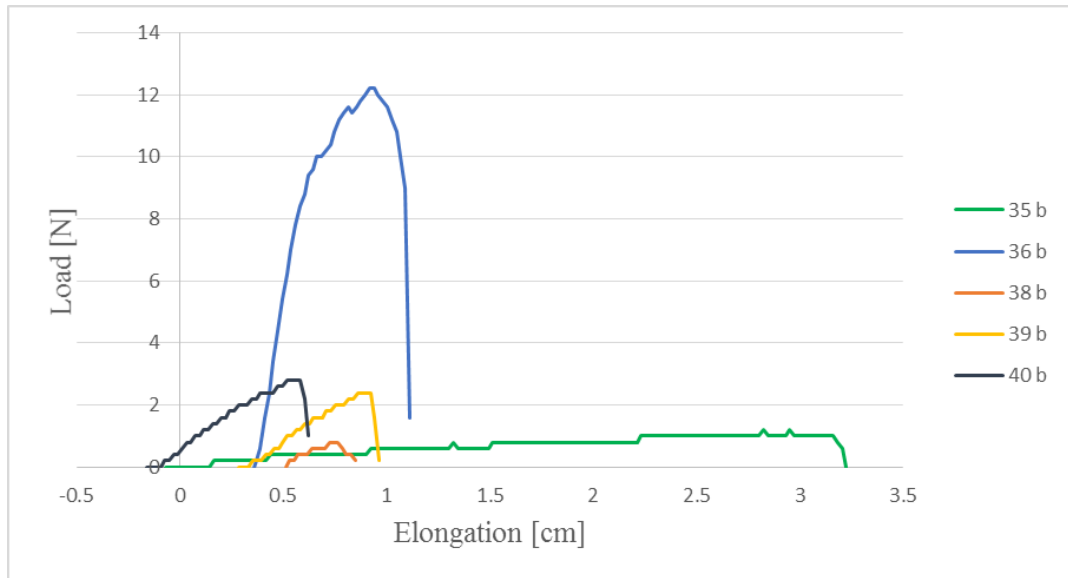


Figure 2-23 Comparing the tensile strength of the **35 b**, **36 b**, **38 b**, **39 b** and **40 b**

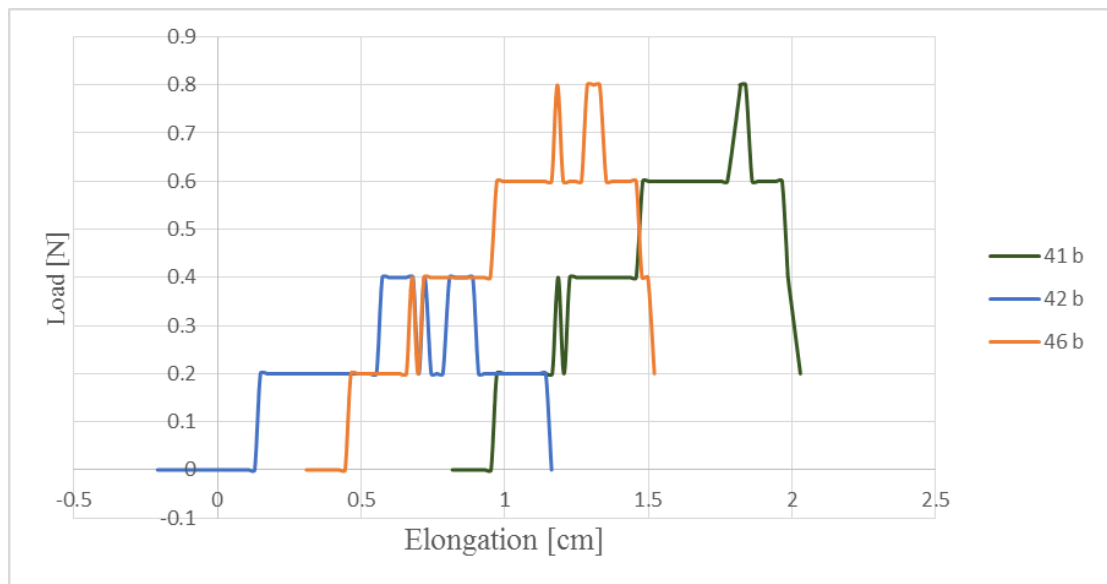


Figure 2-24 Comparing the tensile strength of the **41 b**, **42 b** and **46 b**

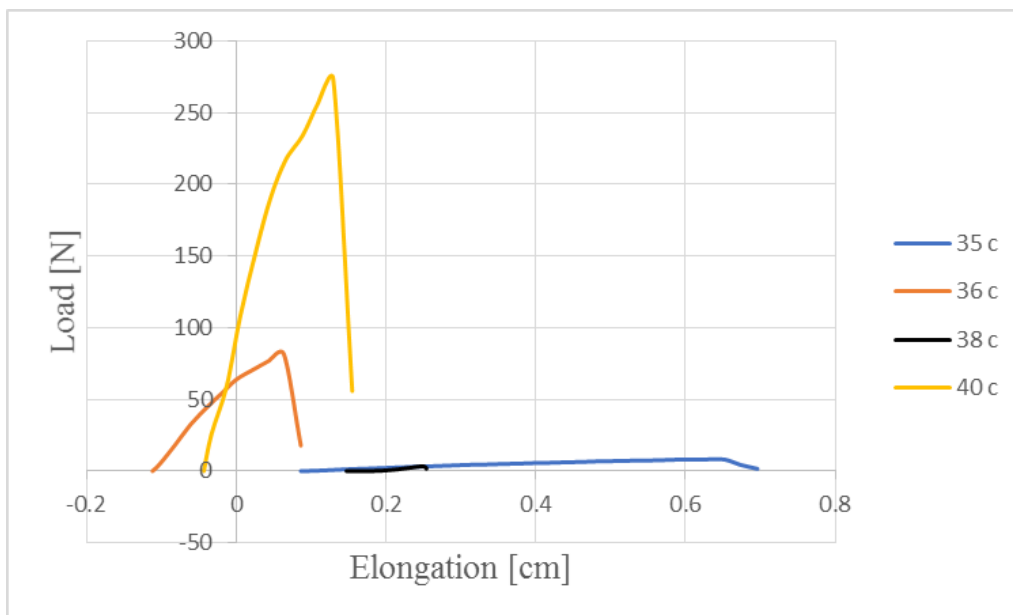


Figure 2-25 Comparing the tensile strength of the **35 c**, **36 c**, **38 c** and **40 c**

The elastomers using **34 c** as diene and compounds **13-18** as dienophiles proved to be too brittle and broke upon attempts to remove them from the moulds. As a result it was not possible to obtain accurate tensile strength measurements for these elastomers.

It was also of interest to compare the tensile strength of the elastomers both before and after healing, with a specific focus on the **35 b** and **35 c** (Figure 2-26). When compared to the virgin elastomer, the healed elastomer **35 b** elongated more after being healed, although a smaller overall force was required before catastrophic failure was observed. Interestingly, with the healed elastomer catastrophic failure did not occur at the scar; failure was always observed within the virgin portion of the elastomer suggesting that the healed portion of the elastomer is in fact more robust than the undamaged areas.

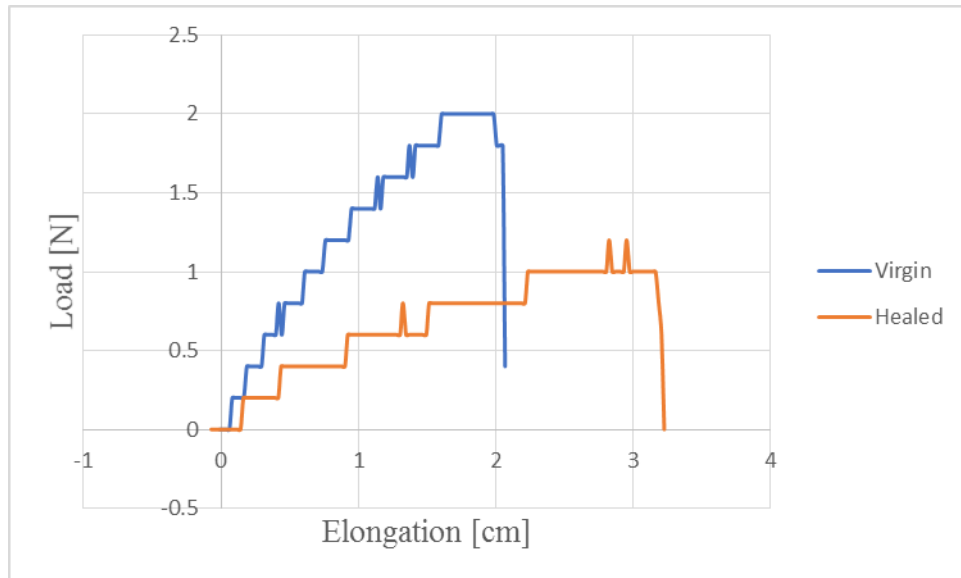


Figure 2-26 Comparing the tensile strength of elastomer **35 b** before and after healing

Given the higher degree of cross-linking found in the PDMS-(iii)-A-4 elastomer, the virgin elastomer possessed a fairly high tensile strength whereas the healed became brittle and lost its elasticity (Figure 2-27).

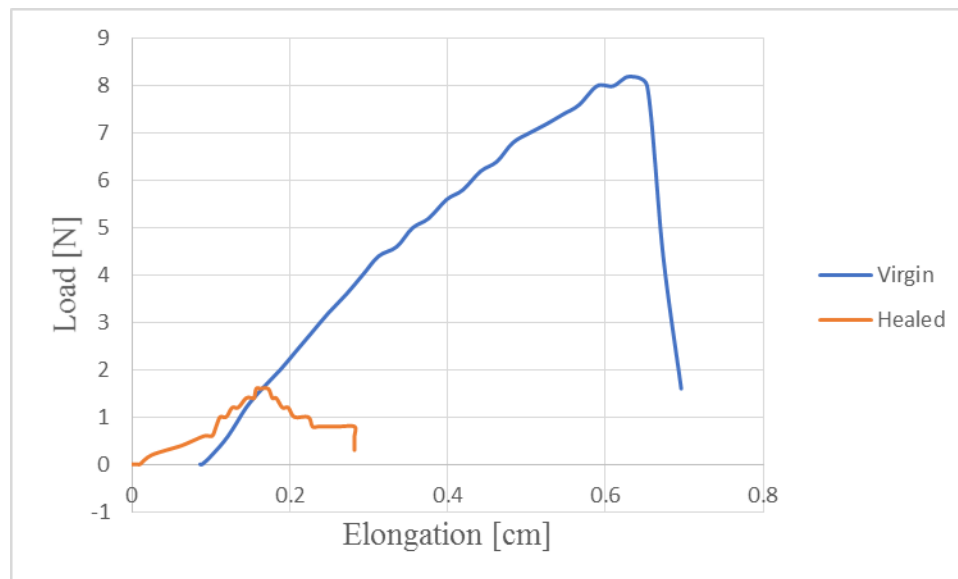


Figure 2-27 Comparing the tensile strength of elastomer **35 c** and after healing

2.6 Differential Scanning Calorimetry (DSC) Analysis of Cross-Linked Elastomers

DSC analysis was performed on model reactions to confirm the temperatures at which DA and rDA reactions were occurring as well as the reproducibility of the reactions. DSC analysis was also performed on the elastomers to ensure that the polymeric networks remained stable, especially for elastomer PDMS-(ii)-A-4 with its low reaction temperature. Seven cycles of heating and cooling were performed from 30 °C to 120 °C with a heating/cooling rate of ± 4 °C and a holding time of 30 min after each step in temperature (Figure 2-28). As was observed with the model reactions, the DA reaction for the elastomer occurred at room temperature. However, since the instrument that was used for this analysis start the heating from 35 °C the DA reaction is observable at approximately 45 °C which is the completion of the reaction not the start point, while the retro DA reaction took place at 100 °C (Figure 2-28). No significant thermal decomposition was observed for the elastomer.

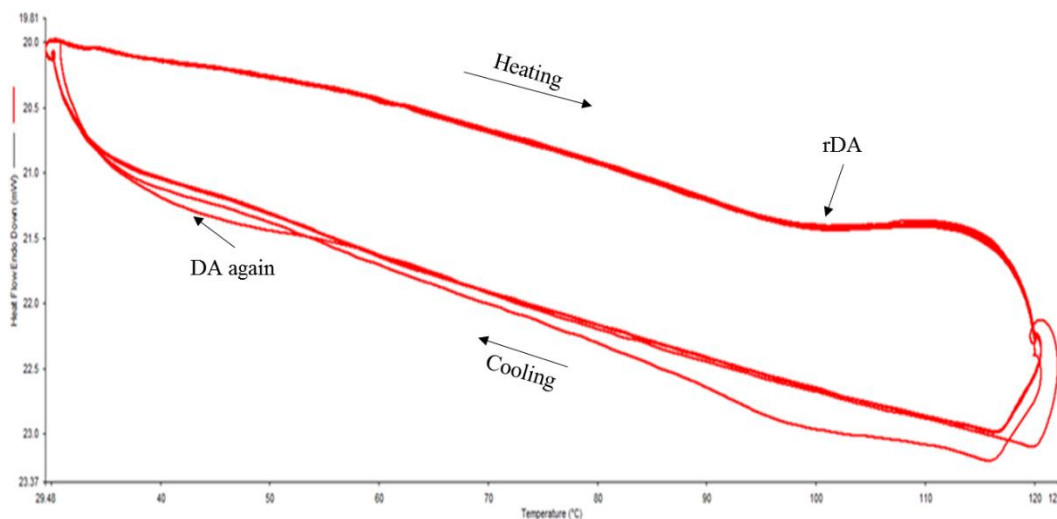


Figure 2-28 DSC thermograms for elastomer 35 b

2.7 Hardness Measurements

The durometer is an instrument used to commonly measure the hardness of polymers, elastomers, and rubbers.¹²⁴ Different scales are applied to different kinds of materials. Silicone polymers typically are subjected to Shore 00 measurements as these materials are typically more resistant to compression stress and indentation. To put the hardness values of the Shore 00 scale into context chewing gum has Shore 00 value of 20 and polyurethane rubbers can have a hardness value between 30 and 70. In this study, the hardness of the elastomers was measured both before damage and after healing (Table 2-4).

Table 2-4 Hardness measurements of synthesized elastomers before and after healing

Elastomer	Shore (00) Hardness		Change in Hardness
	Virgin	Healed	
35 b	66	60.2	-5.8
36 b	62.4	58.7	-3.7
38 b	45.8	36	-9.8
39 b	39.1	31.3	-7.8
40 b	54.8	47.4	-7.4
41 b	34	29.1	-4.9
42 b	32	28	-4
46 b	40	36.7	-3.3
35 c	68.3	56.7	-11.6
36 c	82.4	77.2	-5.2
38 c	76.2	60	-16.2
40 c	64.4	58	-6.4
41 c	78.3	74	-4.3
42 c	70	66.1	-3.9
46 c	66.9	60.2	-6.7

Comparing the hardness of these synthesized elastomers, it can be determined that the elastomers made from higher Si-H percentage (25-30% Si-H) are harder as a result of their higher cross-link density. However, the elastomers made from 7-9% Si-H polymers

are softer and more flexible. The changes in hardness after elastomers being healed varies and no trend can be observed for them.

A summary of the silicone elastomer networks were synthesized is shown in Table 2-5 (the synthesized elastomers' numbers have been written in the coloured boxes). The red boxes represent elastomers that did not cure in the oven after 72 h at 70 °C. The yellow boxes represent elastomers that cured, but did not do so completely; these elastomers were sticky on top or very fragile and could not be removed from the moulds. Green boxes represent perfectly formed elastomers and the black boxes represent elastomers that were not attempted, in spite of the model system results, simply because the cost of the bismaleimide was prohibitive.

The elastomers synthesized from 3-4% Si-H mol% polymer (**33 a** and **34 a**) because of the lower mole percentage of active sites (3-4%) and relatively higher molecular weight ($M_n = 13000$ g/mol) are difficult to be cured and make the elastomers. It seems to be difficult for the dienophiles to find enough diene moieties to do sufficient cross-linking density to get perfect elastomers. So, most of them remained liquid during the 72 h reaction period. Except for the elastomers **35 a** and **36 a** that were using compounds **13** and **14** respectively as the dienophile which produced not perfect elastomers but solid at the bottom and liquid on the top which wasn't solid enough to take out from the mould and do the analysis. Moreover, as it was anticipated none of the DA reactions that were used compound **15** as dienophile went to completion. Because, none of the model DA reactions with this specific dienophile (**15**) yielded DA adducts. Overall, according to the model reactions, the results illustrated in the Table 2-5 were almost predictable.

Table 2-5 Summary of Diels-Alder cross-linked silicone elastomers.^a

Elastomers	Dienophile					
	13	14	15	16	17	18
33 a	35 a	36 a	37 a	38 a	39 a	40 a
33 b	35 b	36 b	37 b	38 b	39 b	40 b
33 c	35 c	36 c	37 c	38 c	39 c	40 c
34 a	41 a	42 a	43 a	44 a	45 a	46 a
34 b	41 b	42 b	43 b	44 b	45 b	46 b
34 c	41 c	42 c	43 c	44 c	45 c	46 c

^a red = systems that did not cure; yellow = elastomers that did not cure completely; green = elastomers that cured completely and could be analyzed further; black = elastomers that were not attempted in spite of the data from the model reactions because the cost of the bismaleimide was prohibitive.

2.8 Conclusions & Future Outlook

The DA reaction was studied in this thesis as a cross-linker for the production of various siloxane elastomer networks. To achieve this goal, furan-modified polysiloxanes with different average molecular weights and different furan concentrations were reacted with a library of bismaleimide compounds. The results illustrated that the novel compound tetramethybis[(N-maleimidomethyl)oxy]disiloxane **13** had the highest maleimide conversion overall, and more importantly the reaction occurred at room temperature and in only 5 h. SEM analysis of these elastomers was used to confirm the self-healing capacity of the elastomers and revealed that, especially with elastomers made with **13**, healing was quite efficient. To the best of my knowledge this is the first, and only, reported case of a self-healing silicone elastomer based on the Diels-Alder reaction where healing occurs at room temperature after the elastomer being heated at around 70 °C – 80 °C for rDA reaction to occur. Which can be a tremendously important property in industry from the view point of using less energy to recycle the elastomers. Moreover, specifically for the

aforementioned elastomer (**35 b**), the double cross-linking in the damaged area made that area stronger than what it was before which can be a really useful property in industry. This was confirmed with the tensile strength measurement of the healed elastomer. As it was illustrated before, the elongation of the healed elastomer compared with the virgin one increased and the breakage of the elastomer did not occur on the same damaged area. Hardness measurements indicated that all of the elastomers after being damaged and healed get softer which can be the result of the smaller amount of cross-link density in the network compared to the virgin elastomers.

The goal of this research was to extend the life-time of the elastomers by making them recyclable and reduce the amount of plastic wastes which leads to less plastic pollution that is a global concern for today's modern lifestyle. The use of bismaleimide molecules as cross-linkers for furan-modified silicone polymers led to the development of recyclable polysiloxane networks whose synthesis, and subsequent healing and recycling, can be temperature controlled because of the DA/rDA reaction and the specific bismaleimide moiety being employed as a cross-linker. Time and temperature are the most important factors in industry of self-healing that was improved in this research by producing clear and colourless elastomers at room temperature in 5 h. For the future studies, the flexibility of the networks can be increased by using silicone polymers modified with both diene and dienophile moieties instead of using molecule bismaleimides.

Chapter 3: Experimental

3.1 Instrumentation

Nuclear Magnetic Resonance (NMR) Spectroscopy. ^1H , ^{13}C , ^{29}Si , variable temperature (VT) and solid-state NMR were carried out using a Bruker AV-300 digital NMR spectrometer with a 7.05 Tesla Ultrashield magnet equipped with a BBFO Z-gradient ATMA probe head.

Infrared Spectroscopy (IR). Attenuated Total Reflectance Fourier Transform IR (ATR-FT-IR) spectra were acquired on a Bruker Alpha Optic GmbH 2012. All spectra were an average of 24 scans at 2 cm^{-1} resolution using neat samples on a diamond window.

Mass Spectrometry (MS). Electron Impact (EI) and Fast Atom Bombardment (FAB) mass spectrometry was performed using a Thermo DFS high-resolution mass spectrometer in positive ion mode.

Thermogravimetric analysis (TGA) and Differential Scanning Calorimetry (DSC). The thermal analyses were conducted using a Perkin-Elmer STA 8000 instrument which has a temperature range from $30\text{ }^\circ\text{C}$ to $1600\text{ }^\circ\text{C}$. Octadecane was used for calibration ($27.95\text{ }^\circ\text{C}$ melting point) while aluminium was used as the standard.

Scanning Electron Microscopy (SEM). The samples were mounted onto SEM stubs with double-sided carbon tape and then placed into the chamber of a Polaron Model E5100 sputter coater (Polaron Equipment Ltd., Watford, Hertfordshire) and approximately 15 nm of gold was deposited onto the stubs. The samples were viewed in a Tescan Vega II LSU scanning electron microscope (Tescan USA, PA) operating at 10kV.

Tensile Strength. A MARK-10 single-column force tensiometer consisting of: a M5-200 force gauge, ESM303 compression test stand, G1101 vise-action grip was used to analyze the tensile strength of the elastomer samples.

Durometer. A digital durometer (*Check-Line* OS-1E) was used to measure Shore 00 according to ASTM D-2240.

3.2 Materials

Toluene, tetrahydrofuran (THF), diethyl ether, n-butyl lithium, furan, 11-bromoundec-1-ene, *N,N'*-(1,3-phenylene)dimalimide, silica gel (230-400 mesh), molecular sieves (4Å beads, 8-12 mesh), 10-undecenoic acid, furfuryl alcohol, Pt(0)-1,3-divinyl-1,1,3,3-tetramethyldisiloxane complex (Karstedt's catalyst, Pt(dvs)) in xylenes, lipase B from *C. antarctica* immobilized on Lewatit VPOC1600 cross-linked divinylbenzene resin (Novozym-435, N435), trimethylsilyl terminated-poly(dimethylsiloxane-co-methylhydrosiloxane) (3-4% methylhydrosiloxane) with an average M_n of 13,000 g/mol (**32 a**), trimethylsilyl terminated-poly(dimethylsiloxane-co-methylhydrosiloxane) (7-9% methylhydrosiloxane) with an approximate molecular weight of 5,500-6,500 g/mol (**32 b**) and trimethylsilyl terminated-poly(dimethylsiloxane-co-methylhydrosiloxane) (25-30% methylhydrosiloxane) with an approximate molecular weight of 2,000-2,600 g/mol (**32 c**) were obtained from Sigma–Aldrich (Oakville, Ontario, Canada). Heptamethyltrisiloxane was obtained from Gelest (Morristown, PA, USA). All compounds were used as received unless otherwise stated.

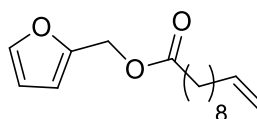
3.3 Synthesis of the Model Compounds

All the reactions were performed under nitrogen atmosphere. Molecular sieves were kept in the oven at least five days prior to being used.

3.3.1 Synthesis of the Diene

Two different diene systems were synthesized in order to make a library of elastomers and to compare their properties.

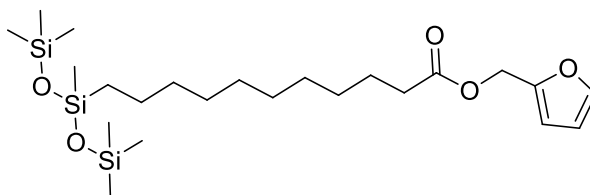
3.3.1.1 Synthesis of furan-2-ylmethyl undec-10-enoate (**3**)



Furfuryl alcohol (1.96 g, 20 mmol) was added to a solution of 10-undecenoic acid (1.85 g, 10 mmol) in toluene (15 mL). Afterwards, the enzymatic catalyst N435 (4% w/w, 0.15 g) was introduced to the flask followed by the addition of molecular sieves (about 1 g). The reaction mixture heated to 110 °C and stirred for 48 h. The reaction mixture filtered through a medium porosity fritted Büchner funnel containing a 2 cm Celite® pad and the solvent was removed using a rotary evaporator. The crude product was dissolved in diethyl ether and washed with distilled water and then extracted with a saturated solution of sodium bicarbonate and brine (x3 each). The organic layer was dried over anhydrous sodium sulfate and the light yellow oil was purified using silica gel column chromatography using 9:1 hexane:ethyl acetate as the elution solvent to yield **3**¹²² as a colourless liquid (28.7 g, 0.11 mol, 83 %). Spectral analyses were consistent with published data¹²⁵. ¹H NMR (300 MHz, CDCl₃) δ 7.42 (dd, *J* = 0.63, 0.57 Hz, 1H), δ 6.35-6.40 (m, 2H), δ 5.74-5.90 (m, 1H), δ 5.74 (s, 2H), δ 4.90-5.02 (m, 2H), δ 2.32 (t, *J* = 7.4 Hz, 2H), δ 2.03 (q, *J* = 6.8 Hz, 2H),

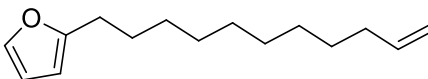
δ 1.60-1.64 (m, 2H), δ 1.27 (s, 10H). ^{13}C $\{^1\text{H}\}$ NMR (101 MHz, CDCl_3) δ 173.45, 149.66, 143.18, 139.18, 114.13, 110.52, 110.45, 57.86, 34.14, 29.25, 29.03, 28.90, 24.85 ppm.

3.3.1.2 Synthesis of furanyl-2-methyl-11-(1,1,1,3,5,5,5-heptamethyltrisiloxan-3-yl)undecanoate (**5**)



After dissolving **3** (2.64 g, 10 mmol) in toluene (10 mL) and heating the reaction to 85 °C in a 100 mL round bottom flask equipped with a condenser, 1,1,1,3,5,5,5-heptamethyltrisiloxane (2.50 g, 11.2 mmol) was introduced to the flask and stirred for 10 min followed by the addition of Karstedt's catalyst (25 μL). The reaction mixture stirred over night until ^1H NMR confirmed that there was no longer a Si-H resonance in the spectrum. After the completion of the reaction, activated carbon was added to the mixture at room temperature and stirred for 2 h. The reaction was then vacuum filtered through a pad of Celite[®] using a Büchner funnel to yield **5**¹²⁵ (4.13 g, 9.1 mmol, 81%) as a light yellow oil. Spectral analyses were consistent with published data¹²⁵. ^1H NMR (300 MHz, CDCl_3) δ 7.42 (s, 1H), δ 6.35-6.39 (m, 2H), δ 5.05 (s, 2H), δ 2.32 (t, $J = 7.5$ Hz, 2H), δ 1.61 (t, $J = 7.2$ Hz, 2H), δ 1.26 (s, 14H), δ 0.44 (t, $J = 7.5$ Hz, 2H), δ 0.08 (s, 18H), δ -0.01 (s, 3H). ^{13}C $\{^1\text{H}\}$ NMR (101 MHz, CDCl_3) δ 173.47, 143.17, 110.52, 110.44, 57.84, 34.16, 33.22, 29.49, 29.46, 29.33, 29.23, 29.09, 24.88, 23.06, 17.62, 1.85, -0.27 ppm. ^{29}Si $\{^1\text{H}\}$ NMR (60 MHz, CDCl_3) δ 6.76 ppm.

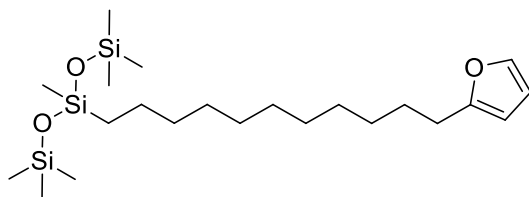
3.3.1.3 Synthesis of 2-(undec-10-en-1-yl)furan (**8**)



The THF was dried over molecular sieves 5 days before being used. Furan was distilled over KOH and under nitrogen immediately before use. THF (80 mL) was cooled in an ice bath prior the addition of n-buthyllithium (20 mL, 48 mmol, 2.5 M solution in pentane). The freshly distilled furan (3.4 mL, 50 mmol) was added drop-wise to the reaction flask and allowed to stir for 30 min at 0 °C. 11-Bromoundec-1-ene (9.32 g, 40 mmol) was introduced to the reaction mixture slowly at room temperature and the reaction was allowed to stir over night. The reaction mixture was quenched with a saturated aqueous solution of NH₄Cl (40 mL) and then extracted with ethyl acetate (3 x 40 mL). After drying the organic phase with MgSO₄ and removing the solvent using a rotary evaporator, compound **8** was obtained from column chromatography using n-hexane (7.5 g, 34.1 mmol, 85%)¹²⁶ as the elution solvent as a clear and colourless liquid. Spectral analyses were consistent with published data¹²⁶. ¹H NMR (300 MHz, CDCl₃) δ 7.29 (d, *J* = 1.2 Hz, 1H), δ 6.27 (dd, *J* = 2.0, 1.9 Hz, 1H), δ 5.98 (t, *J* = 2.8 Hz, 1H), δ 5.75-5.90 (m, 1H), δ 4.91-5.03 (m, 2H), δ 2.62 (t, *J* = 7.5 Hz, 2H), δ 2.05 (q, *J* = 6.7 Hz, 2H), δ 1.60-1.69 (m, 2H), δ 1.30 (s, 12H). ¹³C {¹H} NMR (101 MHz, CDCl₃) δ 156.63, 140.60, 139.24, 114.09, 110.01, 104.49, 33.81, 29.48, 29.45, 29.33, 29.17, 29.12, 28.93, 28.03, 27.98 ppm.

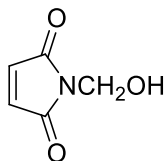
3.3.1.4 Synthesis of 3-(11-(furan-2-yl)undecyl)-1,1,1,3,5,5,5-heptamethyltrisiloxane

(9)



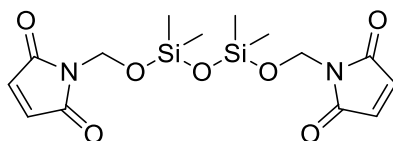
After dissolving **8** (2.64 g, 10 mmol) in toluene (10 mL) and heating the solution to 85 °C in a 100 mL round bottom flask equipped with a condenser, 1,1,1,3,5,5,5-heptamethyltrisiloxane (2.5 g, 11.2 mmol) was added to the solution and stirred for 10 min prior to the addition of Karstedt's catalyst (25 μ L). The reaction mixture stirred over night until ^1H NMR confirmed that there is no Si-H resonances remained in the spectrum. After the hydrosilylation was complete, activated carbon was added to the mixture at room temperature and stirred for 2 h and the mixture was subsequently vacuum filtered through a pad of Celite[®] using a Büchner funnel to compound **9** (4.25 g, 9.6 mmol, 80%) as a light yellow liquid. ^1H NMR (300 MHz, CDCl_3) δ 7.28 (d, $J = 1.2$ Hz, 1H), δ 6.35-6.39 (dd, 2H), δ 5.05 (s, 2H), δ 2.32 (t, $J = 7.5$ Hz, 2H), δ 1.61 (t, $J = 7.2$ Hz, 2H), δ 1.26 (s, 14H), δ 0.44 (t, $J = 7.5$ Hz, 2H), δ 0.08 (s, 18H), δ -0.01 (s, 3H). ^{13}C $\{^1\text{H}\}$ NMR (101 MHz, CDCl_3) δ 156.65, 140.59, 110.00, 104.48, 33.23, 29.65, 29.58, 29.37, 29.19, 29.04, 27.98, 23.06, 17.62, 1.85, -0.27 ppm. ^{29}Si $\{^1\text{H}\}$ NMR (60 MHz, CDCl_3) δ 6.76 ppm.

3.3.1.5 Synthesis of N-hydroxymethylmaleimide (11)



Compound **11** was synthesized from a suspension of maleimide (24.5 g, 0.25 mol) in 37% formalin (20.3 ml, 0.72 mol) to which 0.75 mL of a 5% sodium hydroxide solution was added over 10 min at 30 °C. The reaction was allowed to stir for 3 h at 30 °C. After filtration, the crude product was recrystallized from ethyl acetate to obtain **11** (24 g, 0.19 mol, 76%). Spectral analyses were consistent with published data. ¹H NMR (300 MHz, CDCl₃) δ 6.77 (s, 2H), δ 5.08 (d, *J* = 7.8, 2H), δ 2.95 (t, *J* = 7.9 Hz, 1H). ¹³C {¹H} NMR (101 MHz, CDCl₃) δ 170.07, 134.63, 61.13 ppm.

3.3.1.6 Synthesis of tetramethylbis[(N-maleimidomethyl)oxy]disiloxane (**13**)



Compound **11** (25.5 g, 0.2 mol) was dissolved in dry THF (50 mL), followed by the addition of triethylamine (27.9 mL, 0.2 mol) and 1,3-dichloro-1,1,3,3-tetramethyldisiloxane (20.3 g, 0.1 mol). The reaction mixture stirred at room temperature for 4 h under a nitrogen atmosphere. The crude mixture was filtered through a sintered glass Büchner funnel and the filtered inorganic salts were washed with diethylether. After removing the solvent, diethylether (40 mL) was added to the reaction mixture and it was washed with distilled water (3x20 mL), dried over sodium sulfate, filtered, and concentrated using a rotary evaporator to yield compound **13** as a white, shiny powder (29 g, 0.075 mol, 76.3%). ¹H NMR (300 MHz, CDCl₃) δ 6.75 (s, 4H), δ 5.14 (s, 4H), δ 0.16 (s, 12H). ¹³C {¹H} NMR (101 MHz, CDCl₃) δ 169.82, 134.56, 60.01, -1.11 ppm. ²⁹Si {¹H} NMR (60 MHz, CDCl₃) δ -10.08 ppm. High-Res MS-FAB+ [C₁₄H₂₀N₂O₇Si₂ + NH₄]⁺ : 402

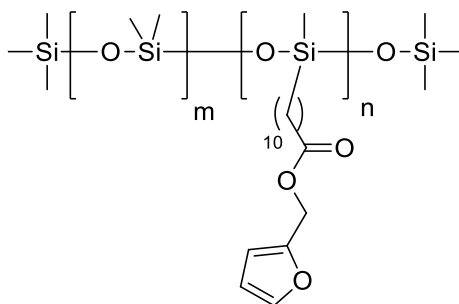
amu, $[\text{C}_{14}\text{H}_{20}\text{N}_2\text{O}_7\text{Si}_2 + \text{Na}]^+$: 407 amu, $[\text{C}_{14}\text{H}_{20}\text{N}_2\text{O}_7\text{Si}_2 + \text{K}]^+$: 423 amu. Elemental Analysis (%): Calculated: C: 43.73, H: 5.24, Found: C: 43.59, H: 5.16.

3.3.1.7 Model Diels-Alder Reactions

All of the 12 model Diels-Alder reactions were set up at one of the following temperatures, five various temperatures 40 °C, 50 °C, 60 °C, 70 °C and 80 °C, in an effort to optimize the reaction temperature and maleimide conversion. The reactions were performed neat in 2 dram vials with a 1:1 mole ratio of diene:dienophile. The reactions were stirred 24 h to yield the DA adduct. The ^1H NMR spectra for these reactions can be found in the appendix.

3.4 Synthesis of the Elastomers

3.4.1 Synthesis of furan-2-ylmethylundecanoatesiloxane-dimethylsiloxane copolymers (33 a, 33 b, 33 c)



Trimethylsilyl-terminated poly(dimethylsiloxane-*co*-methylhydrosiloxane) (**32 a**, **32 b**, **32 c**) was dissolved separately in toluene (80 mL) before the addition of Karstedt's catalyst (180 μL). After 10 min of stirring, compound added to the flask under reflux and stirred overnight. Activated charcoal was added to the reaction after it was cooled to the room temperature and stirring continued for an additional 5 h. The reaction was filtered through a pad of Celite[®] using Büchner funnel to yield polymer after removal of the solvent (Table 3-1). ^1H NMR (**33 a**) (300 MHz, CDCl_3) δ = 7.40 (d, 1.9 Hz, 1H), 6.38-6.34 (m,

2H), 5.04 (s,2H), 2.33-2.28 (m, 2H), 1.63-1.58 (m, 2H), 1.24 (m, 14H), 0.50-0.45 (m, 2H), 0.06 (s, 167H). ^{13}C $\{^1\text{H}\}$ NMR (101 MHz, CDCl_3) δ = 173.38, 149.69, 143.15, 110.51, 110.43, 57.83, 34.15, 33.34, 29.49, 29.39, 29.26, 29.10, 24.88, 22.97, 17.49, 1.77, 1.51, 0.52, -0.50. ^{29}Si $\{^1\text{H}\}$ NMR (60 MHz, CDCl_3) δ = -21.95. IR: ν = 1743 cm^{-1} (C=O), 1258 cm^{-1} (C-O).

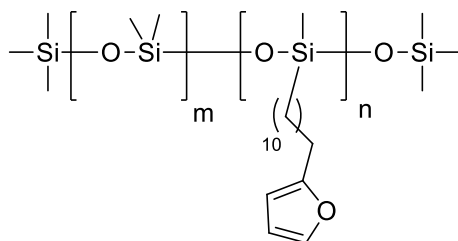
^1H NMR (**33 b**) (300 MHz, CDCl_3) δ = 7.40 (d, 1.9 Hz, 1H), 6.39-6.35 (m, 2H), 5.05 (s,2H), 2.33-2.28 (m, 2H), 1.63-1.58 (m, 2H), 1.24 (m, 14H), 0.51-0.46 (m, 2H), 0.06 (s, 77H). ^{13}C $\{^1\text{H}\}$ NMR (101 MHz, CDCl_3) δ = 173.38, 149.69, 143.13, 110.50, 110.41, 57.81, 34.13, 33.32, 29.49, 29.38, 29.25, 29.09, 24.88, 22.96, 17.49, 1.75, 1.51, 0.52, -0.50. ^{29}Si $\{^1\text{H}\}$ NMR (60 MHz, CDCl_3) δ = 7.20, -21.97. IR: ν = 1742 cm^{-1} (C=O), 1258 cm^{-1} (C-O).

^1H NMR (**33 c**) (300 MHz, CDCl_3) δ = 7.41 (s, 1H), 6.39-6.35 (m, 2H), 5.05 (s,2H), 2.34-2.29 (t, J = 7.5 Hz, 2H), 1.64-1.59 (t, J = 7.0 Hz, 2H), 1.25 (m, 14H), 0.52-0.47 (m, 2H), 0.07 (s, 19H). ^{13}C $\{^1\text{H}\}$ NMR (101 MHz, CDCl_3) δ = 173.36, 149.73, 143.13, 110.50, 110.41, 57.82, 34.11, 33.32, 29.49, 29.38, 29.25, 29.11, 24.88, 22.96, 17.49, 1.51, 0.52, -0.50. ^{29}Si $\{^1\text{H}\}$ NMR (60 MHz, CDCl_3) δ = -21.94. IR: ν = 1742 cm^{-1} (C=O), 1258 cm^{-1} (C-O).

Table 3-1 Moles and masses used for synthesizing compounds **33 a**, **33 b** and **33 c** and their yields

Polymer	Mole required/Mass used		
	32 a	32 b	32 c
	10 mmol/25 g	23 mmol/25 g	35 mmol/10 g
Compound 3	10 mmol/2.64 g	23 mmol/6.1 g	35 mmol/9.2 g
Product (Yield)	33 a (20 g, 80 %)	33 b (21 g, 84 %)	33 c (7.6 g, 76 %)

3.4.2 Synthesis of furan-2-ylmethylundecanoatesiloxane-dimethylsiloxane copolymers (34 a, 34 b, 34 c)



Trimethylsilyl-terminated poly(dimethylsiloxane-*co*-methylhydrosiloxane (**32 a**, **32 b**, **32 c**) was separately dissolved in toluene (80 mL) before the addition of Karstedt's catalyst (180 μ L). After 10 min of stirring, compound **8** was added to the reaction flask. The reaction was heated to reflux and stirred overnight. Activated charcoal was added to the mixture after it had cooled to room temperature and the mixture continued to stir for an additional 5 h. The reaction was then filtered through a pad of Celite[®] using Büchner funnel to yield polymer after rotary evaporation (Table 3-2). ¹H NMR (**34 a**) (300 MHz, CDCl₃) δ = 7.30 (s, 1H), 6.27 (s, 1H), 5.96 (d, J = 2.5 Hz, 1H), 2.63-2.58 (t, J = 7.5 Hz, 2H), 1.66-1.61 (t, J = 7.2 Hz, 2H), 1.28 (m, 16H), 0.53-0.48 (m, 2H), 0.08 (s, 88H). ¹³C {¹H} NMR (101 MHz, CDCl₃) δ = 140.55, 110.00, 104.47, 33.33, 29.68, 29.56, 29.40, 29.22, 28.04, 27.98, 22.96, 17.50, 1.77, 1.51, 1.03, 0.53, -0.47. ²⁹Si {¹H} NMR (60 MHz, CDCl₃) δ = -21.95. IR: ν = 1257 cm⁻¹ (C-O).

¹H NMR (**34 b**) (300 MHz, CDCl₃) δ = 7.29 (s, 1H), 6.27 (s, 1H), 5.96 (d, J = 2.5 Hz, 1H), 2.64-2.59 (t, J = 7.5 Hz, 2H), 1.66-1.61 (t, J = 7.2 Hz, 2H), 1.27 (m, 16H), 0.53-0.48 (m, 2H), 0.08 (s, 88H). ¹³C {¹H} NMR (101 MHz, CDCl₃) δ = 140.58, 109.99, 104.47, 33.35, 29.68, 29.57, 29.40, 29.20, 28.05, 27.98, 22.96, 17.50, 1.77, 1.51, 1.03, 0.53, -0.48. ²⁹Si {¹H} NMR (60 MHz, CDCl₃) δ = -21.95. IR: ν = 1257 cm⁻¹ (C-O).

^1H NMR (**34 c**) (300 MHz, CDCl_3) δ = 7.29 (s, 1H), 6.27 (s, 1H), 5.96 (d, J = 2.5 Hz, 1H), 2.64-2.59 (t, J = 7.5 Hz, 2H), 1.66-1.61 (t, J = 7.2 Hz, 2H), 1.27 (m, 16H), 0.53-0.48 (m, 2H), 0.08 (s, 20H). ^{13}C $\{^1\text{H}\}$ NMR (101 MHz, CDCl_3) δ = 140.58, 109.99, 104.47, 33.35, 29.68, 29.57, 29.40, 29.20, 28.05, 27.98, 22.96, 17.50, 1.77, 1.51, 1.03, 0.53, -0.48. ^{29}Si $\{^1\text{H}\}$ NMR (60 MHz, CDCl_3) δ = -21.95. IR: ν = 1258 cm^{-1} (C-O).

Table 3-2 Moles and masses used for synthesizing compounds **34 a**, **34 b** and **34 c** and their yields

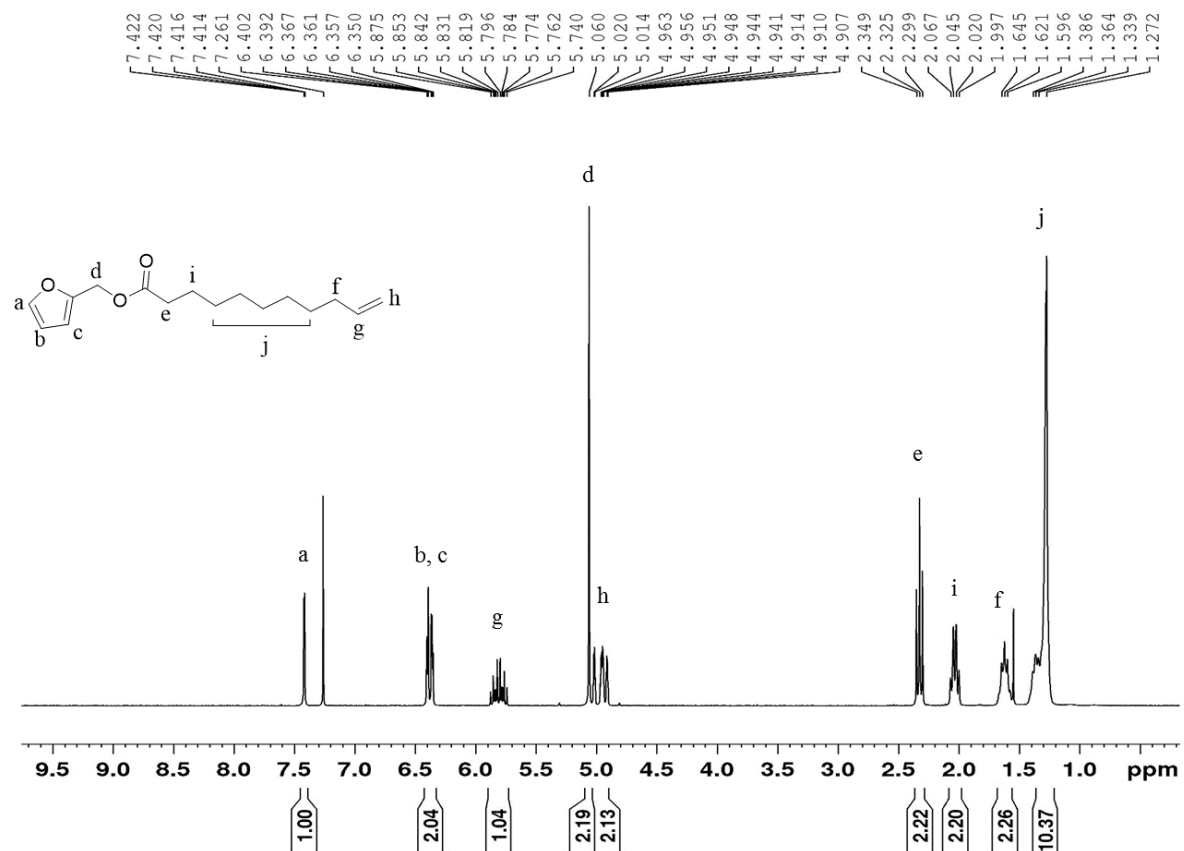
Polymer	Mole required/Mass used		
	32 a	32 b	32 c
	10 mmol/25 g	23 mmol/25 g	35 mmol/10 g
Compound 8	10 mmol/2.20 g	23 mmol/5.06 g	35 mmol/7.7 g
Product (Yield)	34 a (22 g, 88 %)	34 b (23.5 g, 94 %)	34 c (6.8 g, 68 %)

3.4.3 DA Synthesis in the Mould (Elastomers)

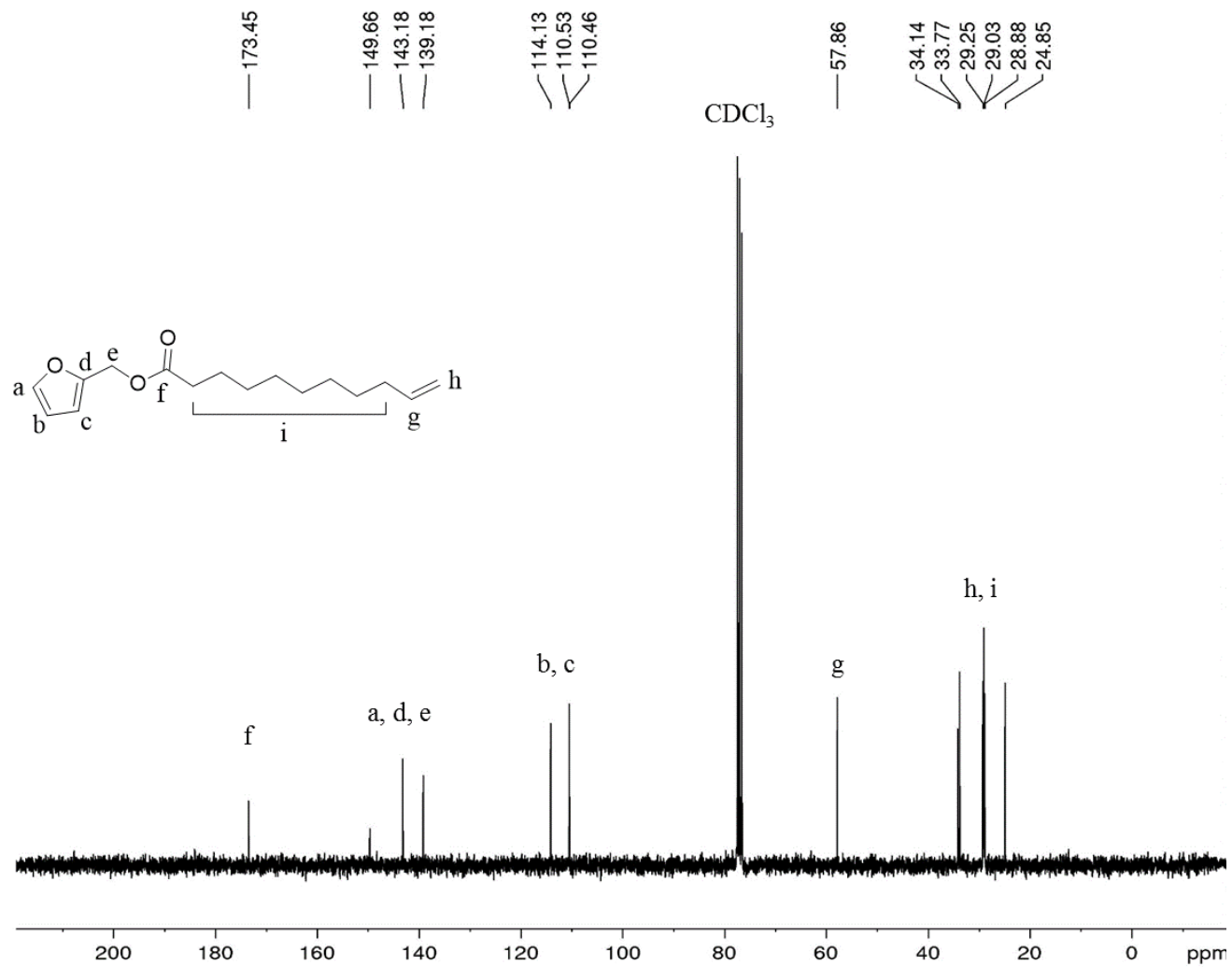
To synthesize the silicone elastomers in the mould, the diene and dienophile compounds were dissolved in chloroform and ultrasonicated for 30 min at 35 °C, to produce a homogeneous mixture. After mixing the solvent was removed *in vacuo* at room temperature and the reaction mixture was added to the mould and put into the oven for 24 h at 60 °C-70 °C in order to form the cross-linked elastomers. This method was applied to the synthesis of all of the elastomers except for the ones involving the tetramethybis[(*N*-maleimidomethyl)oxy]disiloxane **13** as the dienophile as these elastomers were formed at room temperature over 5 h.

3.4.3.1.1 Appendix

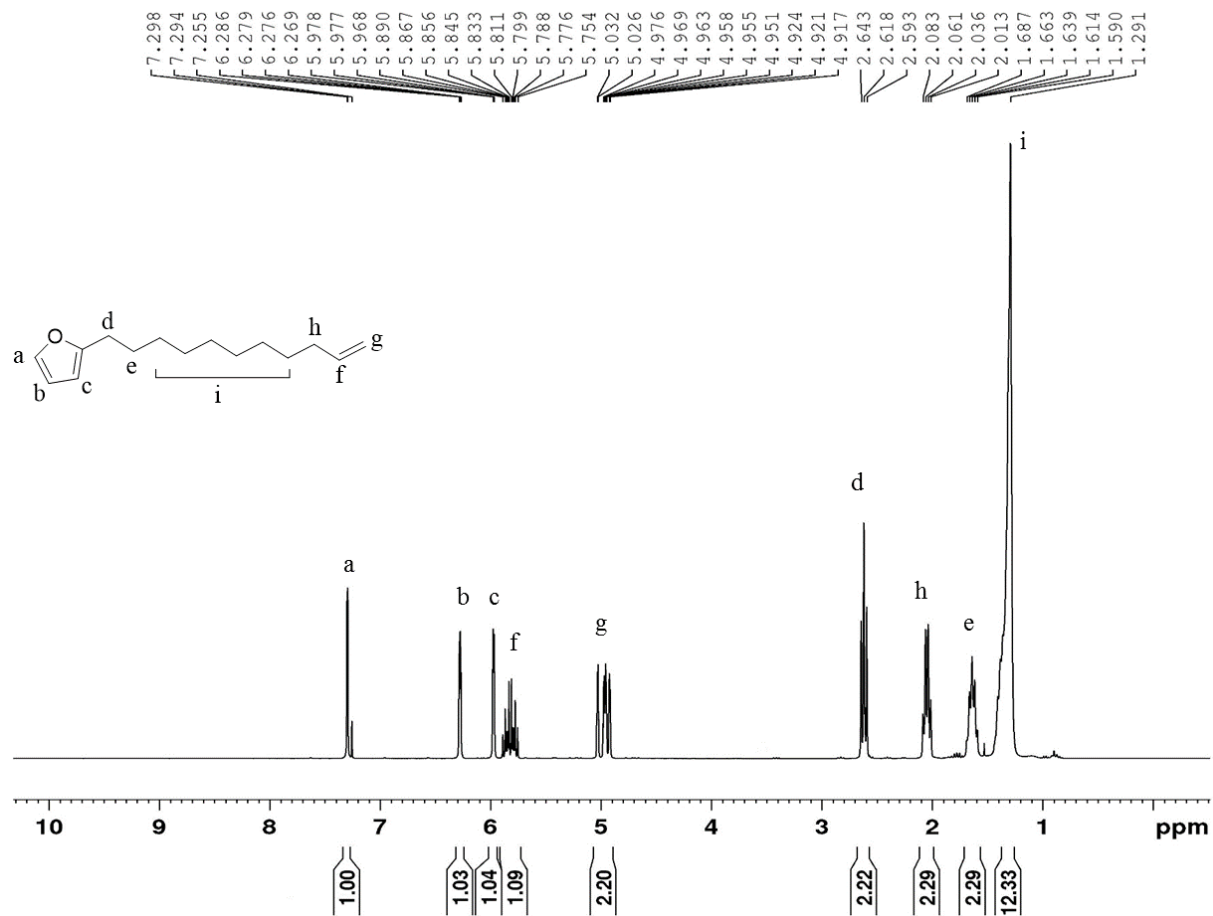
➤ Synthesized Molecules Characterization



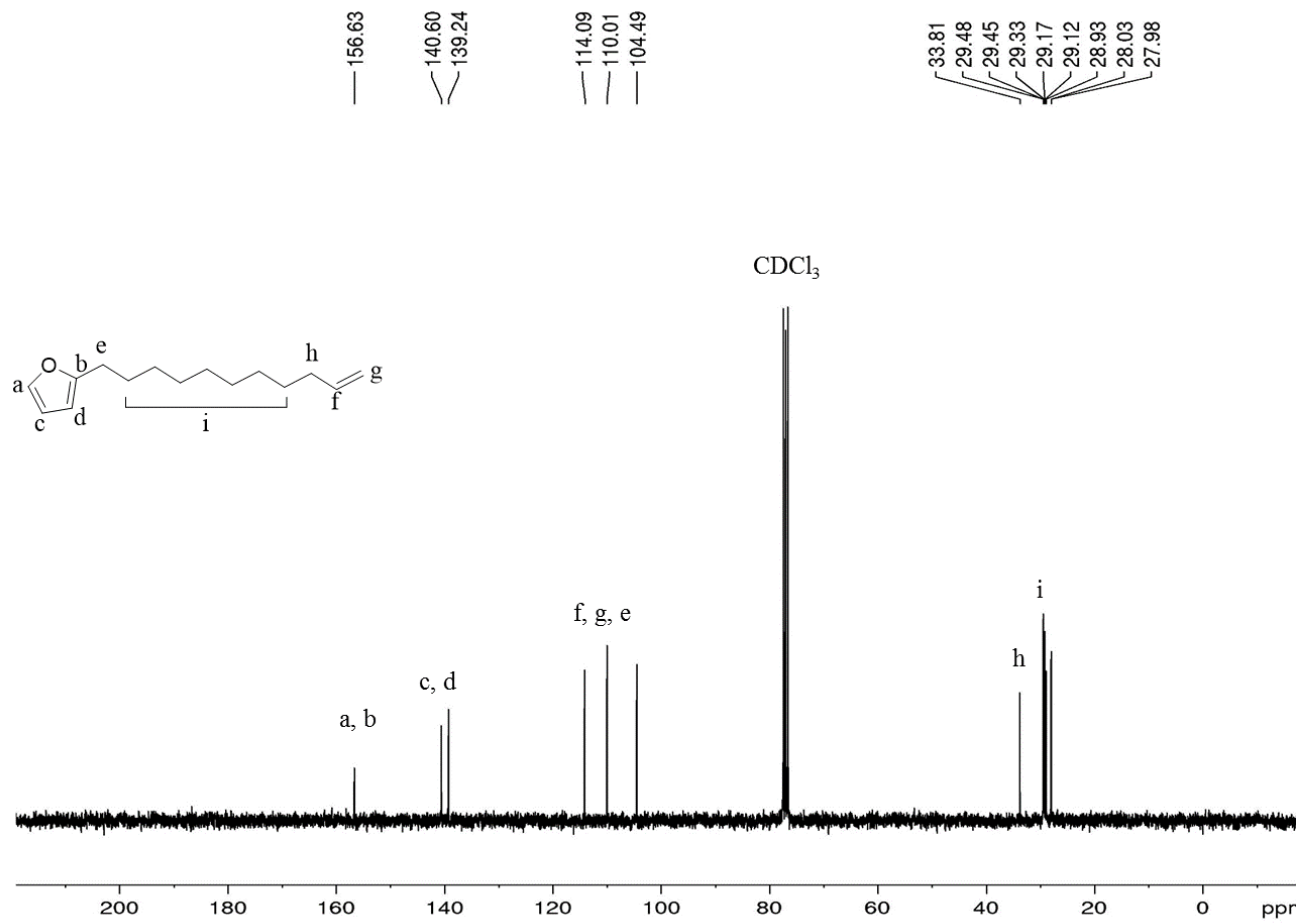
Appendix Figure 1 ¹H NMR of compound 3



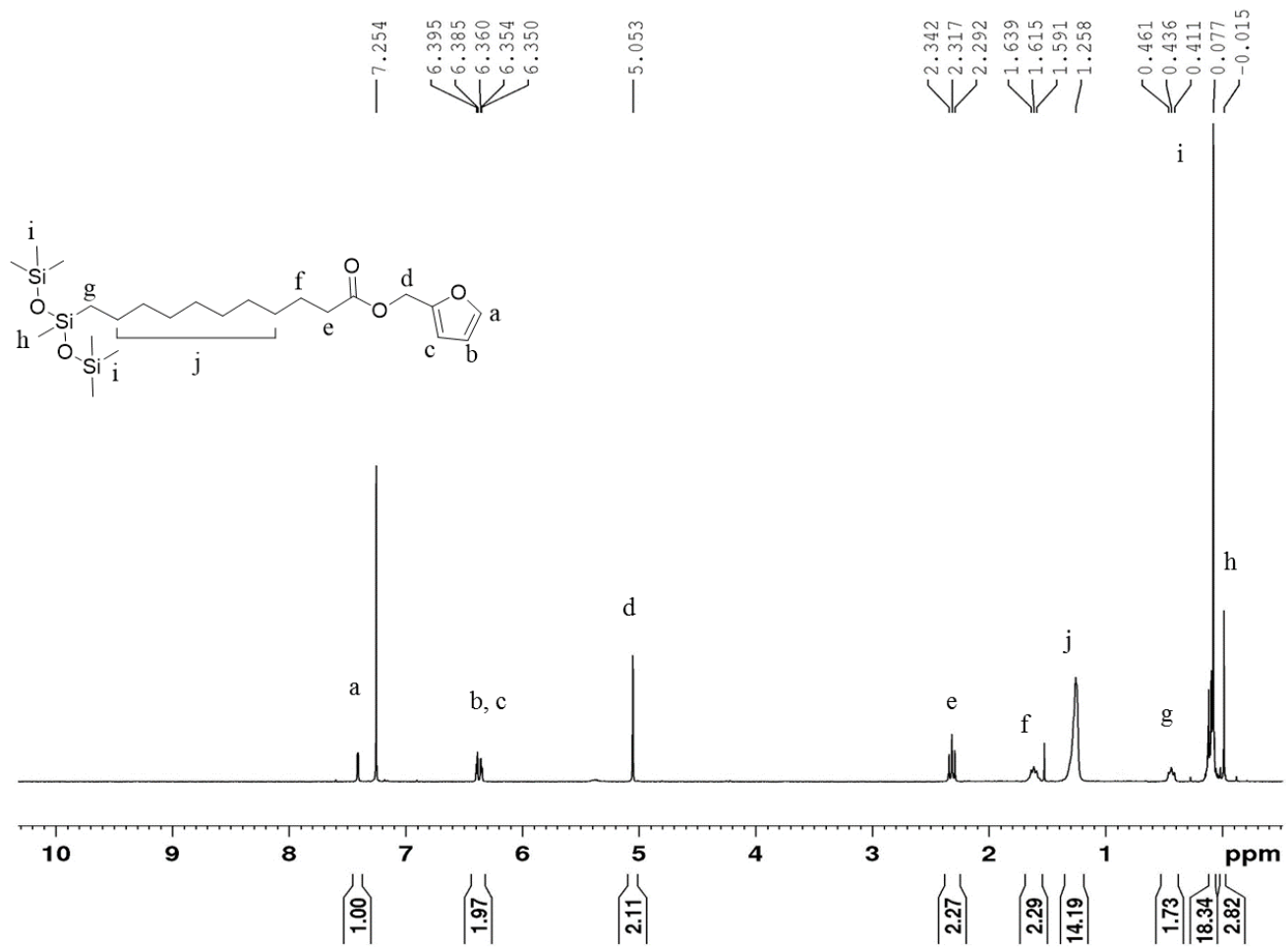
Appendix Figure 2 ^{13}C NMR of compound 3



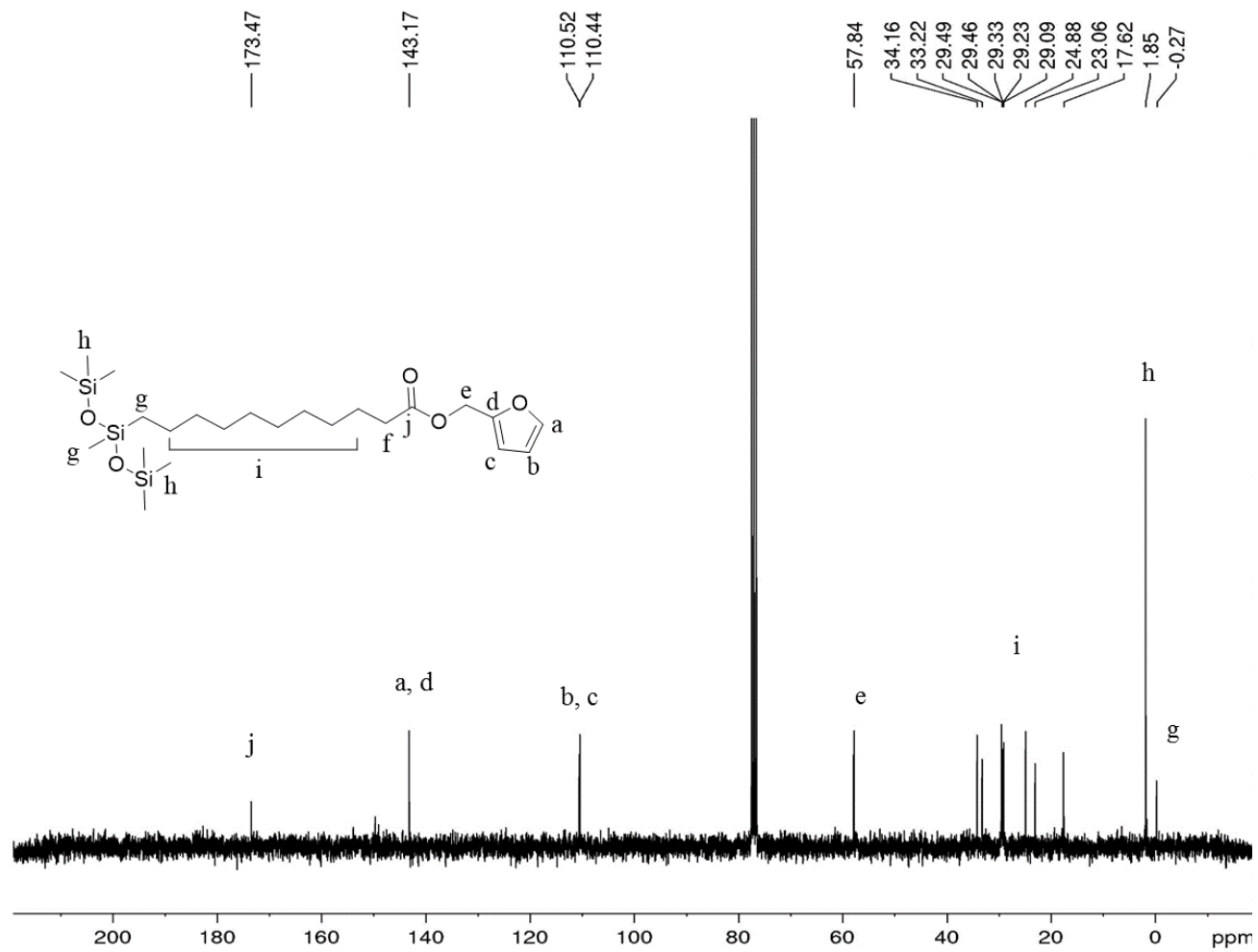
Appendix Figure 3 ¹H NMR of compound 8



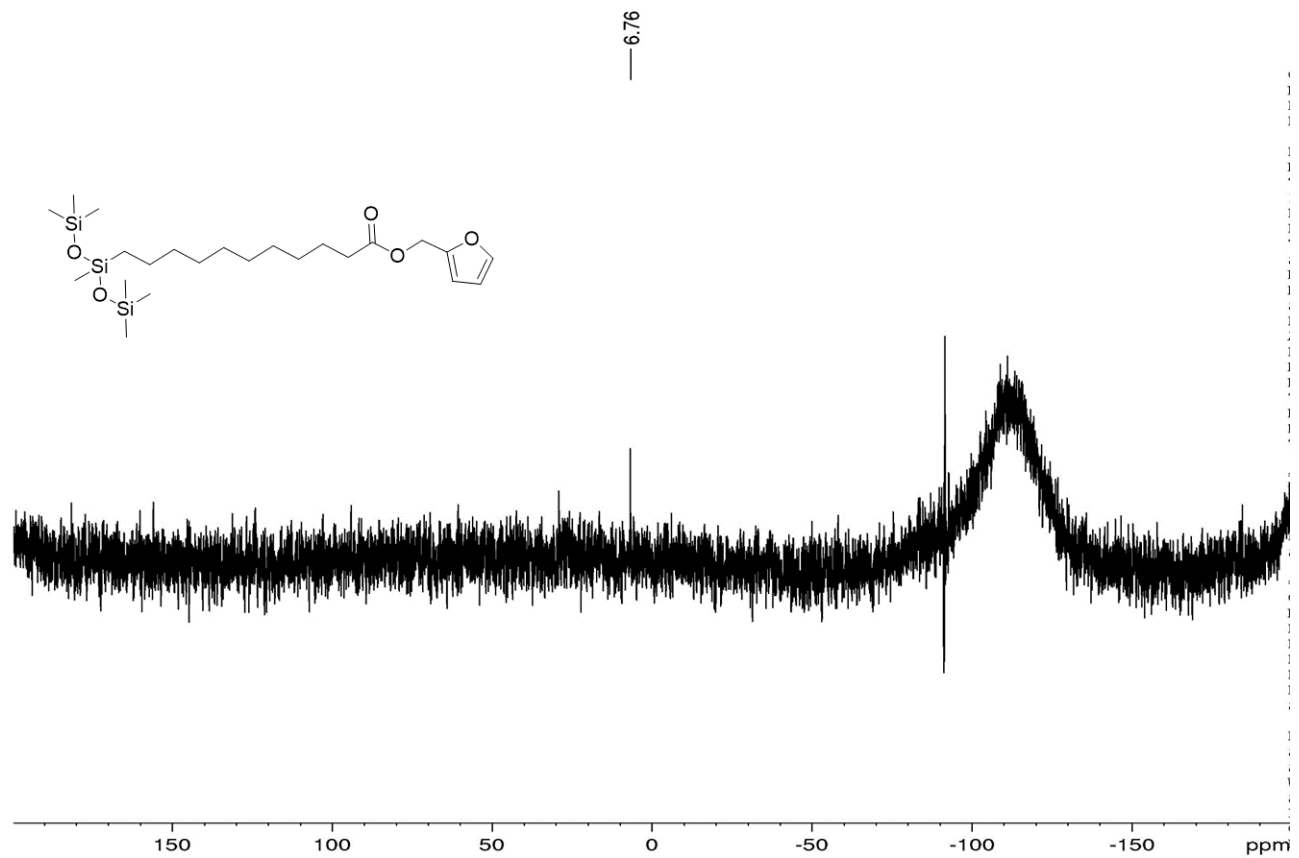
Appendix Figure 4 ^{13}C NMR of compound **8**



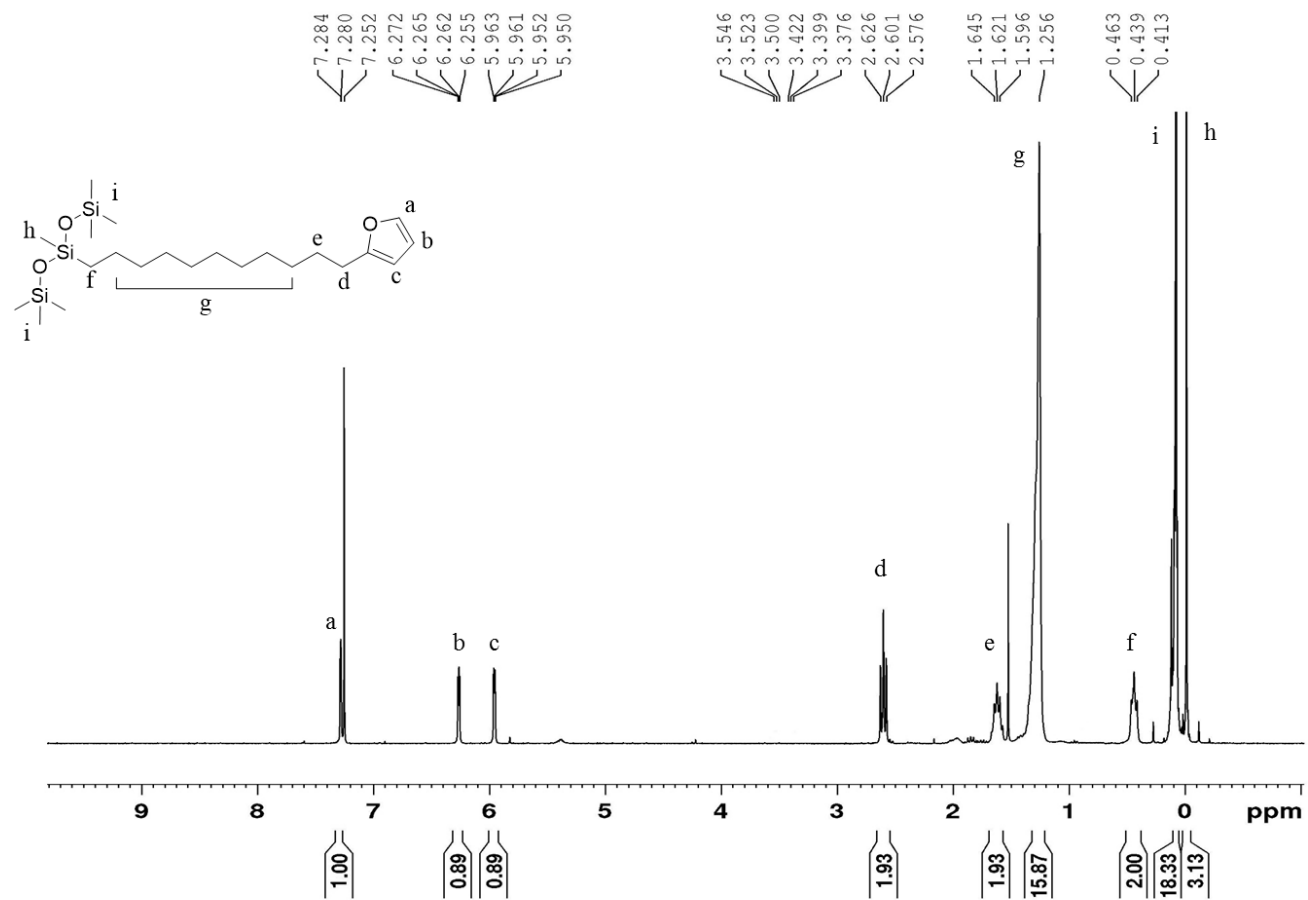
Appendix Figure 5 ¹H NMR of compound 5



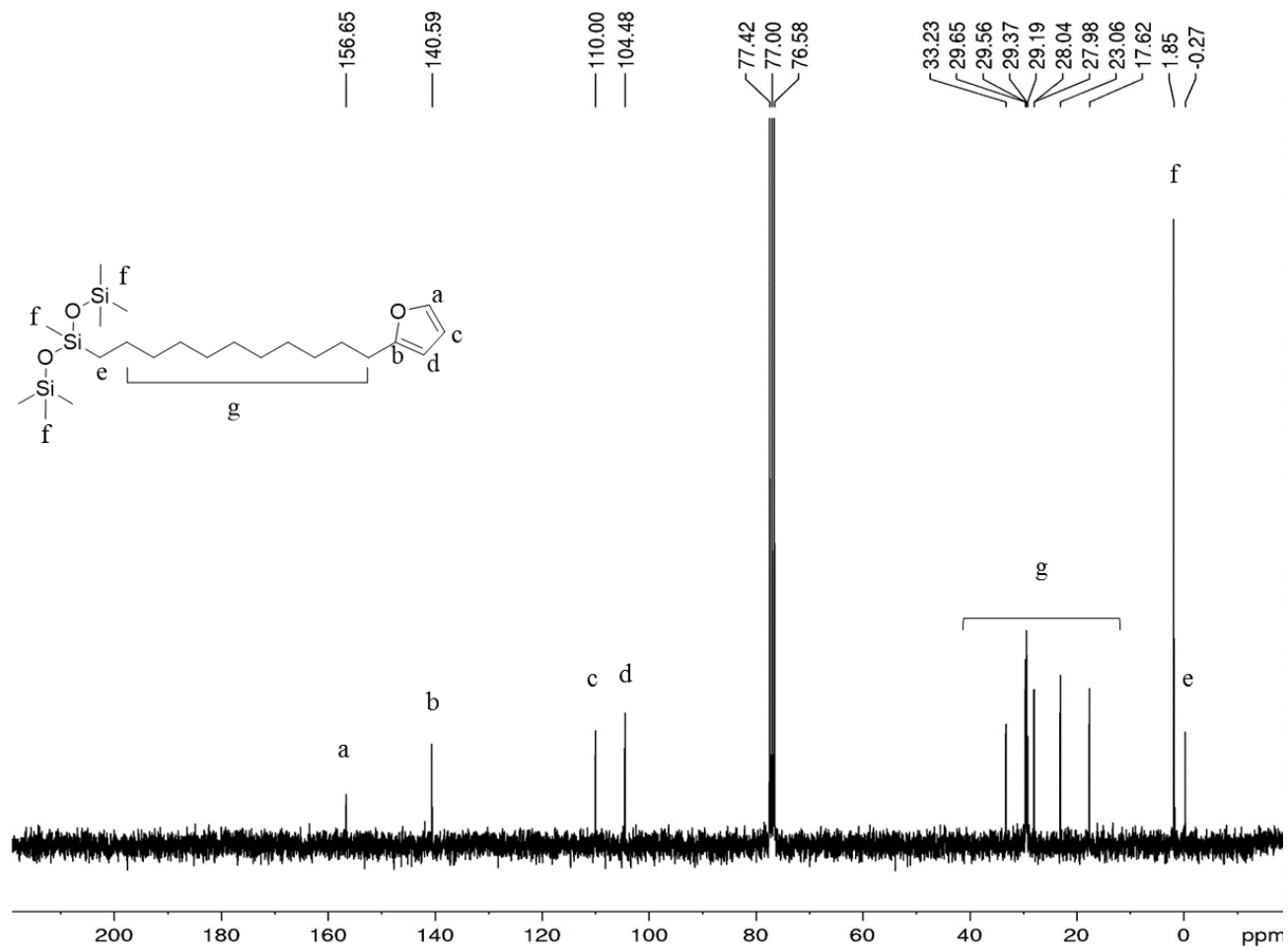
Appendix Figure 6 ¹³C NMR of compound 5



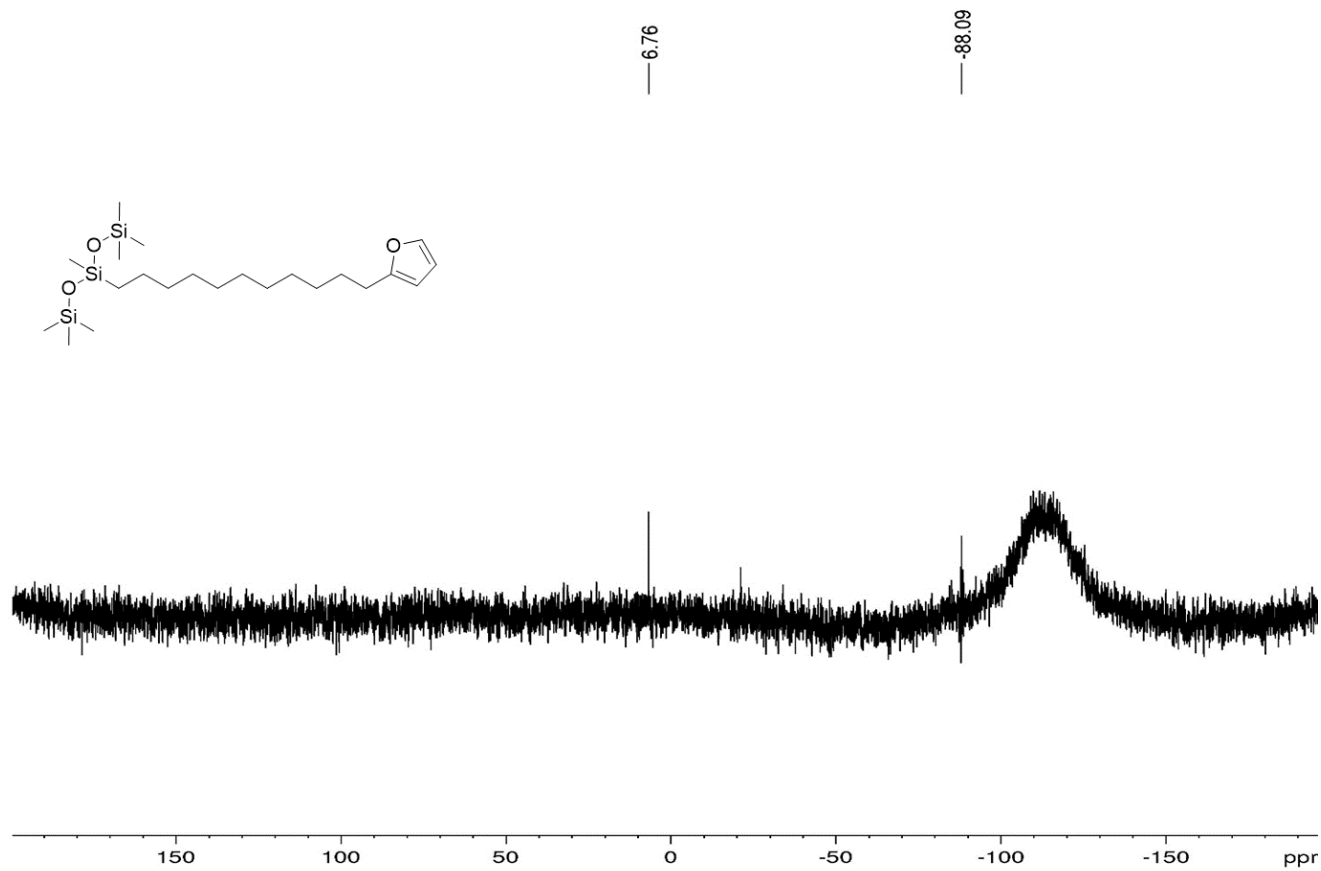
Appendix Figure 7 ^{29}Si NMR of compound 5



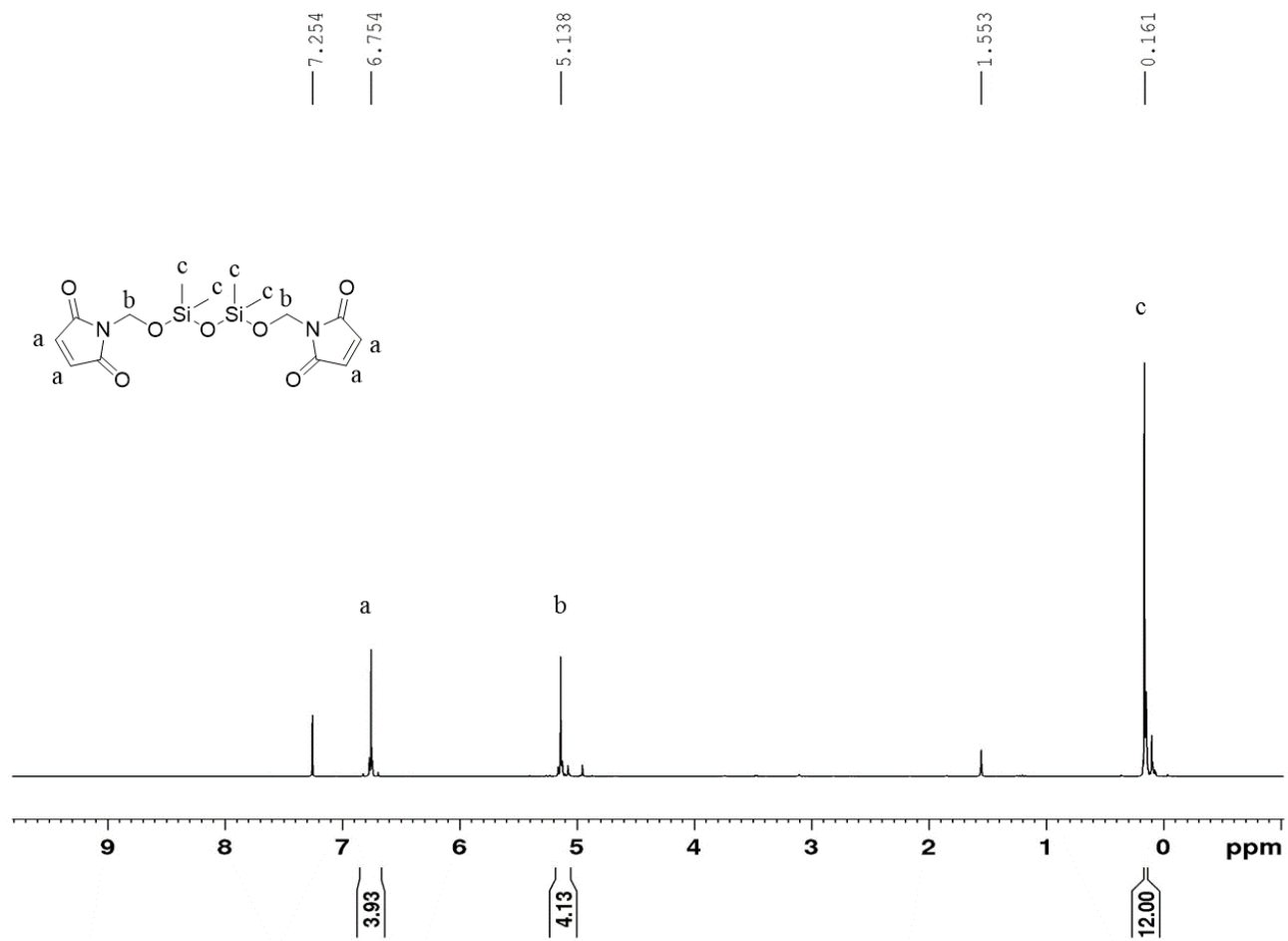
Appendix Figure 8. ¹H NMR of compound **9**



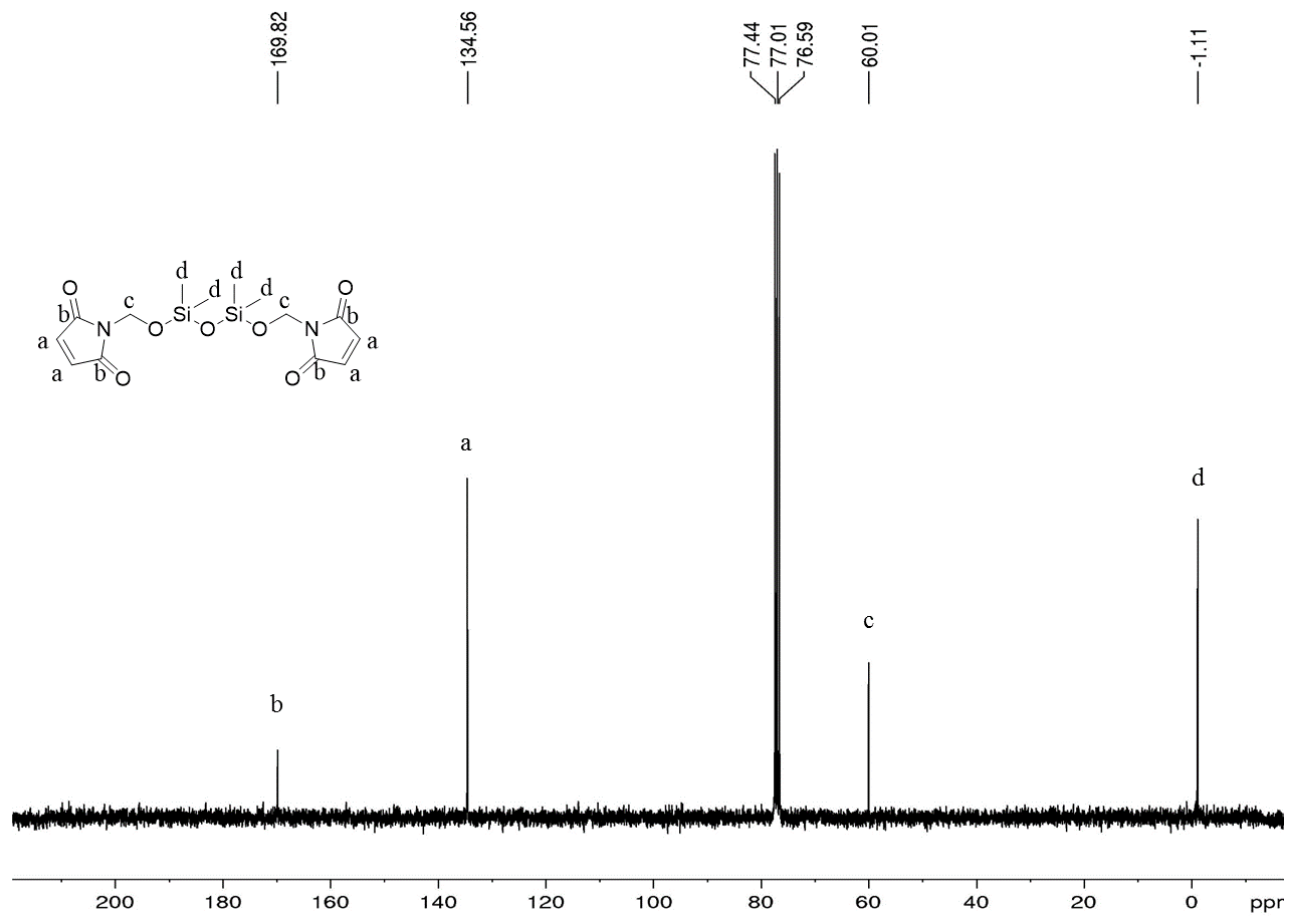
Appendix Figure 9. ¹³C NMR of compound **9**



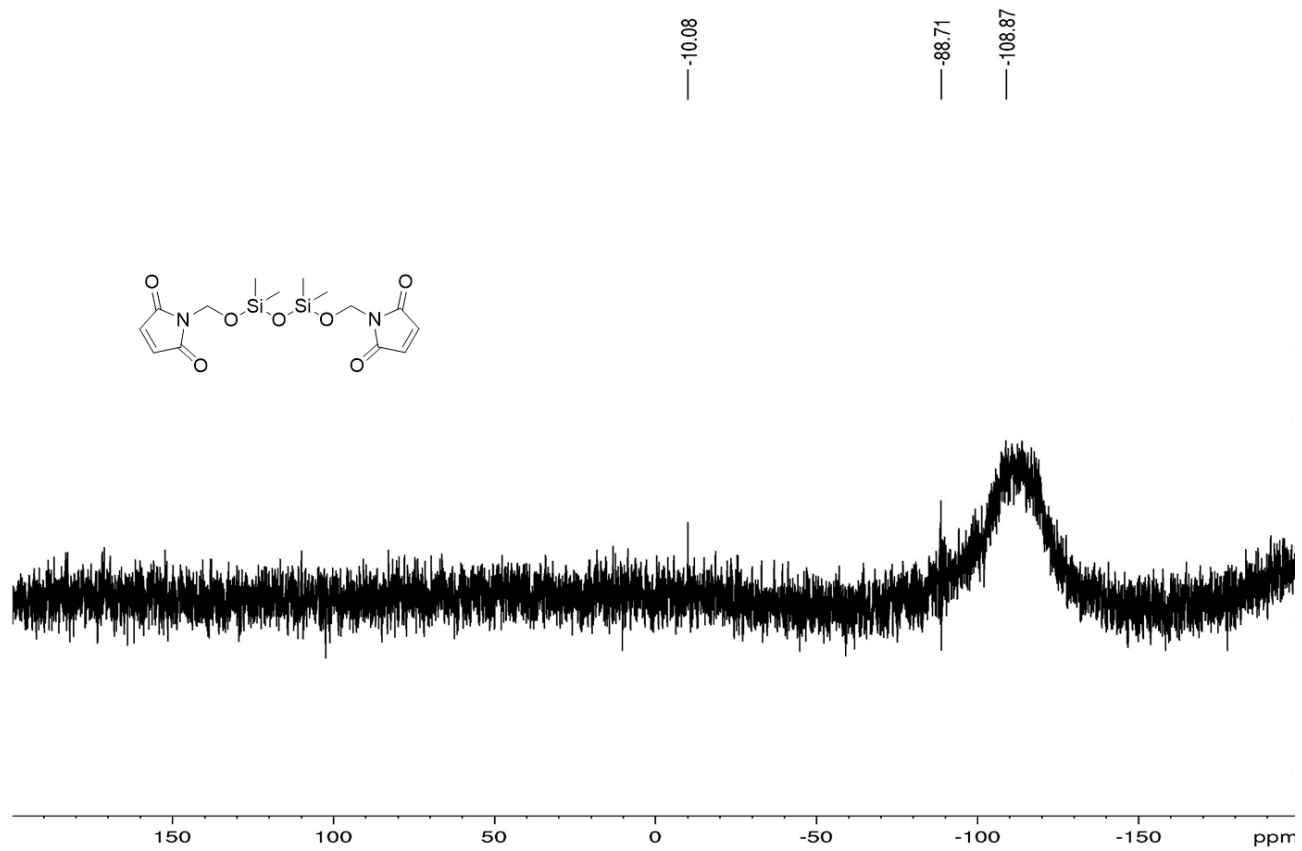
Appendix Figure 10. ^{29}Si NMR of compound 9



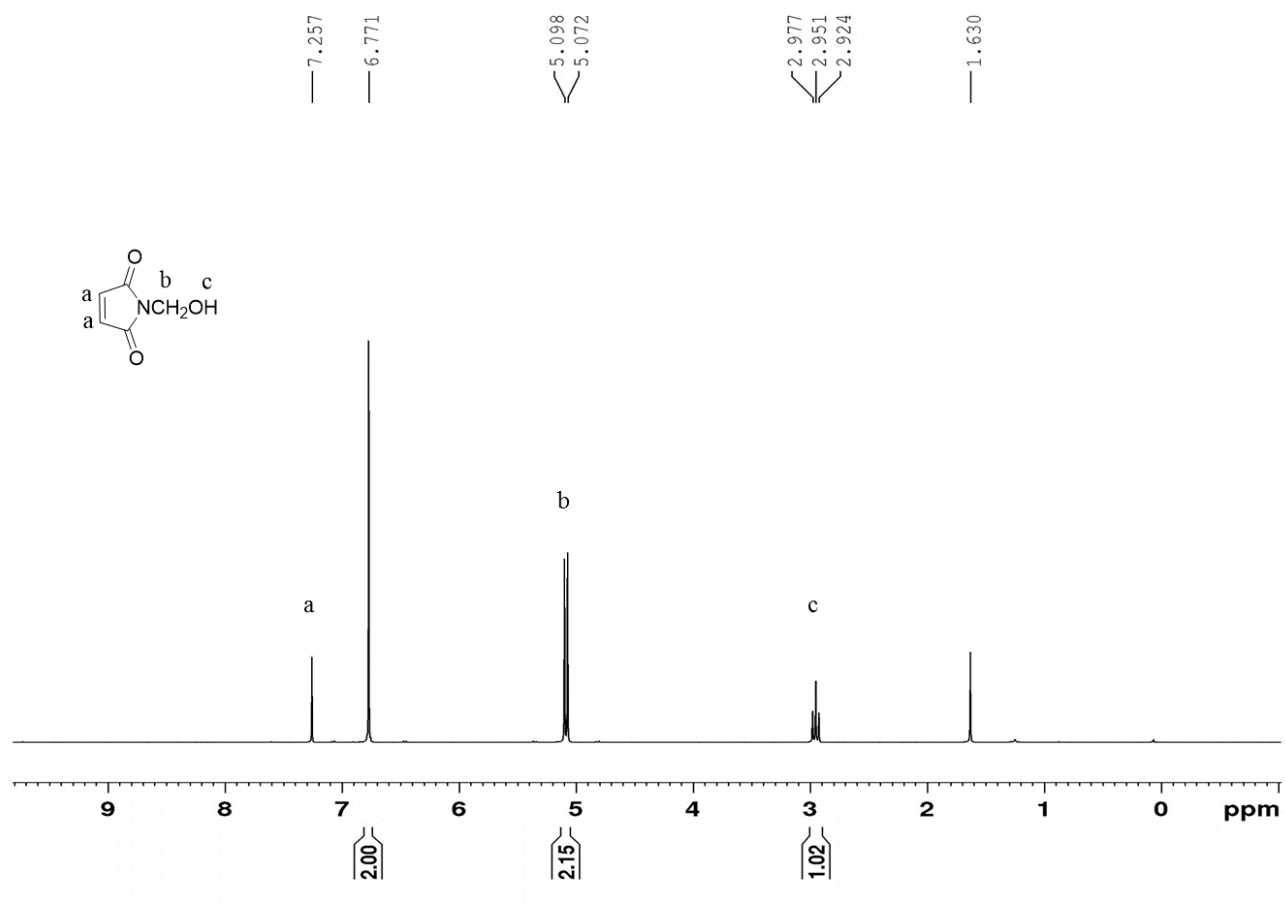
Appendix Figure 11. ¹H NMR of compound 13



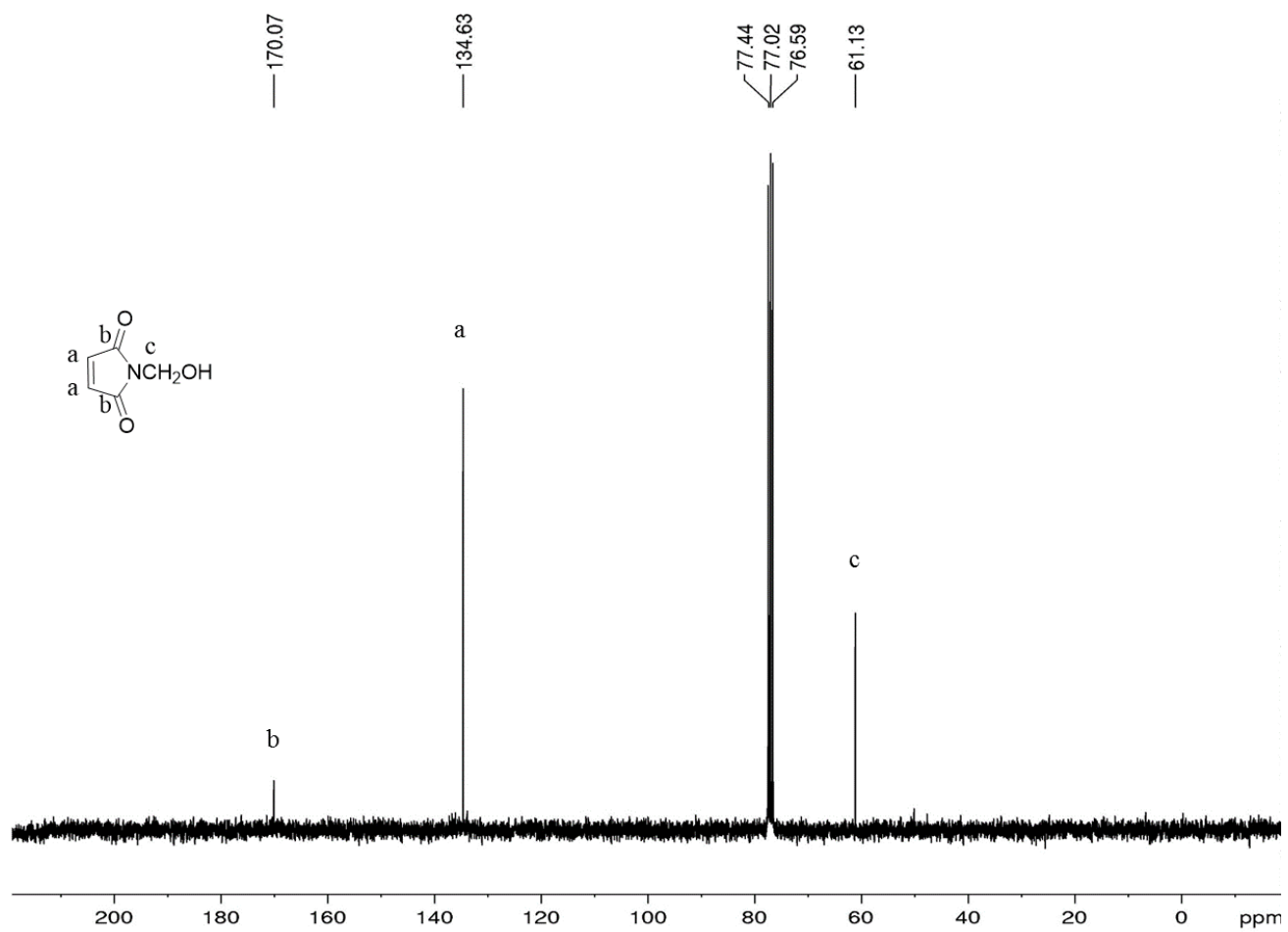
Appendix Figure 12. ^{13}C NMR of compound **13**



Appendix Figure 13. ^{29}Si NMR of compound **13**



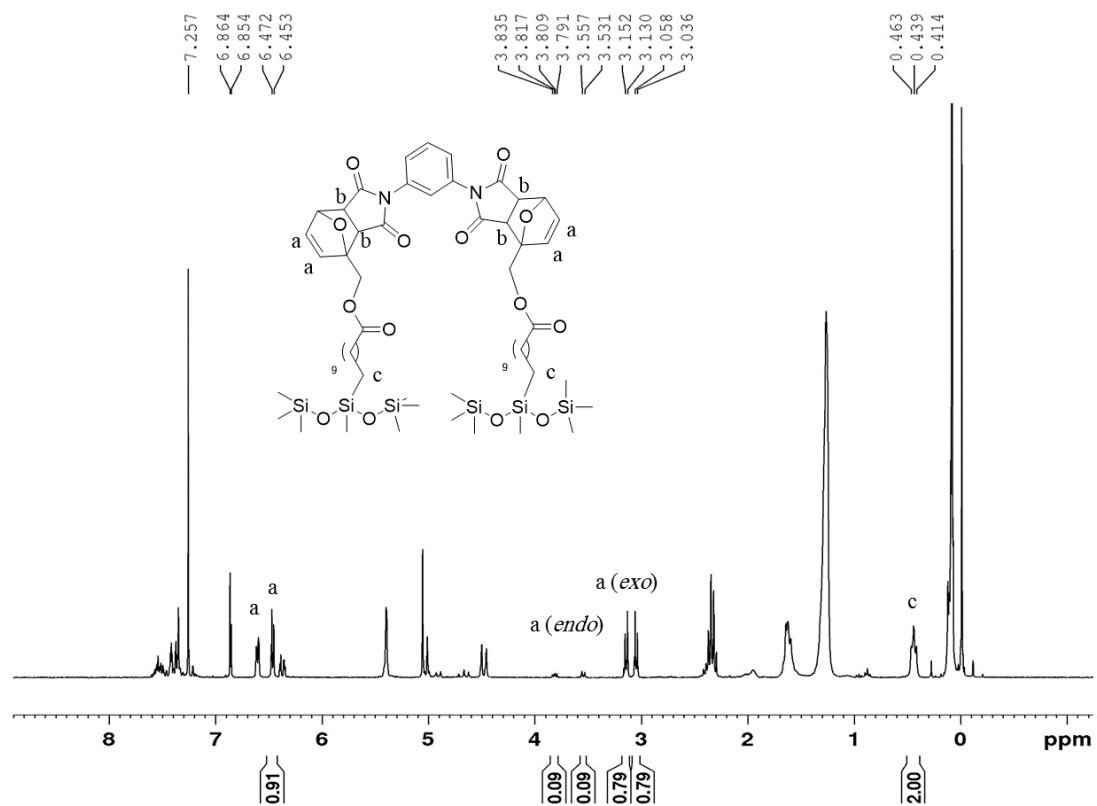
Appendix Figure 14. ¹H NMR of compound **11**



Appendix Figure 15. ^{13}C NMR of compound **11**

➤ Model Diels-Alder Adducts ^1H NMR*

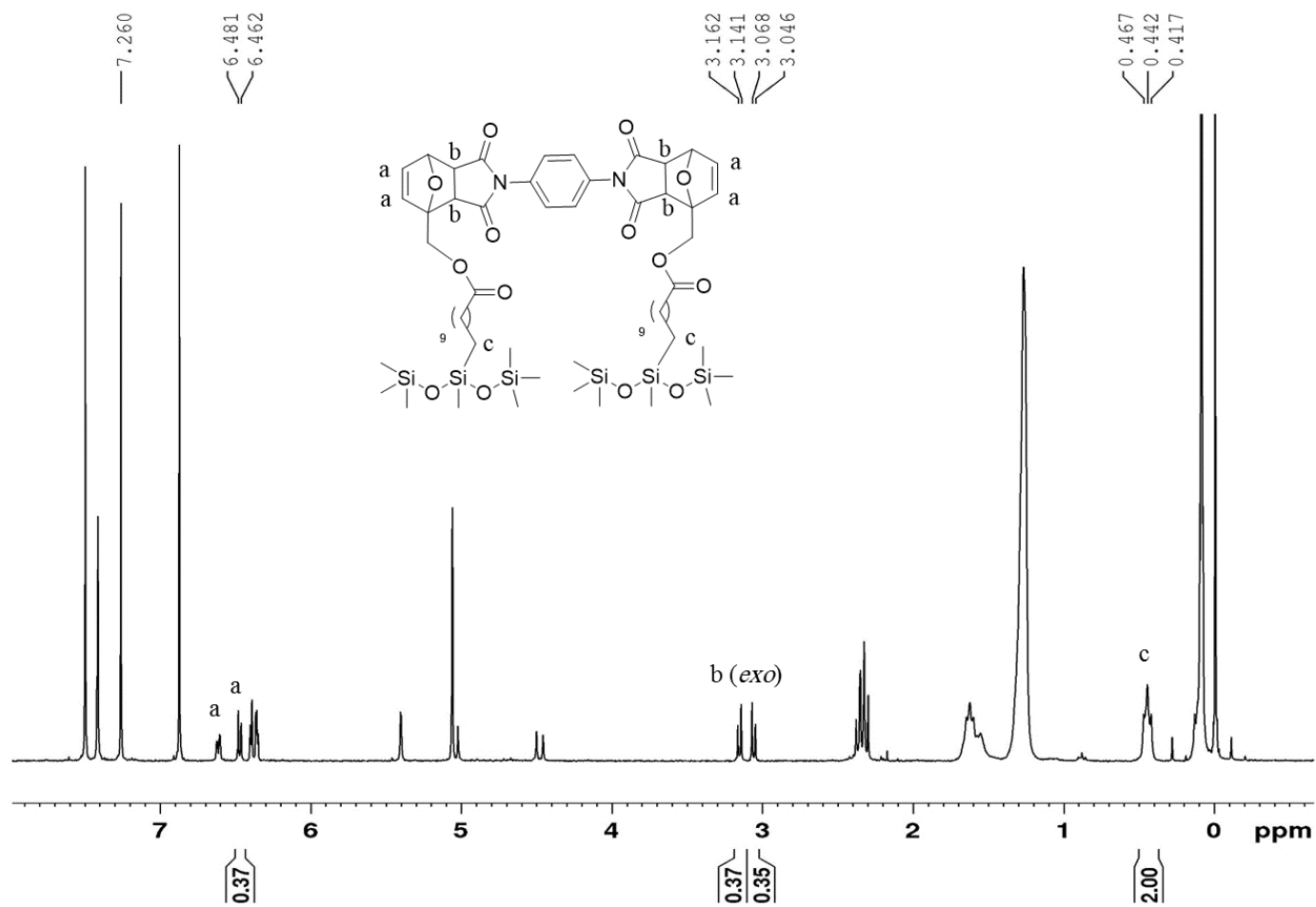
1. Reaction #1



Appendix Figure 16. DA adduct ^1H NMR of reaction number 1

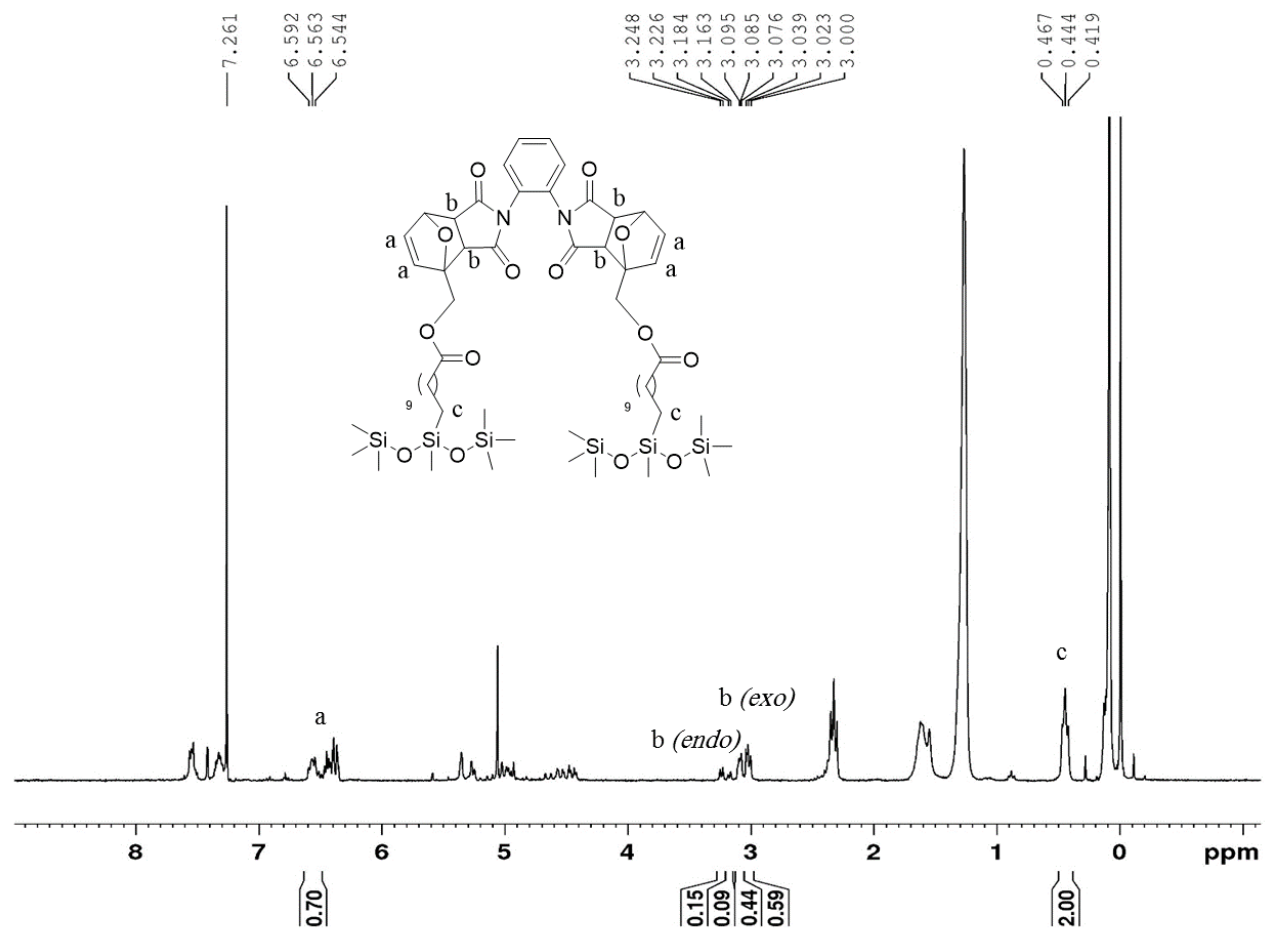
* Reaction numbers correspond to Table 2-1 and 2-2

Reaction #2



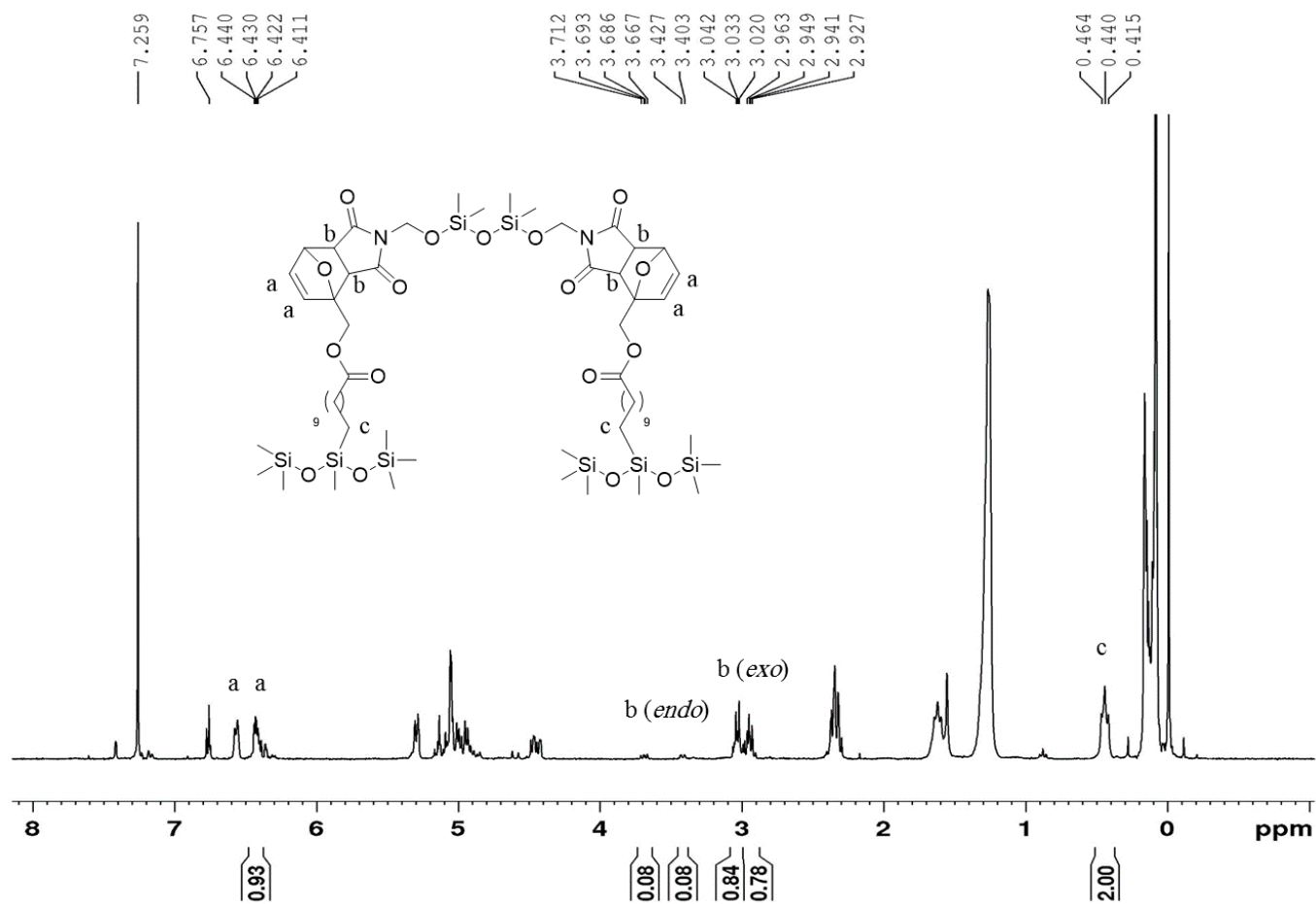
Appendix Figure 17. DA adduct ¹H NMR of reaction number 2

2. Reaction #3



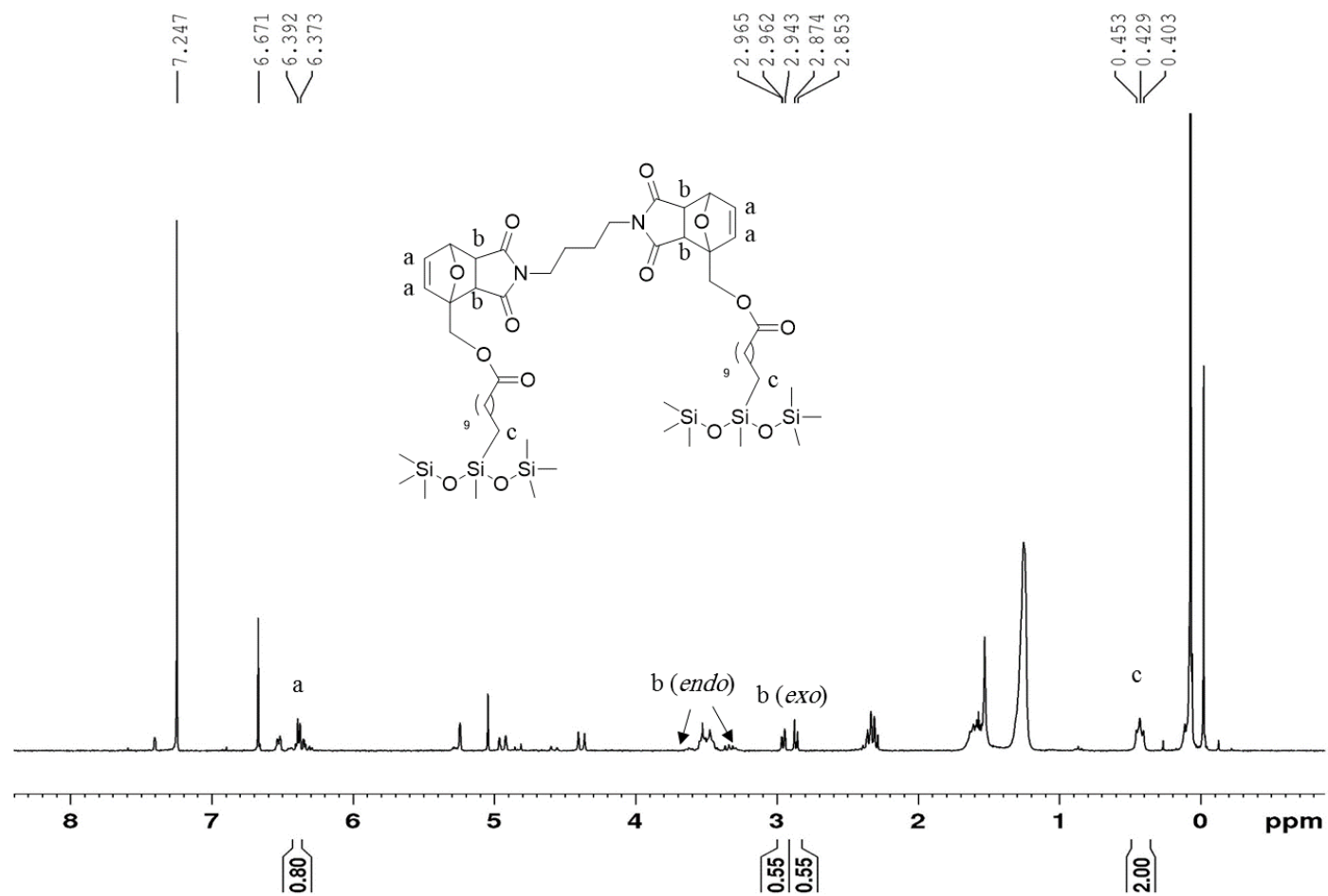
Appendix Figure 18. DA adduct ¹H NMR of reaction number 3

3. Reaction #4



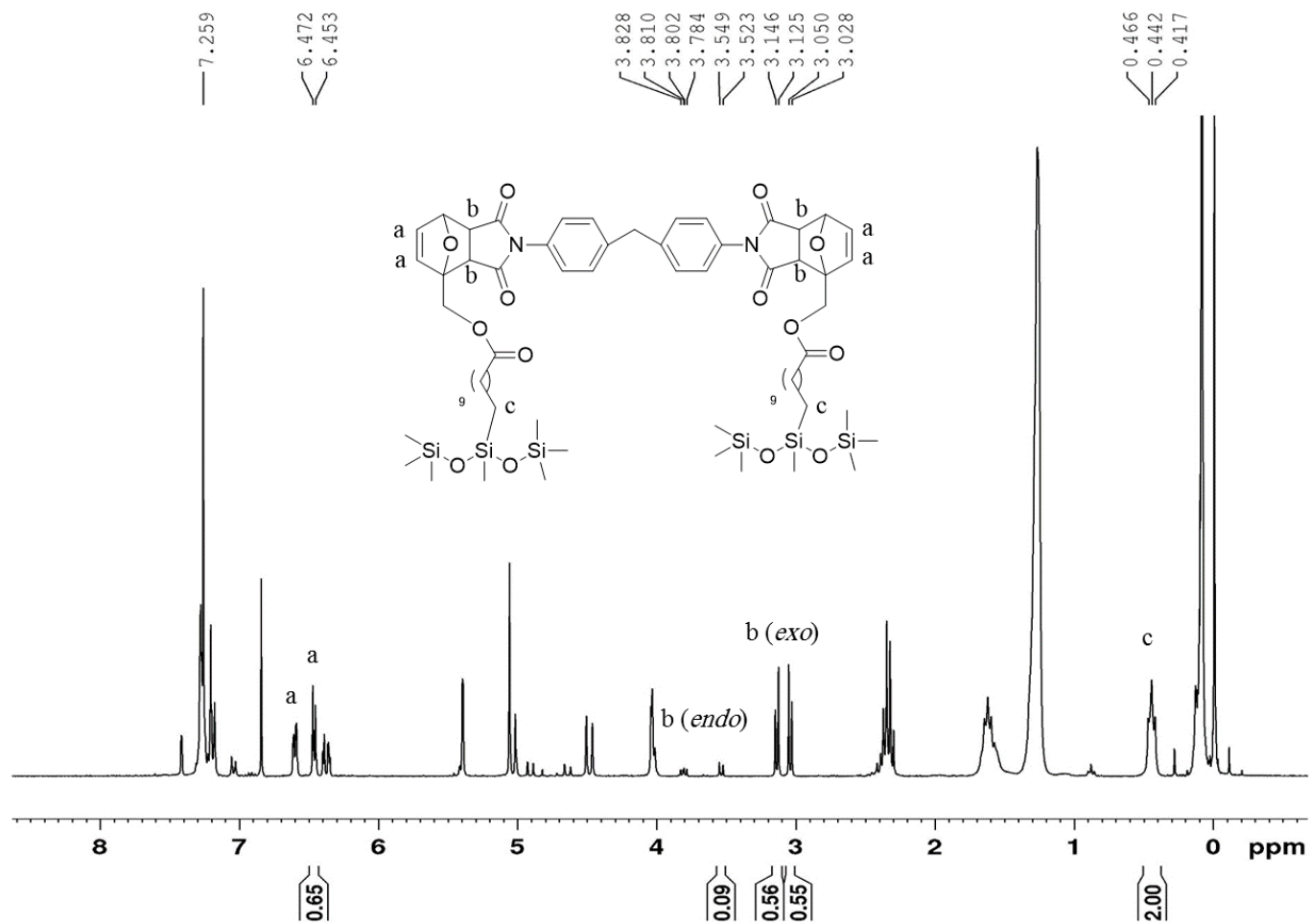
Appendix Figure 19. DA adduct ¹H NMR of reaction number 4

4. Reaction #5



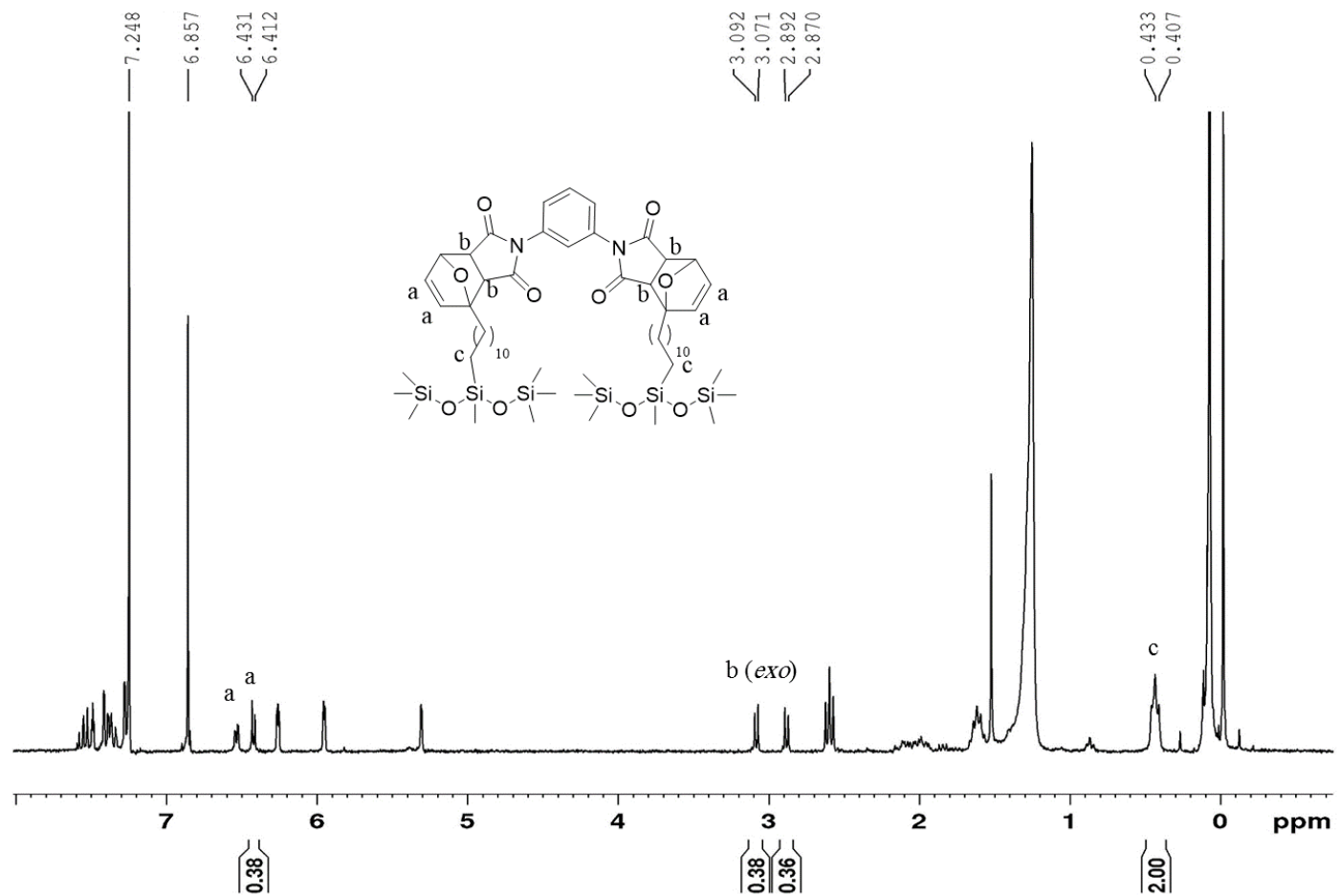
Appendix Figure 20. DA adduct ^1H NMR of reaction number 5

5. Reaction #6



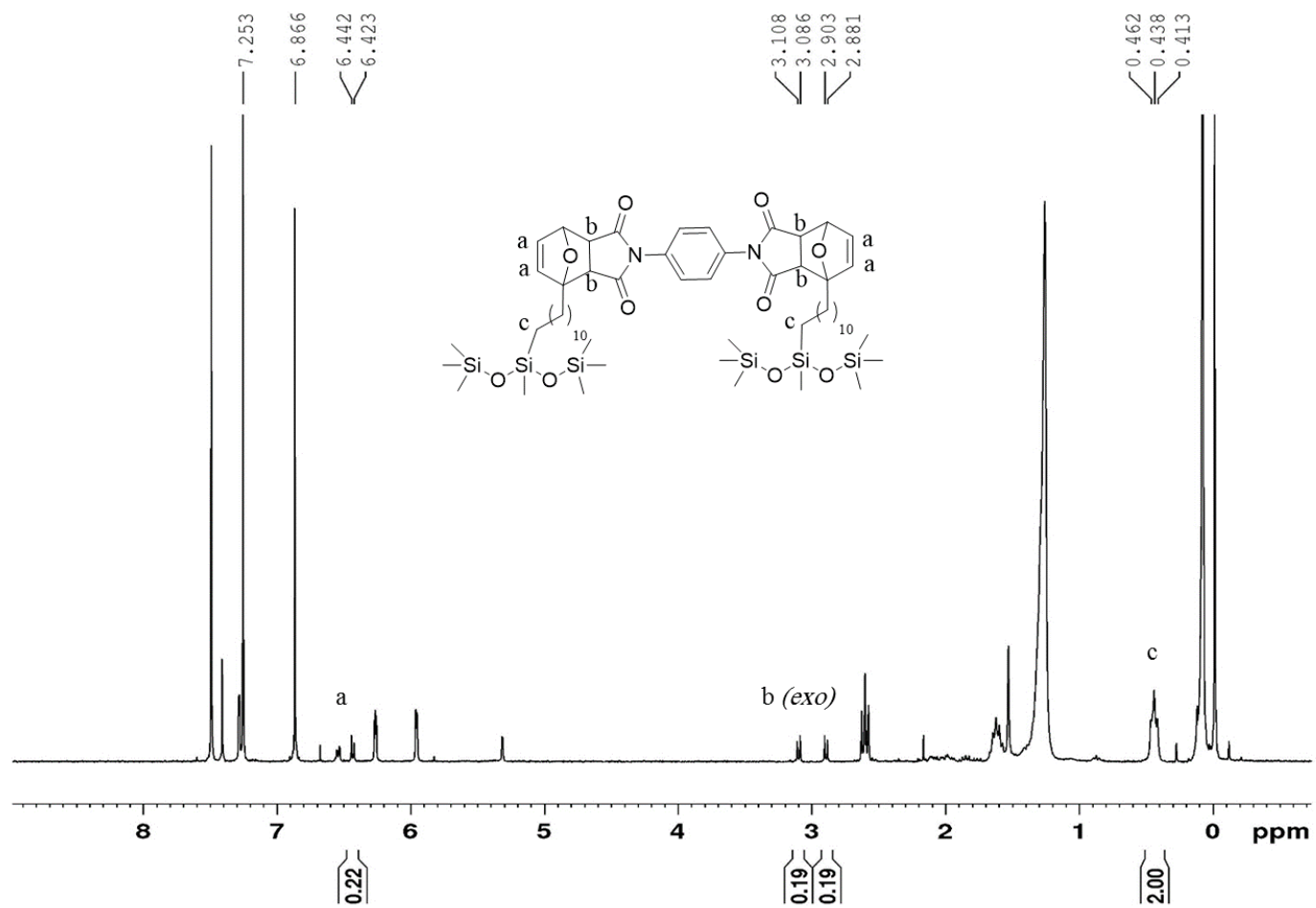
Appendix Figure 21. DA adduct ¹H NMR of reaction number 6

6. Reaction #7



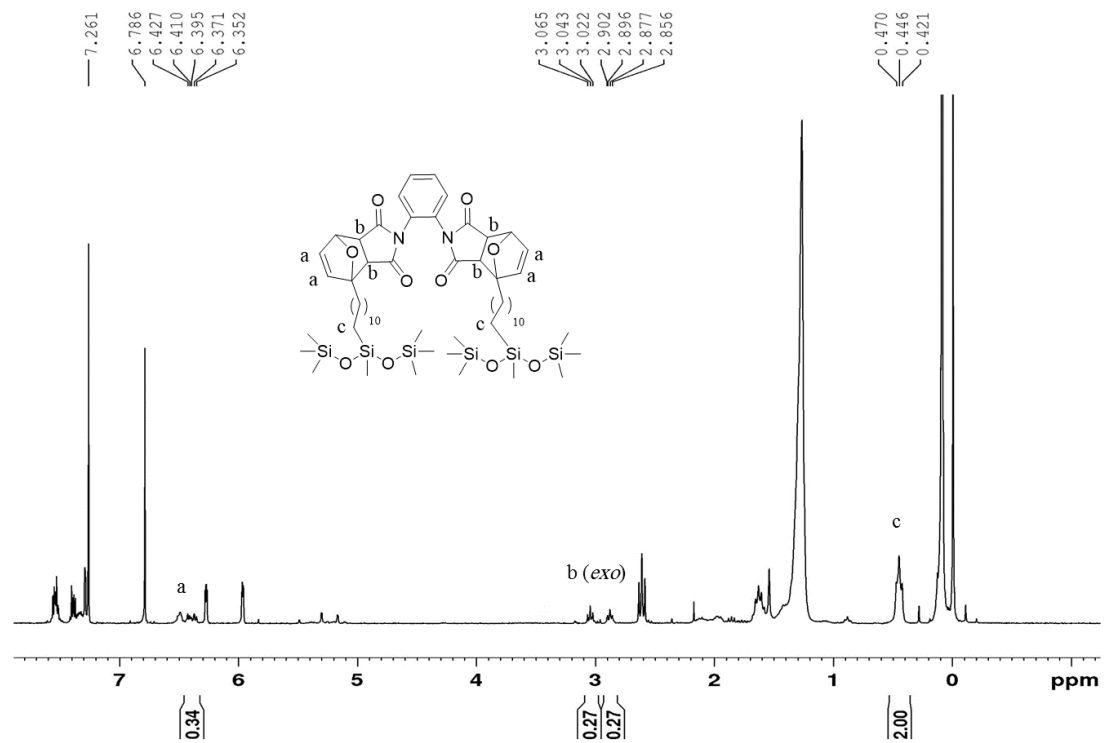
Appendix Figure 22. DA adduct ^1H NMR of reaction number 7

7. Reaction #8



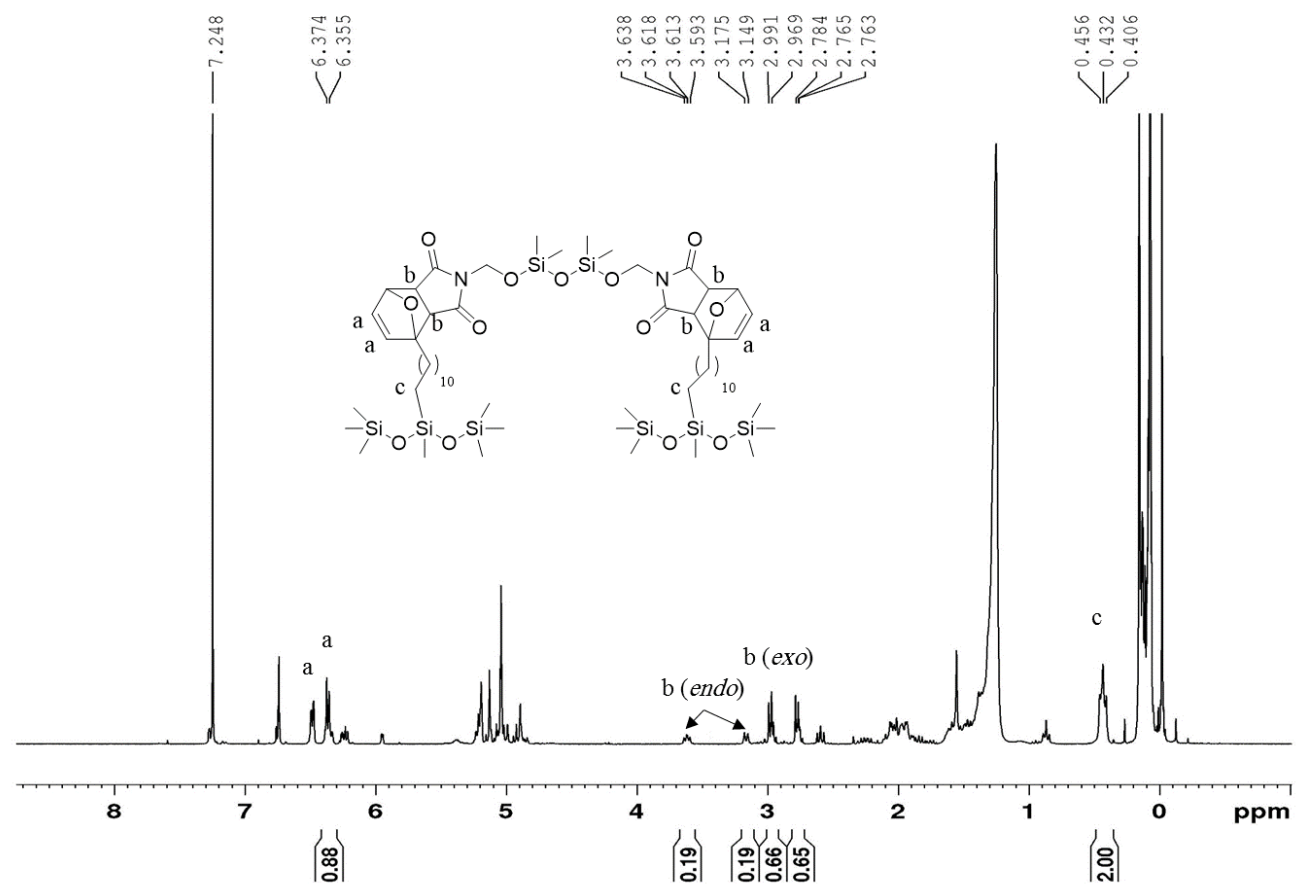
Appendix Figure 23. DA adduct ¹H NMR of reaction number 8

Reaction #9



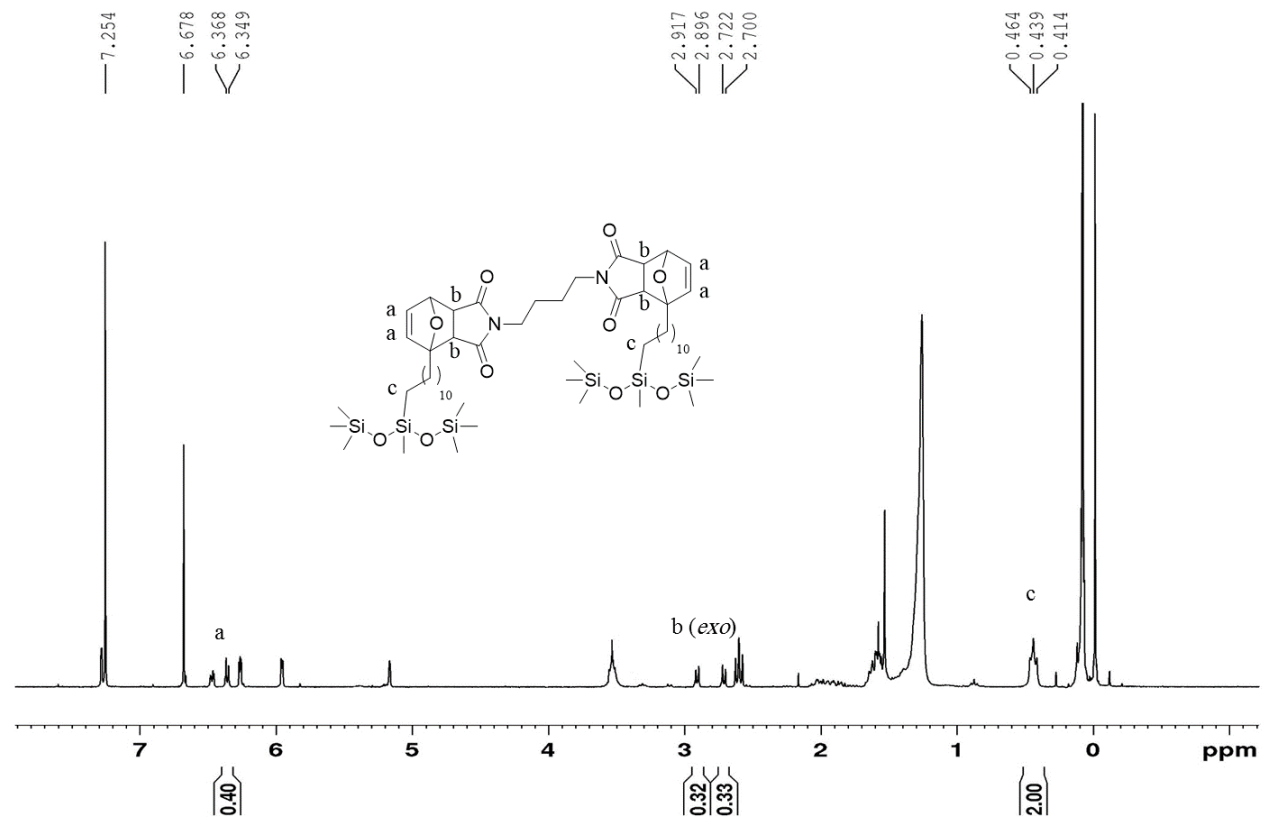
Appendix Figure 24. DA adduct ¹H NMR of reaction number 9

8. Reaction #10



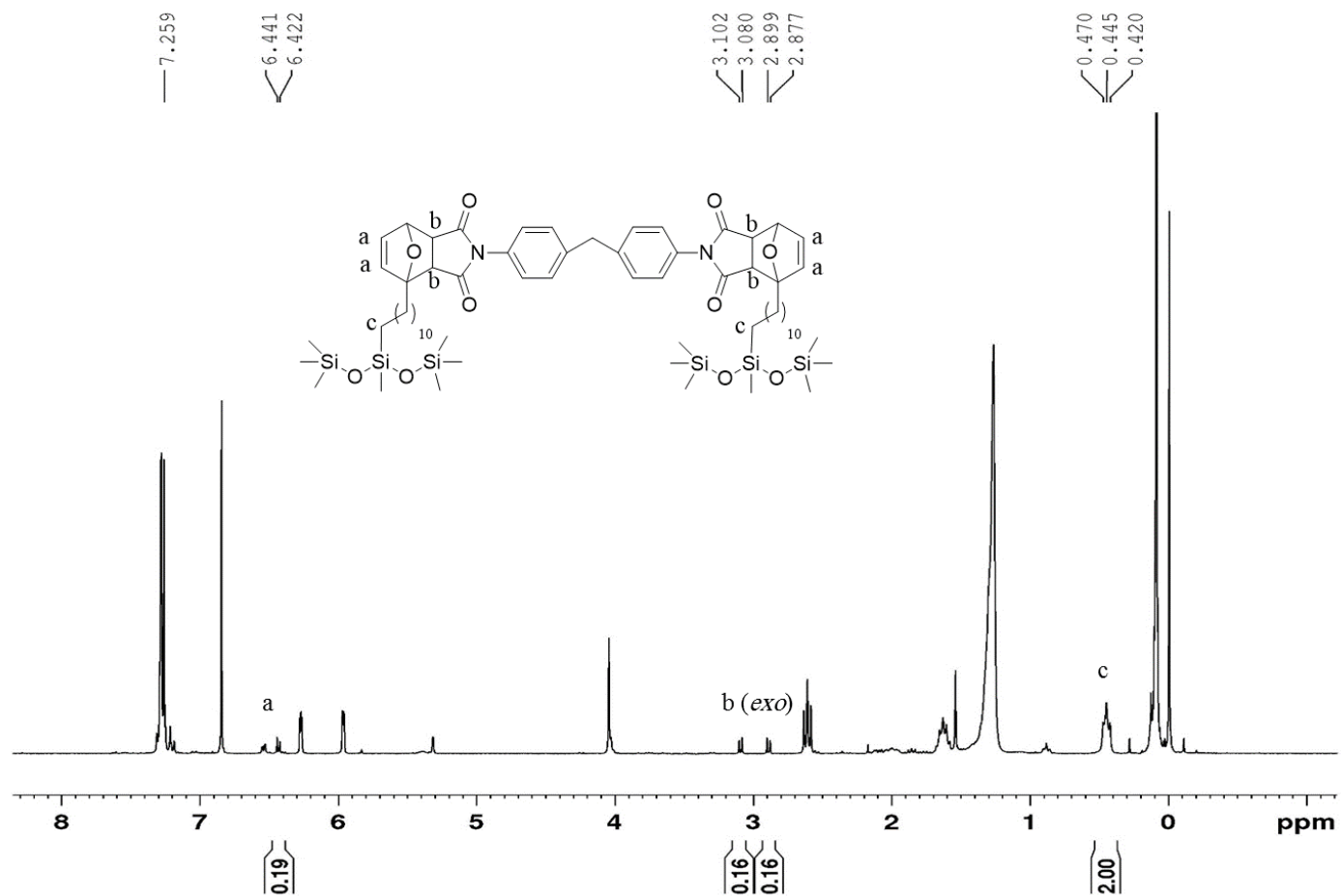
Appendix Figure 25. DA adduct ^1H NMR of reaction number 10

Reaction #11



Appendix Figure 26. DA adduct ¹H NMR of reaction number 11

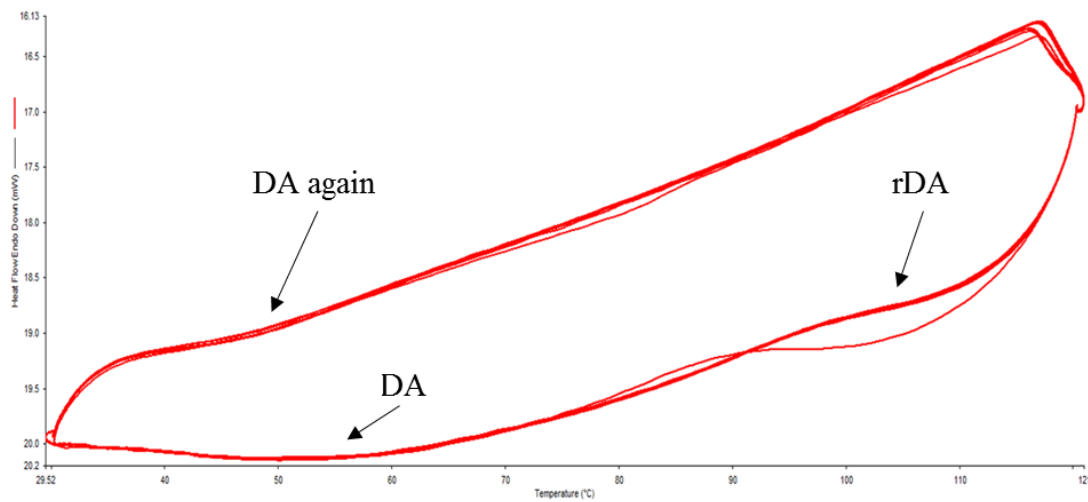
9. Reaction #12



Appendix Figure 27. DA adduct ^1H NMR of reaction number 12

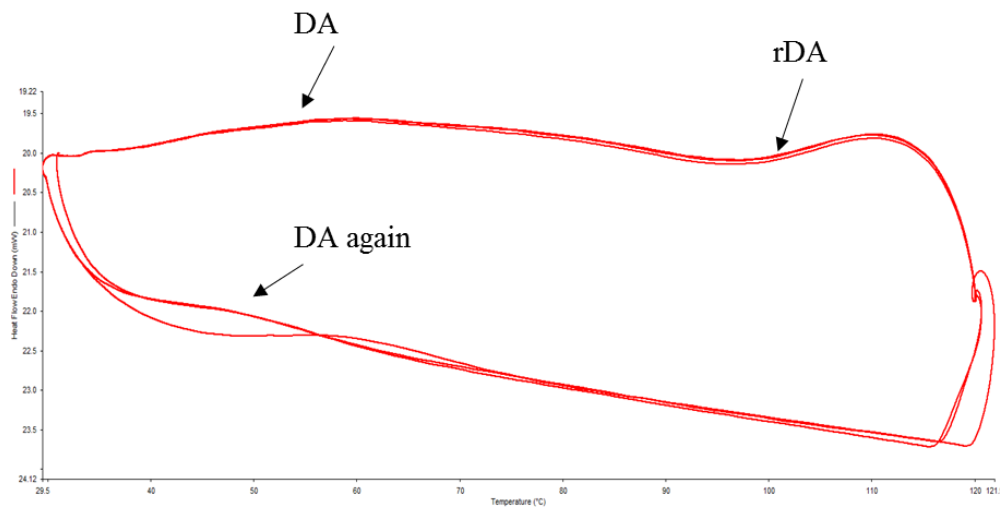
➤ DSC Analysis of Model Reactions *

1. Reaction #1



Appendix Figure 28. DSC analysis of model reaction number 1

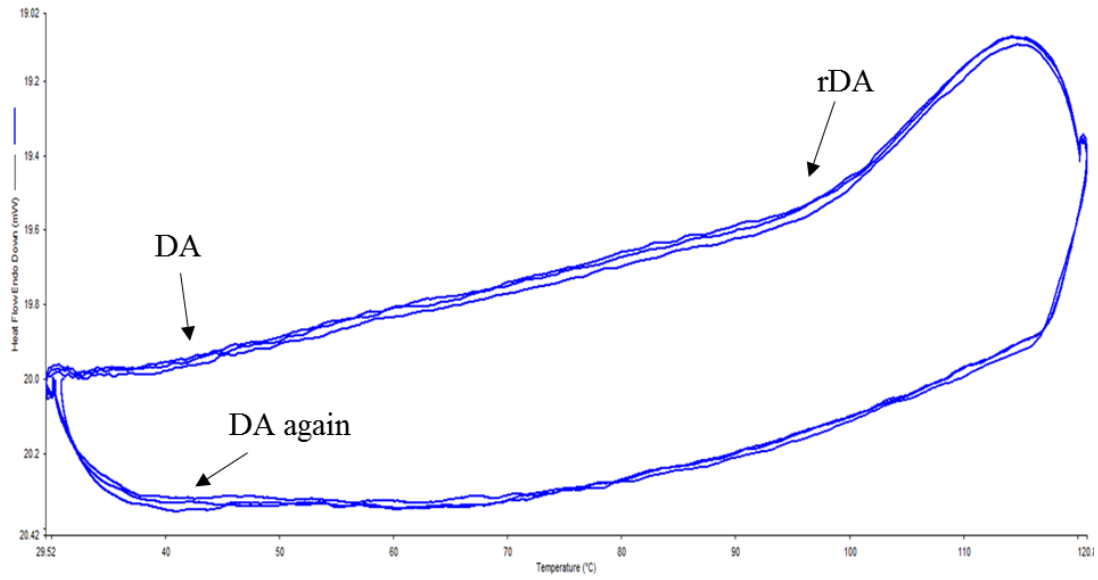
2. Reaction #2



Appendix Figure 29. DSC analysis of model reaction number 2

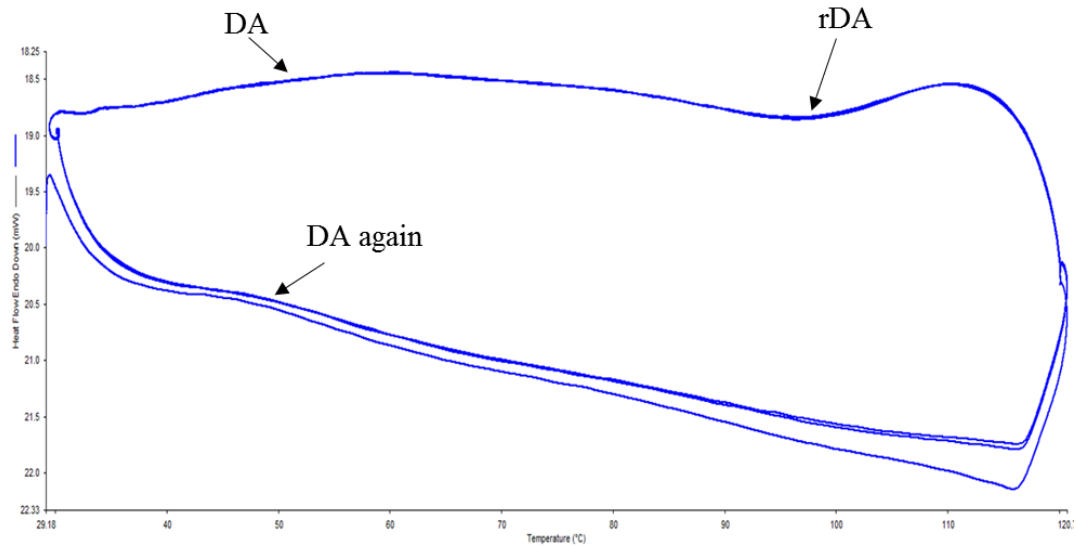
* The reaction numbers correspond to Table 2-1 and Table 2-2

3. Reaction #3



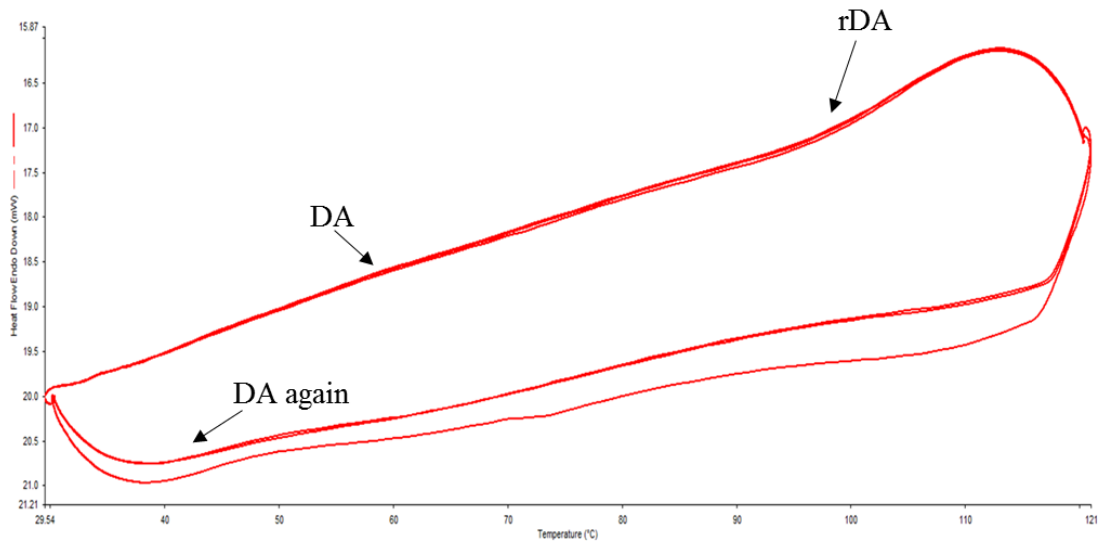
Appendix Figure 30. DSC analysis of model reaction number 3

4. Reaction #4



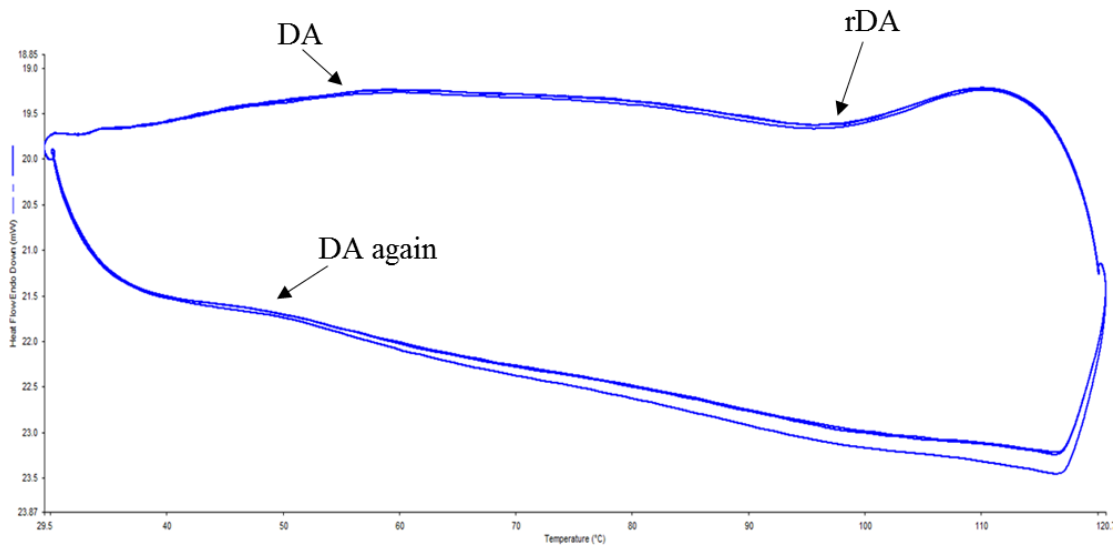
Appendix Figure 31. DSC analysis of model reaction number 4

Reaction #5



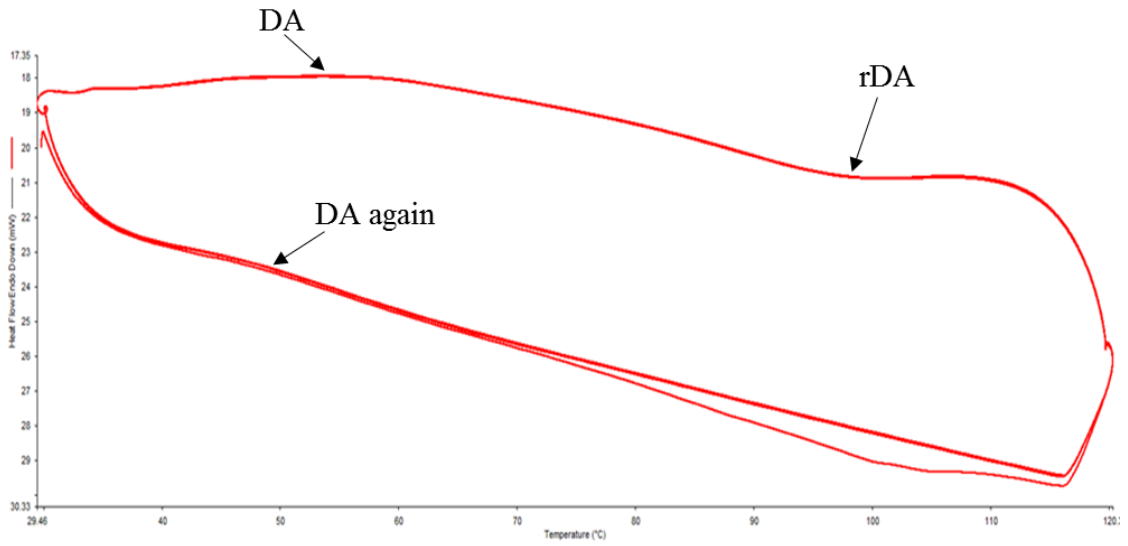
Appendix Figure 32. DSC analysis of model reaction number 5

5. Reaction #6



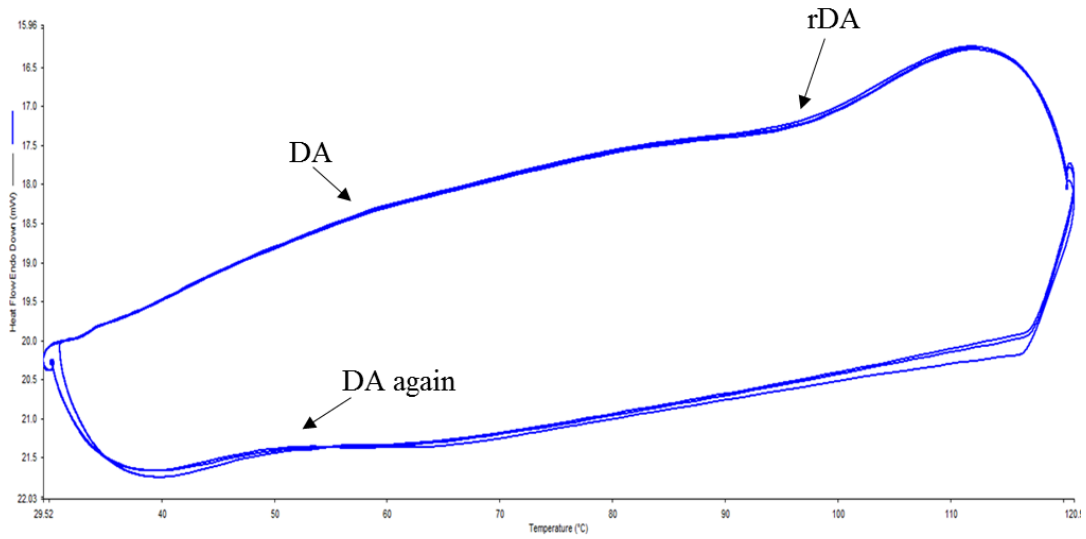
Appendix Figure 33. DSC analysis of model reaction number 6

6. Reaction #7



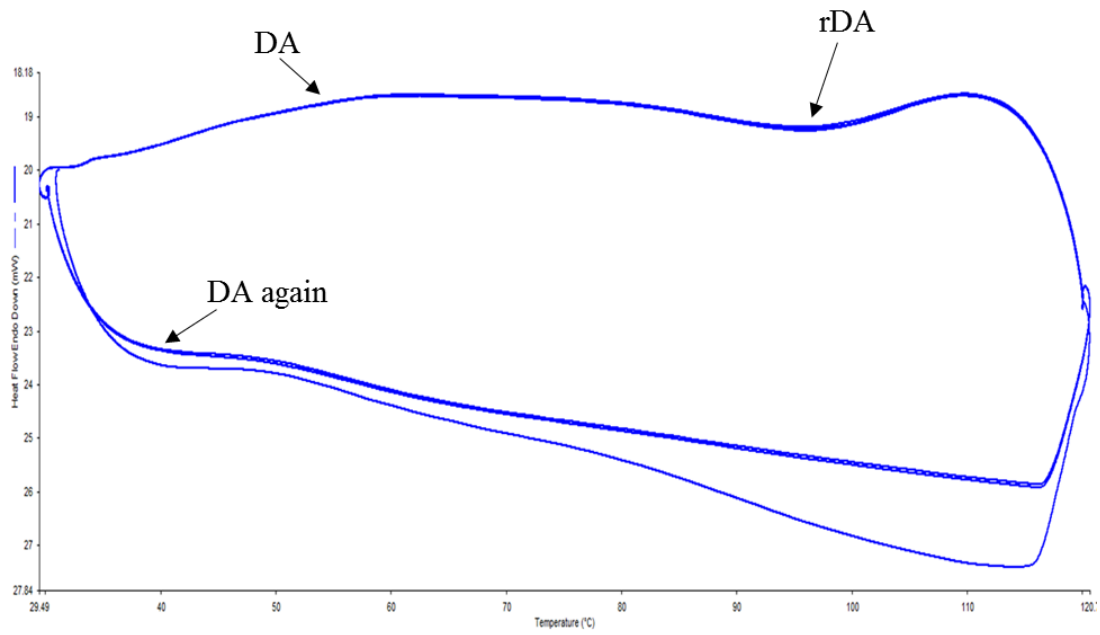
Appendix Figure 34. DSC analysis of model reaction number 7

7. Reaction #8



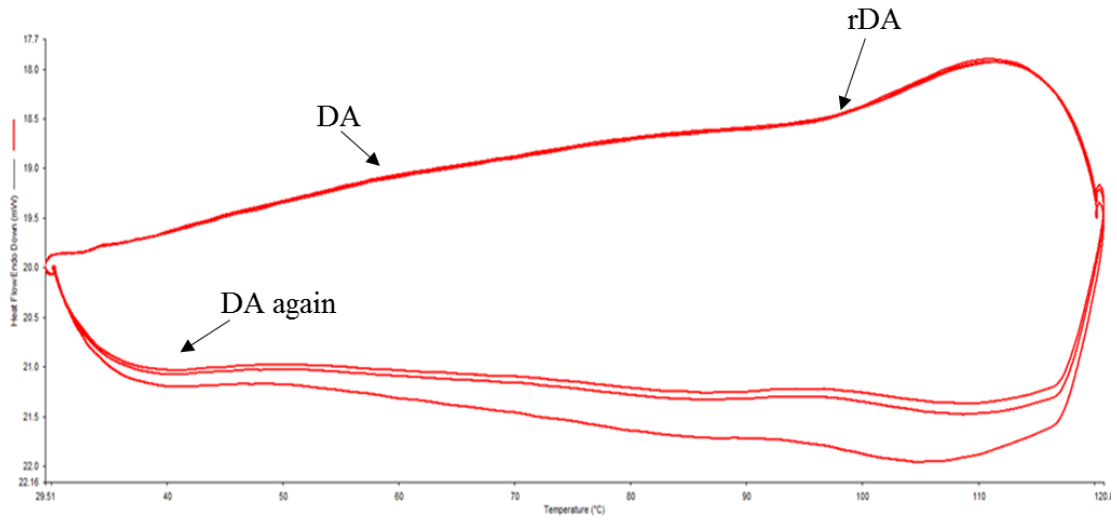
Appendix Figure 35. DSC analysis of model reaction number 8

8. Reaction #9



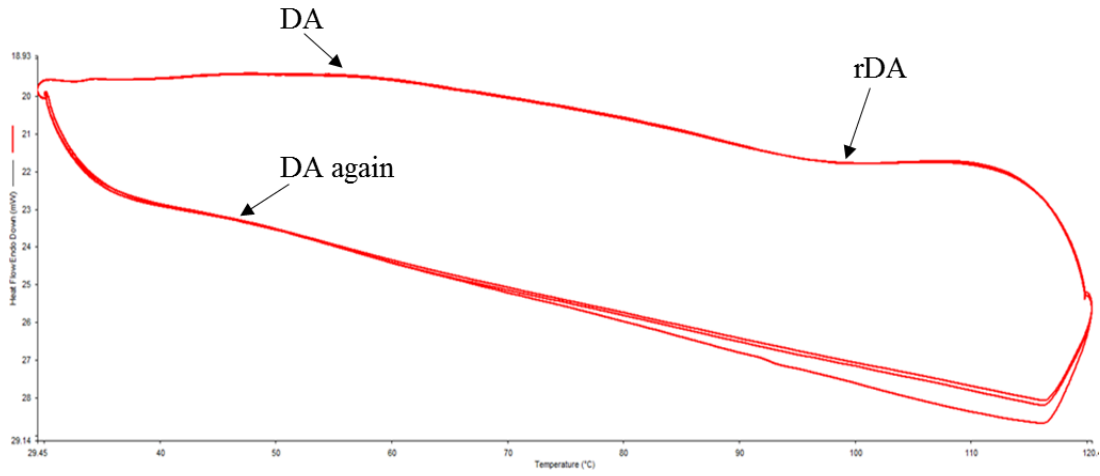
Appendix Figure 36. DSC analysis of model reaction number 9

9. Reaction #10



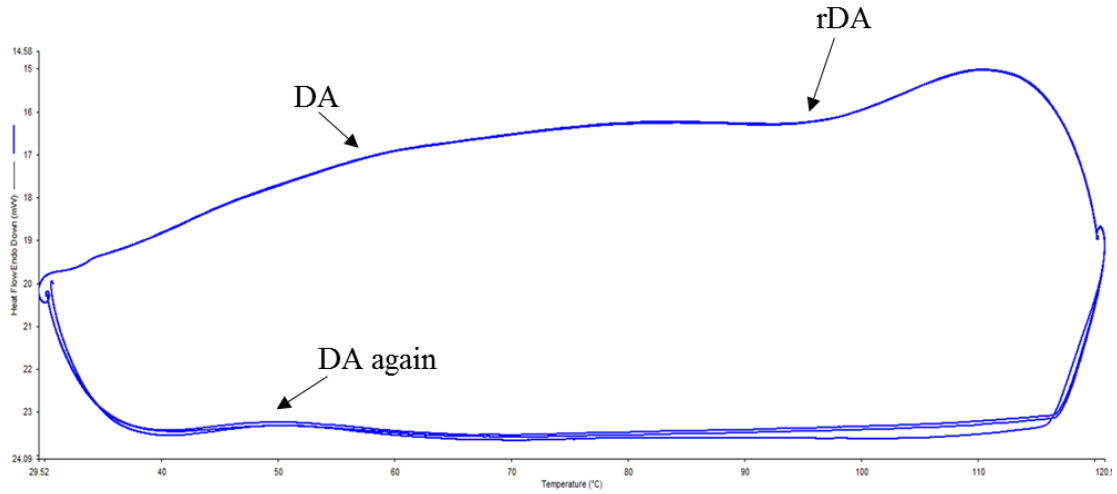
Appendix Figure 37. DSC analysis of model reaction number 10

10. Reaction #11



Appendix Figure 38. DSC analysis of model reaction number 11

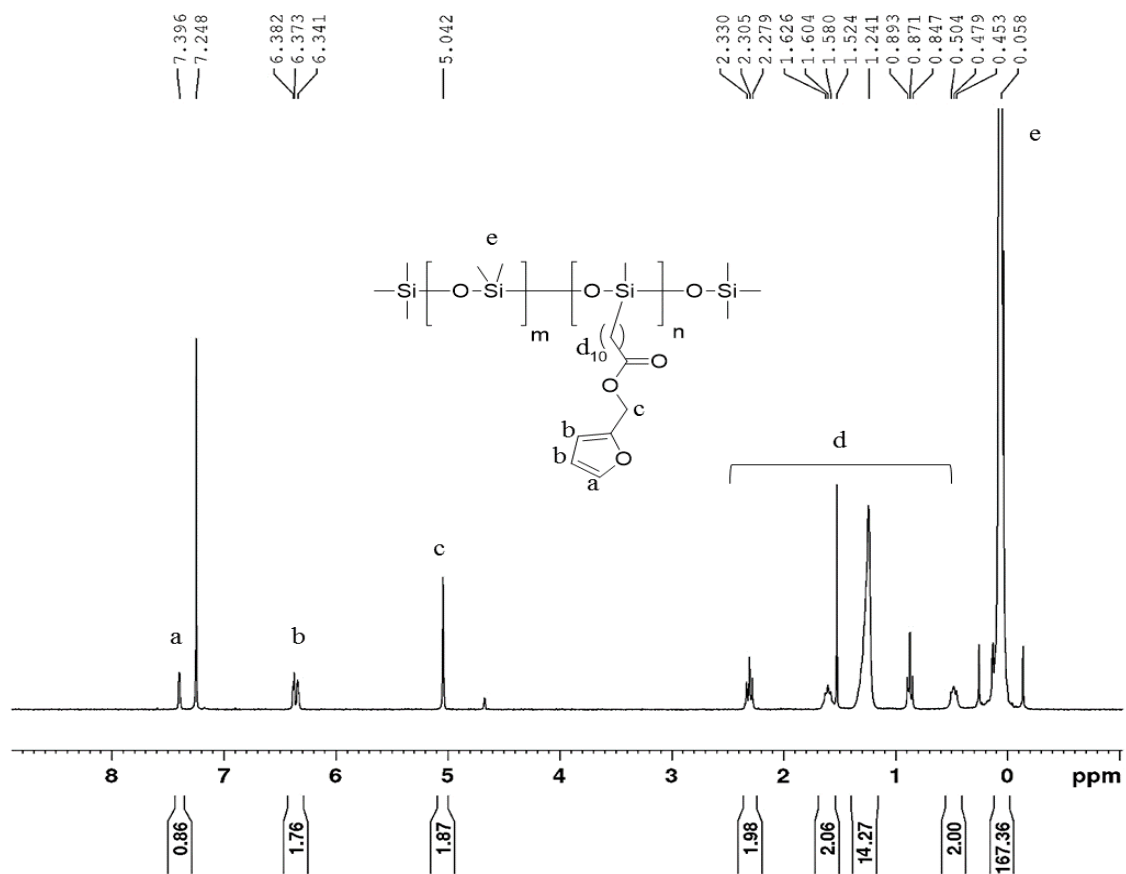
11. Reaction #12



Appendix Figure 39. DSC analysis of model reaction number 12

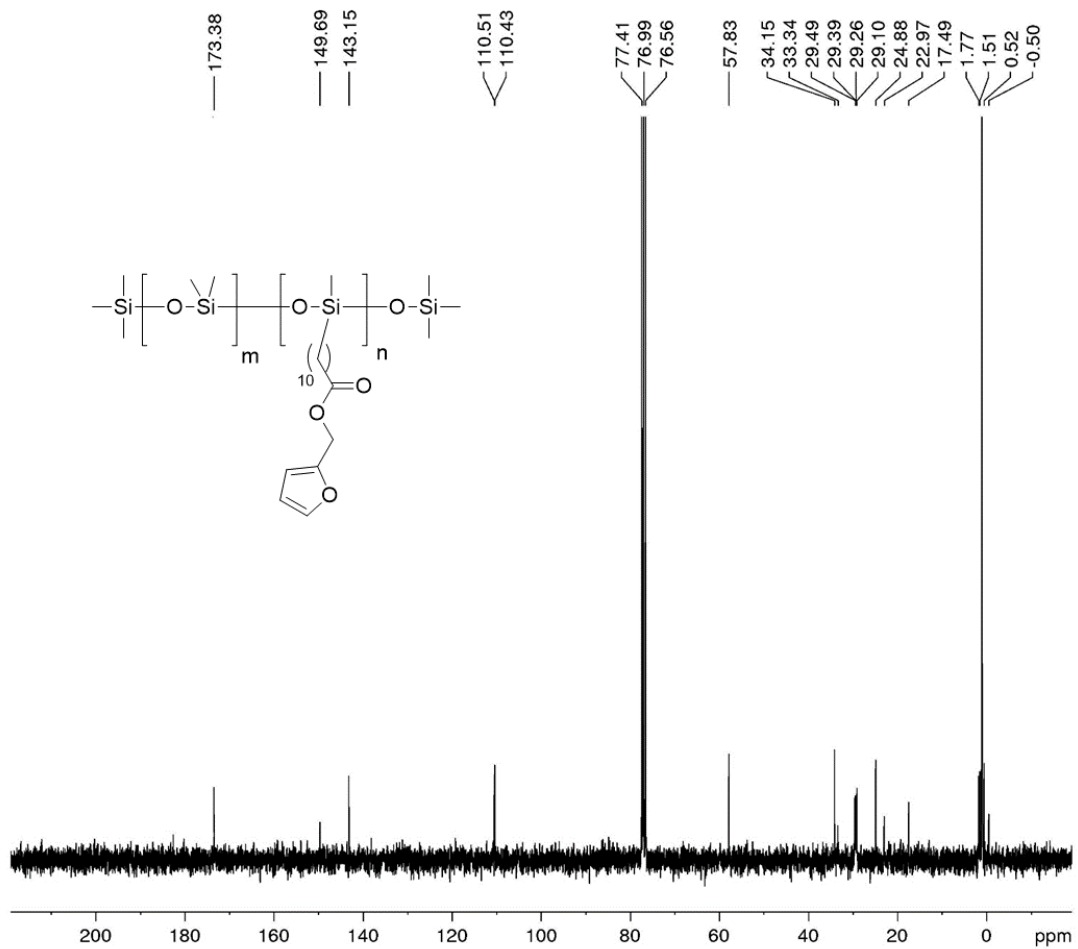
➤ Synthesized Diene polymeric systems Characterization

33 a



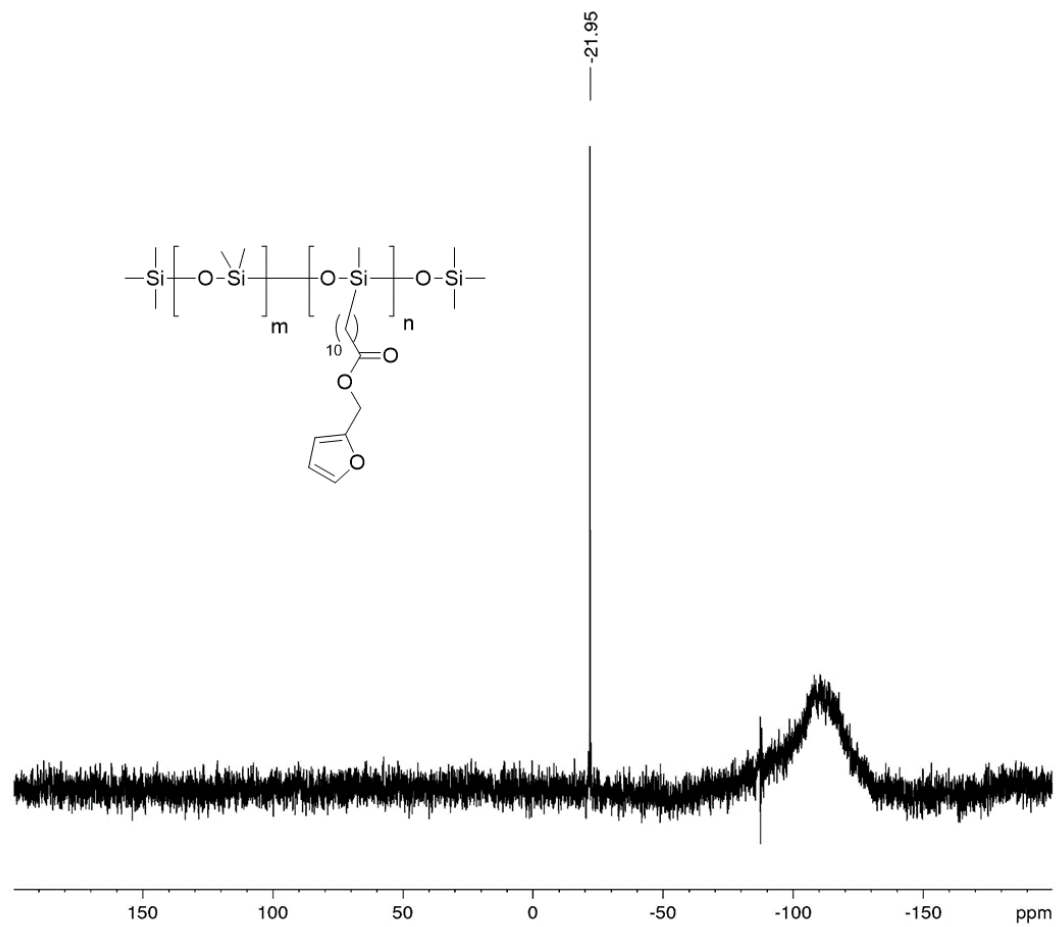
Appendix Figure 40 ¹H NMR of compound **33 a**

33 a



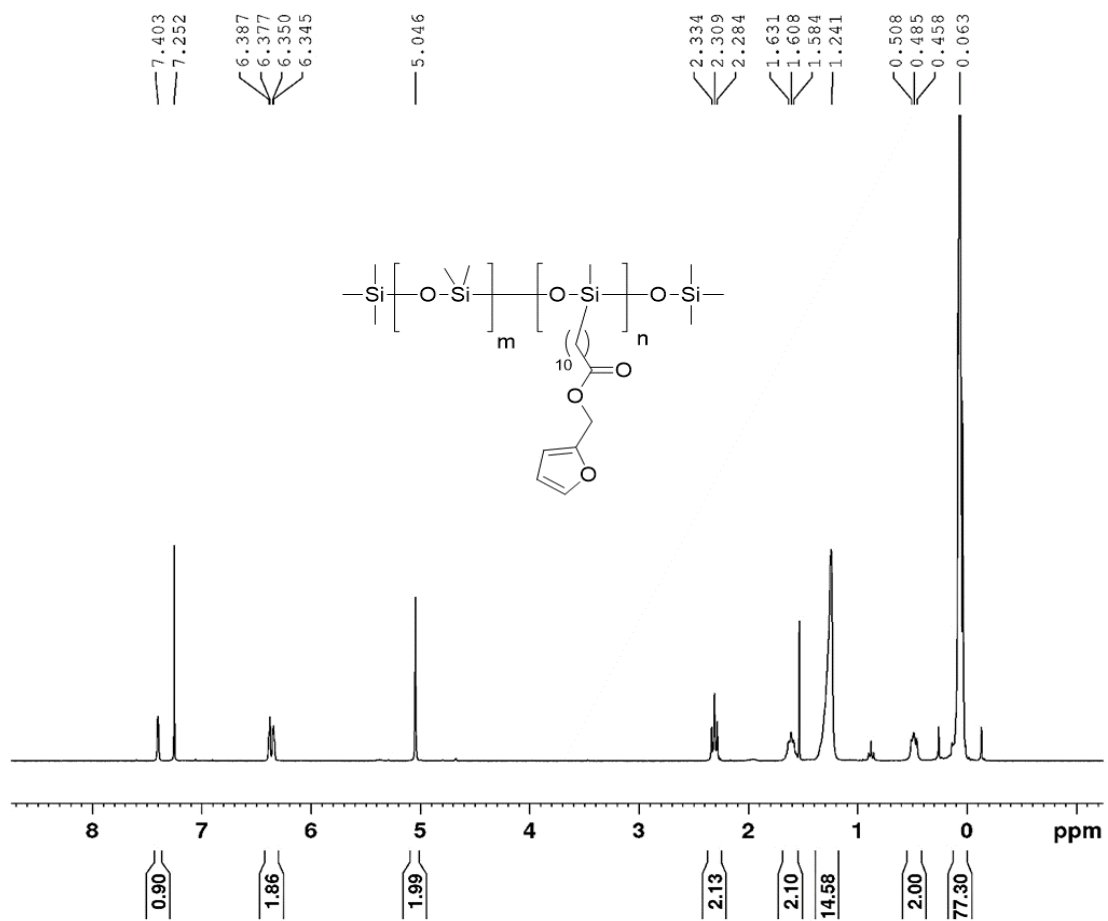
Appendix Figure 41 ^{13}C NMR of compound 33 a

33 a



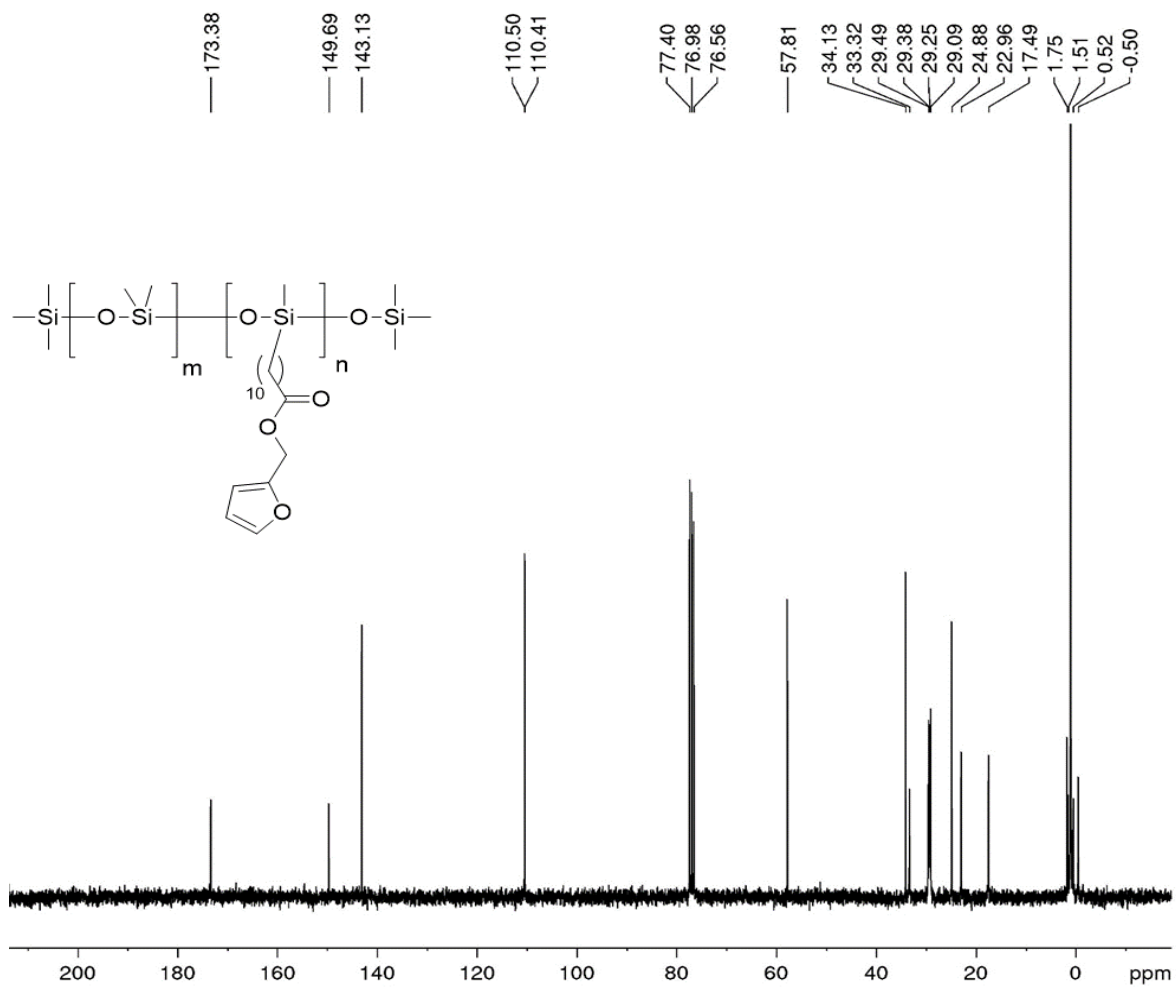
Appendix Figure 42 ^{29}Si NMR of compound 33 a

33 b



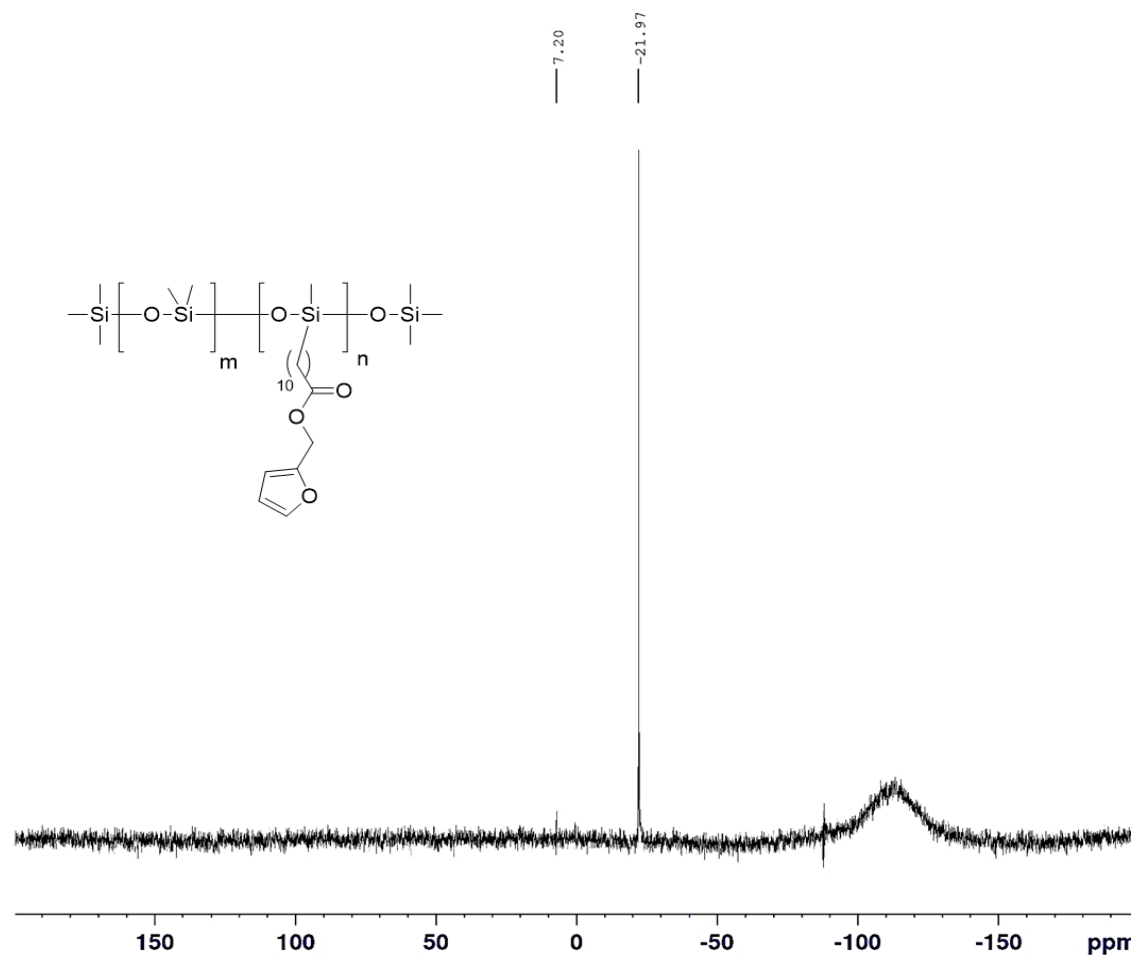
Appendix Figure 43 ^1H NMR of compound 33 b

33 b



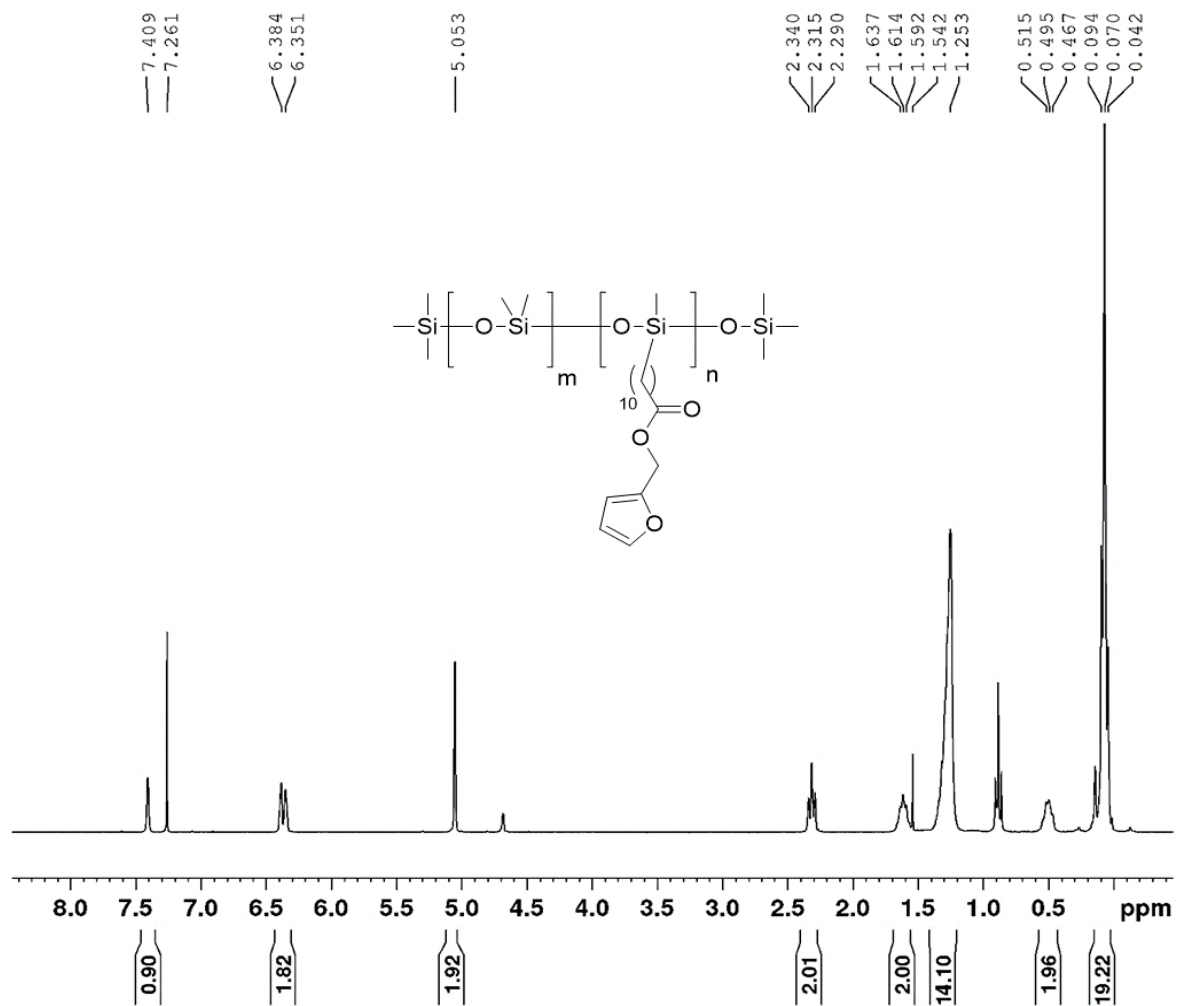
Appendix Figure 44 ^{13}C NMR of compound 33 b

33 b



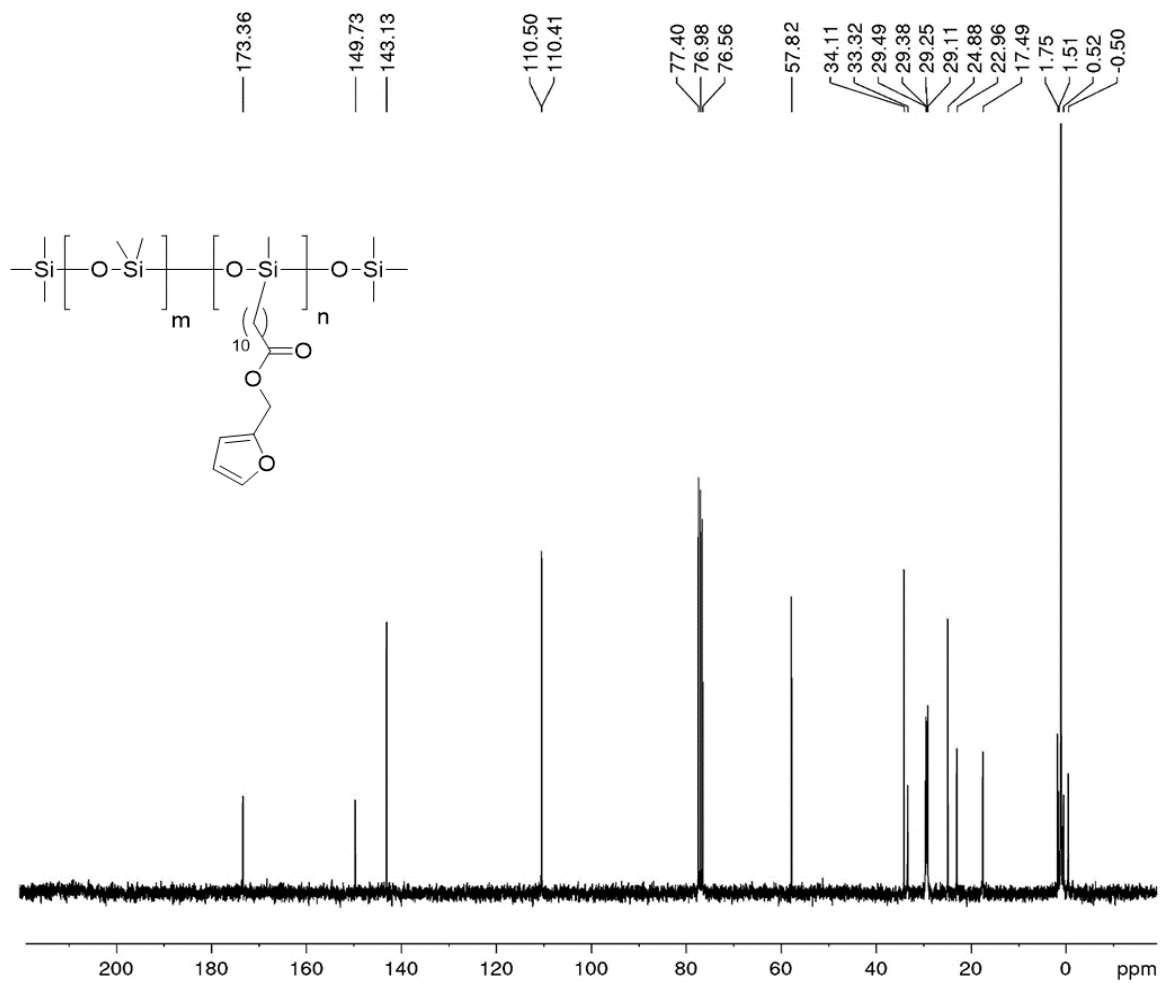
Appendix Figure 45 ^{29}Si NMR of compound 33 b

33 c



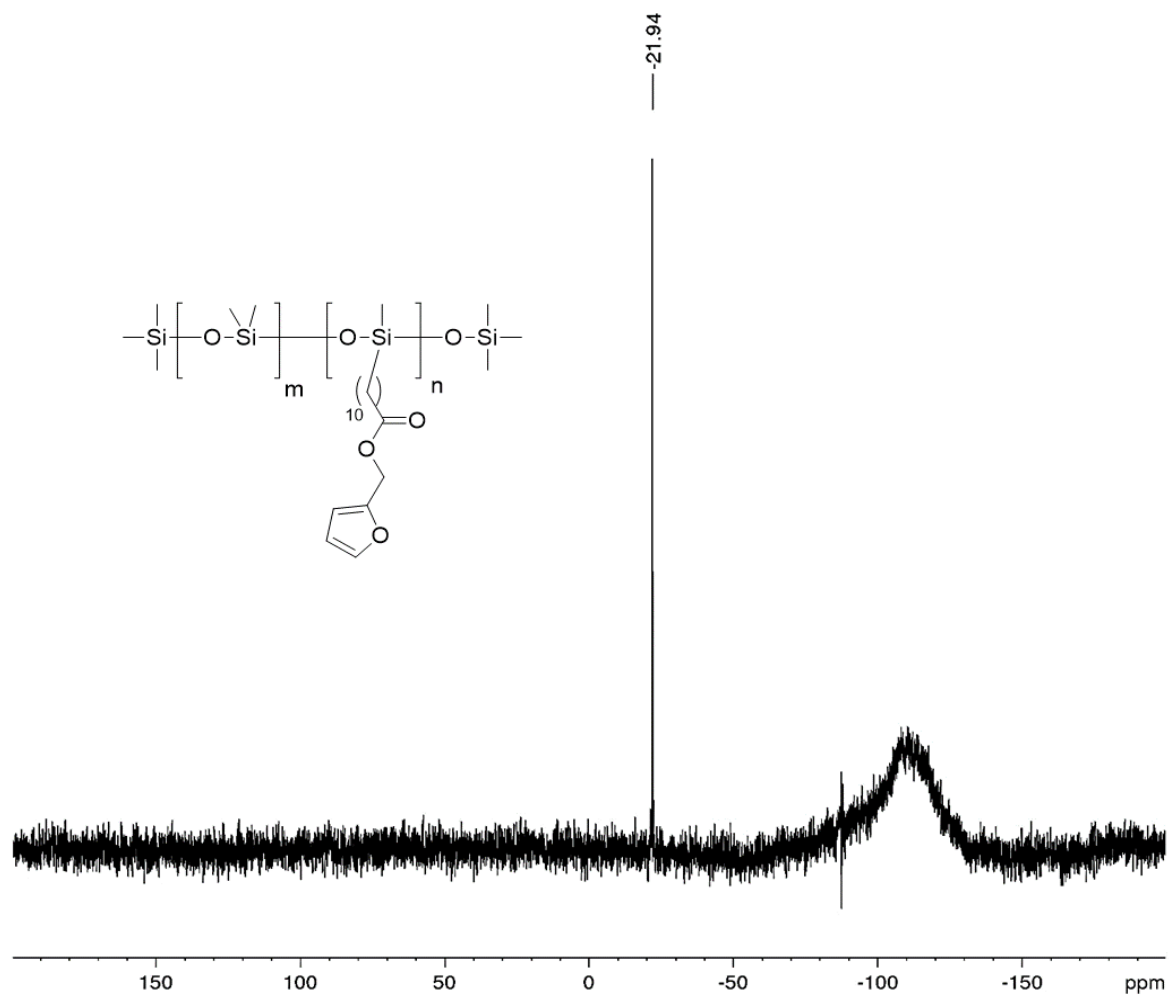
Appendix Figure 46 ^1H NMR of compound 33 c

33 c



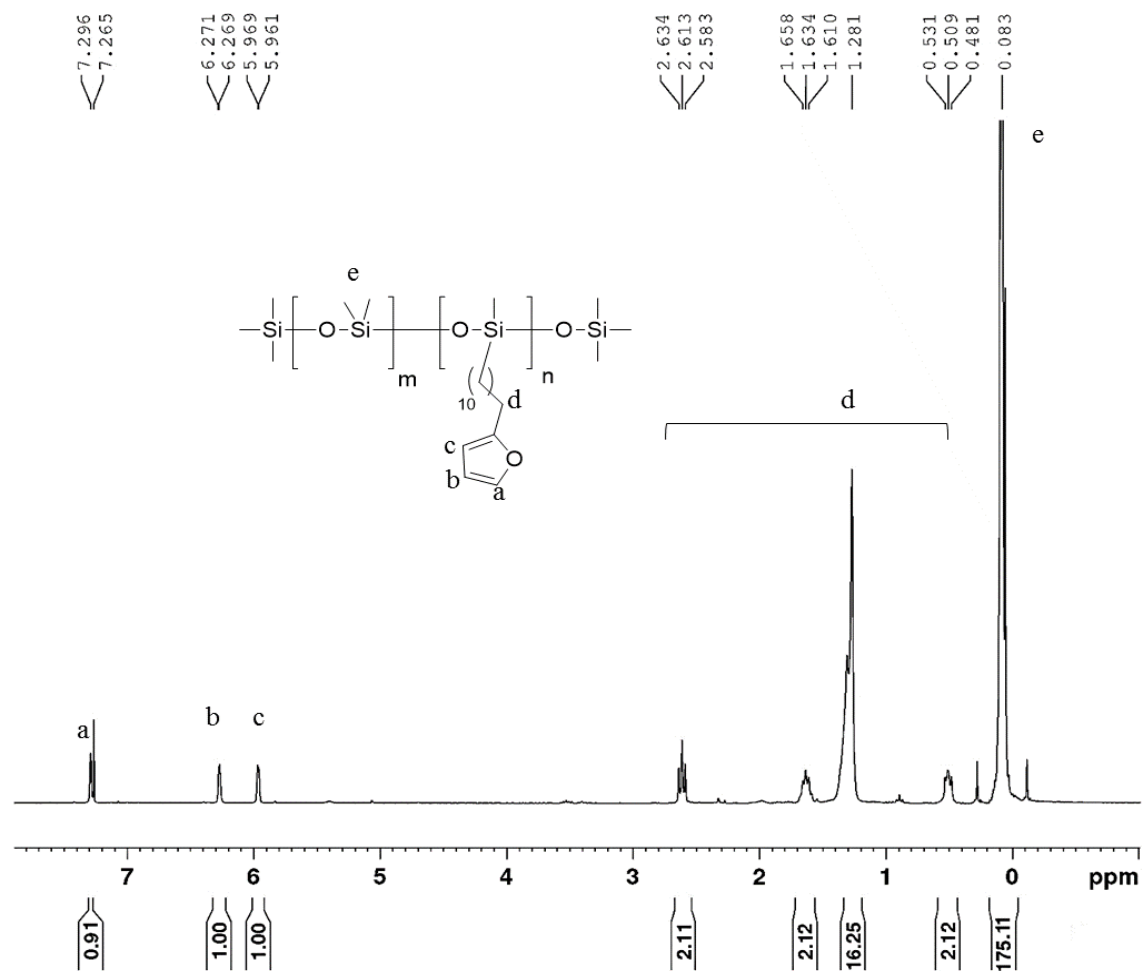
Appendix Figure 47 ^{13}C NMR of compound 33 c

33 c



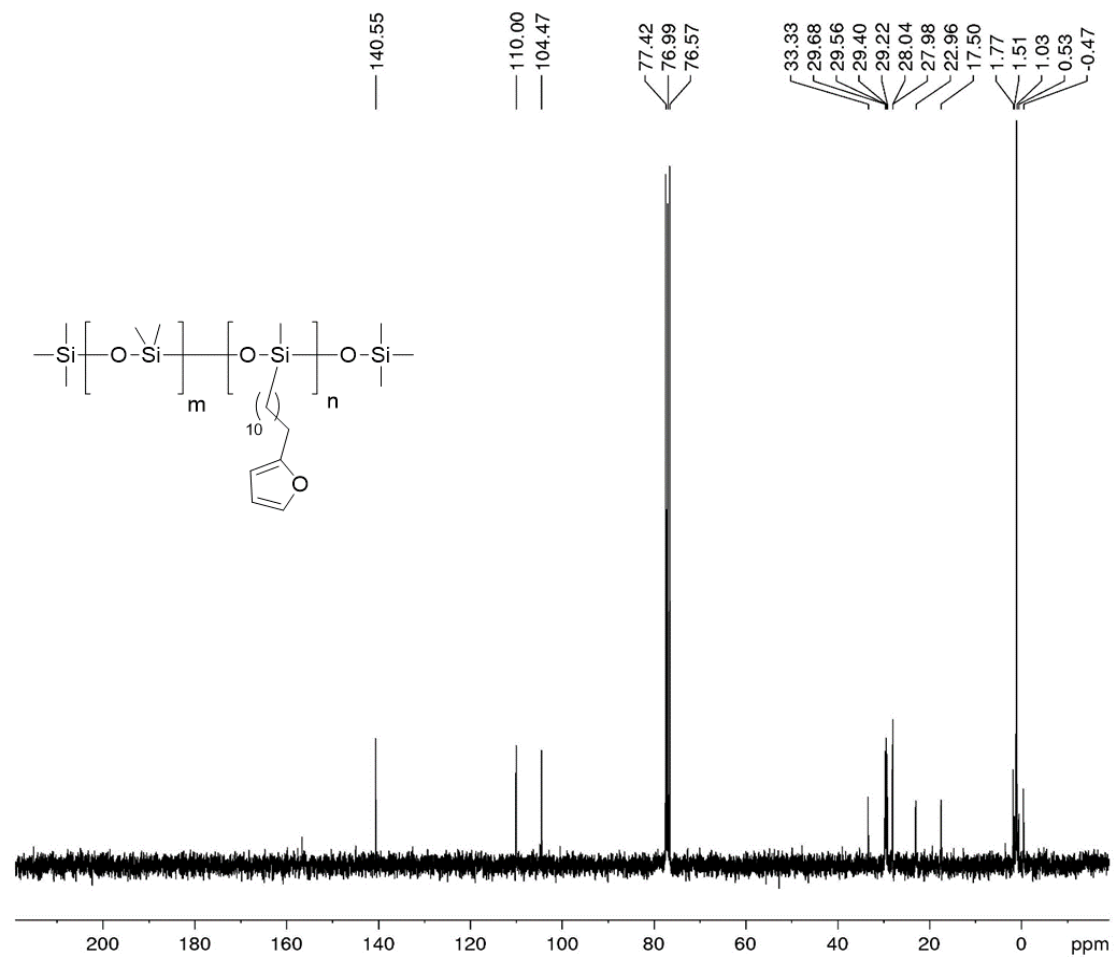
Appendix Figure 48 ^{29}Si NMR of compound 33 c

34 a



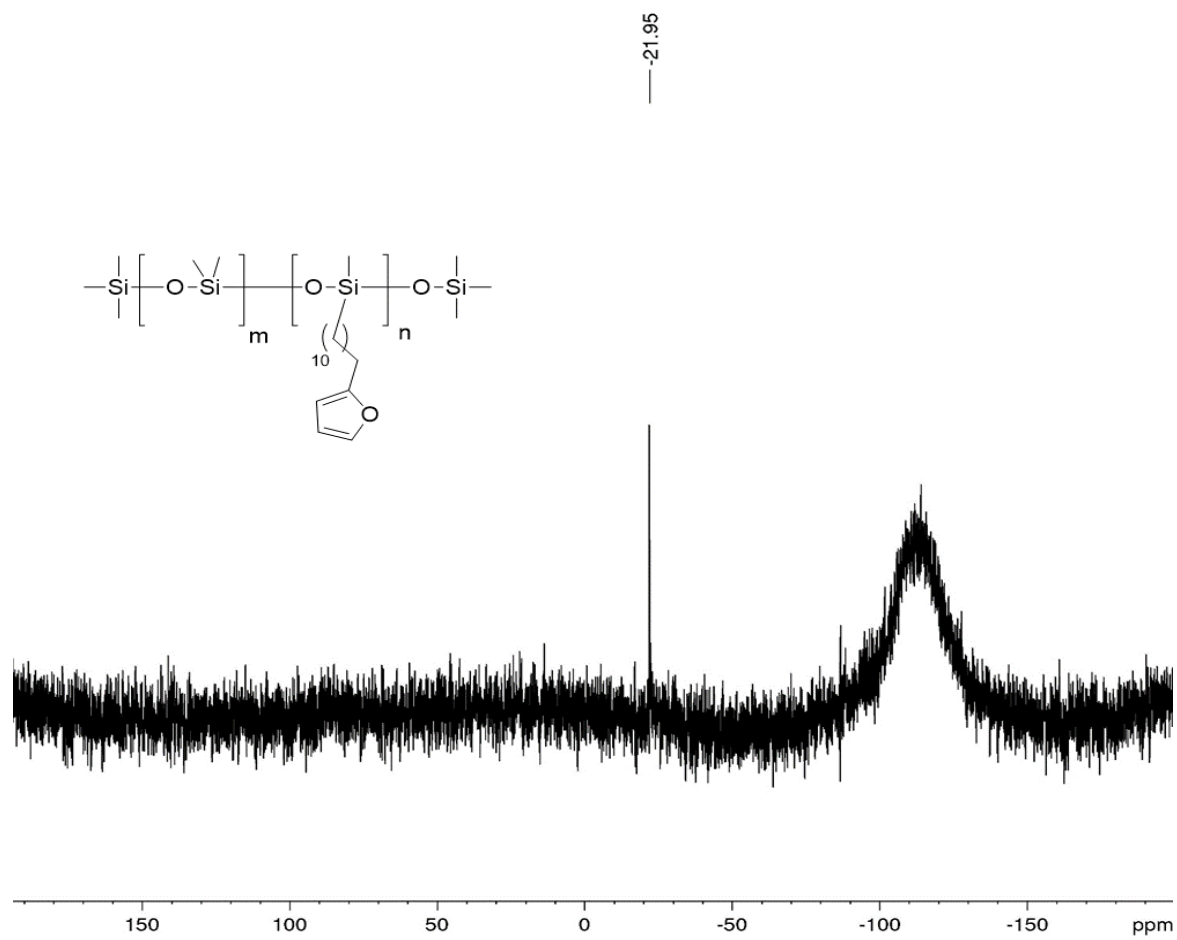
Appendix Figure 49 ¹H NMR of compound 34 a

34 a



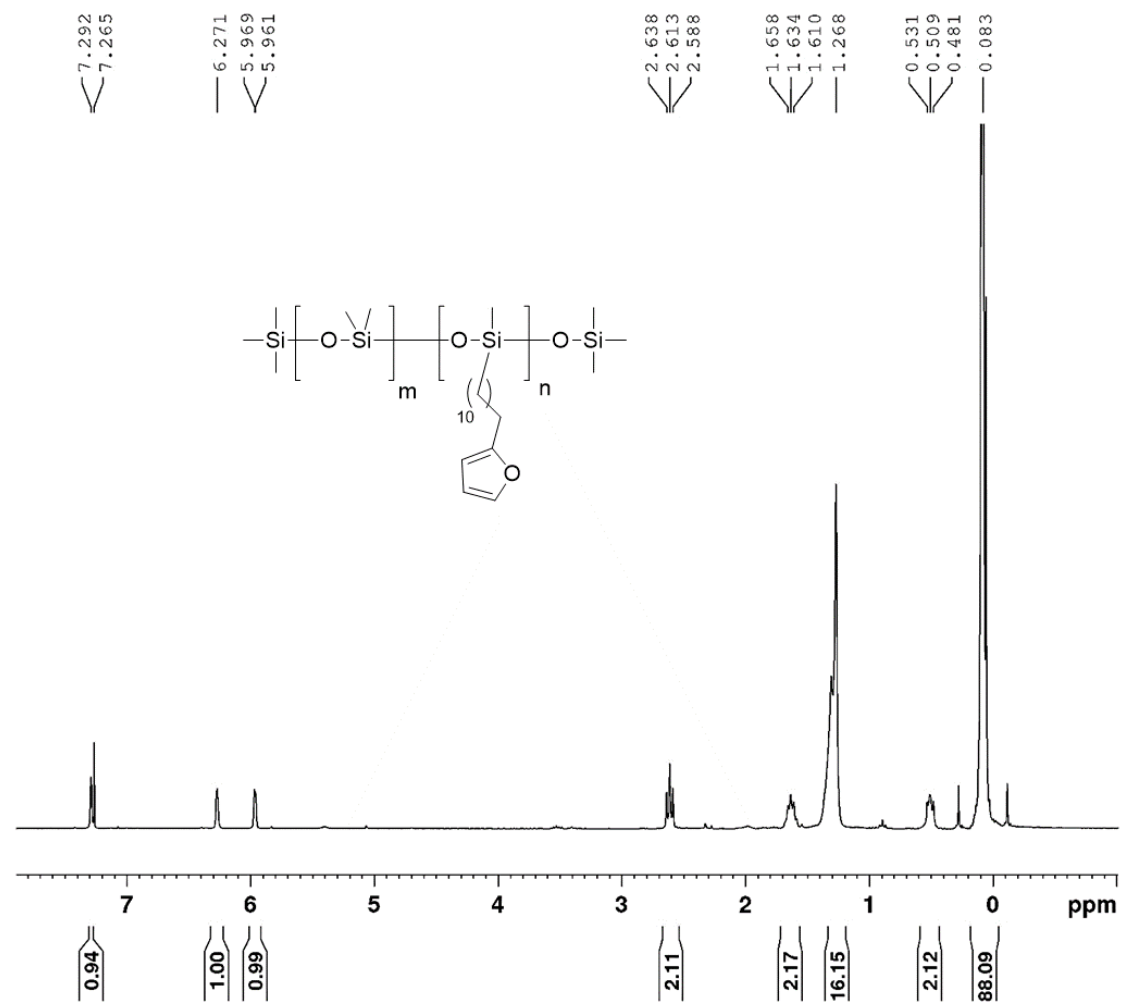
Appendix Figure 50 ^{13}C NMR of compound **34 a**

34 a



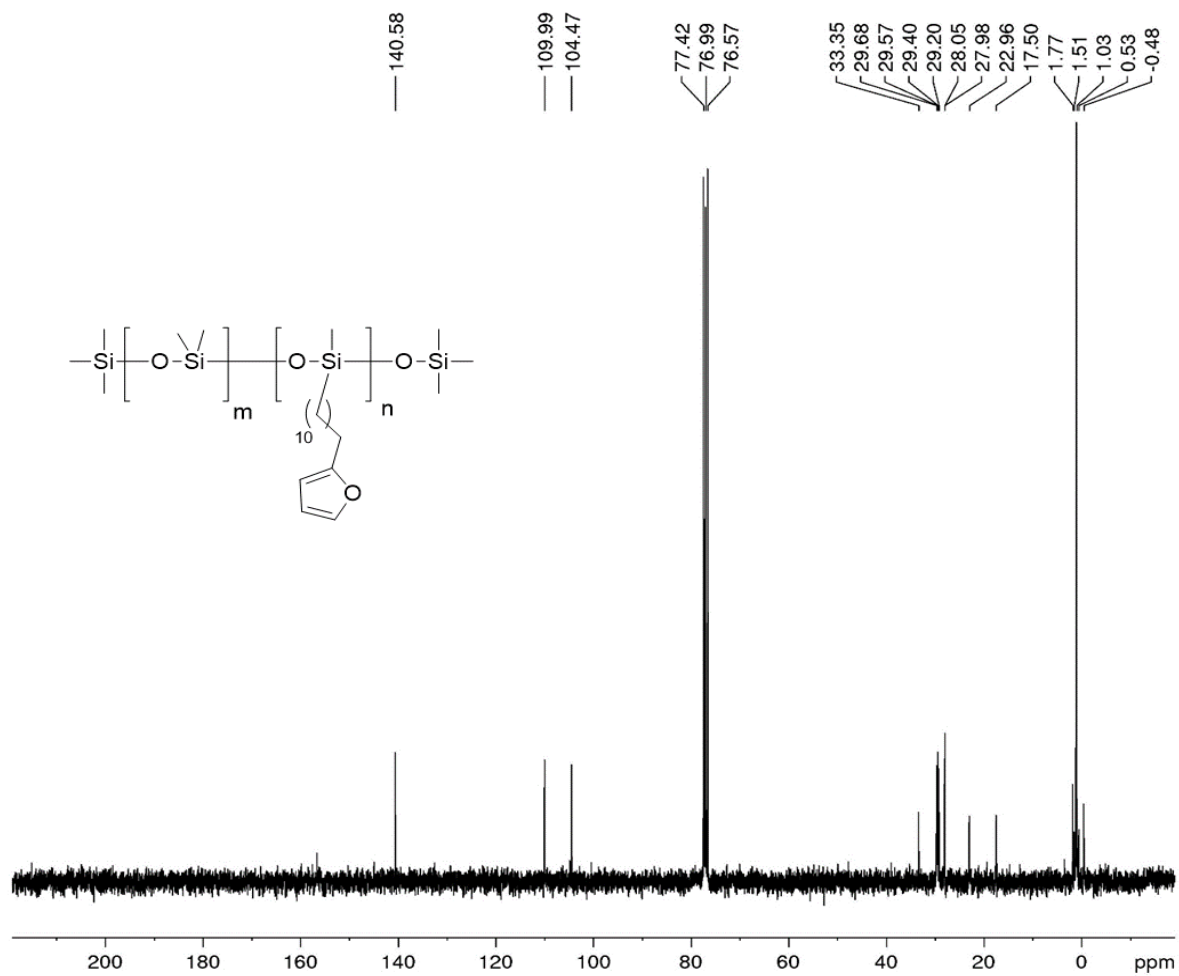
Appendix Figure 51 ^{29}Si NMR of compound 34 a

34 b



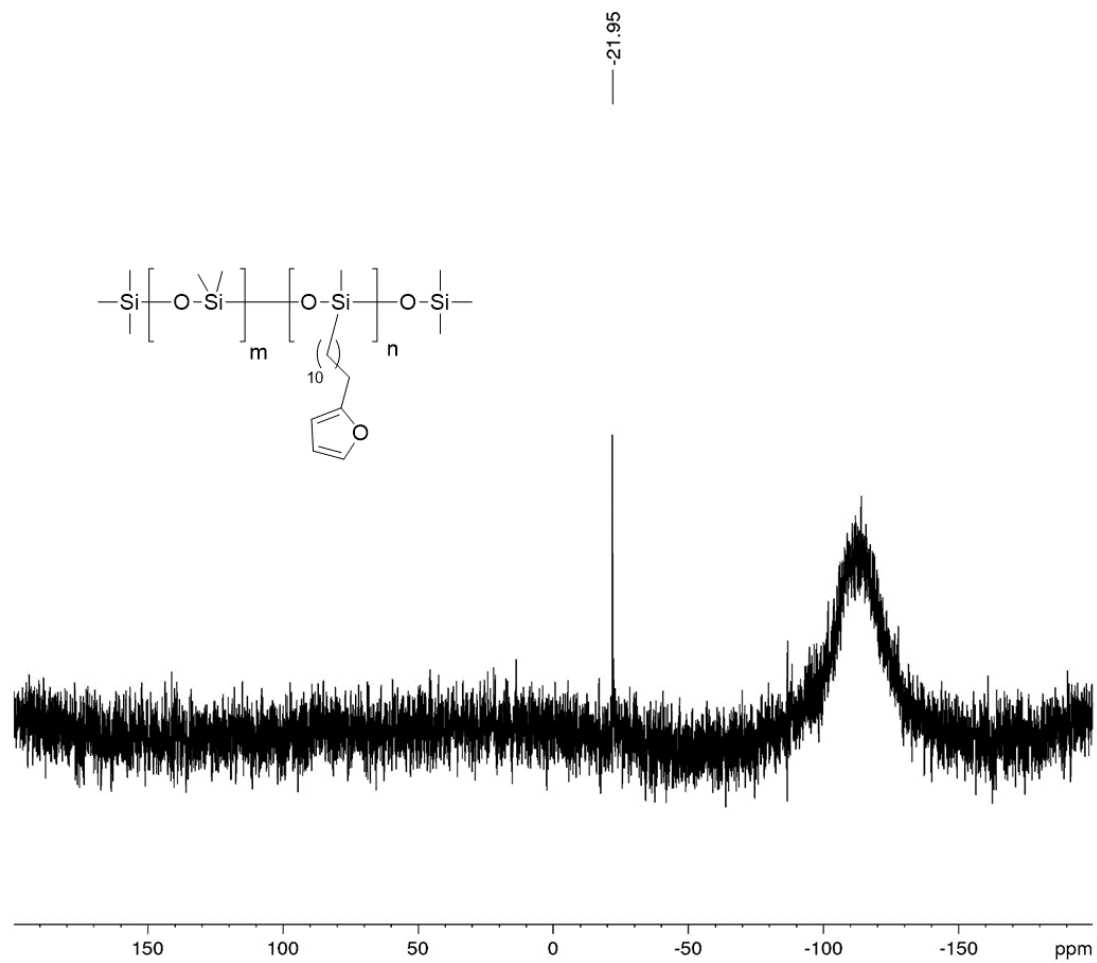
Appendix Figure 52 ¹H NMR of compound 34 b

34 b



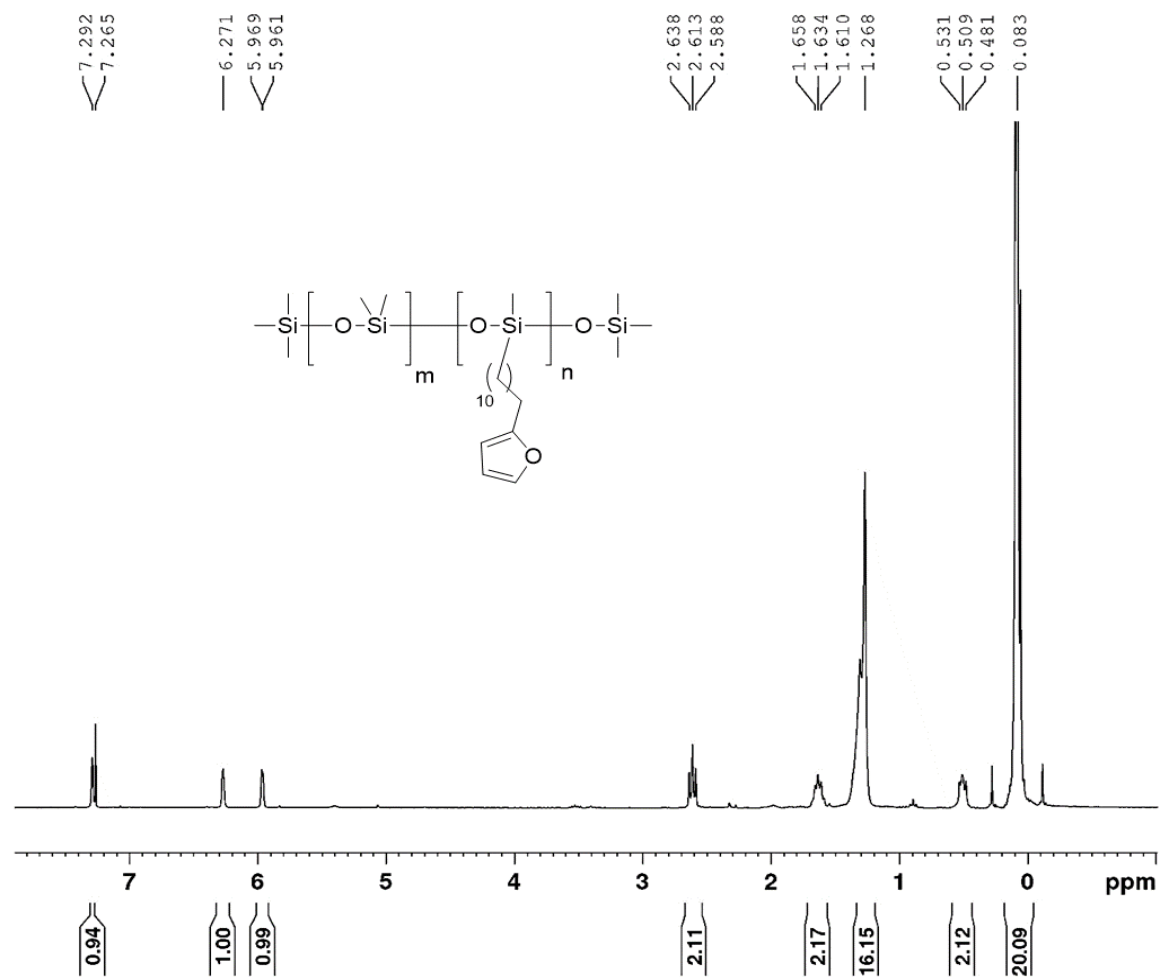
Appendix Figure 53 ^{13}C NMR of compound 34 b

34 b



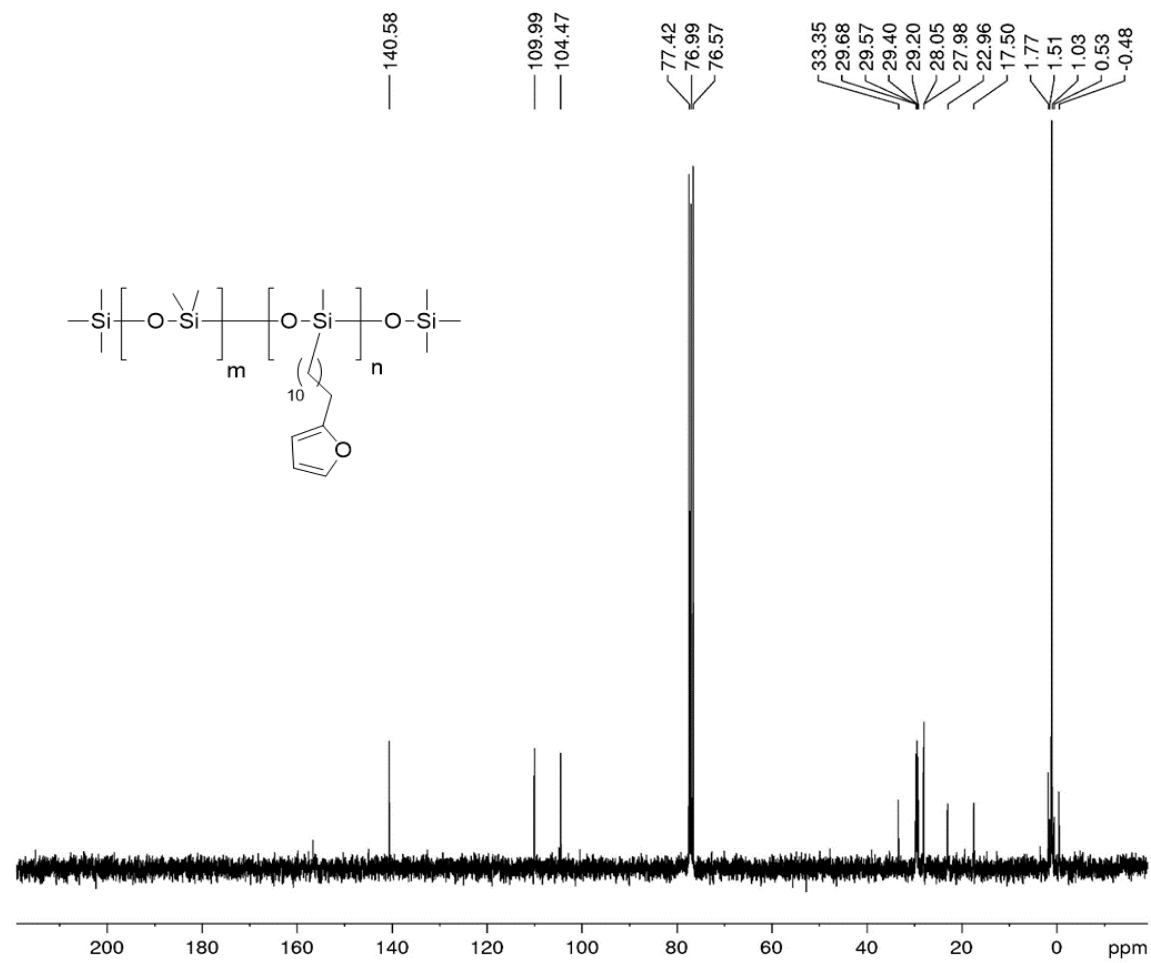
Appendix Figure 54 ^{29}Si NMR of compound 34 b

34 c



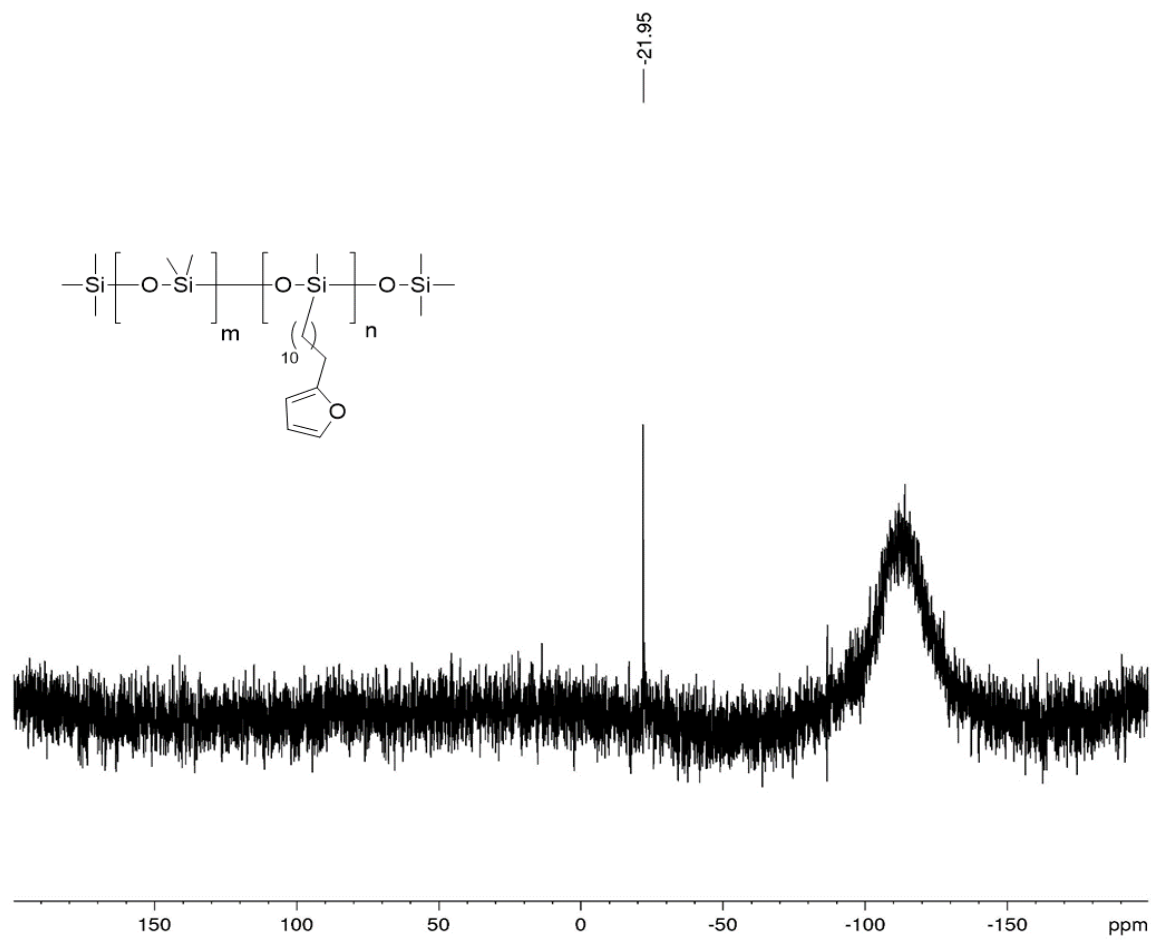
Appendix Figure 55 ¹H NMR of compound 34 c

34 c



Appendix Figure 56 ^{13}C NMR of compound 34 c

34 c



Appendix Figure 57 ²⁹Si NMR of compound 34 c

3.4.3.1.2 Vita

Paria Azadi Namin was born in Tehran, Iran on June 29, 1991. Her high school education was completed at Iran high school in Tehran (capital city of Iran) and got her diploma in mathematics in 2008. Later, she obtained her B.Sc. in applied chemistry from one of the prestigious Universities of Iran, Kharazmi University of Tehran in 2015. Afterwards, she applied for M.Sc. in organic chemistry and worked on her thesis under supervision of Prof. Mohammad Saeed Abae at Chemistry and Chemical Engineering Research Center of Iran and completed her M.Sc. in 2017. She began her second M.Sc. in organic chemistry in 2018 under supervision of Dr. Paul Zelisko.

References

- (1) N. Auner, J. W. *Organosilicon Chemistry III From Molecules to Materials*; WILEY-VCH, **1997**.
- (2) Yuri Magarshak, Sergey Kozyrev, A. K. V. *Silicon Versus Carbon NATO Science for Peace and Security Series*; Springer, **2008**.
- (3) Peter Jutzi, U. S. *Silicon Chemistry. From the Atom to Extended Systems*; Wiley-VCH, **2003**.
- (4) Brook, M. A. *Silicon in Organic, Organometallic, and Polymer Chemistry*; Wiley-VCH, **2000**.
- (5) Li, L.; Matsuo, T.; Hashizume, D.; Fueno, H.; Tanaka, K.; Tamao, K. Coplanar Oligo(p - Phenylenedisilylene)s as Si =Si Analogues of Oligo(p - Phenylenevinylene)s: Evidence for Extended π - Conjugation through the Carbon and Silicon π - Frameworks. *J. Am. Chem. Soc.* **2015**, *137* (47), 15026–15035.
- (6) Sekiguchi, A.; Kinjo, R.; Ichinohe, M. A Stable Compound Containing a Silicon-Silicon Triple Bond. *Science* (80-.). **2004**, *305*, 1755–1757.
- (7) Rich, J.; Drahnak, T.; West, R. Reversible DI-n-Methane Rearrangements of Bicyclic Organosilicon Compounds. *Organomet. Chem.* **1981**, *212*, 7–9.
- (8) Tomadze, A. V.; Yablokova, N. V. The Silicon Oxygen Double-Bonded Intermediates : A New Method for the Formation of Organosilanone. *J. Organomet. Chem.* **1981**, *212* (1), 43–50.
- (9) A. G. Brook J. W. Harris. Silicon-Carbon Double Bonds: New Route, New Substituents, New Behavior. *J. Am. Chem. Soc.* **1976**, *98* (11), 3381–3383.
- (10) Ravve, A. *Principles of Polymer Chemistry*, 3rd ed.; Springer-Verlag New York, **2012**.
- (11) Charles E. Carraher, J. *Introduction to Polymer Chemistry Fourth Edition*; Taylor & Francis Group, **2017**.
- (12) Carothers, W. H. . A. J. A. STUDIES ON POLYMERIZATION AND RING FORMATION. II. POLY-ESTERS. *J. Am. Chem. Soc.* **1929**, *51* (8), 2560–2570.
- (13) Flory, P. J. *Principles of Polymer Chemistry*; Cornell University Press: New York, **1953**.
- (14) Stevens, M. P. *Polymer Chemistry: An Introduction*; Oxford University Press, Inc., **1999**.
- (15) Pascault, J.; Sautereau, H.; National, I.; Verdu, J.; Williams, R. J. J.; Plata, M. *Thermosetting Polymers*, 1st ed.; Marcel Dekker: New York, **2002**.
- (16) Caruso, M. M.; Davis, D. A.; Shen, Qi.; Odom, S. A.; Sottos, N. R.; White, S. R.; Moore, J. S. Mechanically-Induced Chemical Changes in Polymeric Materials. *Chem. Rev* **2009**, *109*, 5755–5798.
- (17) Bhowmick, A. K.; Bhattacharya, M.; Mitra, S.; Dinesh Kumar, K.; Heinrich, G. *Advanced Rubber Composites*; Springer-Verlag Berlin Heidelberg, **2011**.

- (18) Spaeth, G. phenolic-resins-and-phenolic-molding-compounds
<https://www.slideserve.com/barto/phenolic-resins-and-phenolic-molding-compounds>.
- (19) Wool, R. P.; O'Connor, K. M. Time Dependence of Crack Healing. *J. Polym. Sci. Polym. Lett. Ed.* **1982**, *20* (1), 7–16.
- (20) Yonekawa, M.; Furusho, Y.; Takata, T.; Endo, T. Reversible Crosslinking and Decrosslinking of Polymers Containing Alcohol Moiety Using an Acyclic Bifunctional Vicinal Triketone. *Polym. Sci. Part A Polym. Chem.* **2014**, *52*, 921–928.
- (21) Du, P.; Wang, X.; Base, P. H. I.; City, Q. Reversible Cross-Linking Polymer-Based Self-Healing Materials. In *Recent Advances in Smart Self-healing Polymers and Composites*; Elsevier Ltd, **2015**; 159–179.
- (22) Chen, Y.; Guan, Z. Self-Assembly of Core–Shell Nanoparticles for Self-Healing Materials†. *Polym. Chem.* **2013**, *4*, 4885–4889.
- (23) Zwaag, S. V. *Self Healing Materials An Alternative Approach to 20 Centuries Of Materials Science*; Springer, **2007**.
- (24) Balani, K.; Verna, V.; Agarwal, A.; Narayan, R. Physical, Thermal, and Mechanical Properties of Polymers. In *Biosurfaces*; John Wiley & Sons, Inc., **2015**; pp 329–344.
- (25) Davis, J. D. *Polymer Chemistry: A Practical Approach*; Oxford University Press, Inc., **2004**.
- (26) Odian, G. *Principles of Polymerization*, Fourth.; JOHN WILEY & SONS, INC., **2004**.
- (27) Cheng, S. Z. D.; Jin, C. S. *Handbook of Thermal Analysis and Calorimetry*; Elsevier Science B.V., **2002**.
- (28) Gunatillake, P. A.; Adhikari, R. Nondegradable Synthetic Polymers for Medical Devices and Implants. In *Biosynthetic Polymers for Medical Applications*; Elsevier Ltd., **2016**; 33–62.
- (29) Brydson, J. A. Silicones and Other Heat-Resisting Polymers. In *Plastics Materials*; Elsevier Ltd., **1944**; 814–852.
- (30) Hanu, L. G.; Simon, G. P.; Cheng, Y. Thermal Stability and Flammability of Silicone Polymer Composites. *Polym. Degrad. Stab.* **2006**, *91* (6), 1373–1379.
- (31) Lin, S. B. High-Temperature Stability of Silicone Polymers and Related Pressure-Sensitive Adhesives. *J. Am. Chem. Soc.* **1995**, *5*, 37–51.
- (32) Madsen, F. B.; Yu, L.; Skov, A. L. Self-Healing, High-Permittivity Silicone Dielectric Elastomer. *ACS Macro Lett.* **2016**, *5*, 1196–1200.
- (33) Madsen, F. B.; Yu, L.; Daugaard, A. E.; Hvilsted, S.; Skov, A. L. Silicone Elastomers with High Dielectric Permittivity and High Dielectric Breakdown Strength Based on Dipolar Copolymers. *Polymer (Guildf)*. **2014**, *55* (24), 6212–6219.
- (34) Owen, M. J.; Dvornic, P. R. *Silicone Surface Science*, 1st ed.; Springer Netherlands, **2012**.
- (35) Zhu, Y.; Otsubo, M.; Honda, C.; Tanaka, S. Loss and Recovery in Hydrophobicity of Silicone Rubber Exposed to Corona Discharge. *Polym. Degrad. Stab.* **2006**, *91* (7), 1448–

1454.

- (36) Kowalewska, A.; Kupcik, J.; Pola, J. Laser Irradiation of Oligosiloxane Copolymer Thin Films Functionalized with Side Chain Bulky Carbosilane Moieties. *Polymer (Guildf)*. **2008**, *49*, 857–866.
- (37) Mani, S.; Cassagnau, P.; Bousmina, M.; Chaumont, P. Rheological Modelling of the Free-Radical Crosslinking of PDMS Rubber in the Presence of TEMPO Nitroxide. *Polymer (Guildf)*. **2010**, *51* (17), 3918–3925.
- (38) Hoyle, C. E.; Bowman, C. N. Polymer Chemistry Thiol – Ene Click Chemistry. *Polym. Chem.* **2010**, *49*, 1540–1573.
- (39) Lewis, L. N.; Stein, J.; Gao, Y. Platinum Catalysts Used in the Silicones Industry. *Platin. Met. Rev.* **1997**, *41* (2), 66–75.
- (40) Pan, Z.; Liu, M.; Zheng, C.; Gao, D.; Huang, W. Study of Karstedt ' s Catalyst for Hydrosilylation of a Wide Vari- Ety of Functionalized Alkenes with Triethoxysilane and Trimethoxysilane. *Chinese J. Chem.* **2017**, *35* (8), 1227–1230.
- (41) Marciniak, B.; Maciejewski, H.; Pietraszuk, C.; Pawluc, P. Hydrosilylation and Related Reactions of Silicon Compounds. In *Applied Homogeneous Catalysis with Organometallic Compounds: A Comprehensive Handbook in Four Volumes*; Wiley-VCH Verlag GmbH & Co., **2017**; 569–620.
- (42) Sommer, L. H.; Pietrusza, E. W.; Whitmore, F. C. Peroxide-Catalyzed Addition of Trichlorosilane to 1-Octene. *J. Am. Chem. Soc.* **1947**, *69* (1), 188.
- (43) Speier, J. L.; Webster, J. A.; Barnes, G. H. The Addition of Silicon Hydrides to Olefinic Double Bonds. Part II. The Use of Group VIII Metal Catalysts. *J. Am. Chem. Soc.* **1957**, *79* (4), 974–979.
- (44) Karstedt, B. Platinum Complexes of Unsaturated Siloxanes and Platinum Containing Organopolysiloxane, **1973**.
- (45) Lewis, L. N. On the Mechanism of Metal Colloid Catalyzed Hydrosilylation: Proposed Explanations for Electronic Effects and Oxygen Cocatalysis. *J. Am. Chem. Soc.* **1990**, *112* (16), 5998–6004.
- (46) Sabourault, N.; Mignani, G.; Wagner, A.; Mioskowski, C. Platinum Oxide (PtO₂): A Potent Hydrosilylation Catalyst. *Org. Lett.* **2002**, *4* (13), 2117–2119.
- (47) Yang, G.; Wei, Y.; Huang, Z.; Hu, J.; Liu, G.; Ou, M.; Lin, S.; Tu, Y. Rapid and Efficient Collection of Platinum from Karstedt ' s Catalyst Solution via Ligands-Exchange Induced Assembly. *ACS Appl. Mater. & Interfaces* **2018**, *10* (7), 6778–6784.
- (48) Nakajima, Y. . S. S. Hydrosilylation Reaction of Olefins: Recent Advances and Perspective. *RSC. Adv* **2015**, *5*, 20603–20616.
- (49) Gebauer, C.; Fischer, J.; Wassner, M.; Diemant, T.; Bansmann, J.; Hüsing, N.; Behm, R. J. Novel N, C Doped Ti(IV)-Oxides as Pt-Free Catalysts for the O₂ Reduction Reaction. *Electrochim. Acta* **2014**, *146*, 335–345.

- (50) Hofmann, R. J.; Vlatkovic, M.; Wiesbrock, F. Fifty Years of Hydrosilylation in Polymer Science : A Review of Current Trends of Low-Cost and Industrial Applications. *Polymers (Basel)*. **2017**, 9 (10), 534.
- (51) Tsipis, C. A.; Kefalidis, C. E. Hydrosilylation , Hydrocyanation , and Hydroamination of Ethene Catalyzed by Bis (Hydrido-Bridged) Diplatinum Complexes : Added Insight and Predictions from Theory. *J. Organomet. Chem.* **2007**, 692 (23), 5245–5255.
- (52) Matison, J. *Hydrosilylation: A Comprehensive Review on Recent Advances*, 1st ed.; Marciniak, B., Ed.; Springer Netherlands, **2009**.
- (53) Fischer, E.; Speier, A. Darstellung Der Ester. *Chem. Ber.* **1895**, 28 (3), 3252–3258.
- (54) Clausen, T. P. Combining a Standard Fischer Esterification Experiment with Stereochemical and Molecular-Modeling Concepts. *Chem. Educ.* **2011**, 88 (7), 1007–1009.
- (55) Wade, L. G. *Organic Chemistry*; Prentice Hall, **2012**.
- (56) Carey, F. A.; Gullano, R. M. *Organic Chemistry*, 8th ed.; McGraw-Hill, **2011**.
- (57) Ericsson, D. J.; Kasrayan, Al.; Johansson, P.; Bergfors, T.; Sandström, A. G.; Bäckvall, J.; Mowbray, S. L. X-Ray Structure of Candida Antarctica Lipase A Shows a Novel Lid Structure and a Likely Mode of Interfacial Activation. *J. Mol. Biol.* **2008**, 376 (1), 109–119.
- (58) Drauz, K.; Groger, H.; May, O. *Enzyme Catalysis in Organic Synthesis*; Wiley-VCH, **2012**.
- (59) Tuomi, W. V.; Kazlauskas, R. J. Molecular Basis for Enantioselectivity of Lipase from Pseudomonas Cepacia toward Primary Alcohols . Modeling , Kinetics , and Chemical Modification of Tyr29 to Increase or Decrease Enantioselectivity. *J. Org. Chem.* **1999**, 64 (4), 2638–2647.
- (60) Mugford, P. F.; Wagner, U. G.; Jiang, Y.; Faber, K.; Kazlauskas, R. J. Minireviews Enzyme Catalysis Enantiocomplementary Enzymes : Classification , Molecular Basis for Their Enantioselectivity , and Prospects for Mirror-Image Biotransformations. *Angew. Chem. Int. Ed.* **2008**, 47, 8782–8793.
- (61) Kazlauskas, R. J.; Weissflog, A. N. E.; Rappaport, A. T.; Cuccia, L. A. A Rule To Predict Which Enantiomer of a Secondary Alcohol Reacts Faster in Reactions Catalyzed by Cholesterol Esterase , Lipase from Pseudomonas. *J. Org. Chem.* **1991**, 56 (11), 2656–2665.
- (62) Raza, S.; Fransson, L.; Hult, K. Enantioselectivity in Candida Antarctica Lipase B : A Molecular Dynamics Study. *Protein Sci.* **2001**, 10, 329–338.
- (63) Lutz, S. Engineering Lipase B from Candida Antarctica. *Tetrahedron: Asymmetry* **2004**, 15 (71), 2743–2748.
- (64) Frampton, M. B.; Jones, T. R. B.; Zelisko, P. M. Cyclotetrasiloxane Frameworks for the Chemoenzymatic Synthesis of Oligoesters †. *RSC Adv.* **2015**, 5, 1999–2008.
- (65) Binder, W. H. *Self-Healing Polymers From Principles to Applications*; Wiley-VCH, **2013**.
- (66) Hart, L. R.; Harries, J. L.; Colquhoun, H. M.; Hayes, W. Healable Supramolecular Polymers. *Polym. Chem.* **2013**, 4, 4860–4870.

- (67) Kalista, S. J.; Pflug, J. R.; Varley, R. J. . Effect of Ionic Content on Ballistic Self-Healing in EMAA Copolymers and Ionomers. *Polym. Chem.* **2013**, *4*, 4910–4926.
- (68) Ghosh, S. K. *Self-Healing Materials Fundamentals, Design Strategies, and Applications*; Wiley-VCH, **2009**.
- (69) Raimondo, M.; Longo, P.; Mariconda, A.; Guadagno, L. Healing Agent for the Activation of Self- Healing Function at Low Temperature. *Adv. Compos. Mater.* **2014**, *24* (6), 519–529.
- (70) Vimalanandan, A.; Lv, L.; Tran, T.; Landfester, K.; Crespy, D.; Rohwerder, M. Redox-Responsive Self-Healing for Corrosion Protection. *Adv. Mater.* **2013**, *25*, 6980–6984.
- (71) Wool, R. P. Self-Healing Materials : A Review. *Soft Matter* **2008**, *4*, 400–418.
- (72) Prager, S.; Adolf, D.; Tirrell, M. Welding of Polymer Networks. *Chem. Phys.* **1986**, *84*, 5152.
- (73) Herbst, Fl.; Döhler, D.; Michael, P.; Binder, W. H. Self-Healing Polymers via Supramolecular Forces. *Macromol. Rapid Commun.* **2013**, *34* (3), 203–220.
- (74) Zhang, M. Q.; Rong, M. Z. Theoretical Consideration and Modeling of Self-Healing Polymers. **2012**, 229–241.
- (75) Wool, R. P.; O’Connor, K. M. A Theory of Crack Healing in Polymers. *Appl. Phys.* **1981**, *52*, 5953–5963.
- (76) Wool, R. P. Welding, Tack, and Green Strength of Polymers. In *Fundamentals of Adhesion*; Springer, Boston, MA, **1991**; 207–248.
- (77) Khan, N. I.; Halder, S.; Gunjan, S. B.; Prasad, T. A Review on Diels-Alder Based Self-Healing Polymer Composites. In *IOP Conference Series: Materials Science and Engineering*; **2018**; 1–9.
- (78) Greef, T.; Meijer, E. W. Supramolecular Polymers. *Mater. Sci.* **2008**, *453* (8), 171–173.
- (79) Sijbesma, R. P.; Beijer, F. H.; Brunsveld, L.; Folmer, B. J. B.; Hirschberg, J. H. K. K.; Lange, R. F. M.; Lowe, J. K. L.; Meijer, E. W. Reversible Polymers Formed from Self-Complementary Monomers Using Quadruple Hydrogen Bonding. *Science* (80-.). **1997**, *278* (5343), 1601–1604.
- (80) Kumar, S.; Kumar, V.; Singh, S. P. *Pericyclic Reactions : A Mechanistic and Problem-Solving Approach*, 1st ed.; Elsevier Academic Press: London, UK, San Diego, CA, USA, **2016**.
- (81) Fleming, I. *Pericyclic Reactions*; Oxford University Press, USA, **1998**.
- (82) Kumar, S.; Kumar, V.; Singh, S. P. *Cycloaddition Reactions : A Mechanistic and Problem Solving Approach*, 1st ed.; Elsevier Academic Press: London, UK, San Diego, CA, USA, **2016**.
- (83) Azadi-Namin, P. Investigation of Diels-Alder Reaction of Styrylcyclohex-2-Enone Diens with Acrylo Nitrile, Chemistry and Chemical Engineering Reaserch Center of Iran, **2016**.

- (84) Diels, O.; Alder, K. Synthesen in Der Hydroaromatischeii Reihe. *Justus Liebigs Ann. Chem.* **1928**, 460 (1), 98–122.
- (85) Fukui, K.; Yonezawa, T.; Shingu, H. A Molecular Orbital Theory of Reactivity in Aromatic Hydrocarbons. *Chem. Phys.* **1952**, 20 (4), 722–725.
- (86) Fukui, K. Recognition of Stereochemical Paths by Orbital Interaction. *Acc. Chem. Res.* **1971**, 4 (2), 57–64.
- (87) Pohland, A. E.; Badger, R. C. Selection Rules for Sigmatropic Reactions. *Commun. to Ed.* **1965**, 3337 (1949), 2511–2513.
- (88) Houk, K. N. The Frontier Molecular Orbital Theory of Cycloaddition Reactions. *Acc. Chem. Res.* **1974**, 8, 361–369.
- (89) Evans, P. A. *Stereoselective Synthesis. 3, Stereoselective Pericyclic Reactions, Cross Coupling, C-H and C-X Activation*; Thieme: Stuttgart, **2011**.
- (90) Fleming, I. *Molecular Orbitals and Organic Chemical Reactions*, Reference.; John Wiley & Sons Ltd., **2010**.
- (91) Woodward, R. B.; Hoffmann, R. The Conservation of Orbital Symmetry. *Angew. Chem. Int. Ed.* **1969**, 8 (11), 781–932.
- (92) Martin, K. J. Stereochemistry of Electrocyclic Reactions. *Commun. to Ed.* **1964**, 151 (1961), 395–397.
- (93) Amarne, H. Y.; Bain, A. D.; Neumann, K.; Zelisko, P. M. Extensions of a Basic Laboratory Experiment : [4 + 2] and [2 + 2] Cycloadditions. *Chem. Educ.* **2008**, 85 (2), 3–5.
- (94) Pellissier, H. Asymmetric Hetero-Diels – Alder Reactions of Carbonyl Compounds. *Tetrahedron* **2009**, 65 (869), 2839–2877.
- (95) Sustmann, R.; Lopusinski, A. Substituent Effects in Diels-Alder Additions. *Angew. Chem. Int. Ed.* **1972**, 11 (9), 838–840.
- (96) Lu, L.; Yang, S. S.; Wang, Z.; Cooks, R. G. Normal and Inverse Electron Demand Diels-Alder Cycloaddition of Protonated and Methylated Carbonyl Compounds in the Gas Phase. *Mass Spectrom.* **1995**, 30, 581–594.
- (97) Sauer, J.; Heldmann, D. K.; Hetzenegger, J.; Krauthan, J.; Sichert, H.; Schuster, J. 1,2,4,5-Tetrazine: Synthesis and Reactivity in [4+2] Cycloadditions. *European J. Org. Chem.* **1998**, 12, 2885–2896.
- (98) Vivat, J. F.; Adams, H.; Harrity, J. P. A. Ambient Temperature Nitrogen-Directed Difluoroalkynylborane Carboni - Lindsey Cycloaddition Reactions. *Org. Lett.* **2010**, 12, 160–163.
- (99) Mohajeri, A.; Shahamirian, M. Theoretical Study of Diels-Alder Reaction : Role of Substituent in Regioselectivity and Aromaticity. *Iran. Chem. Soc.* **2010**, 7 (3), 554–563.
- (100) Gill, G. B.; Willis, M. R. The Concept of the Conservation of Orbital Symmetry. In *Pericyclic Reactions*; Springer, Dordrecht, **1974**; 99–127.

- (101) Danishefsky, S.; Kitahara, T. A Useful Diene for the Diels-Alder Reaction. *Commun. to Ed.* **1974**, *7*, 7807–7808.
- (102) Kotha, S.; Chavan, A. S.; Goyal, D. Diversity-Oriented Approaches to Polycyclics and Bioinspired Molecules via the Diels-Alder Strategy: Green Chemistry, Synthetic Economy, and Beyond. *ACS Comb. Sci.* **2015**, *17* (5), 253–302.
- (103) Arai, Y.; Matsui, M.; Koizumi, T.; Shiro, M. Powerful Dienophiles for Asymmetric Diels-Alder Reactions: α -(2-Exo-Hydroxy-10-Bornylsulfinyl)Maleimides. *J. Org. Chem.* **1991**, *56* (6), 1983–1985.
- (104) Sauer, J.; Sustmann, R. Mechanistic Aspects of Diels-Alder Reactions : A Critical Survey. *Angew. Chem. Int. Ed.* **1980**, *19*, 779–807.
- (105) Ginsburg, D. The Role of Secondary Orbital Interactions in Control of Organic Reactions. *Tetrahedron* **1983**, *39* (13), 2095–2135.
- (106) Sauer, J. Diels-Alder Reactions II: The Reaction Mechanism. *Angew. Chemie Int. Ed. English* **1967**, *6* (1), 16–33.
- (107) Meir, R.; Chen, H.; Lai, W.; Shaik, S. Oriented Electric Fields Accelerate Diels-Alder Reactions and Control the Endo/Exo Selectivity. *ChemPhysChem* **2010**, *11* (1), 301–310.
- (108) Fernández, I.; Bickelhaupt, F. M. Origin of the “Endo Rule” in Diels-Alder Reactions. *J. Comput. Chem.* **2013**, *35* (5), 371–376.
- (109) Wiggins, K. M.; Syrett, J. A.; Haddleton, D. M.; Bielawski, C. W. Mechanically Facilitated Retro [4 + 2] Cycloadditions. *J. Am. Chem. Soc* **2015**, *137* (9), 3430–3430.
- (110) Zhou, J.; Guimard, N. K.; Inglis, A. J.; Namazian, M.; Lin, C. Y.; Coote, M. L.; Spyrou, E.; Hilf, S.; Schmidt, G.; Barner-kowollik, C. Thermally Reversible Diels – Alder-Based Polymerization : An Experimental and Theoretical Assessment †. *Polym. Chem.* **2012**, *3* (3), 628–639.
- (111) Sanyal, A. Diels – Alder Cycloaddition-Cycloreversion : A Powerful Combo in Materials Design. *Macromol. Chem. Phys.* **2010**, *211*, 1417–1425.
- (112) Murphy, E. B.; Wudl, F. Progress in Polymer Science The World of Smart Healable Materials. *Prog. Polym. Sci.* **2010**, *35*, 223–251.
- (113) Zhao, J.; Xu, R.; Luo, G.; Wu, J.; Xia, H. A Self-Healing, Re-Moldable and Biocompatible Crosslinked Polysiloxane Elastomer. *Mater. Chem. B* **2016**, *4*, 982–989.
- (114) Gheneim, R.; Perez-berumen, C.; Gandini, A. Diels - Alder Reactions with Novel Polymeric Dienes and Dienophiles: Synthesis of Reversibly Cross-Linked Elastomers. *Macromolecules* **2002**, *35* (19), 7246–7253.
- (115) Reutenauer, P.; Buhler, E.; Boul, P. J.; Candau, S. J.; Lehn, J. M. Room Temperature Dynamic Polymers Based on Diels-Alder Chemistry. *Chem. - A Eur. J.* **2009**, *15* (8), 1893–1900.
- (116) Polgar, L. M.; Duin, M. V.; Broekhuis, A. A.; Picchioni, F. Use of Diels – Alder Chemistry for Thermoreversible Cross-Linking of Rubbers : The Next Step toward Recycling of

Rubber Products ? *Macromolecules* **2015**, *48*, 7096–7105.

- (117) Kickelbick, G.; Schafer, S. Self-Healing Polymer Nanocomposites Based on Diels-Alder-Reactions with Silica Nanoparticles : The Role of the Polymer Matrix. *Polymer (Guildf)*. **2015**, *69*, 357–368.
- (118) Nasresfahani, A.; Zelisko, P. M. Synthesis of a Self-Healing Siloxane-Based Elastomer Cross-Linked via a Furan-Modified Polyhedral Oligomeric Silsesquioxane: Investigation of a Thermally Reversible Silicon-Based Cross-Link†. *Polym. Chem.* **2017**, *8*, 2942–2952.
- (119) Leidner, J.; Akovali, G.; Bernardo, C.; Utracki, L.; Xanthos, M. *Derivation and Validation of Models to Predict the Properties of Mixtures of Virgin and Recycled Polymers*; Springer Netherlands, **1998**.
- (120) Haider, T. P.; Völker, C.; Kramm, J.; Landfester, K.; Wurm, F. R. Plastics of the Future? The Impact of Biodegradable Polymers on the Environment and on Society. *Angew. Chemie - Int. Ed.* **2019**, *58* (1), 50–62.
- (121) Gross, R. A.; Kalra, B. Biodegradable Polymers for the Environment. *Science (80-)*. **2002**, *297* (5582), 803–807.
- (122) Nasresfahani, A.; Zelisko, P. M. Synthesis of a Self-Healing Siloxane-Based Elastomer Cross-Linked via a Furan-Modified Polyhedral Oligomeric Silsesquioxane: Investigation of a Thermally Reversible Silicon-Based Cross-Link. *Polym. Chem.* **2017**, *8* (19), 2942–2952.
- (123) Small, J. H. Methods of Making Thermally Removable Polymeric Encapsulants. US 6,271,335 B1, **2001**.
- (124) QI, H. J.; Joyce, K.; Boyce, M. C. Durometer Hardness and the Stress-Strain Behavior of Elastomeric Materials. *Rubber Chem. Technol.* **2002**, *76*, 419–435.
- (125) Nasresfahani, A.; Zelisko, P. M. Polymer Chemistry of a Thermally Reversible Silicon-Based Cross-Link †. **2017**, 2942–2952.
- (126) Sandra Schafer Guido Kickelbick. Self-Healing Polymer Nanocomposites Based on Diels-Alder-Reactions with Silica Nanoparticles: The Role of the Polymer Matrix. *Polymer (Guildf)*. **2015**, *69*, 357–368.